THÈSE DE DOCTORAT

Etude du vieillissement des aciers ferritiques par simulations atomiques

Présentée et soutenue publiquement à
L'UNIVERSITÉ DE LILLE

École Doctorale Sciences de la Matière, du Rayonnement at de l'Environnement
Unité de Matériaux et Transformation, UMR CNRS 8207, ENSCL

Pour obtenir le grade de
DOCTEUR

Spécialité : Sciences des matériaux
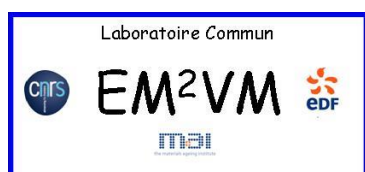par
Romain Candela

Thèse dirigée par
Prof. Charlotte Becquart et Dr. Christophe Domain

Soutenance prévue le 19 décembre 2019 devant la Commission d'Examen composée de :

Prof. Anne Hemeryck	LAAS-CNRS	Rapporteure
Prof. Sandrine Brochard	Université de Poitiers	Rapporteure
Prof. Philippe Carrez	Université de Lille	Examinateur
Prof. Michel Perez	INSA-Lyon	Examinateur
Dr. Christophe Domain	EDF	Encadrant de thèse
Prof Charlotte Becquart	ENSCL	Directrice de thèse

Ph.D. MANUSCRIPT

Study of the ageing of ferritic steels by atomic simulations

Submitted and defended at
UNIVERSITY OF LILLE

École Doctorale Sciences de la Matière, du Rayonnement at de l'Environnement
Unité de Matériaux et Transformation, UMR CNRS 8207, ENSCL

For the degree of
Ph.D.

Field: Materials sciences
by
Romain Candela

Supervised by
Prof. Charlotte Becquart and Dr. Christophe Domain

Ph.D to be defended on 19 december 2019 before the Examination Committee:

Prof. Anne Hemeryck	LAAS-CNRS	Committee Member
Prof. Sandrine Brochard	University of Poitiers	Committee Member
Prof. Philippe Carrez	University of Lille	Examiner
Prof. Michel Perez	INSA-Lyon	Examiner
Dr. Christophe Domain	EDF	Co- supervisor
Prof. Charlotte Becquart	ENSCL	Ph.D. supervisor

Table of contents

List of figures

List of Tables

List of acronyms

AKMC	Atomic Kinetic Monte-Carlo
AP	Atom Probe
AP-FIM	Atom-Probe Field Ion Microscopy
ART	Activation-Relaxation Technique
BMRM	Basin Mean Rate Method
CG	Conjugate Gradient
CNN	Carbon Nearest Neighbour
DD	Dislocation Dynamics
DFT	Density Functional Theory
DL	Dislocation Loop
DSA	Dynamic Strain Ageing
EAM	Embedded Atom Method
EKMC	Event Kinetic Monte-Carlo
EP	Empirical Potential
FIM	Field Ion Microscopy
FIRE	Fast Inertial Relaxation Engine
FISE	Final Initial State Energy
GGA	Generalized Gradient Approximation
HAC	H-Assisted Cracking
HELP	H Enhanced Local Plasticity
K-ART	Kinetic Activation-Relaxation Technique
KMC	Kinetic Monte-Carlo
KRA	Kinetically Resolved Activation
MC	Monte Carlo
MD	Molecular Dynamics
MEP	Minimum Energy Path
MLKMC	Mixed-Lattice Kinetic Monte-Carlo
MMC	Metropolis Monte-Carlo
MS	Molecular Statics
NEB	Nudged Elastic Band
OKMC	Object Kinetic Monte-Carlo
PAW	Projector Augmented Wave
PD	Point Defect
PF	Phase Field
PBC	Periodic Boundary Conditions
PKA	Primary Knock-on Atom
PLC	Portevin-Le Chatelier
PWR	Pressurized Water Reactor
RPV	Reactor Pressure Vessel
TEP	Thermo-Electric Power
SD	Steepest descents
SIA	Self-Interstitial Atom
SSA	Static Strain Ageing
TEM	Transmission Electron Microscopy
VWN	Vosko-Wilk-Nursair

Acknowledgements

First of all, I would like to deeply thank Charlotte Becquart for the trust she put on me for this Ph.D. Then, thank you again for everything you taught me, both in technical aspects and in scientific rigor. Finally, thanks for supporting me all the way from the beginning to the end of this Ph.D., in addition to be a pleasure, it was an honour working with you.

I would also like to thank Christophe Domain for his supervision, for all the help he provided me during this Ph.D. and for all the talks we had that made me think more and more about the subject. You're clearly a part of why I enjoy doing simulations.

I would like to thank the reviewers, Anne Hemeryck and Sandrine Brochard, for agreeing to review my manuscript and for their relevant comments and corrections about the Ph.D. More broadly, thanks to the jury members, Michel Perez and Philippe Carrez, that took the time to listen to my presentation and to dive into my manuscript.

Then I would like to thank the "Canadians", especially Normand Mousseau, who welcomed me to Montreal and helped me a lot to develop the MLKMC. Every conversation I had with you was a pleasure, and working with you was delightful. Thanks also to Sergeï, Vincent who made me feel like home. Lastly, thanks to Simon Geslin for all the laughs, especially when you escaped dying, when you showed us your arm wrestling mastering, and of course for the lesson in humility you taught me.

As for you, Roberto Veiga, thanks for all the discussions I could have with you and all the help you provided me, and more specifically thanks for, in my view, have paved the way for my Ph.D. to be completed. Thanks also to Michel Perez and Osamu Waseda with whom I have had great discussions about my and their models.

I would also like to thank all the people I met at the UMET, they're all a small part of my work. Firstly, Isa and Coco for all the small breaks and fun you bring to this laboratory, and your smiles are always nice to see. Carmen for being yourself, sometimes too cute, sometimes too frank. Speaking of frank people, Damien, you're clearly the funniest around here. Ahmed for all the good talks we had, it was always cool to spend time with you. Ludo for all the jokes you told me, I am still laughing at them. Rémy for introducing me to the world of simulation, you took me as an intern when I did not know anything about this world. Thank you everyone I could speak to during this work, I think particularly to Phillippe, Pierre, Jeremy, Jean-Bernard, Ingrid, Michel and Alexandre.

As for the Ph.D. candidates (and also fresh doctors) I want to thank, my first thought goes to Jérôme, who made me the Linux fanboy I am now, teaching me the beauty of awk, bash, simulations in general, all of this without a smile but with a single philosophical sentence. Marco for all the games we did together, it's always fun when you're around. Max for bringing the coffee breaks to another level, when drinking a coffee could mean spitting it out by the nose. Saadia for your honesty, it's always good to have you nearby. The "ancient ones", Rudy, Kaoutar, Gulzar, Benjamin, Carla, Adi, Chao and Claire. Pierre-Marie for being always available and motivated for futsal. Xie xie chun huo Yu for teaching me Chinese, I can now flirt with girls in Chinese. Devadas for almost all the things that you did, I want to tell you "nyahaha nyahaha", sums up pretty much our relationship. Charlotte for the little breaks we had together, it's always cool to have your hand in my face. Thanks to all the "new ones" that made me laugh, Julie, Isadora, Laïs, Maïra, Arthur, Marco, Thomazs, Ines, Thibault, Sabrina the Boss, Jianlei and Adi. Finally, thank you Gabriel for being the one and only love of my life, the second part of the

Bogdanov brothers, the one whose laugh could be heard from Jupiter thus revealing his soon-to-be crushed teeth.

As for my friends, thanks to the CGCG, Pedro, Piiiiins, Gadon the Loser, Diegz, Stéphane, Léo, Paulo, Zozo… The Parisians, Medhi, Craps, Romrom and Ben. I missed you bros but now I'll come more annoying than ever in every discussion that we will have.

And there's the family, the only reliable pillar we have whatever happens to you. The Barbier family, even there at my defense, you have my special thanks. All the Candela that I can think of, especially my godfather Michel, you also have my special thanks. Thanks again to my close family, my grand-parents, my dear mother, my dear father, my dear Pouchine. Last but not least, I would like to thank my wife, Kimmy-Laure, without whom I would not have had enough support to carry on this Ph.D..

Introduction

Steels are the most used metallic materials in the industry because of their very large range of properties and fields of applications. They regroup Fe-based alloys containing C as alloying element between 0.02 % and 2.11 % in mass. Steels are mainly used for their good mechanical properties such as enhanced hardness compared to Fe alone due to the presence of carbon. The macrostructural properties of materials arise from their microstructure, therefore studying the microstructure of steels and their evolution in service is important to understand the mechanisms governing their properties at the macro scale. The main parameters impacting metal microstructures are the temperature and more precisely the heating and cooling history, the methods used to give them the appropriate form and the C content or more generally the alloying element content. Indeed, other alloying elements are often added in steels to enhance their mechanical properties or to grant them specific properties such as corrosion or high temperature resistance. The Fe matrix phase can be changed by adjusting one or several of these parameters. Indeed, as seen on the Fe-C phase diagram Figure 1, different allotropes are present depending on the temperature and the carbon content.
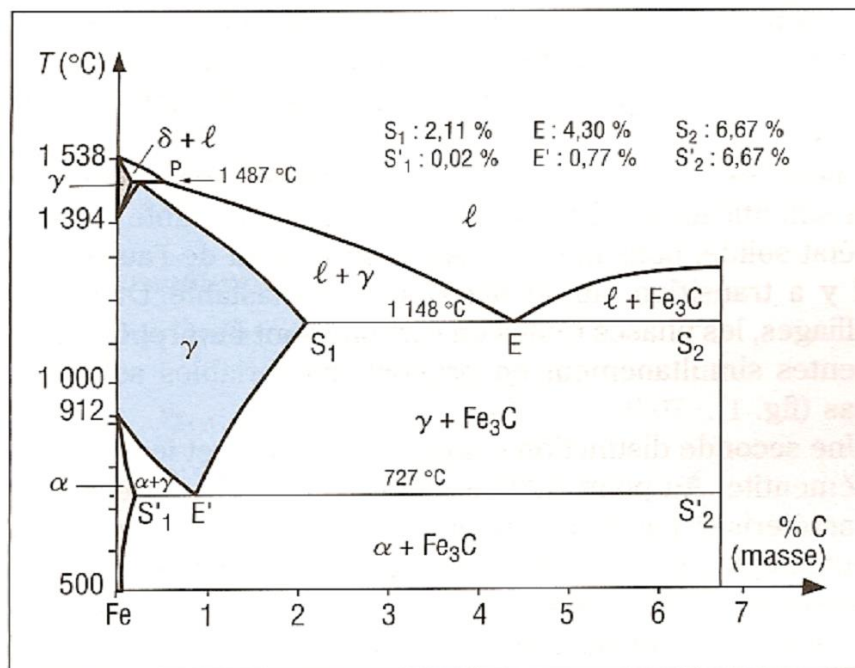
Figure 1: Fe-C phase diagram taken from reference (Barralis and Maeder, 2005).

The ferrite, also known as α-Fe, is a C solid solution within a body-centred cubic Fe matrix. This phase has a small domain of stability and contain low C content (Figure 1). The austenite, or γ-Fe on Figure 1, is a C solid solution like α-Fe, but unlike the ferrite the Fe crystal is arranged in a face-centred cubic arrangement. The Fe_3C phase, known as the cementite, is an iron carbide formed when carbon is added in ferrite or austenite. For a C content between 0.02 % and 6.67 % and a temperature below 727 °C, microstructure is arranged in two phases of ferrite and cementite (Figure 1). This two-phased is known as pearlite and can take two forms depending on the cooling parameters, as pearlite is usually obtained by cooling down γ or γ+Fe_3C. If the cooling rate is high (T decrease at a high speed), the unstable lamellar pearlite, constituted of lamellas of cementite and ferrite, will be formed. However, if the cooling rate is low, the pearlite is qualified as spheroid because the cementite will form spheres within

the ferrite. The spheroid pearlite is more stable than the lamellar pearlite, therefore the lamellar pearlite will become spheroid pearlite when waiting for a sufficient time in a process known as the globulisation. Another microstructure of the Fe worth presenting is the martensite, known for its hardness. It is a C solid solution body-centred tetragonal Fe matrix. Martensite is obtained by quenching γ-Fe (i.e. very high cooling rate), inducing a very fast phase transformation where the C atoms do not move. Therefore, this structure is metastable and is not seen on the phase diagram in Figure 1. Finally, the bainite, a ferrite and cementite two-phased (like martensite and pearlite), is obtained by cooling γ-Fe with a cooling rate between those of martensite and pearlite.

C is the most common addition to Fe because it is the easiest and cheapest alloying element to harden Fe. Nonetheless, it is common to add other alloying element to change the properties of the steel, like W which is added to harden the steels even more and enhance their mechanical properties at high temperatures, Mn which is used to increase the hardness and the machining ability of steels, or Cr which is commonly added to prevent steels from corrosion. For instance, the reactor vessel of a Pressurize Water Reactor (PWR) is constituted of bainitic steel with Mn and Ni as alloying elements (France and Commissariat à l'Energie Atomique, 2016) and the pipes of the secondary circuit are constituted of Fe-Mn-C steels.

The nuclear industry is one of the contributors to the researches in the field of material sciences as the conditions experienced by the components of the reactors are very specific. A PWR can be divided in three major parts, namely the primary circuit containing the nuclear vessel where all the nuclear reactions happen, the secondary circuit containing the alternator where the heat is converted to electricity and the cooling circuit allowing the water to reactor to cool down. An overview of a PWR is provided on Figure 2.
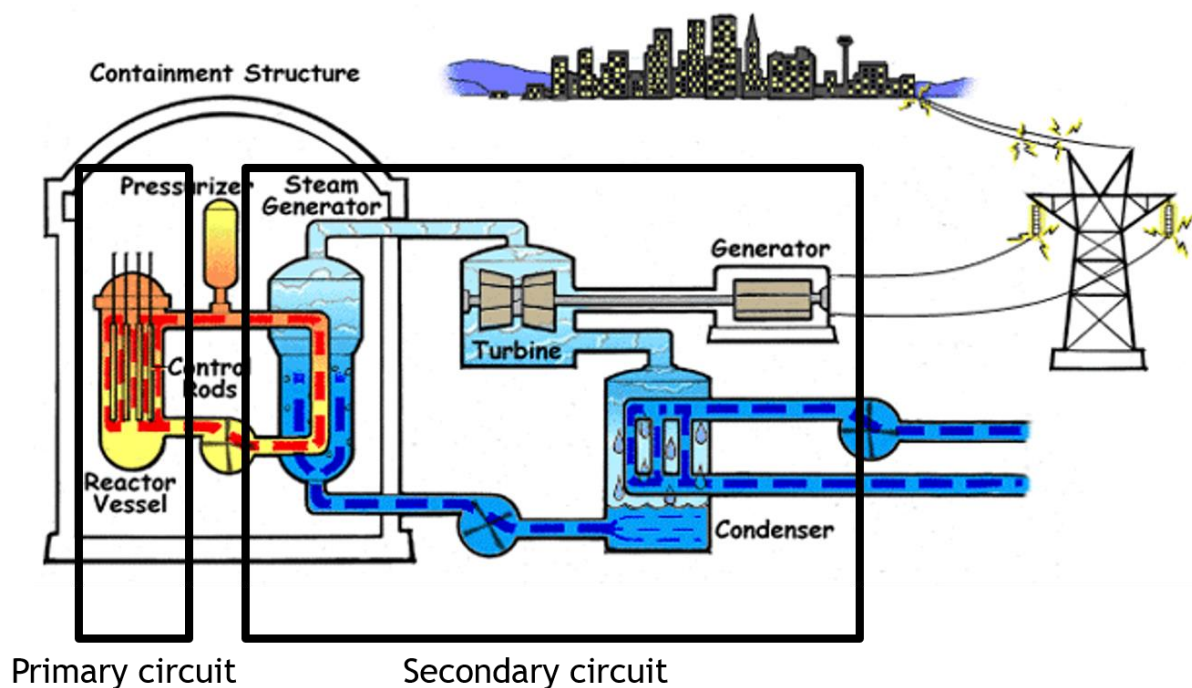
Figure 2: Primary and secondary circuit of a typical pressurized water reactor (taken from (U.S.NRC)).

Even though a constant oversight of the materials constituting the nuclear reactor was done to ensure its good functioning, the ageing of steels under irradiation or not is a phenomenon which needs a special attention. Furthermore, within the framework of E.D.F. major refit, nuclear power plants

initially built for forty years may see their lifespan extended by ten or twenty years. It is in this context that I started my Ph.D., aiming to understand the kinetics of the ageing of pipes in PWR.

In PWR, only the reactor vessel of a nuclear plant is subject to irradiation damage, the other parts are not directly connected to the nuclear reactor. High-energy particles coming from the nuclear reactor will come and hit atoms in the steels constituting the internals and the vessel of the nuclear reactor, thus inducing a displacement cascade. These cascades come from the first atom being hit by the high-energy particle (also known as the Primary Knock-on Atom or PKA) which will leave its lattice site and displace the surrounding atoms that in turn will leave their lattice sites and displace their surrounding atoms and so on. As such, several defects are created due to the irradiation, among others self-interstitial atoms (SIA) who are signature defects of irradiation damage in steels due to their high formation energy. After a displacement cascade where a lot of self-interstitial atoms are created, in α-Fe, these SIA tend to regroup to form clusters called dislocation loops. Several notions need to be introduced before going any further, namely the formation energy, the migration energy and the binding energy. These energies are often used to characterize the mechanisms happening at the microscale of materials. The formation energy of a defect is the energy that needs to be brought to the system to create that defect. For example, the formation energy of a self-interstitial atom (SIA) in a α-Fe matrix is the energy needed for a Fe atom to move from its lattice site to an interstitial site. The migration energy of an atom (or a vacancy) is the energy needed to make this atom move from its site to another site. For instance, the migration energy of a C atom in the α-Fe matrix is the energy needed to move the C atom from its interstitial site to an adjacent one. The binding energy between two defects is the energy of the interaction between these defects, whether it is a repulsive or an attractive energy. It is defined as the difference between the energy of the defects interacting and the energy of the defects not interacting. We will come back to these notions later in the manuscript. Let's just add that the binding energy between SIAs is quite high. This is the reason why dislocation loops form under irradiation. These loops were observed to be very mobile defects (Arakawa et al., 2014)' (Arakawa et al., 2007) which will interact with numerous other defects and thus induce a lot of changes in the material microstructure. Among others, a dislocation loop can interact with another loop in order to form a less mobile loop (Xu et al., 2013), alloying elements such as C (Terentyev and Martin-Bragado, 2015a) (Candela et al., 2018), Mn, Cu, Ni (Bonny et al., 2014)'(Terentyev et al., 2015) or Cr (Arakawa et al., 2004) resulting in a loss of mobility of dislocation loops, and even dislocations (Terentyev et al., 2012)'(Kuramoto et al., 2005). The loops can then be absorbed by grain boundaries (Gao et al., 2018) or even by dislocations (Terentyev et al., 2010).

Another crucial defect found in metals is the dislocation. Volterra was the first to conceptualize the principle of dislocations, which are linear defects in the matrix distorting their surrounding environment. Unlike dislocation loops in α-Fe, dislocations are not found only in radiation damaged steels but in every steel piece. In his Ph.D. (Volterra, 1907), Volterra introduces several equilibrium states of distorted materials as well as the mechanism to induce these deformations in the material. Dislocations will be explained more in details in section: "Chapter I. Bibliography 2. B. Linear defects". Nonetheless, it is important to know that the movement of these dislocations is responsible for the plasticity of the material. Therefore, hindering the movement of dislocations will change the macrostructural properties of the material. As mentioned with the dislocation loop, dislocations can interact with other defects thus changing their mobility, and so the properties of the material. Remember that C is added in α-Fe to harden the material. This is in fact due to C atoms hindering the movement of dislocations, especially the carbides or C precipitates that represents obstacles that dislocations have to cross in order to move. Another impact of alloying elements was discovered by Cottrell and Bilby (Cottrell and Bilby, 1949) with the now known Cottrell atmospheres. In this article, Cottrell and Bilby explain that a dislocation can act as a sink for hetero-interstitial atoms such as C in

Fe. Therefore, the hetero-interstitials will move towards the dislocation to form clouds of interstitials hindering the dislocation movement. These atmospheres were later directly observed especially by Atom-Probe Field-Ion Microscope (AP-FIM) (Blavette, 1999),(Smith et al., 2013),(Miller, 2006). It is also possible to deduce the amount of C in Cottrell atmosphere with the thermoelectric power (TEP) (Lavaire et al., 2001).

Several issues arise from the formation of the Cottrell atmospheres. Taking the α-Fe-C system as an example, one can deduce several of these issues. The most intuitive issue linked to the formation of Cottrell atmosphere is the spatial distribution of C atoms. Indeed, the C enrichment of dislocations induce a C depletion zone near these dislocations and thus a spatial organization of the C atoms different than the original solid solution. This effect alone can influence the macrostructural properties of the Fe-C system. As enlightened by Kather & al. (Khater et al., 2014), the C atoms in solid solution may have a softening effect in iron. Moreover, the second issue linked with the formation of the Cottrell atmospheres is the atmosphere itself. It is well-known that these atmospheres hinder the movement of dislocations and because the movement of dislocations is responsible for the plasticity in a material, this leads to an hardening effect observed at the macrostructural scale of the material (Caillard, 2011). Unfortunately, the hardening of a material often goes along with a loss in ductility and is not always a desired effect. This phenomenon arising with time refers to Static Strain Ageing (SSA) and is part of the more general concept of ageing of a material. The other part of the ageing of a material is known as Dynamic Strain Ageing (DSA). While SSA occurs on a material left on rest, DSA occurs during a material deformation. The main effect of DSA was explained by Le Chatelier in 1909 and is now called the Portevin-Le Chatelier (PLC) effect (Le Chatelier, 1909). The explanation came after the observations of jerky elongation of steel wires during a tensile test in a short range of temperature, which can be directly related to the serrations observed in a stress-strain curve of material during a tensile test. These serrations are shown in Figure 3 b) and are compared to a non-serrated curve Figure 3 a).
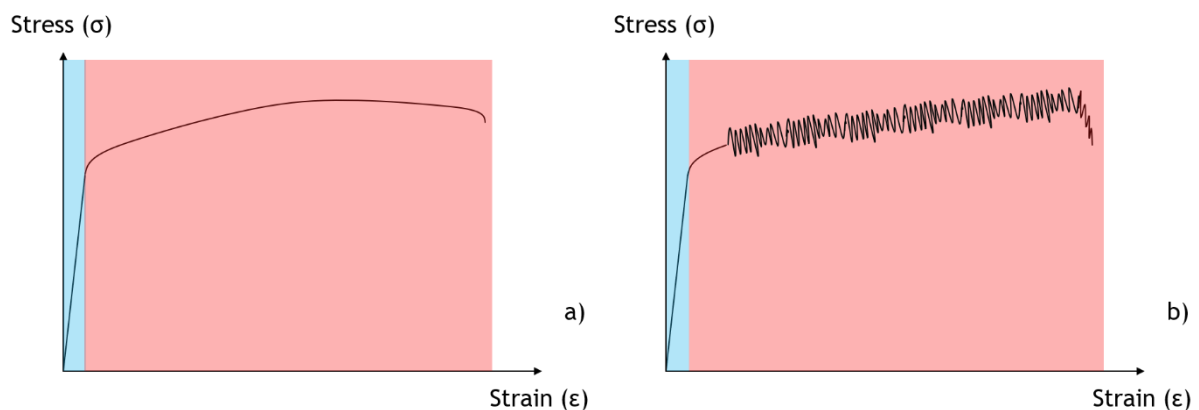
Figure 3: Examples of stress-strain curves exhibiting a typical behaviour (a) and the characteristic serrations of the PLC effect (b) during a material deformation. The blue zone represents the elastic zone of the material and the red zone represents the plastic zone of the material.

This effect happens at a macroscopic scale but as always in material sciences, arise from the micro-structure of the material. The explanation to this phenomenon is itself linked to the Cottrell atmosphere. At the beginning of a serration (Figure 4 step 1), Cottrell atmospheres are decorating dislocations. A high stress is needed to unpin the dislocation from its atmosphere, thus the stress increases (Figure 4 step 2) to a critical point (Figure 4 step 3) where the dislocations will unpin from their Cottrell atmospheres. The dislocations can move again, resulting in a lowering of the stress

(Figure 4 step 4). Eventually, the cloud of C atoms will catch back the dislocations leading to another beginning of a serration until the material fracture.
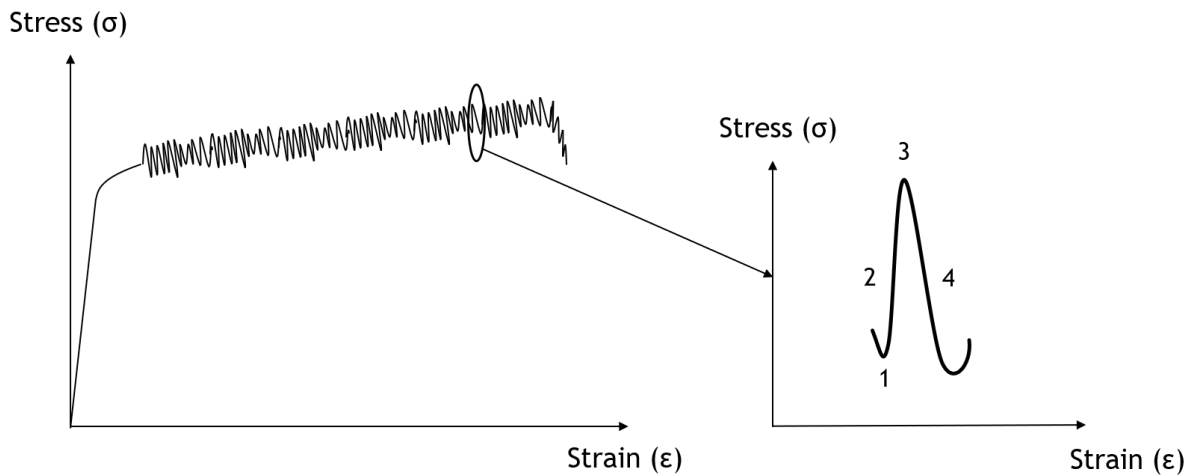
Figure 4: Zoom of a serration with the different steps of the evolution of the material microstructure. The numbers on the zoomed serration represent the different steps occurring during a serration. Step 1: Cottrell atmospheres are decorating dislocations; step 2: stress increase to unpin dislocations from their Cottrell clouds; step 3: dislocations are unpinned from their clouds and can move; step 4: dislocations movement and lowering in the stress.

Two complementary fields exist for the study of materials. The first one, the experimental approach, relies on observations and several other techniques to explain the properties or behaviours of materials. The second one, the numerical approach, relies on simulations and models to bring comprehensive elements of the behaviour or evolution of a material. The major aim of the numerical approach is to bring a multi-scale analysis of a material, i.e. explaining the macrostructural properties of a material starting from the atomic scale.

The aim of this Ph.D. is to investigate the kinetics of formation of C atmospheres around dislocation loops and dislocations using atomic scale modelling and compare with experimental data available. Indeed the carbon enrichment factor of a dislocation has been calculated by 3D AP-FIM studies (Blavette, 1999) or TEP measurements (Lavaire et al., 2004). This was done for instance by R.G.A. Veiga in his Ph.D. work, where he compared the carbon enrichment factor of the dislocations he created with experimental results (Veiga, 2011). However, Veiga & al. studied the dislocation from a thermodynamic point of view only, i.e. investigating the stability of a Cottrell atmosphere and how the atoms are placed when decorating a dislocation and we aim to add kinetics to Veiga's contribution and model the formation of the Cottrell atmosphere.

This manuscript is organized in five major parts. The first one is a bibliographic summary of the studies done close to this research theme. The second one describes the methods used to investigate the thermodynamics and the kinetics of the system. A focus is drawn on the Kinetic Monte-Carlo (KMC) method which constitutes the main algorithm used in this work. The third part of this manuscript will present the program developed during this Ph.D. based on a combination of two different KMC. This program was designed to study atomic systems using different approximations depending on the simulation zone: a very precise algorithm when studying the vicinity of a dislocation or a dislocation loop, and a fast algorithm when studying the bulk which is less distorted than the vicinity of a dislocation. The fourth part presents the results obtained for the C-loop and the C-screw dislocation

system, especially with the above-mentioned developed program. The fifth part presents simulations of a Cottrell atmosphere already formed (provided by Veiga). A conclusion summarizing the main results and proposing future perspectives will end the manuscript.

Chapter I. Bibliography

In this chapter, we present a selection of bibliographical data. We start by presenting the Fe-Mn-C system and the defects present in materials, especially the dislocations and the dislocation loops. The stability of defects and the interactions between different defects in steels is also discussed. The migration of C in steels is addressed as well as the mobility of dislocations. Finally, several experimental methods allowing to confront the simulations with real observations are presented.

1. Fe-Mn-C alloys

Many enhancements can be made to steels when adding some alloying elements. These alloying elements can be classified in two different families, namely the α-genics referring to elements stabilizing the ferritic Fe matrix (such as Cr or Si) and the γ-genics referring to elements stabilizing the austenitic Fe matrix (such as C or Ni). The corrosion resistance can be improved with Cr, with the addition of Ni if the desired steel is austenitic ; Mo, W, and V can be used as alloying elements in iron to increase the hardness of the steel ; Ni will enhance the mechanical properties of the steel at low temperature, while W and V will enhance the mechanical properties of the steel at high temperatures.

Fe-Mn-C is used in the pipes of the secondary circuit of pressurized water reactors. Contrary to C atoms which will occupy interstitial sites, Mn is a substitutional atom in Fe, meaning that it will occupy a lattice site normally filled by a Fe atom. Mn is often added in Fe alloys to improve its hardenability and the hardness. It also influences the mobility of interstitial atoms and the duration of the ageing (Marais, 2012).

2. Defects in metals

A. Point defects

In a pure metal, considering that the atoms are placed on sites (and thus not considering the impact of the atoms vibrations due to the temperature), point defects (PD) either refer to a vacancy or to a self-interstitial atom, as illustrated on Figure 5 b). An atom leaving its atomic site to move in an interstitial site will create both a vacancy and a self-interstitial atom, defect known as a Frenkel pair which is shown in Figure 5 b). Vacancies and interstitials can be introduced in metals during plastic deformation of the material or under radiation, especially in nuclear reactors for the latter (Hull and Bacon, 2001). In bcc and fcc crystallographic structures, SIA will rearrange most of the time either in dumbbells or in crowdions (Amino et al., 2016). Two atoms sharing a lattice site describes the dumbbell arrangement; if the SIA relaxes its strain in the close-packed direction (the crowdion axis), the arrangement is a crowdion. The major difference between these two arrangements is that dumbbells can perform a 3D diffusion, whereas the crowdion is restricted to a one dimension motion along the crowdion axis. In α-Fe, the formation energy of a SIA is high (around 4 eV). Therefore, SIA and SIA clusters are considered signature defects of irradiated steels (Kuramoto et al., 2005).
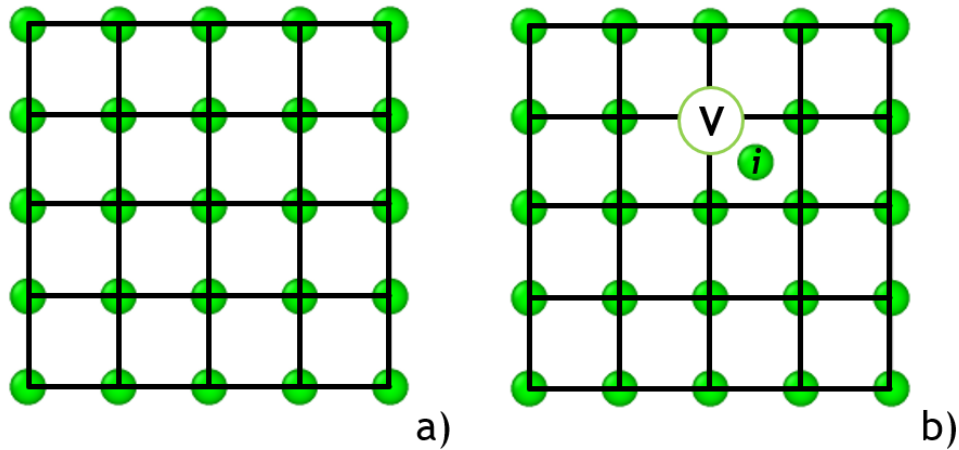
Figure 5: Difference for a pure metal between a perfect lattice a) where all the atoms (green spheres) are placed on their sites (nodes on the black grid) and a lattice containing a Frenkel Pair, i.e. the combination of a vacancy (represented by a V in a circle, an atom left its original site) and a self-interstitial atom (represented by atom labelled "i"). The interstitial atom will then interact with another lattice atom to form a dumbbell or a crowdion.

Adding some impurities in the system redefines the term point defects. As such, the impurities are seen as point defects too. Two different kinds of these point defects can be considered, depending on the place the defect will occupy within the matrix. If the PD is placed in an atomic site, it is labelled as substitutional; on the contrary, an impurity atom placed in an interstitial site will be labelled as interstitial atom.

B. Linear defects

The most common and studied defect is the dislocation, the motion of which is responsible for the plasticity of the material. Two kinds of pure dislocations exist, namely the edge dislocation and the screw dislocation that can be seen on Figure 6 and Figure 7. The concept of edge dislocation was introduced by Taylor (Taylor, 1934) to give an explanation to the low stress needed for the occurrence of a slipping in a mono-crystal at high temperatures.
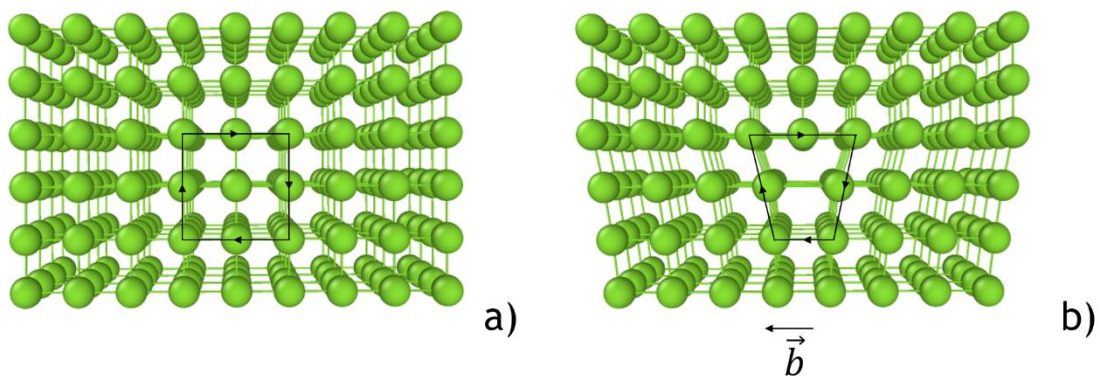
Figure 6: Comparison of a perfect lattice (a) and an edge dislocation (b) in bcc Fe. The Burgers vector $\vec{b}$ is represented.
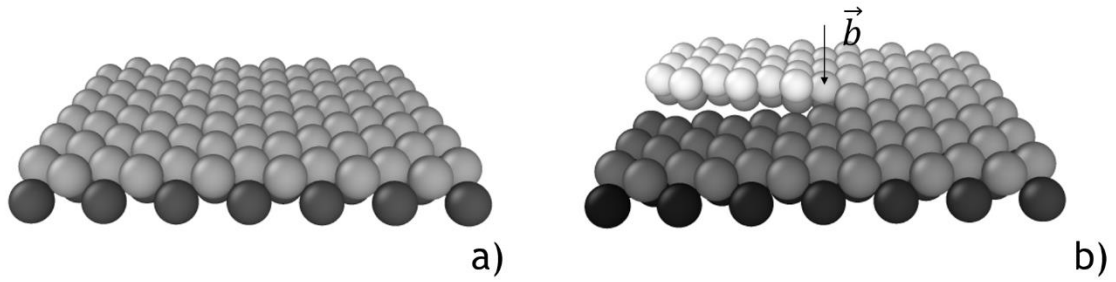
Figure 7: Comparison of a perfect lattice (a) and a screw dislocation (b) in hcp Zr. The atoms are colorized according to their height. On the perfect lattice (a), the atoms are placed in two planes, while in the screw dislocation (b), the atoms have different heights. The Burgers vector $\vec{b}$ is represented.

A dislocation can be characterized by its Burgers vector: it is defined as the vector needed to close a drawn loop in the perfect lattice opened by the presence of a dislocation (the Burgers circuit), thus representing the deformation induced by the presence of the dislocation. As such, dislocations can be defined with their Burgers vector: an edge dislocation has its Burgers vector perpendicular to the dislocation line, a screw dislocation has its Burgers vector parallel to the dislocation line, and what is called a mixed dislocation, i.e. a combination of both a screw and an edge dislocation, has neither its Burgers vector parallel nor perpendicular to its dislocation line.

The atomic study of the mobility of dislocations is of primary importance to have a better comprehension of the mechanisms underlying the plasticity in a material. For that purpose, the Peierls stress of a dislocation is defined as the stress needed to make the dislocation move. The Peierls stress thus accurately reflects the dislocation mobility. Indeed, the lower the dislocation Peierls stress, the lower the energy needed to make the dislocation move and thus the higher the dislocation mobility.

The dislocation density ρ is defined as the distance of dislocation line per volume of material. For a perfect crystal, this value would be null. However, in most of the cases, annealed crystals such as steels have a dislocation density close to $\rho = 10^6 \; cm^{-2}$ (Hirth and Lothe, 1992). The dislocation density rises up along with the straining of the material (Johnston and Gilman, 1959). Thus, a cold-rolled material will have its dislocation density around $10^{10} \; cm^{-2}$ (Hirth and Lothe, 1992). Among ferritic steels, martensite is perhaps the one with the highest dislocation density due to the process to make it; especially in a lath martensite, the dislocation density was found to be between $10^{14} \; m^{-2}$ and $10^{15} \; m^{-2}$, corresponding to $10^{10} \; cm^{-2}$ and $10^{11} \; cm^{-2}$ (Cong and Murata, 2011).

The dislocation loops were previously introduced in this manuscript. In pure α-Fe dislocation loops either refers to SIA dislocation loops or vacancy dislocation loops. However, vacancy loops were not studied in this Ph.D., and every occurrence of the dislocation loop will from now on only refer to SIA dislocation loops (DL). DL are constituted of several crowdions formed during a displacement cascade, and a dislocation loop constituted of 19 SIA is shown on Figure 8. These defects are more mobile than dislocations and can even become obstacles for dislocations.
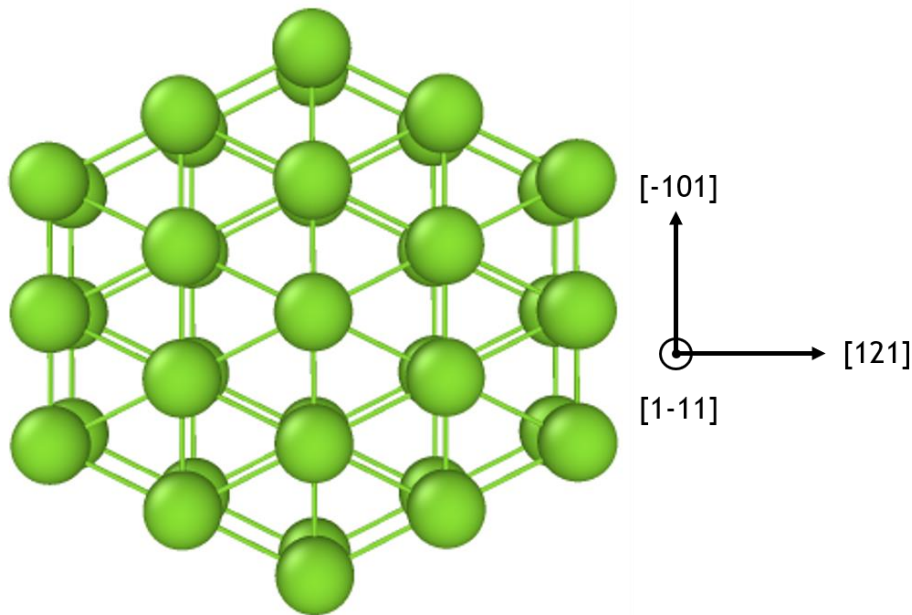
Figure 8: dislocation loop constituted of 19 crowdions.

Vacancies are also defects that can be found in irradiated steels. They have tendencies to bind with a lot of different defects to form more massive defects such as cluster of vacancies, vacancy loops formed during displacement cascades (Soneda et al., 2001) or even carbon-vacancies complexes (Anento and Serra, 2013).

3. Modelling of steels

A. Thermodynamics – Stability of the system

a. C and Mn in α-Fe steels

Many different methods allow one to study the stability of a system containing iron as a matrix. *Ab initio* calculations have the lowest scale among all these methods but provide very reliable results. *Ab initio* has thus become the state-of-the-art method to investigate the thermodynamics of a system. Bcc iron has been widely studied by DFT (i.e. *ab initio* calculations), and especially the interaction between the bcc matrix and the defects. The first important result is the tendency for a C atom to favour O sites rather than T sites[1] (Domain et al., 2004) (Jiang and Carter, 2003). As for Mn, due to its size closeness to Fe, will rather occupy substitutional sites. The addition of Mn can play an important role in the evolution of the microstructure of the steel. For example, Olsson & al. proved that Mn bonds strongly with other interstitials and even vacancies in α-Fe using DFT calculations (Olsson et al., 2010). It also is one of the substitutional alloying element that will segregate the most to interstitial clusters (Ngayam-Happy et al., 2013). Mn will even strongly interact with SIA dislocation loops in Reactor Pressure Vessel (RPV) steels going to their core, thus making it harder for a dislocation to cross the Mn-enriched loop as proven by Terentyev & al. (Terentyev et al., 2015). On the other hand, C atoms have tendencies to precipitate into carbides. These precipitates are known to pin dislocations and harden steels.

---

[1] O sites and T sites refer respectively to octahedral and tetrahedral sites which are the interstitial sites in a crystalline structure

b. Dislocations in pure bcc materials

The dislocations have been investigated as well. The dislocation core controls several properties of a system containing a dislocation such as the dislocation mobility or the short range interaction between the dislocation and other defects such as interstitials. Rodney & al. summarized the different major discoveries about dislocation cores studied by *ab initio* computations (Rodney et al., 2017). After providing the evolution of the dislocation core modelling methods – from the Peierls-Nabarro model (Peierls, 1940) (Nabarro, 1947) to the current *ab initio* modelling of the dislocation cores -, the article displays in details the different lattice types as well as the interesting facts discovered for each of these lattice types. It is a well-known fact that the plasticity in bcc metals is dominated by the thermally activated $\frac{1}{2}\langle 111\rangle$ screw dislocations motion due to their low mobility compared to edge dislocations, especially at low temperatures. As said previously, the core of the screw dislocation is mainly responsible for some of the properties of the dislocation such as its mobility, hence the plasticity behaviour of the bcc metal where the dislocation is in. Two main different configurations of the $\frac{1}{2}\langle 111\rangle$ screw dislocation cores are found in the bcc metals, namely the easy core and the hard core (the split-core[2] will not be addressed in this manuscript). The hard core of a screw dislocation consists in putting the 3 atoms closest to the dislocation line are in the same plane. On the contrary, the 3 closest atoms form a helix on an easy dislocation core. The easy core is believed to be more stable than the hard core and thus the state that the screw dislocation cores are likely to be found (Rodney et al., 2017).
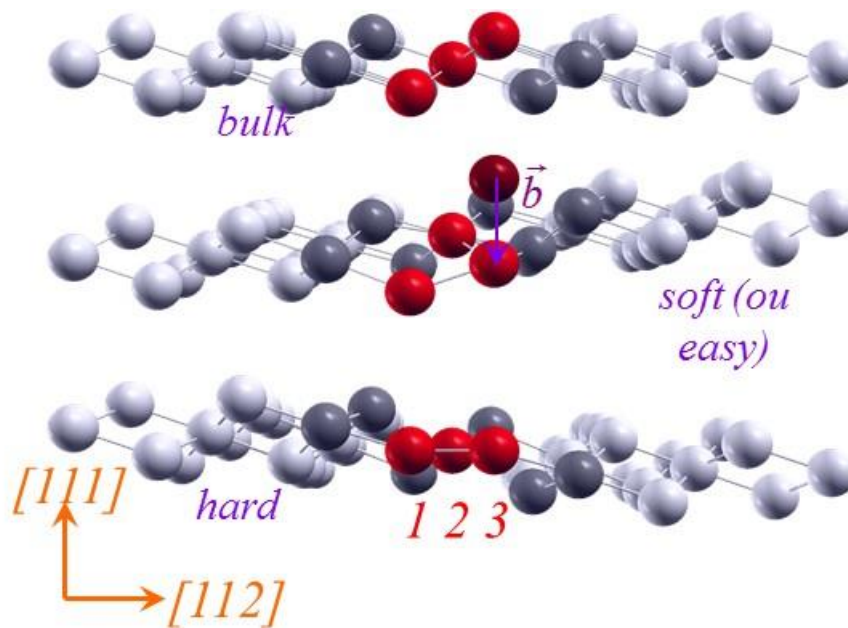
Figure 9: Atomic arrangements of the bulk, the soft core and the hard core of a screw dislocation. The red atoms represent the dislocation. In the hard core configuration, the three atoms constituting the dislocation are in the same {111} plane. Figure taken from reference (Nguyen, 2009).

A method has been developed by Vítek & al. to characterize the structure of the screw dislocation core in bcc materials. It consists in drawing arrows that represent the difference between the vector connecting two atoms in the simulation box containing the screw dislocation and the vector connecting the two same atoms in the perfect bulk (Vítek et al., 1970). More practically, these arrows show the

---

[2] The split-core of a screw dislocation is an unstable or metastable core where the threefold symmetry of the screw dislocation is broken (Ventelon et al., 2013).

displacement of the atoms induced by the dislocation. A representation of the soft core of a $\frac{1}{2}\langle 111\rangle$ screw dislocation in Fe is presented in Figure 10 (taken from reference (Domain and Monnet, 2005)).
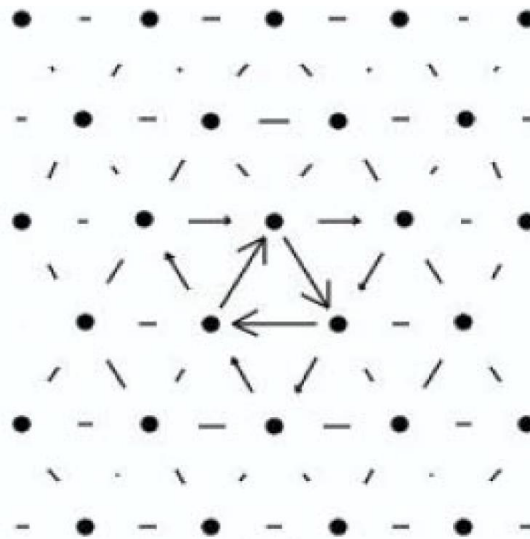
Figure 10: Vitek arrows showing the displacement induced by a $\frac{1}{2}\langle 111\rangle$ screw dislocation in bcc Fe (soft core). The figure is taken from reference (Domain and Monnet, 2005).

The addition of a dislocation within a matrix induces a stress field that distorts the lattice. The properties of this stress field have been investigated. For instance, far from the dislocation, the stress and displacement fields can be easily predicted. As the eye of an observer focuses on the field closer to the dislocation line, i.e. the dislocation core, Clouet shows that another elastic field has to be accounted to explain the discrepancies between the Volterra solution (that describes well the elastic field far from the dislocation) when applied close to the dislocation and the reality (Clouet, 2011).

c. Interaction between dislocations and other defects in Fe alloys

The addition of interstitials in the pure iron system impacts a lot the thermodynamics of the system, especially in the presence of a dislocation. An edge dislocation, which can be seen as the addition (or depletion) of half an atomic plane, therefore has a tension zone and a compression zone. During his Ph.D., Veiga presented the mean displacement of a C atom near an edge and a screw dislocation (Veiga, 2011). For the edge dislocation, the C atoms tend to go away from the compression zone (where they have less space) to join the tension zone (where they have more space).

The effect of a single C atom on dislocations was studied in many different works. For instance, Clouet & al. computed the binding energy between a C atom and both screw and edge dislocations by Molecular Statics (MS) simulations with the help of an Embedded Atom Method (EAM) interatomic potential and compared the results to the elasticity theory predictions (Clouet et al., 2008). An attraction was found to exist between these two defects thus leading to an increase of the stress needed to make the dislocation move compared to a dislocation with no C atoms. Another interesting fact stated in this article is the near perfect agreement of the elasticity theory predictions and the EAM potential predicted binding energies especially for the screw dislocation (results are very close for a C atom at a distance of more than 2 Å of the screw dislocation core, 20 Å for the edge dislocation). It was also found that C atoms bind more strongly with edge dislocations than with screw dislocations; this is also the case for the smaller interstitials H and He in α-Fe (Zhao and Lu, 2011). However, contrary to C atoms, it was found that H atoms tend to enhance the dislocation mobility. This observation is consistent with the H-Assisted Cracking (HAC) (Beachem, 1972), later called H Enhanced Local Plasticity (HELP) (Myers et al., 1992), stating that dislocations move more easily in the presence of H as observed

experimentally. C atoms were found to expel H atoms when in an edge dislocation core (Simonetti et al., 2003).

Interstitials may even influence the dislocation core itself. As shown by Ventelon & al. (Ventelon et al., 2015), the presence of C atoms within a screw dislocation core will induce a change in its structure. As such, the hard core of the dislocation will become more stable than the usual easy core, in a configuration close to the Fe_3C cementite which is an Fe trigonal prism with a C atom in its centre. More generally, solute atoms (B,C,N and O) tend to stabilize the hard core of the dislocation (Lüthi et al., 2018). The presence of hydrogen was also observed to stabilize a quasi-split core[3] of screw dislocations compared to the easy core (Wang et al., 2013).

If the hardening effect of a single C atom on a dislocation - leading to an increase of the Peierls stress - was observed (Chockalingam et al., 2014) (Clouet et al., 2008), the opposite effect has been observed for C atoms in solid solution. Indeed, even if it is a well-established fact that introducing C atoms in a Fe matrix hardens the system, a softening of iron by C atoms was observed by Caillard with TEM in the temperature range of 150 K to 300 K, when a hardening occurs for temperatures below 150 K and above 300 K (Caillard, 2011). Furthermore, the stress needed to make an edge dislocation move in α-Fe was computed and found to be lower for a dislocation surrounded by C atoms in solid solution than the Peierls stress without C atoms (Khater et al., 2014). This effect is due to the attractive nature of the interaction between C atoms and the dislocation: C atoms in solid solution can pull the dislocation and thus contribute to the overall mobility of the dislocation. A consequence of the softening effect that C atoms can have on Fe is that the traditional method to harden Fe (i.e. adding C atoms in the system) may not be as straightforward as thought. Depending on many different factors such as the temperature, the C content, the possibility for C to form atmospheres or to precipitate, or even screw dislocation lengths, C atoms may induce a softening. On the contrary, solute atoms forming precipitates or Cottrell atmospheres always lead to a hardening of the material. For example, using a MC/MD approach, Ganesan & al. show that a screw dislocation in α-Fe does not move when decorated by a C Cottrell atmosphere and when applying a sufficient stress to make a naked dislocation move (Ganesan et al., 2018a). Furthermore, as proven by Pascuet & al. (Pascuet et al., 2017) who studied the influence of alloying elements (Cu, Mn, Ni and P) on an edge dislocation in Fe matrix, the precipitation or the segregation of these alloying elements hinder the dislocation motion. Firstly, configurations containing precipitates near the dislocation line were created with a MC method, then MD simulations while applying a force to the dislocation line allowed the computation of the resistance of the precipitate to the dislocation motion and observe the hardening of the material. Precipitates can interact in other ways with dislocation, e.g. can be totally or partially absorbed by the dislocation such as loops in iron (Bacon and Osetsky, 2009). Depending on the dislocation type, solutes may precipitate to specific zones of the dislocation. This is especially the case for edge dislocations, whereas the screw dislocation stress field has no hydrostatic pressure, thus no positions are favoured for the solutes to form precipitates (Pascuet et al., 2019). Furthermore, Pascuet & al. also show that dislocations reduces the solubility of solutes due to their strain field, and conversely enhances the precipitation: this phenomenon is known as heterogeneous precipitation, with the dislocation acting as a catalyst for the solutes to precipitate.

Concerning the computational costs of simulations, it is important to note the work achieved by Ganesan & al. who developed a parallelized MC algorithm allowing the study of the thermodynamics of the C Cottrell atmosphere in α-Fe (Ganesan et al., 2018b). In this work, the system is divided into several parts, each handled by a manager core who handle worker cores which can compute the transitions in the system. The different managers communicate between them, thus allowing to not overflow the usual single manager used in parallelized simulations.

---

[3] The quasi-split core of a screw dislocation is close to the split-core mentioned previously in note 2 but will not be addressed in this manuscript.

d. Dislocation loops interaction with other defects

Contrary to dislocations, self-interstitial ⟨111⟩ dislocation loops are much more mobile defects than dislocations as observed with Transmission Electron Microscopy (TEM) by Arakawa (Arakawa et al., 2014). This kind of loop has been observed to have a one dimensional glide plane along their Burgers direction, moving with no external stress in the bulk on the ⟨111⟩ directions, with a higher diffusivity for smaller clusters (Arakawa et al., 2007). Their high mobility suggest that they will collapse on other defects such as dislocations or even other dislocation loops: in a mechanism proposed by Xu & al., two ⟨111⟩ dislocation loops interacting can result in a less mobile ⟨100⟩ dislocation loop (Xu et al., 2013), which then can become a strong obstacle for edge dislocations (Terentyev et al., 2008). ⟨111⟩ dislocation loops were also observed to perform a change in their Burgers vector to form another ⟨111⟩ dislocation loop or even ⟨100⟩ dislocation loops with only heating or electron irradiation, as well as the opposite reaction (Arakawa et al., 2006).

The interaction between loops and other defects has also been investigated. For instance, Terentyev and Martin-Bragado investigated the effect of C atoms on the mobility of dislocation loops using an Object-KMC (Terentyev and Martin-Bragado, 2015b). The mobility of the loop was concluded to be driven by the C trapping of the loops and thus the stability of carbon - vacancy clusters. Tapasa & al. found the C atoms to move at the periphery of SIA clusters larger than 19 atoms, directly observing the trapping of the SIA cluster by C atoms for temperatures up to 1200 K (Tapasa et al., 2007a). Using a soft-lattice KMC (i.e. k-ART), Candela & al. showed a stability zone at the external periphery of the loop where the C atom can move with a very low migration energy path and pin the loop for times up to 10^{-1} s at 300 K (Candela et al., 2018), thus confirming the trapping of SIA clusters by C atoms observed by Tapasa & al. (Tapasa et al., 2007a). The effect of Cr on the mobility of DLs in α-iron was also studied with in-situ TEM experiments (Arakawa et al., 2004). Cr atoms were observed to decrease the mobility of loops, especially above 450 K. Another important result in this article is that the main factor impacting the SIA dislocation loop diffusivity is the density of loops: the higher the loop density, the more the loops interact with each other, and the higher the overall mobility of the loops. Domain and Becquart studied the interaction between solute atoms and small (7, 19 and 37 SIA) ⟨111⟩ dislocation loops (Domain and Becquart, 2018). Using DFT calculations, they showed that, big solute atoms such as Mo or W do not bind to the loop, solutes such as P, Si, Mn, Ni and Cu are strongly bound to the loop when at the border of the dislocation loop, whether they are within or outside the loop. It was also found that Cr has a very small interaction with loops, in agreement with the fact that Cr is known not to interact strongly with small SIA clusters. Vacancies were also observed to bind strongly with SIA loops (Anento and Serra, 2013), and vacancy-carbon clusters were found to bind very strongly (more than a single C atom, or even a C-C pair), therefore constituting traps for the SIA loops (Terentyev et al., 2011). SIA loops can then be trapped, e.g. be absorbed by dislocations (Bacon and Osetsky, 2009) or by grain boundaries (Gao et al., 2018).

While SIA loops are omnipresent defects in irradiated α-iron, vacancy loops are way more likely to be found in fcc metals according to Soneda and co-workers (Soneda et al., 2001). Out of 100 MD simulations, only one was able to conduct to the formation of a vacancy loop in α-Fe by a mechanism described by the authors as a collapse of a void into a loop after the formation of a very mobile SIA cluster (thus leaving a vacancy rich zone). Indeed, as pointed out by Soneda and De La Rubia, vacancies in bcc iron being less mobile than interstitials, an atom depleted zone will be created through the leaving of SIA clusters (Soneda and de la Rubia, 1998). Gilbert & al. later confirmed that spherical voids are the most stable configuration for a cluster of vacancy in α-Fe and in W (which can perhaps be generalized to all bcc materials), and affirming that vacancy loops are metastable in such materials (Gilbert et al., 2008). These results however may very well be related to the interatomic potentials as

a recently built database of cascades done with many different Fe interatomic potentials seems to indicate that the respective amount of vacancy and SIA dislocation loops is potential dependent.

B. Kinetics – Diffusion of C in α-iron

The diffusion of C atoms in the α-iron is the first step of the study of the kinetics of the formation of a Cottrell atmosphere. The C migration energy in bcc Fe was estimated to be close to 0.8 eV with a minimum energy path going from an O site to another O site with the saddle point being C in the T site (Restrepo et al., 2016) (Jiang and Carter, 2003).

A lot of computational simulation studies of the C-dislocation interaction were done these past years. A comparison between elastic anisotropy and AKMC simulation was performed by Veiga (Veiga et al., 2011) for C atoms near both edge and screw dislocations. In this article, Veiga & al. show that the anisotropic elasticity fails when the C atom comes too close to the dislocation core, giving an idea of the complexity to study the kinetics of C diffusion from the bulk to the dislocation core and thus the necessity of powerful tools to reproduce the real C behaviour under the dislocation induced distortion. Taking into account the previously introduced "dislocation core field" (Clouet, 2011) to the anisotropic elasticity theory allowed Clouet to find a higher binding energy between the C atom and a screw dislocation in α-Fe than what was predicted by anisotropic elasticity theory alone.

Veiga & al. simulated the diffusion mechanism of a single C atom under the stress field of an edge dislocation in α-Fe using a combination of an AKMC and molecular statics (Veiga et al., 2010). It was shown in this article the slight attraction of the C atom towards the dislocation core. Furthermore, as the temperature rises, the capture radius of the C atom decreases, i.e. the C atom is less likely to get trapped inside the dislocation core.

The diffusion of C atoms was studied in even more distorted systems. Tapasa & al. observed the diffusion of a C atom within the core of an edge dislocation (Tapasa et al., 2007b) where the molecular dynamics simulations showed an enhanced diffusivity of the C atom within the dislocation core. This phenomenon is now widely known as the pipe diffusion. A model was proposed by Love to explain to enhanced diffusivity of defects near the dislocation line (Love, 1964).

Concerning the formation of a Cottrell atmosphere, Veiga constructed a carbon Cottrell atmosphere in iron around a screw dislocation with a combination of MC and MD methods (Veiga et al., 2015), showing the high stress needed to unpin the dislocation from its atmosphere and deducing that the decorated screw dislocations may be obstacles for other moving dislocations. Another important result was put on display by Waseda & al. (Waseda et al., 2017): creating a C Cottrell atmosphere in Fe around an edge dislocation with a MMC, they observed that the only factor impacting the saturation of the Cottrell atmosphere is the C-C interaction. As such, they even observed C atoms occupying the compression zone of the dislocation after filling the tension zone.

C atom was also observed to move when bound to other defects such as a vacancy (Restrepo et al., 2016) and a DL (Candela et al., 2018), both with the same soft-lattice AKMC.

C. The movement of dislocations
a. Pure iron

As said previously, the mobility of dislocations is crucial to study for a better understanding of the mechanical behaviour observed at the macro scale as the movement of dislocations is responsible for the plasticity in a material. For instance, the $\frac{a_0}{2} \langle 111 \rangle$ screw dislocation in pure bcc iron was observed by MD simulations to move accordingly to the double kink mechanism under a shear strain (Domain and Monnet, 2005). This mechanism shows that a screw dislocation segment will move to an adjacent

triangle if the observer looks at the dislocation in the [111] direction, and that this segment will drag the rest of the dislocation with it resulting in a shift of the dislocation position. Because after this double kink the screw dislocation has passed from an easy core to a more unstable hard core, another double kink follows the first one to retrieve the easy core of the dislocation. Another important result shown in this article is that the dragging of the whole dislocation after a double kink occurred is very fast, and thus that the rate-determining step of the screw dislocation motion is the apparition of a double kink, itself proportional to the dislocation length. The usual slip planes of screw dislocations in bcc irons are {110}. However, for temperatures above 300 K, a change of the effective slip planes from {110} to {112} was observed, even if kinks pairs occurred only in the {110} planes (Gilbert et al., 2011). This change of effective slip planes, thus not having a huge effect on the screw dislocation movement, may be linked to the "spreading" of the dislocation core observed by the same authors for temperature above 350 K.

As for the $\frac{a_0}{2} \langle 111 \rangle$ edge dislocation in bcc iron, it will also move along a slip plane, the easiest activated slip planes being {110} and {112}. However, the motion of edge dislocations in α-iron at low temperatures (below 100 K) was observed to occur by kink-pairs propagation, in a manner close to the screw dislocation kink-pair mechanism (Monnet and Terentyev, 2009). Furthermore, Queyreau & al. observed the same behaviour to happen only for the $\frac{a_0}{2} \langle 111 \rangle \{112\}$ edge dislocation (not for {110} slip planes) when the applied stress was low (Queyreau et al., 2011).

The Peierls stress has been mostly studied using interatomic potential simulations (Domain and Monnet, 2005). However, using DFT calculations, Ventelon & al. (Ventelon et al., 2013) discovered that none of the commonly used Fe interatomic potentials are adapted to this kind of study, as they overestimate a lot the energy of the dislocation hard core. As such, the hard core configuration of the dislocation must be considered when looking at the displacement of the screw dislocation.

b. *Material with defects*
Except in pure materials, the motion of dislocations is not smooth. In fact, many obstacles will hinder or enhance the movement of these dislocations, such as interstitials, precipitates, other dislocations, dislocation loops and even grain boundaries.

Bhatia & al. studied the influence of vacancies and hydrogen on the mobility of an edge dislocation using MS and MD calculations (Bhatia et al., 2014). As expected, hydrogen in the tension zone of the dislocation and vacancies in the compression zone reduces the dislocation mobility. However, a hydrogen atmosphere first enhances the dislocation mobility (due to the attractive interaction between the atmosphere and the dislocation) and pins the dislocation after. Moreover, with the increase of the strain applied, a single vacancy was observed to mimic the Portevin-Le Chatelier effect, where the vacancy follows the dislocation movement with a speed of the same order.

SIA dislocation loops can also hinder the movement of dislocations. Especially depending on the orientation of the loop, the interaction between a dislocation and a SIA DL can result in various situations, from the whole loop absorption to the dislocation not absorbing the loop at all (Terentyev et al., 2008). It was shown by Terentyev & al. that ⟨100⟩ SIA loops with their Burgers vector in the edge dislocation slip plane can make strong obstacles for a moving dislocation. Furthermore, at low temperatures, loops are not absorbed by the dislocation thus providing strong pinning points for the dislocation (Terentyev et al., 2010).

Concerning precipitates, Nedelcu & al. studied the influence of different sized Cu precipitates on the motion of an edge dislocation in α-iron by MD simulations (Nedelcu et al., 2000). Firstly, two opposite dislocations are introduced in the simulation supercell, leading to an attraction between them and

thus a movement of these dislocations. This attraction is sufficient enough to allow a dislocation to cross small Cu precipitates but not large ones as an external pressure had to be applied for a large Cu precipitate for the dislocation to cross it. The Cu precipitate is strongly bound to the dislocation, even making the dislocation bow. For a big enough precipitate, the dislocation can not cut it. Therefore, the moving dislocation must circle the precipitate to pass it, leaving new dislocations around the precipitate. This mechanism, known as the Orowan process, has been studied by Monnet using Dislocations Dynamics (DD) simulations in irradiated in a Zr-1%-Nb alloy (Monnet, 2006). It was even shown by Pascuet & al. that precipitation near the dislocation line can make the screw dislocation almost immobile (Pascuet et al., 2019).

4. Experimental comparison

Investigating the thermodynamics of a system can be achieved by many different methods, *ab initio* calculations being the state of the art method. Methods derived from *ab initio* are also used for that purpose, such as the use of interatomic potential derived from DFT calculations allowing one to perform greater sized and faster computations than DFT, e.g. molecular statics. MMC methods also allow the user to investigate the thermodynamics of a system, such as predicting the shape of a Cottrell atmosphere decorating a dislocation (Waseda et al., 2017).

Such a created atmosphere can be linked to the enrichment factor of solute atoms within the dislocation, which can itself be determined by experimentations. For example, the Thermo-Electric Power (TEP, a difference in tension) which is measured on two samples, i.e. a reference sample (pure iron) and an aged steel, can lead to the enrichment factor of dislocations in the aged steel. In fact, TEP is very sensitive to solutes in solid solution, precipitates and dislocations. The effect of each of these defects is assumed to be decorrelated (Lavaire et al., 2001), especially in low alloyed steels, and can therefore be linked to the variations of the TEP measurements. For more details about this technique, see the methodology proposed by Lavaire & al. who determined the activation energy of C diffusion in Fe using TEP (Lavaire et al., 2001). A more straightforward method than TEP consists in directly observe the dislocations using Atom-Probe methods (AP). This method consists in the decomposition of the studied sample with a laser "atom by atom" and reconstruct the map of the atoms desorbed. Like this, atomic maps can be achieved and a Cottrell atmosphere can even be visualised (Lavaire et al., 2001) (Hatakeyama et al., 2014) (Miller, 2006). It is also possible to link the observations at the micro-scale to the behaviour at the macro-scale, such as the serrations in a stress-strain curve linked to Cottrell atmosphere following an unpinned dislocation.

Concerning the study of dislocations, it is interesting to note that many studies consider that the core of a dislocation needs an atomic-scale precision modelling when the bulk can be described using easier approximations (Clouet, 2011) (Veiga et al., 2011) (Tchitchekova et al., 2014). Several methods allow to simulate the evolution in time of an atomic system. At the atomic scale, depending on the studied system, perhaps the most used method is MD. To achieve greater simulated time than MD, AKMC method can be favoured without losing the atomic description (Soisson et al., 2010) or temperature-accelerated MD (Sorensen and Voter, 2000). At the mesoscopic scale, DD, OKMC or phase field can simulate the behaviour or more massive objects than atoms. However, it is harder to study experimentally the kinetics of a system. Nonetheless, in-situ TEM observations can be carried out to study the behaviour of dislocations (Caillard, 2010a) (Caillard, 2010b) (Caillard and Bonneville, 2015) and even dislocation loops (Arakawa et al., 2014).

Several defects are present in steels, and the interactions between these defects will dictate the evolution of the microstructure of the material. As such, in α-Fe, dislocations act as sinks for hetero-interstitials like the C atoms. This can lead to the formation of Cottrell atmospheres which will hinder the dislocation mobility and thus impact the macro properties of the material. The simulated results can be compared to experimental data, for example the enrichment factor of a dislocation in C atoms can be determined either with simulations or with AP-FIM.

Chapter II. Methods

In this chapter, we present the computational methods used during the Ph.D. to study the thermodynamics and the kinetics of a system of Fe atoms containing an extended defect such as a dislocation loop or a screw dislocation and C atoms. The full description on how to simulate the kinetics of a system is displayed in this section, starting from the calculation of the energy of a system. A particular attention is drawn on the kinetic Monte-Carlo method, as it constitutes the main method used during the Ph.D.

1. Cohesive model: computing the energy of a system

The first step of studying at the atomic scale a system by numerical simulation is to compute the energy of a system as well as the forces on atoms. This can be achieved by different kinds of cohesive models, and two of these models are presented, i.e. the density functional theory (DFT) and the empirical potentials (EP). The density functional theory is considered the state-of-the art method to study the thermodynamics of a system especially because of its precision and its ability to predict accurate results, at the cost of a lot of CPU resources with simulation box sizes typically between a hundred and a thousand atoms. On the contrary, empirical potentials are faster than DFT and allow to relax a simulation box containing few millions of atoms on a single node within hours. The information searched by DFT are precise ones, such as the formation energy of defects, the binding energy between two defects or even the precise geometry of a cluster of atoms, while EP results are semi-quantitative or trends, such as the tendency of point defects to cluster, and mechanisms like the dislocation motion.

A. Ab initio calculations and Density Functional Theory (DFT)

Ab initio calculations have become the standard method to investigate the stability of a system at the atomic level. In principle, to properly investigate the thermodynamics of a system, one needs to solve the Schrödinger equation (equation 1) for all the particles present in the system.

$$\widehat{H}\Psi = E\Psi \tag{1}$$

Where Ψ is the wave function, E is the total energy of the system and $\widehat{H}$ is the Hamiltonian of the system composed by N nuclei of mass M_N and charge Z_N, and n electrons of mass m_n. For simplification sake, the atomic units system is used: the mass is based on the electron mass ($m_n = 1$), the electric charge is based on the proton charge ($e = 1$), the reduced Planck Constant is also set to 1 ($\hbar = 1$) and $4\pi\varepsilon_0 = 1$. The Hamiltonian can thus be written:

$$\widehat{H} = \sum_{\alpha} -\frac{1}{2M_\alpha}\nabla_\alpha^2 + \sum_{j} -\frac{1}{2m_i}\nabla_i^2 + \frac{1}{2}\sum_{\alpha,\beta}^{\alpha\neq\beta} \frac{Z_\beta Z_\alpha}{|r_\alpha - r_\beta|} + \frac{1}{2}\sum_{i,j}^{i\neq j} \frac{1}{|r_i - r_j|} - \sum_{\alpha,i} \frac{Z_\alpha}{|r_\alpha - r_i|} \tag{2}$$

Where α and β represents nuclei, i and j are electrons, and r_x are the positions of the particle depending on x (nucleus if $x = \alpha, \beta$; electron if $x = i, j$). The five different sums correspond to different contribution to the total energy of the system, from the left to the right respectively the nuclei kinetic energy, the electrons kinetic energy, the electrostatic energy between the different nuclei, the electrostatic energy between the different electrons and the electrostatic energy between electrons and nuclei.

This Hamiltonian can be solved analytically only for hydrogen and hydrogenoïds where the total number of particles is equal to one electron and one proton. To study more complex systems, assumptions must be made.

a. The Born-Oppenheimer approximation

The Born-Oppenheimer approximation consists in decorrelating the electron motion from the nuclei motion. The observation that the X-ray emission spectra are the same for a solid and for free particle allows us to precise the precedent approximation: the decorrelation occurs between the valence electrons and the resulting ions when because, as justified, the ion structure is not changed by its environment. Therefore, the Hamiltonian in equation 2 can be written as a decomposition of the contribution of the ions and the contribution of the electrons to the Hamiltonian:

$$\hat{H} = \hat{H}_{ions} + \hat{H}_{electrons} \tag{3}$$

Where

$$\hat{H}_{ions} = \sum_{\alpha} -\frac{1}{2M_{\alpha}} \nabla_{\alpha}^2 \tag{4}$$

And

$$\hat{H}_{electrons} = \sum_{j} -\frac{1}{2m_i} \nabla_i^2 + \frac{1}{2} \sum_{\alpha,\beta}^{\alpha \neq \beta} \frac{Z_{\beta} Z_{\alpha}}{|r_{\alpha} - r_{\beta}|} + \frac{1}{2} \sum_{i,j}^{i \neq j} \frac{1}{|r_i - r_j|} - \sum_{\alpha,i} \frac{Z_{\alpha}}{|r_{\alpha} - r_i|} \tag{5}$$

The fact that the nuclei are far less mobile than the electrons allows one to consider the position of the nuclei as parameters in the Hamiltonian, resulting in a wave function depending only on electrons.

b. The mono-electronic approximation

This approximation states that the wave function $\Psi(x_1, x_2, \dots, x_n)$ of n particles can be written as the product of n spin-orbitals $\psi_m(x_m)$:

$$\Psi(x_1, x_2, \dots, x_n) = \psi_1(x_1) \times \psi_2(x_2) \times \dots \times \psi_n(x_n) \tag{6}$$

The Schrödinger equation (equation 1) is then simplified a lot, as the total energy of the system is simply the sum of each electronic contribution:

$$E = \varepsilon_1 + \varepsilon_2 + \dots + \varepsilon_n \tag{7}$$

This method is thus decorrelating the electrons position and movement with each other, the system is seen as a sum of n functions describing one electron progressing through a field of other electrons. The anti-symmetry principle, which states that the electrons can be swapped resulting in a sign change on the wave function, is not respected by the mono-electronic approximation. Two different methods will be presented to cope with this problem, namely the Hartree-Fock approximation most used in chemistry and the Density Functional Theory often used in material sciences.

c. The Hartree-Fock approximation

To consider the correlation between the electron motion and respect the anti-symmetry principle, one can combine the product of the spin orbitals. The wave function can then be written as a Slater determinant for a n electrons system:

$$\Psi(x_1, x_2, \dots, x_n) = \frac{1}{\sqrt{n!}} \begin{vmatrix} \psi_1(x_1) & \psi_2(x_1) & \cdots & \psi_n(x_1) \\ \psi_1(x_2) & \psi_2(x_2) & \cdots & \psi_n(x_2) \\ \vdots & \vdots & \ddots & \vdots \\ \psi_1(x_n) & \psi_2(x_n) & \cdots & \psi_n(x_n) \end{vmatrix} \tag{8}$$

The Pauli principle, which excludes the possibility of having two electrons in the same spin-orbital, is respected as the wave function is null if two electrons shares the same quantum-numbers, i.e. the same spin-orbital. Furthermore, because of the Pauli principle, the same spin electrons are correlated but not the opposite spin electrons.

d. The Density Functional Theory (DFT)

The DFT principle is to reduce the complexity of the $3n$ variables problem (with n the number of electrons and the 3 coordinates in cartesian coordinates) to a 3 variables problem using the electronic density instead of the coordinates of each electron. The justification of this change of variable was given by Hohenberg and Kohn (Hohenberg and Kohn, 1964) as they proved that the fundamental energy of a system of electrons immersed in an external potential can be determined with the sole knowledge of the electronic density. The energy function of the system is thus written as:

$$E(\rho) = \int V(r)\rho(r)d^3r + F(\rho) \tag{9}$$

B. Interatomic potentials

An interatomic potential is a function which returns the potential energy between two or several different atoms from the knowledge, most of the time, of the distance between them. A potential is developed according to the type of bonds involved (metallic bonds, ionic bonds, …). The potential is optimized on parameters to match experimental or ab initio data. These parameters are fit on physical properties which are chosen according to their relevance, i.e. fulfilling the two necessary conditions: the physical properties must be known with precision and they must be somehow related to the use of the interatomic potential, e.g. the Fe bcc elastic constant for the study of dislocation in bcc Fe. However, because the potential is optimized to accurately reproduce precise data, it may lack of versatility and can sometimes be confined to the study of resembling systems. Indeed, an interatomic potential fit for the C diffusion in the pipe of a dislocation Fe will not necessary predict the same carbides found in the bulk compared to the ones observed in real materials. Several different kinds of potentials exist depending on the system studied. Among the existing potentials, the Embedded Atom Method (Daw and Baskes, 1983) (Daw and Baskes, 1984) (EAM) potentials are one of the most commonly used for the study of metals. Contrary to DFT calculations where the energy of the system is written as a non-local functional of the electron density, the EAM approximates this functional by a local function (Ackland, 2012). Under the EAM hypothesis, the energy of an atom is given by a combination of the energy between two atoms versus their distances (pairwise part of the potential) and the energy needed to put an atom in a cloud of other atoms (embedding part of the potential):

$$E_i = F_\alpha(\rho)\left(\sum_{i \neq j} \rho_\beta(r_{ij})\right) + \frac{1}{2}\sum_{i \neq j} \phi_{\alpha\beta}(r_{ij}) \tag{10}$$

Where E_i is the energy of the atom i, $F_\alpha(\rho)$ is the embedding energy, $\rho_\beta(r_{ij})$ is the electron density, r_{ij} is the distance between the atoms i and j, α and β are the atomic types of respectively i and j, and $\phi_{\alpha\beta}(r_{ij})$ is the pairwise interaction between atoms i and j.

The potential used in this work was developed by Becquart and co-workers (Becquart et al., 2007) and later slightly modified by R.G.A. Veiga (Veiga et al., 2014). The Fe-Fe interactions of the potential are provided by the potential developed by Ackland, Mendelev & al. (Mendelev et al., 2003) (Ackland et al., 2004), which is still considered one of the most accurate Fe-Fe potential that can describe accurately a wide variety of defects (Malerba et al., 2010) even if the development of Fe potentials is still a very active field. The Fe-C interactions were fitted on two sets of ab initio data, namely a single

C atom in an O site and a single C atom in a T site to accurately predict the C migration energy (Becquart et al., 2007).

This potential has proven its worth on numerous different Fe-C based systems, such as predicting the dynamics of C in bulk Fe (Restrepo et al., 2016) or focusing more on the C-dislocation interaction (Veiga et al., 2015) (Clouet et al., 2008) (Veiga et al., 2011).

2. Looking for a potential energy minimum: minimization algorithms

A. Statistical ensembles

Before addressing the minimization algorithms, the notion of statistical ensemble must be defined. A system can be thermodynamically characterized by several parameters, e.g. the number of particles, the temperature and the energy of the system. The other thermodynamics parameters can be retrieved from the fundamental equations of thermodynamics and the equations of state. Furthermore, quantities such as the diffusion coefficient or the shear viscosity are state functions, i.e. their value depends on the set of thermodynamic parameters (Allen and Tildesley, 1987). Therefore, fixing this set of parameters allows to easily retrieve other thermodynamic properties of the system; this is what is called a statistical ensemble. The parameters most often fixed are the number of particles N, the pressure P, the temperature T, the energy E and the chemical potential μ. These variables can be fixed simultaneously to create the most used statistical ensembles: the microcanonical ensemble (NVE fixed), the canonical ensemble (NVT fixed), the grand canonical ensemble (μVT fixed) and the isothermal-isobaric ensemble (NPT fixed). In practice, a system is studied in one of these statistical ensembles, e.g. a simulation will occur in a defined volume, with a fixed number of particles and at a certain temperature so in the canonical ensemble. The simulations in this work were all done in the canonical ensemble.

To accurately describe the kinetics of a system, the initial system must be relaxed in a local potential energy minimum. Several families of algorithm can investigate the local potential energy landscape of a configuration and allow the system to relax its energy into a minimum of energy. Among them, the Molecular Statics (MS) calculations are the most commonly used, and four of the most used algorithms in MS are presented, namely the quench, the steepest descents (SD), the fast inertial relaxation engine (FIRE) and the conjugate gradient (CG). Note that all these methods are iterative, i.e. going from a configuration to a minimized configuration by a succession of steps. What differentiate these methods is the manner to pass from a configuration to the following one.

B. Quench

The quench is a simple algorithm which consists in computing the forces, velocities and then the displacement of each atom for many steps thanks to an empirical potential. If the total energy at the step $n + 1$ is higher than the total energy at the step n, the velocities of all the atoms are set to 0. An alternative way to perform molecular statics is to apply the previous algorithm not for the total energy but for the energy of each atom (i.e. put the velocity of an atom at 0 if its energy at step $n + 1$ is higher than its energy at step n). Note however than this can be done too with DFT instead of the empirical potential, but molecular statics are faster methods than DFT to relax a system into a local potential energy minimum. This method is used in the code DYMOKA (Becquart et al., 1997).

C. Steepest descents

Among the possible algorithms allowing the relaxation of a system, the steepest descents is one of the simplest (Sheppard et al., 2008). It simply consists in following the force vector from a configuration towards a force equal to zero. More practically, the SD will go from a configuration to another following the equation:

$$C_{n+1} = C_n + \alpha F_n \tag{11}$$

Where C_{n+1} and C_n represents the configuration at steps $n+1$ and n, α is an adjustable parameter allowing to control the speed of the SD, and F_n is the force. Therefore, one simply has to compute the forces on atoms to perform this minimization method. This method is used by k-ART to relax configurations.

D. Fast inertial relaxation engine

The FIRE method was introduced by Bitzek & al. in 2006 (Bitzek et al., 2006). Contrary to the SD method, in the FIRE algorithm the steps to go from a configuration to another are dynamical, i.e. take into account the velocity and the acceleration and thus relies on time. Furthermore, to avoid atoms climbing up the energy landscape, an atom is stopped when the scalar product of the velocity and the force is negative, i.e. when the force tend to draw back the atom to the energy minimum while the velocity tend to make the atom climb to energy landscape.

E. Conjugate gradient

The conjugate gradient method was developed in 1952 (Hestenes and Stiefel, 1952). It is still at this time perhaps the most commonly used algorithm in molecular statics. Contrary to SD where the atoms are following the force only, on the CG method atoms are also searching conjugate directions (Sheppard et al., 2008). The method is described precisely step by step by Shewchuk (Shewchuk, 1974).

3. Calculating the binding energy between several defects

One of the property that will be used throughout this work is the binding energy between objects which characterizes their interaction. In a bcc Fe lattice, the total binding energy between n objects, i.e., vacancies, self-interstitial atoms, Fe or solute atoms, is the energy difference between the configuration where all the objects interact and the configuration where all the objects are far enough from one another to not interact anymore. Due to the limited supercell size, the total binding energy is calculated as follows:

$$E_{D_1,D_2,\dots,D_n}^{binding} = \sum E_{D_i} - (E_{D_1-D_2-\dots-D_n} + (n-1)E_{perfect\ lattice}) \tag{12}$$

With $E_{D_1,D_2,\dots,D_n}^{binding}$ the binding energy between all the objects, $D_1, D_2, \dots, D_n$ the objects number 1, 2, …, n, E_{D_i} the energy of the simulation box containing the object i and $E_{D_1-D_2-\dots-D_n}$ the energy of the simulation box containing all the objects.

For example, the binding energy between a C atom and a dislocation loop is defined as the difference between the energy of the simulation box with the loop and the C atom interacting and the energy of the simulation box with the loop and the C atom not interacting (i.e. far from each other):

$$E_{C-loop}^{binding} = E_C + E_{loop} - (E_{C-loop} + E_{perfect\ lattice}) \tag{13}$$

Where E_C is the energy of the simulation box containing 1 C atom, E_{loop} is the energy of the box containing an dislocation loop, E_{C-loop} is the energy of the simulation box containing both the loop and the C atom interacting and $E_{perfect\ lattice}$ is the energy of the simulation box with no defect.

With our definition, a positive value of the binding energy corresponds to an attraction between the defects. On the contrary, a negative binding energy indicates repulsion between the defects. More

practically, for the C-loop example, the higher the binding energy, the higher the attraction between the loop and the C atom, the more stable the configuration.

4. Going from an energy minimum to another

Cohesive models provide the total energy of a system of particles and the methods described above can be used to find stable states of the system of particles. To investigate how the system of particles can evolve from one stable or meta stable state to another, different methods can be applied. These algorithms will often search for the so-called "minimum energy path" (MEP) connecting two different potential energy minima and going through a saddle point.

A. Drag method

Among all the transition path searching methods, the drag method is the simplest and the easiest. It requires the knowledge of two local energy minima that constitutes the initial and the final point of the drag method. It consists of fixing one and only one degree of freedom, named the drag coordinate, while the other ones are relaxed (Henkelman et al., 2002). The drag coordinate is then incremented from its initial value to its final value, i.e. from the initial local minimum to the adjacent local minimum. The minimum energy path emerges as the iterative process goes on. More pragmatically, for the study of the C atom diffusion in bcc Fe, the drag method consists in moving the C atom from an O site (the local energy minimum for a C atom in bcc Fe) to another adjacent O site in a straight line (the reaction coordinate) by little steps. At each step, the system is relaxed with a restriction on the C atom, as it can relax only perpendicularly to the reaction coordinate. The C atom will thus climb the potential energy landscape to the saddle point and fall back to the adjacent local energy minimum. The major downfall of this method is that it fails as the system becomes more complicated. In fact, the drag method is efficient only for transitions involving a minimum energy path close to the linear interpolation. On Figure 11, the example of a MEP with the drag method is provided. At first, the C atom (in green) within an O site (blue circle) is pushed towards an adjacent O site (Figure 11 a). Then the system is relaxed (especially the Fe atoms in red), but the C atom is forbidden to move along the direction of the push (represented by the dotted line in Figure 11 b). The process is repeated until the C atom arrives at a saddle point (Figure 11 d), and finally to another energy minimum (Figure 11 f).
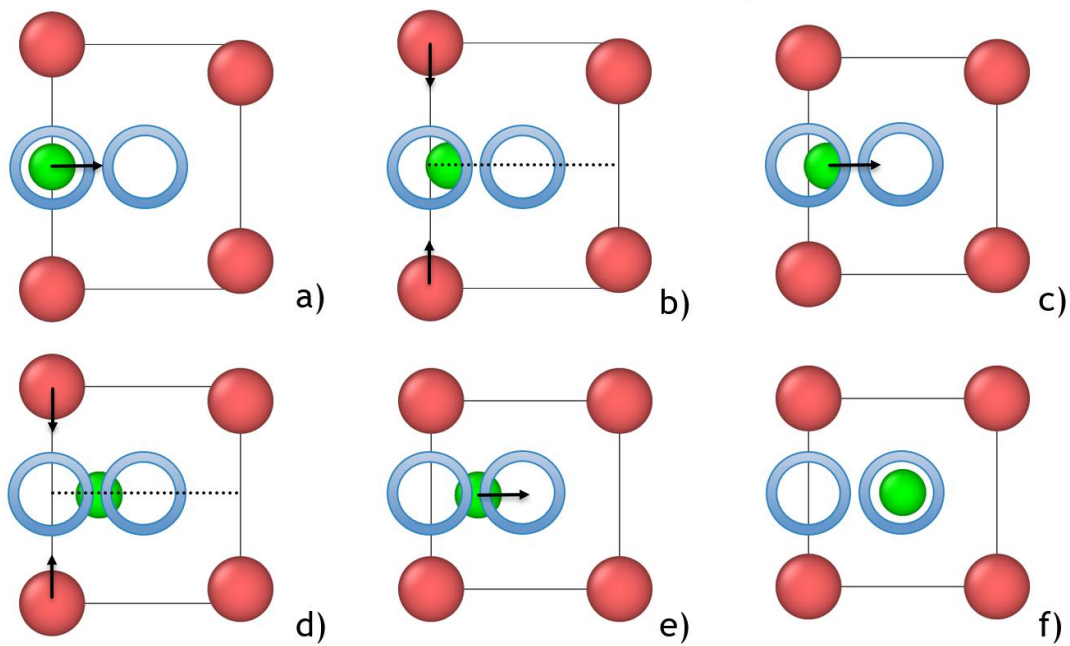
Figure 11: Example of a drag method finding the MEP for a C atom in Fe. The C atom is represented by the green atom, the Fe atoms are the red atoms. The blue circles represent the O sites, the arrows represent movement and the dotted lines represent the line along the C atom is forbidden to relax along. First, the C atom is pushed towards an adjacent O site (a) and the system is relaxed (b). The C atom is pushed again (c) and the system is relaxed again until it arrives at the saddle point (d). The C atom is now pushed (e) many steps to the adjacent O site (f).

B. Nudged Elastic Band (NEB)

Another more precise minimum energy path searching method is the Nudged-Elastic Band (NEB). This method is still the state-of-the-art method to investigate the MEP between two different energy minima, namely the initial configuration and the final configuration. The NEB is defined as a chain-of-states method meaning that different states (or images) of the system along the migration path are created by the algorithm (Jonsson et al., 1998). These images can be created at first by an interpolation between the first minimum (the initial configuration) and the second minimum (the final configuration). Once done, the images are connected by springs to create a representation of the path from the initial configuration to the final configuration, which are now the start and the end of the chain of images. Naming the initial configuration I_0 and the final configuration I_n with $n-1$ images created, it is possible to list the images: $I_0, I_1, \ldots, I_{n-1}, I_n$. All these intermediates states between I_0 and I_n are relaxed to fit the minimum energy path. Then, the chain of strings, equivalent to an elastic band, is put under tension, with I_0 and I_n fixed. With this elastic band method, two main issues arise. The first one is that the images tend to fall close to the energy minima I_0 and I_n, neglecting the area close to the saddle point, i.e. the most interesting area as it is the aim of the method. The second issue is linked to the tension applied to the springs that tends to shortcut the MEP. These two effects are represented on Figure 12 where the tension applied to the springs drifted the path from the perfect minimum energy path (in black) to a more energetic one (in light grey). The intermediate images $I_1, I_2, \ldots ; I_{n-1}$ are represented by the dots on Figure 12, and a depletion zone of images is observed for the path found (grey) compared to the MEP (black).
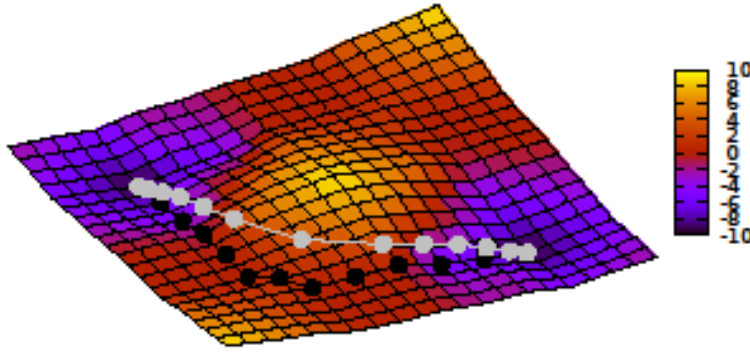
Figure 12: Perfect minimum energy path (black) and minimum energy path found by the elastic band method (light grey). The dots reprensent the intermediate images. The tension applied to the springs drifted the elastic band from the perfect minimum energy path to a more energetic one. The color code represents the energy of the system with highest energies in yellow.

These two issues are solved by a force projection, balancing the spring force and the attraction force to the local minimum energy. This step is referred as "nudging", hence the method name.

C. Activation-Relaxation Technique (ART)

Unlike the drag method and the NEB, the Activation-Relaxation Technique (ART, also called ART-nouveau) (Barkema and Mousseau, 1996)'(Malek and Mousseau, 2000)'(Mousseau and Barkema, 1998) does not need two energy minima to connect them; ART can find all the minimum energy paths as well as all the energy minima connected to a single local energy minimum. The activation-relaxation technique is a two-steps process. Firstly, ART will move the system from a local energy minimum to a local near energy saddle point (activation step). Secondly, the system is forced to relax into another energy minimum (relaxation step).

The activation is achieved by slightly moving an atom towards a random direction to get away from the local energy minima. Therefore, a non-zero term emerges in the $3N$ (N the number of atoms in the system) dimensional force $\vec{F}$ given by the interatomic potential meaning that the system wants to be driven back to the local energy minimum. The system is then forced to follow iteratively until the reaching of a saddle point a force $\vec{G}$ defined as:

$$\vec{G} = \vec{F} - (1 + \alpha)(\vec{F}.\hat{r})\hat{r} \qquad (14)$$

With α a positive number to control the speed of the algorithm (the greater α, the faster the algorithm, the more chance to miss the saddle point), $\hat{r}$ a normalized vector parallel to the displacement vector from the actual position to the local minimum $\vec{r}$. The forces $\vec{F}$ and thus $\vec{G}$ are reassessed at each step of the iterative process. The forces $\vec{F}$ and $\vec{G}$ are equal to 0 as the system reaches the saddle point, the activation is complete. Note however that if only one atom was slightly moved at the beginning of the activation step, all of the system atoms may move during the activation as only 1 component of $\vec{F}$ is

changed directly in equation 14 while the other components are minimized. A simple example of the activation is provided in Figure 13.
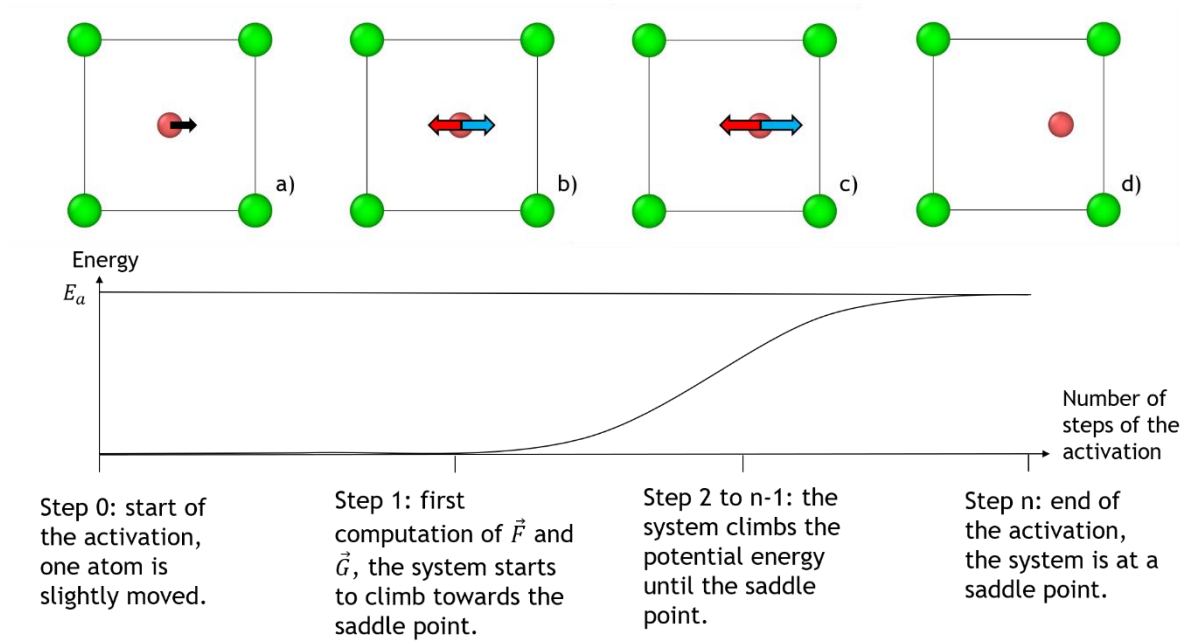
Figure 13: Activation iterative process of ART for the displacement of a C atom in an Fe matrix. The black arrow represents the push given at the atom to induce a non-zero term in the force, the red and blue arrows represents the forces F and G, for different steps of the activation: the initial state a), first step b), a step between the first and the last step c) and the last step, i.e. the reaching of a saddle point d). The total energy curve of the system is provided below, and the difference between the energy at the last step and the first step is defined as the activation energy of the transition.

The relaxation step starts from the saddle point, where the atom pushed at the activation step is pushed again towards the same direction and relaxed to a new local energy minimum thanks to a minimization algorithm. This method is especially suitable to investigate the potential energy landscape of an unknown system.

5. Making the system evolve in time: kinetic methods

Now that a starting point and a way to go from a potential energy minimum to another are known, the kinetics of a system can be investigated. Two main methods will be described, namely the Molecular Dynamics, allowing one to study the evolution in time of the whole system step by step, and the Kinetic Monte-Carlo, algorithm performing event by event steps.

A. Molecular Dynamics

Molecular dynamics (MD) is known as the standard method to study the evolution in time of a system at the atomic scale. It works by integrating the equation of motion for each particle for a small enough time step to consider the forces on the atoms constant, usually around the smallest atomic vibration duration which will result in a time step close to 10^{-15} s:

$$\sum \vec{F_i} = m\vec{a} = m\frac{d\vec{v}}{dt} = m\frac{d^2\vec{r}}{dt^2} \qquad (15)$$

Where $\sum \vec{F_i}$ is the sum of the forces applied on atom i (due to other atoms nearby), $\vec{a}$ is the acceleration, $\vec{v}$ the velocity of the atom, $\vec{r}$ its position and t the time. The forces on each atom can be spatialized along the x, y, z directions of the coordinate system using the Laplacian operator:

$$\vec{F_i} = -\vec{\nabla}E = -\left(\frac{\partial Ex}{\partial x_i} + \frac{\partial E}{\partial y_i} + \frac{\partial E}{\partial z_i}\right) \tag{16}$$

In equation 16, E is the total energy of the system, E_x, E_y, E_z are the energies of the system along the x, y, z directions and x_i, y_i, z_i are the coordinates of atom i. The forces of all the atoms of a system can be computed with an interatomic potential. The position of each atom can then be found at each step with the knowledge of the two previous steps as proposed by Verlet (Verlet, 1967):

$$r_i(t + dt) = r_i(t - dt) + 2r_i(t) + \sum \vec{F_i}\big(r_i(t)\big)dt^2 \tag{17}$$

The velocities can be computed as well:

$$v_i(t) = \frac{r(t + dt) - r(t - dt)}{2dt} \tag{18}$$

Therefore, to model the evolution in time of system with this algorithm, the knowledge of the two previous steps must be known. The algorithm was later modified to minimize the error and not depend on the two previous step (Swope et al., 1982):

$$r_i(t + dt) = r_i(t) + dtv_i(t) + \frac{dt^2 a(t)}{2} \tag{19}$$

$$v(t + dt) = v(t) + \frac{1}{2}dt\big(a(t) + a(t + dt)\big) \tag{20}$$

B. Kinetic Monte-Carlo (KMC)

a. The MC methods

Historically, the Monte-Carlo methods are named after the city, famous for the casinos present there, reflecting the stochastic character of the method. It was developed by von Neumann, Ulam and Metropolis (Metropolis and Ulam, 1949) to study the diffusion of neutrons. In these methods, the evolution of the system is seen as a Markov chain whose characteristic feature is to advance to the next step with the only knowledge of the present step (Allen and Tildesley, 1987). In other words, the algorithm needs an initial state and the probability to go from one state to another, often given under the form of a matrix named the transition matrix. The second and last necessary condition for a chain to be Markovian is that the possible transitions to advance in the chain, or to sample the different configurations the system can adopt, forms a finite set, i.e. the number of transitions can not be infinite. The sampling must be handled with care to explore the whole configuration space. The importance sampling was designed by Metropolis for that purpose (Metropolis et al., 1953). It states that the transition matrix needs be constructed to satisfy equation 21:

$$\rho\Pi = \rho \tag{21}$$

Where ρ is the limiting distribution and Π is the transition matrix of the system. The usual method to satisfy equation 21 is to respect the unnecessary strong condition of micro reversibility, also called the detailed-balance, presented in equation 22:

$$\rho_i\Pi_{ij} = \rho_j\Pi_{ji} \tag{22}$$

Where i and j are 2 separate microstates of the system, ρ_i is the limiting distribution of i and Π_{ij} is the probability to go from state i to state j. More pragmatically, the detailed-balance condition ensures that for a system at equilibrium, the probability to go from a microstate i to a microstate j is the same as the probability to go from the microstate j to the microstate i.

b. The KMC

The KMC approach is a method designed to model the evolution in time of a system (Fichtorn and Weinberg, 1991). **The motivation behind the KMC relies on the fact stated by the Transition State Theory (Eyring, 1935) that the system is most of the time in a state close to a local minimum, except when overcoming large energy barriers. Therefore, when focusing on high energy barriers events, the system can be seen as a chain of high energy events from a local minimum to another local minimum, allowing to get rid of the atomic vibration.** Contrary to MD, the time step is not fixed but a variable to be determined in the simulation according to the time residence algorithm (Bortz et al., 1975). At each step the algorithm will search or be given all the possible transitions that the system can undergo and randomly chose one; the time step is then computed and depends on all the possible transitions. Because of the proportionality between the energy of an event and the time it takes to occur, and because the atomic vibration is not taken into account thus allowing one to focus on high energy barriers, the time that can be reached by a KMC is way greater than the time reachable for MD (whose time step is set after the smallest atomic vibration). An overview of the KMC algorithm is shown and in Figure 14. This algorithm will be explained in detail for the Atomic-KMC in section "C. The Atomic Kinetic Monte-Carlo (AKMC) method".
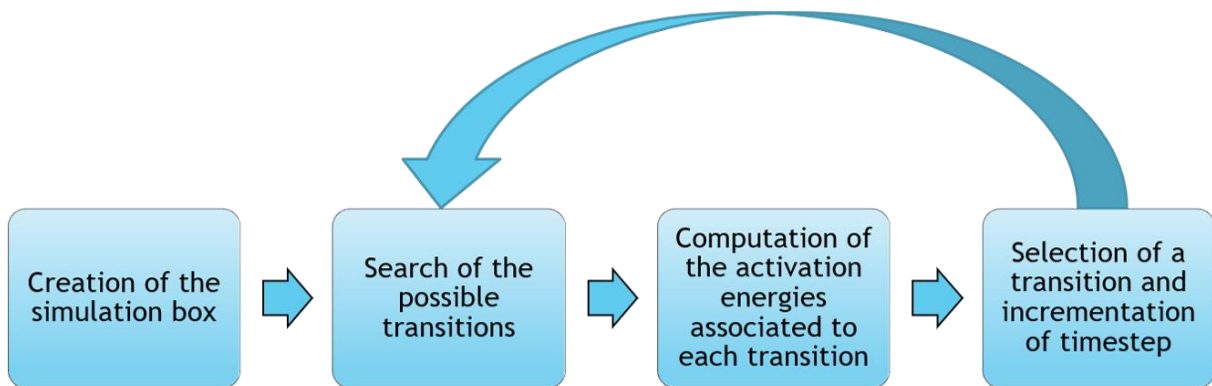
Figure 14: A typical KMC algorithm.

Several kinds of KMC exists depending on the studied system. On the next section, three different kinds of KMC are presented.

c. Different approaches of the KMC

The first and perhaps the most common KMC used is the Atomic KMC. It simply consists in applying the KMC method to an atomic system. As such, the evolution of the microstructure can be known for each atom. The Object KMC (OKMC) trades some of the precision of the Atomic KMC for computational time. It no longer treats all the atoms but some objects as well such as atom clusters. An object is treated as one unity, not as the object constituents, and is given some emission and migration properties. As such, an object can move by itself, and in the case of a cluster of atoms, will move instead of having an atom by atom migration of the cluster. This is where the computational cost is saved, but the lack of knowledge of the microstructure reduces the precision of this method. It is also important to note that the OKMC can reach the mesoscopic scale, depending on the objects defined. The Event Kinetic Monte-Carlo (EKMC) is a variant of OKMC where some of the events are directly related to the stability of the objects ; as such, the objects can be destructed or reconstructed (Dalla Torre et al., 2006).

C. The Atomic Kinetic Monte-Carlo (AKMC) method

The AKMC refers to a kind of KMC where each atom is treated independently. When applied to a system, the evolution of its microstructure can be simulated.

a. Search for transitions and computation of their associated migration energies

In an Atomic KMC, a transition is characterized by the displacement of one atom and its associated activation energy, called the migration energy. The migration or energy $E_m^{i \to j}$ of an atom to go from state i to state j is computed as the difference between the energy of the system at the saddle point of a transition $E_{saddle\ point}$ (normally the highest energy of a system for a given transition) and the energy of the system at the state i E_i (a local energy minimum):

$$E_m^{i \to j} = E_{saddle\ point} - E_i \qquad (23)$$

The energy of the state j is not considered for the calculation of the migration energy because the atom doing the transition is expected to fall to state j after reaching the saddle point. **For an AKMC to perform a step, all the transitions that the system can perform as well as their migration energies must be known.** This is the hardest task to achieve for an AKMC and therefore a very special attention needs to be put in the migration energy computation to properly investigate the kinetics of a system. Several methods have been developed for that purpose.

i. Methods using the initial and final states of a transition

These methods require the knowledge of any equilibrium microstate that the system can undergo, i.e. a Hamiltonian. The migration energy can be computed according to the Kang and Weinberg decomposition of the migration energy (Kang and Weinberg, 1989) displayed in equation 24:

$$E_m^{i \to j} = E_{m0}^{i \to j} + \frac{E_j - E_i}{2} \qquad (24)$$

Where $E_m^{i \to j}$ is the migration energy from state i to state j, $E_{m0}^{i \to j}$ is the migration energy from state i to state j without taking into account the chemical interactions (depends on the migrating atom type), E_i and E_j are the total energy of the system at state i and j, so respectively at the initial state and the final state of the transitions. This model shows his best performances when applied to the migration of point defects. Therefore, with these methods, the knowledge of the saddle point is not even required. This method can be found under the name of kinetically resolved activation (KRA) (Van der Ven et al., 2001) or Final Initial State Energy (FISE) (Vincent et al., 2008).

ii. The broken bond models

This model theorizes the activation energy E_m as the difference between the energy at the saddle point and the energy due to the interactions of the bonds broken during the transition (Soisson et al., 1996), as presented in equation 25:

$$E_m = E_i^{saddlepoint} - \sum_j \varepsilon_{i-j} - \sum_{j \neq i} \varepsilon_{PD-j} \qquad (25)$$

Where $E_i^{saddlepoint}$ is the binding energy of the atom i at the saddle point, the two sum terms represent the bonding interaction. A different form of cut bond model has been developed by Vincent & al. (Vincent et al., 2008) where the atom performing the migration does not involve broken bonds but now the replacement of bonds.

iii. Direct calculation of the migration energy

This approach is the most intuitive, the energy barrier of an event is computed as the event is discovered. The values of the activation energies can be tabulated to speed up the calculations, like in

the rigid-lattice approximation (explained in detail in section "5. d. The rigid lattice"), but other techniques allow the user to compute the barriers on-the-fly, such as ART (explained in details in section "4. C. Activation-Relaxation Technique (ART)") or the SEAKMC (Xu et al., 2011).

b. Selection and execution of a transition among all the possible ones

Once all the transitions are known, only one is selected and executed. For each possible transition from the current state i to a state j, the transition rate $T_r^{i \to j}$ is computed as such:

$$T_r^{i \to j} = \omega_0 e^{-\frac{E_m^{i \to j}}{k_B T}} \tag{26}$$

Where ω_0 is the prefactor in Hz, $E_m^{i \to j}$ is the activation energy in eV, k_B is the Boltzmann constant in eV.K^{-1} and T is the temperature in K. This quantity is directly linked to the probability of a transition to occur; the lower the activation energy of a transition, the higher the transition rate, the higher the chance for a transition to occur. Note that in the transition rate definition, k_B is a constant and the temperature T is fixed at the beginning of a simulation. Therefore, the only quantities that impact the transition rate are the activation energy of this transition and the prefactor on a lower scale. The prefactor can be either fixed or changed for each transition according to the Meyer-Neldel law (Meyer and Neldel, 1937).

The sum of the transition rates at the nth KMC step is noted Ω_n. Once it is obtained, a transition can be selected using the method proposed initially proposed by Young et al. (Young and Elcock, 1966), then by Bortz & al. (Bortz et al., 1975) and explained below. A random number r_Ω between 0 and Ω_n is then selected to determine which transition will be performed. For a step containing n_{T_r} possible transitions, the algorithm will compare r_Ω to the first transition rate of the system T_{r_1}. If T_{r_1} is greater than r_Ω, the transition 1 is selected. If T_{r_1} is lower than r_Ω, the algorithm will compare r_Ω to the second transition rate of the system T_{r_2}. If T_{r_2} is greater than r_Ω, the transition 2 is selected... and so on until n_{T_r} or if a transition is chosen before. The system is now changed according to the previously selected transition.

c. Computation of the time step and update of the total simulated time

Once the sum of the transition rates Ω_n is known, the time step τ_n can be computed as such:

$$\tau_n = -\frac{1}{\Omega_n} \tag{27}$$

The time step thus does not depend only on the chosen transition, but on all the transitions that the system can undergo at step n. Quite logically, numerous possible transitions for a step result in a lower time step than a step with few transitions (assuming the energy of the transitions are close).

d. The rigid lattice approximation

In the simplest cases, the atoms can be put on a rigid grid derived from the real lattice of the system making the transition searches and the migration energy computations very fast. A simple example of this assumption, called the "rigid-lattice approximation", is displayed for a Fe-C system in Figure 15.
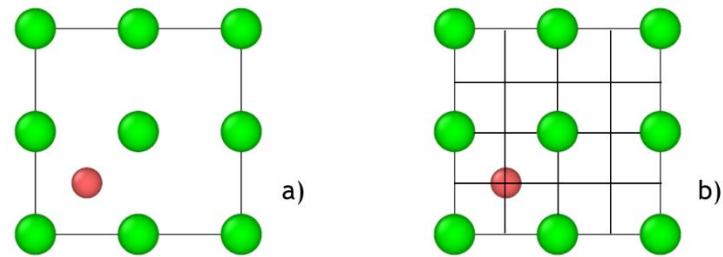
Figure 15: Example of the "rigid-lattice approximation". At first the system is read a), then all the atoms are placed on the nodes of a rigid lattice b). The green atoms represent Fe atoms, and the red atom represents the C atom.

Putting the atoms on a rigid grid allows one to find the possible transitions very fast. For example, on the α-Fe-C system, it is known that a C atom can jump from an O site to an adjacent O site. Placing the Fe atoms on a rigid grid also means that the positions of all O sites will be fixed. Therefore, the O sites positions can be easily found and computed to know the possible transitions of each C atom. This rigid-lattice approximation is valid when studying low distorted systems such as the diffusion of carbon in Fe bulk. Unfortunately, this approach does not produce reliable results when studying distorted systems such as the core of a dislocation.

e.   The Kinetic-Activation Relaxation Technique (K-ART)

i.   Finding the transitions

K-ART (El-Mellouhi et al., 2008) (Béland et al., 2011) is an off-lattice AKMC which means that the atoms are not forced to be placed on a rigid lattice. At each step, the possible transitions are found by ART (explained in "4. C. Activation-Relaxation Technique (ART)") (Barkema and Mousseau, 1996) (Malek and Mousseau, 2000) for all the different topologies (local maps containing only the links between the different atoms) found in a given atomic system. More practically, a topology is centered at a specific atom, and the transitions for this specific atom will be searched. An example of a topology is given in Figure 16 c).
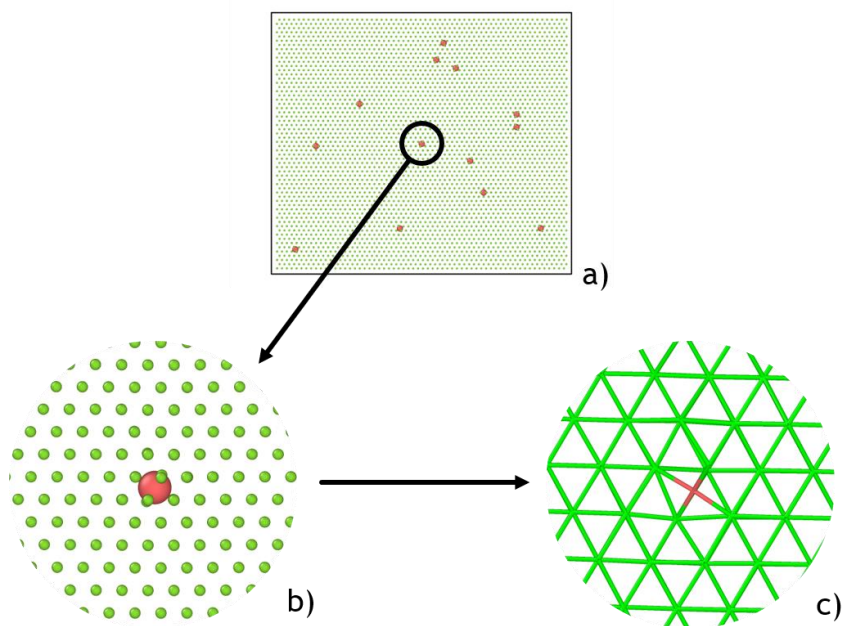
Figure 16: From the simulation box a) in this example containing Fe (green atoms) and C (red atoms), a small portion centred at an atom (here the C atom) is taken b), and the atoms are replaced by only the links between these atoms c) to become a topology.

It is assumed that for a topology, all the possible transitions will remain the same. This means that for a topology, the transitions must be computed only once and can then be stored in a catalogue to be reused each time the topology is encountered, hence the qualifier self-learning for k-ART. The topologies are managed by NAUTY (McKay, 1981). The migration energy associated to a relevant enough transition (probability of the event of at least 0.01 %) are recomputed at each step, thus allowing k-ART to fully consider the elastic deformation on the migration energy calculation. This algorithm can thus potentially fully and accurately explore a totally unknown system. Furthermore, note that k-ART is able in the same time to compute the migration energy of the inverse events found.

ii.   Important k-ART parameters

In k-ART, many features help the user to overcome common issues linked to the KMC. Probably the most useful of these features is the Basin Mean Rate Method (BMRM). In a distorted system, different order of magnitude in the migration energies of events may arise, and the KMC is driven by the lowest energy transitions, meaning that the interesting high energy transitions are likely to be missed even with a many steps simulation. These low energy transitions are called flickers. The BMRM provides an interesting way to deal with flickers: the events with a migration energy below a certain threshold defined by the user are considered to be within a basin. Therefore, the system has no longer a small energy barrier to overcome, but the basin itself with an energy barrier of a least the user-defined threshold. A way out of the basin is found and the time corresponding to this way is computed analytically allowing the KMC to perform a more energetic step than the flicker and increasing the time step as well. The BMRM can be set or not in the k-ART input file, as well as the energy of a transition to be considered in a basin.

To predict the correct kinetics of the system and have a better efficiency, several parameters must be adjusted in k-ART. As such, the topology cut-off, which corresponds to the radius of the topologies, is therefore set to a value superior to the potential cut-off. In this manuscript, the topology cut-off was set to 6 Å for all the simulations, meaning that the transitions for a specific atom will be searched on a sphere containing all the atoms closer than 6 Å to this specific atom. Another important parameter to

adjust is the number of searches per topology. This parameter is specific to the system, for example setting the number of searches on a topology to 20 ensures k-ART to find the 4 possible transitions of a C atom in the bcc Fe bulk. However, for more distorted systems, some transitions may be harder to find, and the number of searches per topology must be higher.

Another important feature is the possibility to use local forces to search for the possible transitions of the system. Indeed, as the events in k-ART are intrinsically local (due to the topology cutoff), it is not necessary to compute the forces between the atoms in the topologies and all the other atoms. More practically, only a certain number of atoms around the topologies is necessary to find the possible transitions of the system. In k-ART, it is therefore possible to stipulate in the k-ART input file that the forces on the atoms in a topology are computed taking into account only the atoms surrounding the topologies. For that purpose, the k-ART user has to define two different parameters, namely the number of cubic cells surrounding the topologies, and their lengths. The use of local forces is a necessity to allow k-ART to study large system, i.e. systems containing more than 10 000 atoms.

It is also important to note that specific conditions can be added for each system. For this purpose, some code must be written in a file named "additional_conditions.f90", allowing to change the outcome of the simulations, such as forbidding a group of atoms to move.

iii.   Summary of k-ART

Theoretically, k-ART is suitable for any atomic system given in input. However, for large systems (> 10 000 atoms), the CPU time needed to perform transitions is too high to have great simulated times. Moreover, larger systems generally imply more possible transitions and so a diminution in the KMC step. The only downfall about k-ART is its computational cost. This is the reason why we propose in this Ph.D. to create a program using combination of a rigid and a soft lattice, respectively for quasi-crystalline and distorted regions of the studied system: the mixed-lattice KMC.

6. Boundary conditions

In a simulation, the supercell is finite and thus restricts the possibility of atoms to diffuse. Therefore, the boundary conditions, i.e. the approximation at the limits of the simulation box, must be defined. The most used approximation is called the Periodic Boundary Conditions (PBC), which means that the simulation box is periodic, thus allowing atoms to interact across the boundaries. Moreover, a particle exiting the side of the simulation box is assumed to enter the box at the other side. Under the PBC approximation, the system is fictitiously infinite and the number of atoms in the simulation box stays the same. Other conditions at the boundaries can be also defined. For example, the free surfaces forbid atoms to cross the limits of the simulation box. Furthermore, with this approximation, the boundaries are not periodic, meaning that the atoms do not interact across the boundaries. Note that different approximations can be used on a same simulation. Indeed, it is possible to set different boundary conditions for the three different directions of the simulation box: the system can be periodic in a direction and not in other directions.

7. Programs used in this work

The codes used throughout this work are DYMOKA (Becquart et al., 1997) and LAMMPS (Plimpton) for the molecular statics and dynamics simulations. DYMOKA has already been used in iron, e.g. for the study of a screw dislocation motion (Domain and Monnet, 2005) and was used in this work both for relaxation and MD simulations of a SIA loop in iron interacting with C atoms. As for LAMMPS, perhaps the most known MD open-source code, it was also used to study Iron, especially a C Cottrell atmosphere formation (Veiga et al., 2015). In the code we have developed, LAMMPS was used in combination with k-ART as well as for relaxation purposes (dislocations in bcc iron).

The DFT calculations were done using the Projector Augmented Wave (PAW) method through the code VASP (Kresse and Hafner, 1993)'(Kresse and Hafner, 1994a)'(Kresse and Hafner, 1994b)'(Kresse and Joubert, 1999) and were performed in this work on the same simulation boxes as the one launched with DYMOKA to provide a comparison for the DYMOKA relaxed configurations: supercells of 1458 Fe atoms ($9 \times 9 \times 9$ bcc, unit cell containing 2 Fe atoms with a lattice parameter of 2.831 Å) were constructed with Gamma point representation because of the supercell size. The cut-off of the plane wave energies was set at 300 eV. The relaxation of all atoms was done with the constant volume condition. A perfect $\frac{1}{2}a_0 \langle 111 \rangle$ SIA loop is introduced in the centre of the supercell. The pressure induced by the addition of this loop (and due to the constant volume condition) was taken into account with the method introduced by Varvenne (Varvenne et al., 2013). The point defect energies are computed and then corrected by subtracting the energy due to the periodic images of the loop. The Generalized Gradient Approximation (GGA) was used with the Perdew and Wang parametrization (Perdew et al., 1992). The improved Vosko-Wilk-Nursair (VWN) interpolation has been used for the spin interpolation of the correlation potential.

The soft-lattice KMC k-ART has been used with success in the Fe-C system (Restrepo et al., 2016) and was used for that reason in this work. It is also what we will refer to as "the precise part" of the mixed-lattice Kinetic Monte-Carlo.

Atomsk (Hirel, 2015) was used to construct the simulation boxes in combination with Babel (Clouet, 2007) to provide the anisotropic elasticity calculations.

> **To simulate the evolution in time of a system using an AKMC, several ingredients are needed. Firstly, a cohesive model needs to be defined that can determine the energy of the system. Secondly, one needs to find ways to minimize the energy of the system, i.e. to find its closest local potential energy minimum. Thirdly, it is necessary to find paths between the different energy minima (the MEP) which will constitute the possible transitions that the AKMC can perform. These transitions can be easily found when the atoms are put on a rigid grid (the rigid lattice approximation). However, this approximation fails for distorted systems, as the rigid grid does not reproduce the real geometry of the system. Therefore, it may be necessary to find these transitions on-the-fly by using an AKMC such as k-ART. We propose to implement in k-ART the possibility to use the rigid-lattice approximation in the bulk (zone very-low distorted) and restrain the use of k-ART to the distorted zones.**

Chapter III. Results: the Mixed-Lattice Kinetic Monte-Carlo

In this chapter, we present the Mixed-Lattice KMC (MLKMC) program we have developed. The mixed-lattice KMC is a combination of different lattices within the same KMC simulation. As such, different parts of a simulation box are treated by different methods, either with a rigid lattice or a soft lattice (i.e. k-ART). Choosing wisely the zones of the different lattices can speed up the KMC a lot without biasing the kinetics, as the time needed to perform a step on a rigid lattice is a lot lower than the time needed to perform a step on the soft lattice. More precisely, the rigid lattice should be used when the rigid lattice approximation and the soft lattice returns the same results, otherwise the soft-lattice should be used.

1. Justification of the mixed-lattice KMC

Two k-ART simulations, each containing a 19 SIA loop and 1 C atom in a bcc Fe matrix, were launched with their only difference situated in the bulk size (to study the influence of the matrix size on the CPU time). The first simulation is a $9 \times 9 \times 9$ box (1478 atoms), the other one is a $30 \times 30 \times 30$ box (54020 atoms). The CPU time versus the number of steps is plotted on Figure 17.
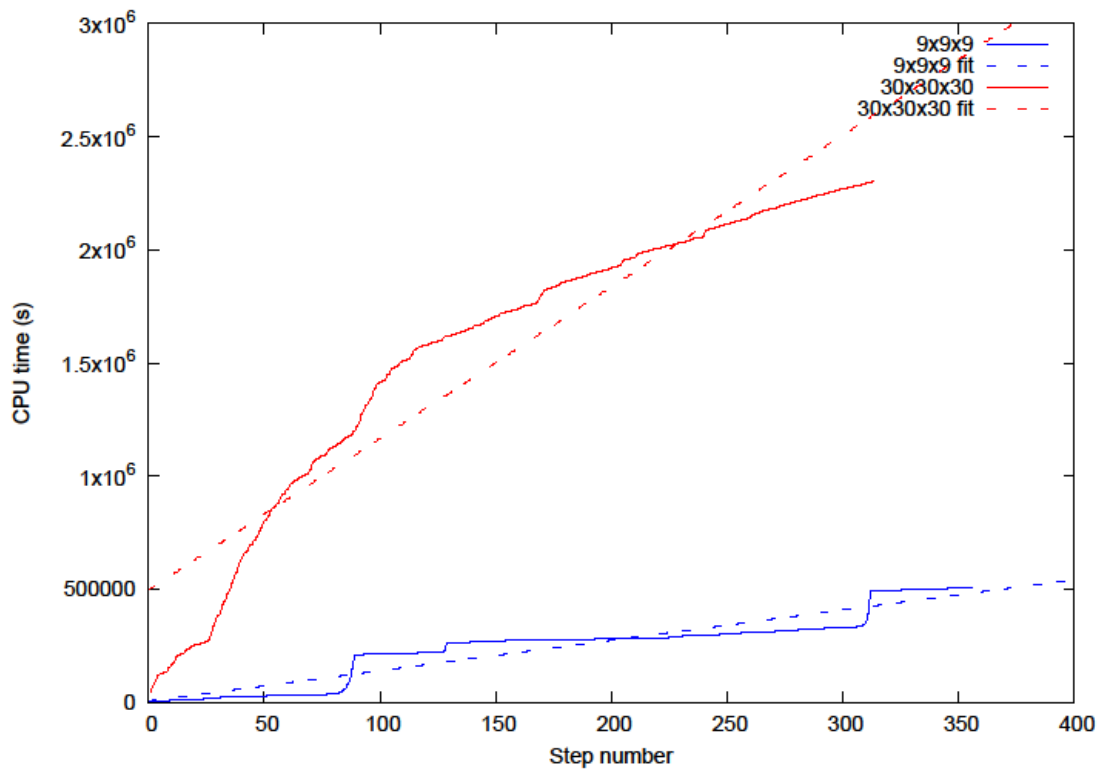
Figure 17: CPU time versus the number of steps for two sizes of box, i.e. a 9×9×9 (blue line) and a 30×30×30 (red line). The dotted lines are linear fits of the function. The first 6 steps of the simulation are not represented in this plot not to bias the fit because the first steps are longer to perform than the last ones because the system is unknown.

The slope of the fit is the average time needed for a step to be performed by k-ART. For a $30 \times 30 \times 30$ box, the average step is done in 4000 s of CPU time whereas for a $9 \times 9 \times 9$ box, the average time

needed for a step to be performed is 1200 s of CPU time. Therefore, even if the time for k-ART to perform a jump is especially linked to the number of transitions of the system, there is still an influence of the matrix size. Furthermore, even without taking into account the matrix size, k-ART needs some time to perform a step, approximatively 100 s for the $9 \times 9 \times 9$ box containing a SIA dislocation loop. On the other hand, the on-lattice KMC is known for its speed, with more than 1000 steps per second depending on the system (Veiga, 2011).

The mixed-lattice KMC is thus a necessity to study large systems and reduce the size of the zone managed by k-ART. In our case, the aim is to reduce the k-ART zone to a dislocation or a dislocation loop and use a rigid lattice far from the dislocation or the DL. More precisely, as seen on Figure 18**, the possible transitions for the zone within the circle (the k-ART zone) will be found by k-ART while the transitions outside the circle (the rigid-lattice zone) will be found using the rigid-lattice approximation**. On Figure 18, a screw dislocation in the centre of the box in bcc Fe (red atoms) is decorated by a Cottrell atmosphere of C atoms (blue atoms). The circle delimiting the off-lattice zone has its centre coinciding with the screw dislocation core. The radius of the circle is chosen to be as small as possible without impacting the kinetics of the system (the method developed to determine this k-ART zone size is presented in the subsection "4. B. Determination of the k-ART zone").
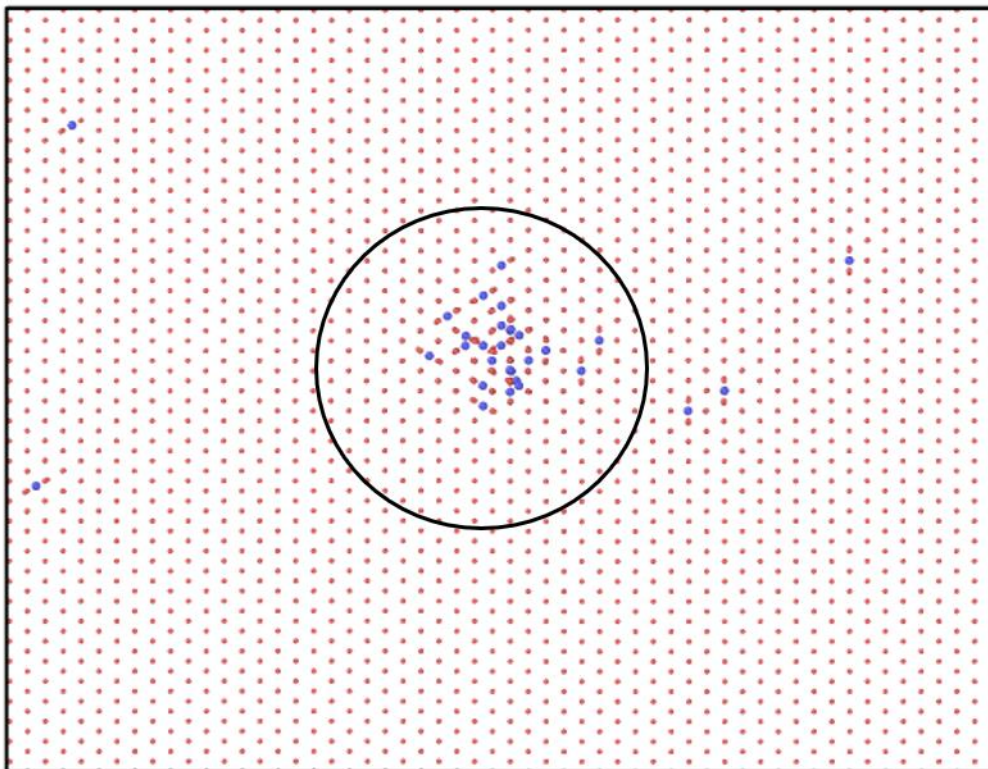
Figure 18: Mixed-Lattice KMC simulation of a screw dislocation in bcc Fe (red atoms) decorated by a Cottrell atmosphere of C atoms (blue atoms). The zone within the circle is handled by k-ART and the rest of the box is a rigid-lattice KMC.

2. Code language

At first, the mixed-lattice KMC was a mix between DYMOKA for the on-lattice part and k-ART for the off-lattice zone. DYMOKA is mainly a F77 code with few C subroutines, k-ART is a F90 code. K-ART calls the C++ code LAMMPS for the force calculations. With this combination, the KMCs are operative and the calls of the different codes needs to be done. For an optimum portability, DYMOKA and k-ART

codes must remain unchanged. Furthermore, a new main had to be created and was created in C (this choice was guided by the two main languages which DYMOKA and k-ART are written in, i.e. either FORTRAN or C) thus imposing the constraints of a mixed-language compilation (C, C++, F77 and F90). The compilation, especially the linkage, was a very harsh task to accomplish. Therefore, this approach was abandoned and it was decided to add some new code, written in F90 language, directly in k-ART, putting aside the DYMOKA part. In this approach, the compilation is an easy task to complete, and the code can furthermore be distributed at will (DYMOKA is an E.D.F. code and distribution problems would have arisen).

3. Overview of the algorithm

The algorithm of the program can be summarized as the sum of two different KMCs just communicating the possible transitions on two different parts of the same simulation box. Moreover, some interactions may occur between atoms in the k-ART zone and atoms in the rigid-lattice zone. Therefore, a special attention is required for the interaction between the two different KMCs. An overview of the functioning of the Mixed-Lattice KMC based on the previously shown algorithm of the KMC (in section "Chapter II. Methods 5. B. b. The KMC") is provided in Figure 19.
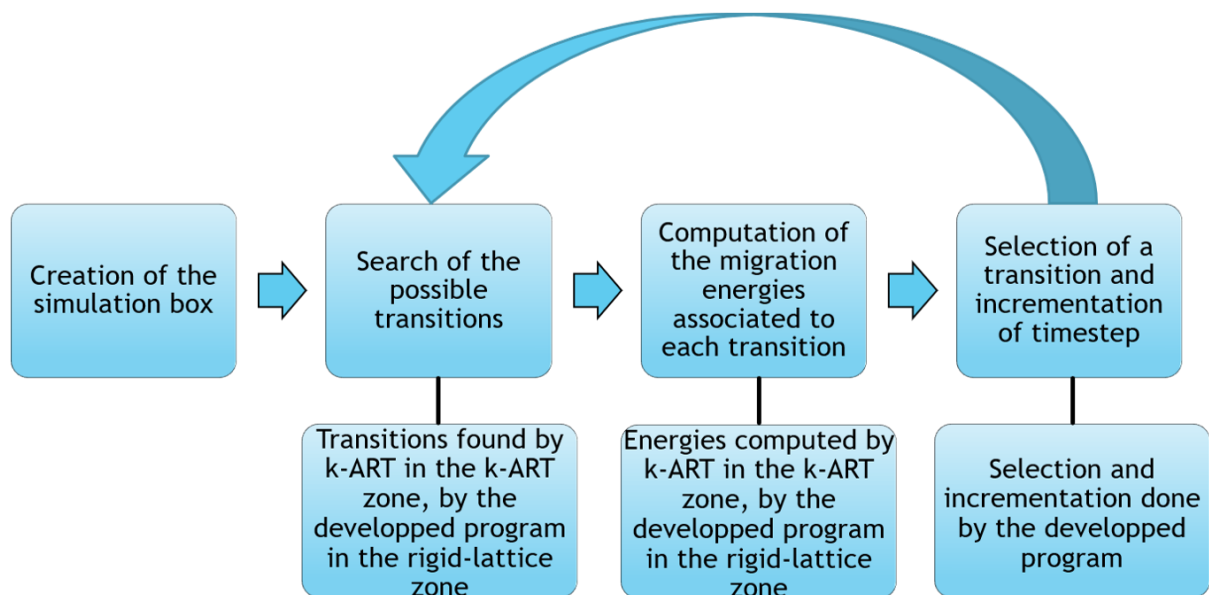
Figure 19: Overview algorithm of the mixed-lattice KMC.

Each of the presented steps will be detailed in the following subsections, as well as a focus on the interface between the two k-ART zone and the on-lattice zone (and therefore between the two programs).

4. Construction of the simulation box

A. Introduction of the defects in the simulation box

Before launching a simulation, the simulation box must be created. Considering a dislocation or a dislocation loop and interstitials as the only defects, the creation of the simulation box can be seen as a succession of different steps:

1) Creation of the bulk in the desired orientation. This is usually done by creating a unit cell oriented as wanted by the user and multiplied along the X, Y and Z directions;

2) Introduction of the defects. The dislocation(s) or the dislocation loop(s) should be put first, and the system can be relaxed. After that, the interstitials can be put within the simulation box, and the whole box is relaxed once again.

These two steps are enough to perform a k-ART simulation. However, for the MLKMC simulations, another step between the step 1 and the step 2 must be added. A list of O sites and T sites linking to adjacent O and T sites must be constructed before the introduction of carbon within the system. More practically, the possible transitions (provided by the list of O and T sites) on the rigid-lattice zone must be computed before the start of the simulation.

B. Determination of the k-ART zone

Once the simulation box is prepared, another important step is to determine the size of the k-ART zone. **Indeed, for the simulation to accurately predict the kinetics of the system, it is of primary importance that a continuity in the migration energies exists for an atom going from a zone to another.** More practically, it means that if the rigid-lattice approximation is used for an atom at a particular place in the simulation box, the migration energies predicted within the rigid-lattice approximation must be the same as the one predicted by k-ART otherwise this means that the rigid-lattice computations are false. Furthermore, a more prudent approach would be to take a large k-ART zone to ensure good kinetics of the system. However, this would lead to a significant increase in the computational cost of the simulation as this computational cost directly relies on the size of the k-ART zone. **Therefore, the size of the k-ART zone must be chosen to be as small as possible without impacting the kinetics of the system.**

A preliminary study is thus needed to find the optimal size of the k-ART zone. For that purpose, the example of C diffusion in a bcc Fe matrix containing a screw dislocation is presented. The screw dislocation is well known to induce a long-range strain field on bcc Fe. Therefore, the migration energies of the C atoms in the rigid-lattice zone are computed within the anisotropic elasticity theory. More details about the computation of the migration energies with the anisotropic elasticity theory are presented in section "5. c. Taking into account the distortion of the system induced by defects such as dislocations".

Veiga & al. observed a large difference in the C-dislocation binding energies predicted by atomistic calculations and by anisotropic elasticity theory calculations (more than 100 meV) for C-screw dislocation distances up to 1 nm, but almost no differences for distances greater than 1 nm (Veiga et al., 2011). As the elastic contribution to the migration energy of a C atom directly relies on the C-dislocation binding energy, this means that the k-ART zone must cover this discrepancy zone to ensure a continuity between the migration energy given by the anisotropic elasticity theory and the ones given by k-ART.
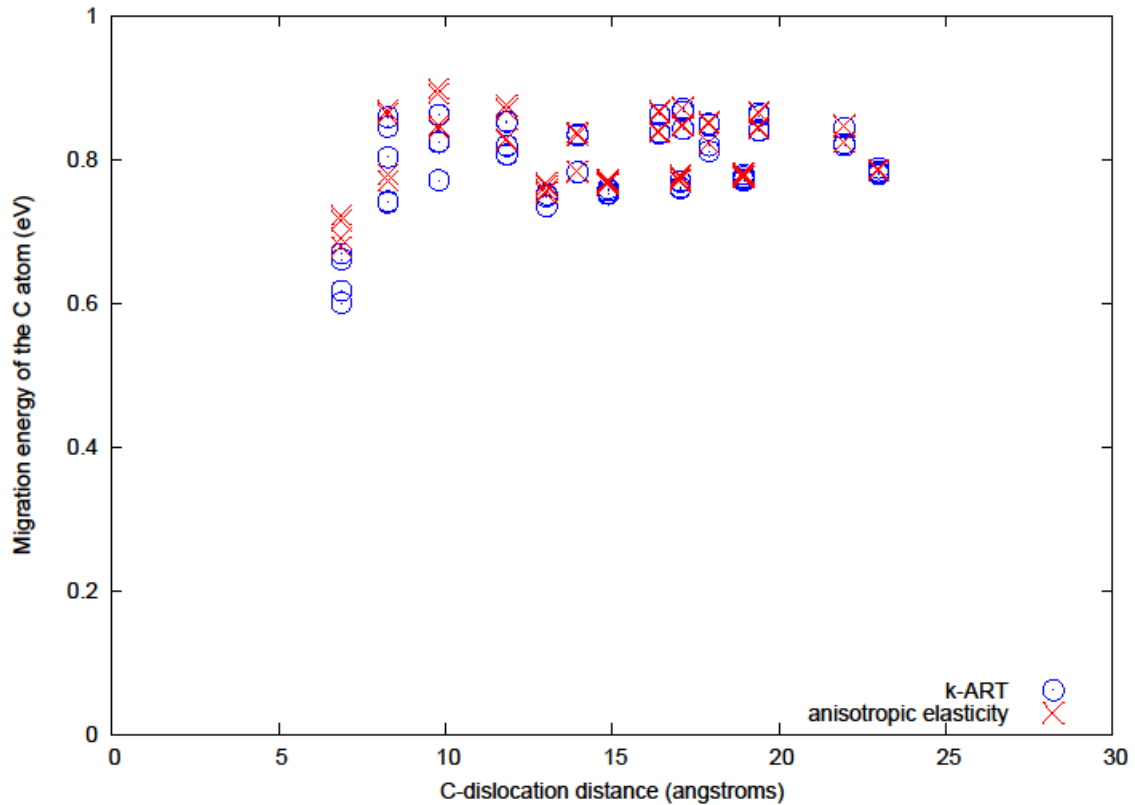
Figure 20: Migration energy of the C atom versus the C-screw dislocation distance predicted by k-ART (blue circles) and anisotropic elasticity (red crosses).

A lot of issues arise from the interface between the k-ART zone and the rigid-lattice zone. Figure 20 shows the C migration energy for different C-screw dislocation distances predicted by both anisotropic elasticity (red crosses) and k-ART (blue circles). One can observe that for C-dislocation distances greater than 1.2 nm, both methods return results with a difference smaller than 10 meV. On the contrary, for C-dislocation distances up to 1.2 nm, the differences in the predicted migration energies by the different methods indicates the limits of the anisotropic elasticity theory and thus the necessity for atomistic computations. As such, for this system, the size of the k-ART zone must be at least of 2.4 nm, centred on the dislocation line. Furthermore, as the C atom gets close to the dislocation, other C migration patterns than the usual 4 C jumps in the Fe bulk can be found (such as small C oscillations around its equilibrium position), thus reinforcing the need of k-ART. This preliminary study is a necessity for the kinetics not to be biased and needs to be performed for each system launched (without taking the C atoms into account, the k-ART size box is valid for a given type of dislocation in the same material).

Note however that the k-ART zone is chosen as a rectangular parallelepiped and not a cylinder. In fact, several issues may arise from the use of a cylinder-shaped k-ART zone, such as the difficulty to define proper boundaries to the k-ART zone and interfaces problems. Indeed, a C atom crossing the interface could be seen simultaneously in the k-ART zone and in the rigid-lattice zone (or neither in these zones), as k-ART relaxes the C position when a C arrives in the k-ART zone. With a rectangular k-ART zone, just looking at the system to precisely define the boundaries of the k-ART zone allows one to get rid of this issue.

5. <u>Search of the possible transitions and computation of the migration energies</u>

The beginning of each KMC step is to find the possible transitions that all the atoms can perform at this step as well as their migration energies. In the MLKMC approach, the transitions are either found by k-ART if the concerned atom is within the k-ART zone, or by the developed program if the concerned atom is within the rigid-lattice zone.

A. <u>K-ART zone</u>

In k-ART, the migration energies are computed with the search of events, as each saddle point is "discovered" during the search of events. The method is explained in section "Chapter II. Methods 4. C. Activation-Relaxation Technique (ART)". Note however that if the events have a probability of more than 0.01 % to happen, their migration energy is recomputed to take into account all the elastic interactions of the current configuration.

B. <u>Rigid-lattice zone</u>

Remembering that C can only jump from an O site to an adjacent O site, knowing the positions of each of the O sites within the simulated system allows one to easily find the transitions of the C atoms in the rigid-lattice zone. **Therefore, the transitions are computed only once before the simulation starts. In other terms, to each O site is associated each four adjacent O sites representing the four possible transitions for a C atom in the bulk. Note however than another method was developed to find the transitions on-the-fly on the rigid-lattice zone, but is less reliable than finding the transitions before the simulation starts (presented in "Annexes 1. On-the fly computation of the migration energies in the rigid-lattice zone").** A list containing the positions of each O sites is constructed. To each O site is associated each adjacent O site and T sites, allowing the MLKMC program to retrieve the positions of the four possible transitions for each C atom just by knowing the O sites the C atoms are within.

On the rigid-lattice zone, the migration energies of these transitions are computed as:

$$E_m = E_m^0 + \Delta E_{C-C} + \Delta E_{elastic} \tag{28}$$

Where E_m is the migration energy of a particular migrating event (i.e. a C jump), E_m^0 is the migration energy of a C atom in a perfect bcc Fe lattice (predicted by our potential to be 0.815 eV), ΔE_{C-C} is the corrective term associated with the C-C interactions, and $\Delta E_{elastic}$ is the corrective term associated with the distortion of the matrix (in our case due to a dislocation). The correctives terms ΔE_{C-C} and $\Delta E_{elastic}$ will be detailed in the next sections. To take into account the C-C interactions, C-C and C-Fe distances must be found at each step (the details will be explained in subsection "a. Computing the distances between atoms"). This step can take a lot of time and therefore requires a particular attention which is why we need to address the notion of scaling of a program which refers to its capability to how the computing of the expected results change with the size of the system n.

a. *Computing the distances between atoms*

In methods such as MD or KMC where interactions between atoms must be computed, a loop on each atom within a loop on each atom is performed to compute all the atomic interactions. The scaling is thus said to be $O(n^2)$ with n referring to the system size. For the MD and KMC cases, n often refers to the number of atoms. This means that if one increases the number of atoms in the system, the increase in the computational cost will be squared (e.g. doubling the size of the system will require four times the computational effort to perform a step). Several tricks may allow to speed up the calculations, such as getting rid of spurious calculations. For instance, the fact that the interaction between the atoms i

and j is the exact same whether it is computed as i interacting with j or computed as j interacting with i means that half of the computational cost can be saved. Indeed, the fact the interactions between the different atoms are computed in a loop on each atom within a loop on each atom means that these interactions are computed twice. However, even if the computational time is halved with this trick, the time gain is not sufficient enough when comparing to the scaling of the program, especially for usual MD box sizes of few tens of thousands up to few millions atom. The two most widely used method to get rid of this $O(n^2)$ scaling (and thus having only a $O(n)$ scaling) are the link cells method and the list of neighbours.

i.   The link cells method

The link cells method, also known as the cell-linked list method or cell index method, consists in dividing the whole system into small cells, which are small parts of the system containing few atoms. Like this, when searching for neighbours atoms to a particular atom, instead of searching through the whole system, only the neighbouring cells to the cell containing this particular atom will be searched (Allen and Tildesley, 1987).

For this method to work, the cells must be constructed to cover entirely the interaction zone. More precisely, for a system of $X \times Y \times Z$ Å, and the cut-off of the cohesive model (often a potential) equal to $C_{potential}$ Å, the cells can be constructed as such:

-   Determination of the number of cells along each direction as well as their size. For instance, the number of cells along the X direction is equal to: $N_X = integer\ part\left(\frac{X}{C_{potential}}\right)$. With this definition, $L_X = \frac{X}{N_X}$, the length of each cell along the X direction, is assured to be at least equal to $C_{potential}$. The same logic applies for the other directions. Therefore, the size of the cell being greater but close to the potential cut-off, searching only the 27 neighbouring cells instead of the whole system is sufficient enough to ensure that the interactions will be accurately computed.
-   Association of atoms to each cell. Now that each cell is created, a variable containing the cell IDs and the atoms present in this cell is created. To find which atom belongs to which cell, one simply has to perform this operation: $X_i = \frac{x_i}{X} * N_x$ where X_i is the nth cell number along the X direction where the atom i is in, and x_i is the coordinate of the atom i along the X direction. Once again, the same logic applies for the other directions.

A 2D example of a box divided in cells in presented on Figure 21. However, the extrapolation to a 3D system is straightforward and presenting a 3D system is not necessary to understand the principle. On Figure 21, each cell is filled with its ID, i.e. the number of the box along the X direction and the number of the box along Y direction: $(X_i; Y_i)$. For a system of $X \times Y = 11 \times 10$ Å and the cut-off of the potential $C_{potential} = 2$ Å, there are thus $N_X = integer\ part\left(\frac{11}{2}\right) = 5$ boxes along the X direction ($N_y = 5$ as well) of lengths $L_x \times L_y = 2.2 \times 2$ Å². An atom with the coordinates $(x_i; y_i) = (6; 6)$ will be in the cell $(3; 3)$, in red on Figure 21. Therefore, when searching for nearest neighbours of this atom, only the cell containing the above-mentioned atom as well as the 8 (26 for a 3D system) surroundings cells will be searched, in yellow on Figure 21.
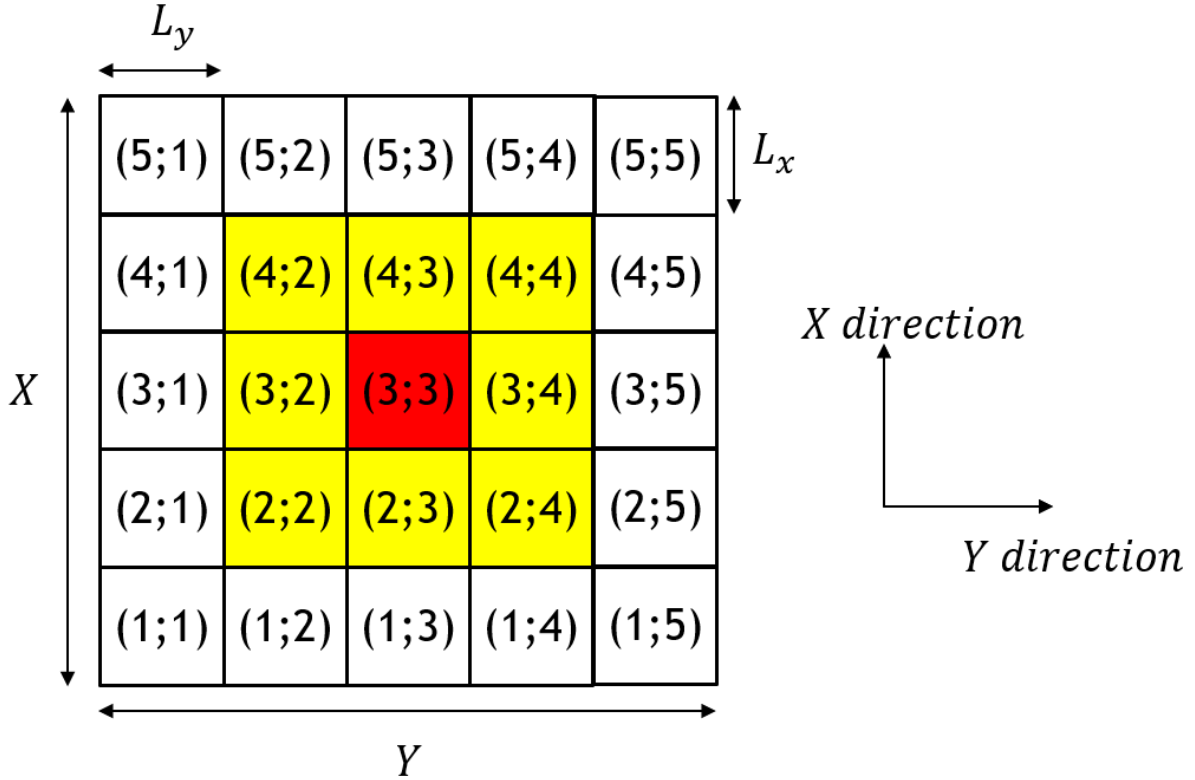
Figure 21: Example of a box divided in small cells in 2D. Each cell is filled with its ID. The red cell represents the cell containing the atom on which the nearest neighbours are searched, the yellow cells represents the cells where the nearest neighbours of the above-mentioned atom will be searched (in addition to the red cell).

With this distribution of the system, finding the nearest neighbours of an atom is a fast task (Allen and Tildesley, 1987). The main downfall of this method is the great number of spurious computations. Indeed, restricting the neighbouring search to few cells allow to get rid of a lot of spurious calculations, but the whole zone covered by each of the cells is still too great to perfectly describe an atom environment.

ii.   The list of neighbours

Keeping a list of neighbours for each atom is the other usual method to get rid of the $O(n^2)$ scaling. For that purpose, to each atom is associated a list of all the neighbouring atoms. This list is computed at the first iteration of the KMC or MD algorithm and updated each desired iteration. To construct/update this list of neighbours, the distances between atoms are computed and stored if this distance is below r_{skin}. r_{skin} is a value determined by the user and is chosen to be slightly larger than the cut-off of the potential (10 %) in order to not rebuild the list at each step.

This method is especially suitable if the atoms are not moving too much (Fomin, 2010). However, usually in KMC methods, the atoms are moving way faster than in MD, thus making the update of the list of neighbours a task made more often than in MD.

iii.   Implementation in the MLKMC algorithm

The MLKMC works with a combination of the two methods, namely a list of neighbours and the linked-cells list. Given that only C atoms are allowed to perform jumps in the on-lattice zone, the neighbour list was built only for the C atoms. However, to keep track of the Fe atoms that can impact the migration energies of the C atoms (especially for 2 C atoms at a_0 Å having a Fe between them), the

linked-cells list is used. After each step, a check is done on whether the atom who performed a jump changed cells during the jump. If so, the variable storing each atom to its cell is updated.

b. Taking into account the C-C interactions

As previously seen in equation 28, the migration energy is computed with ΔE_{C-C} being the corrective term associated to the C-C interactions. **ΔE_{C-C} was chosen to be computed according to the FISE model (seen previously in section** Chapter II. Methods **5. C.** "Search for transitions and computation of their associated migration energies"):

$$\Delta E_{C-C} = \frac{E_{after} - E_{before}}{2} \tag{29}$$

Where E_{before} is the energy of the configuration before the transition is done and E_{after} is the energy of the configuration after the transition is done. The energies E_{before} and E_{after} are computed according to the C-C distances, hence the necessity of using the cell-linked list method and the list of neighbours. The values of these energies are showed on Figure 22. Note that two different energies are found for a distance equal to $a_0 = 2.85532$ Å between the two C atoms, depending on whether a Fe atom is found between these two C atoms. The configuration where a Fe atom is between 2 C atoms at a_0 Å is more unstable than the configuration where no Fe atom is between 2 C atoms at a_0 Å, hence the higher energy for the first configuration.
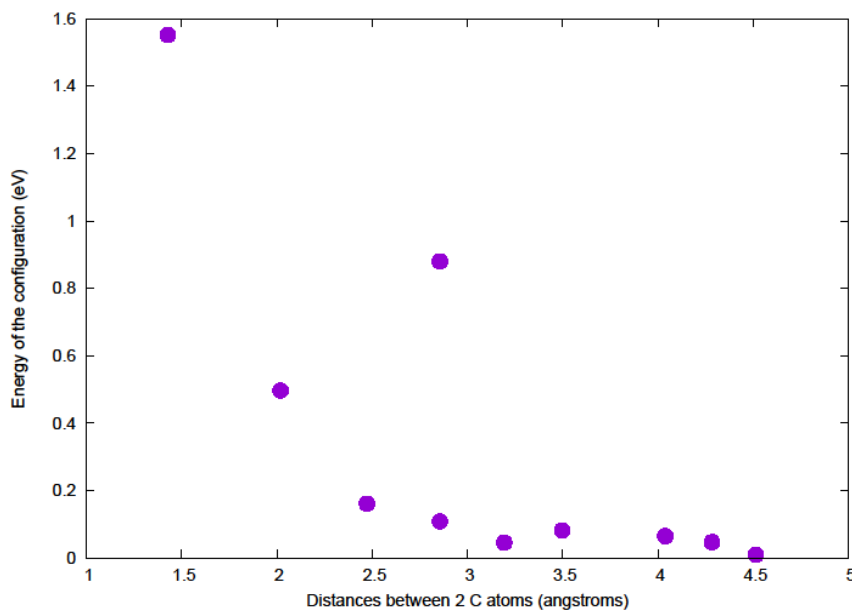
Figure 22: Energy of a C-C pair versus the distance between the C atoms. 2 different energies are found for the same distance (distance between the C atoms $d = a_0 = 2.85532$ Å) depending on whether a Fe atom is found between the C atoms.

An example on how ΔE_{C-C} is computed is presented for comprehension sake. On Figure 23, 4 different transitions are possible for the C atom on the left (state i). These transitions are shown on the configuration on the right (possible states j). Note that the distances between the C atoms are not represented, the number of CNN is. However, the number of CNN can be easily linked to the distance between the C atoms: 2 C atoms 4th NN are for example separated by a_0 Å. One of the possible

transitions in Figure 23 leads to a configuration where the 2 C atoms are separated by precisely a_0 Å with a Fe atom between these 2 C atoms (labelled as 4NN 2). For this transition, ΔE_{C-C} will be computed as such:

$$\Delta E_{C-C} = \frac{E_{after} - E_{before}}{2} = \frac{0.880 - 0.0457}{2} = 0.4172 \; eV$$

This leads to a migration energy to go from the initial state i to the possible state j where the 2 C atoms are in the configuration 4NN 2:

$$E_m^{5NN \rightarrow 4NN2} = E_m^0 + \Delta E_{C-C} = 0.8145 + 0.4172 = 1.2317 \; eV$$

State i   Possible states j
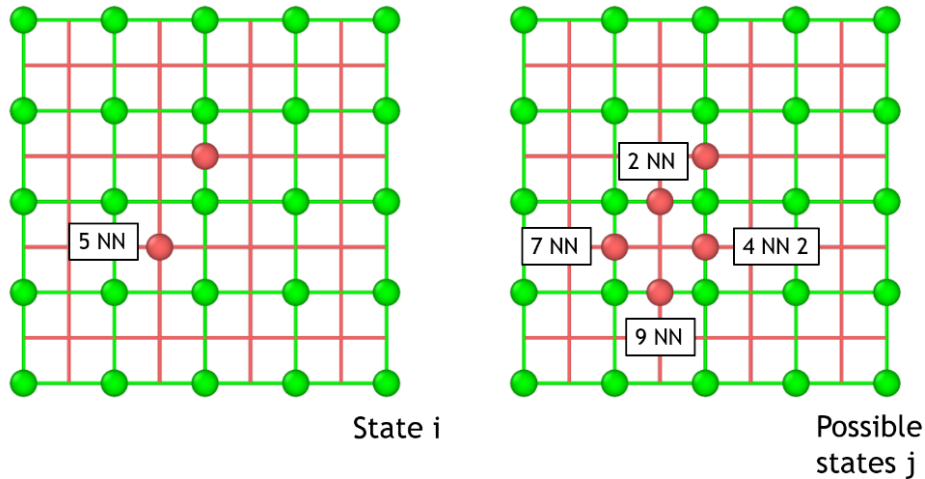
Figure 23: Example of the four possible transitions possible for the C atom on the left, i.e. the four possible states j from the state i. The green atoms represent Fe, the red atoms represent C.

Note that our model considers the C-C interactions up to the 9th NN (distance between the C atoms of 4.51 Å), because the impact of 2 C atoms 9th NN on each other is close to 0 (Figure 22). Therefore, 2 C atoms at greater distances are expected to have less impact and are thus not relevant. The maximum distance between C atoms to consider that they have an impact on each other is seen on Figure 24.
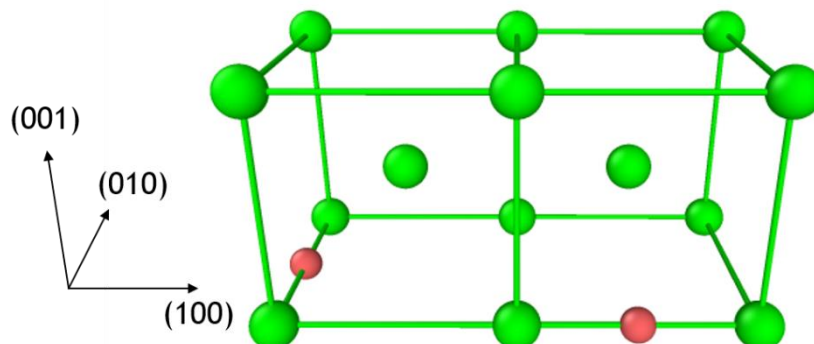
Figure 24: Representation of two C atoms 9 NN (red atoms) in a bcc Fe lattice (green atoms).

c.   Taking into account the distortion of the system induced by defects such as dislocations

Defects introduce deformations or distortions of the matrix which can be more or less large and localised depending on the defect and its size. These deformations will have an impact on the migration energies of moving species (Becquart et al., 2007) (Tchitchekova et al., 2014) (Liu et al., 2011) (Li et al., 2011) and in particular the distortion zone induced by dislocations has a non-negligible impact on the interstitial migration energies. The strain field of a dislocation is known to be long-ranged and influences the C migration in bcc Fe. **Concerning the MLKMC simulation, this means that it may be necessary to take into account the dislocation induced distortion of the system on the migration energies in the rigid-lattice zone.** The migration energies in the rigid-lattice zone are computed with equation 28, with $\Delta E_{elastic}$ the term reflecting the dislocation impact on the C migration energies. As the migration energy of the C atom is also equal to the difference of the C atom in the T site with the C atom in the O site, the $\Delta E_{elastic}$ term is dependent only on the C position on the T and the O sites (Veiga et al., 2011):

$$\Delta E_{elastic} = E_{C_O-dislocation}^{binding} - E_{C_T-dislocation}^{binding} \qquad (30)$$

Where $E_{C_O-dislocation}^{binding}$ represents the binding energy between the dislocation and a C atom in a O site and $E_{C_T-dislocation}^{binding}$ represents the binding energy between the dislocation and a C atom in a T site. These two terms are crucial values that can be computed with the help of anisotropic elasticity theory. The advantage of computing the binding energies between a C atom and a dislocation with the anisotropic elasticity rather than with atomistic calculations (as seen on equation 12) is the speed of the method. Indeed, while atomistic calculations can be difficult (especially for a C atom in a T site) and long, the anisotropic elasticity calculations are almost instantaneous. The first step of computing $E_{C_O-dislocation}^{binding}$ and $E_{C_T-dislocation}^{binding}$ is to determine the strain field of the dislocation.

i.   Determining the strain field of the dislocation

Within the elasticity theory, the system is seen as a continuum (Veiga et al., 2011). It is assumed that for small distortions, the stresses are proportional to the deformation (as stated by Hooke's law) (Hirth and Lothe, 1992). Mathematically, this statement can be translated in equation 31:

$$\sigma_{ij} = c_{ijkl}\epsilon_{kl} \qquad (31)$$

With σ_{ij} the stress, c_{ijkl} the elastic constants (intrinsic properties of a material) and ϵ_{kl} the strain.

Because $\sigma_{ij} = \sigma_{ji}$ and $\epsilon_{kl} = \epsilon_{lk}$, the following relation can be expressed:

$$c_{ijkl} = c_{jikl} = c_{ijlk} = c_{jilk} = c_{klij} \qquad (32)$$

Equation 31 can be rewritten with a matrix notation (Hirth and Lothe, 1992):

$$\{\sigma_{ij}\} = \{c_{ijkl}\}\{\epsilon_{kl}\} \qquad (33)$$

Because of the relation $c_{ijkl} = c_{klij}$, the $\{c_{ijkl}\}$ matrix is diagonally symmetrical. For a more convenient understanding, the pair of indices $n = ij$ and $m = kl$ are often rewritten:

$ij\ or\ kl$	11	22	33	23	31	12	32	13	21
$m\ or\ n$	1	2	3	4	5	6	7	8	9

Table 1: equivalence between the pair of indices $n = ij$ and $m = kl$

For example, c_{1123} can be reduced to c_{14} with this notation. By combining this notation with equation 32, the equation 31 can be even more reduced:

$$\begin{bmatrix}\sigma_{11}\\\sigma_{22}\\\sigma_{33}\\\sigma_{23}\\\sigma_{31}\\\sigma_{12}\\\sigma_{32}\\\sigma_{13}\\\sigma_{21}\end{bmatrix} = \begin{bmatrix}c_{11}&c_{12}&c_{13}&c_{14}&c_{15}&c_{16}&c_{14}&c_{15}&c_{16}\\c_{12}&c_{22}&c_{23}&c_{24}&c_{25}&c_{26}&c_{24}&c_{25}&c_{26}\\c_{13}&c_{23}&c_{33}&c_{34}&c_{35}&c_{36}&c_{34}&c_{35}&c_{36}\\c_{14}&c_{24}&c_{34}&c_{44}&c_{45}&c_{46}&c_{44}&c_{45}&c_{46}\\c_{15}&c_{25}&c_{35}&c_{45}&c_{55}&c_{56}&c_{45}&c_{55}&c_{56}\\c_{16}&c_{26}&c_{36}&c_{46}&c_{56}&c_{66}&c_{46}&c_{56}&c_{66}\\c_{14}&c_{24}&c_{34}&c_{44}&c_{45}&c_{46}&c_{44}&c_{45}&c_{46}\\c_{15}&c_{25}&c_{35}&c_{45}&c_{55}&c_{56}&c_{45}&c_{55}&c_{56}\\c_{16}&c_{26}&c_{36}&c_{46}&c_{56}&c_{66}&c_{46}&c_{56}&c_{66}\end{bmatrix}\begin{bmatrix}\epsilon_{11}\\\epsilon_{22}\\\epsilon_{33}\\\epsilon_{23}\\\epsilon_{31}\\\epsilon_{12}\\\epsilon_{32}\\\epsilon_{13}\\\epsilon_{21}\end{bmatrix}$$

Due to the symmetry, the matrices can be further reduced:

$$\begin{bmatrix}\sigma_{11}\\\sigma_{22}\\\sigma_{33}\\\sigma_{23}\\\sigma_{31}\\\sigma_{12}\end{bmatrix} = \begin{bmatrix}c_{11}&c_{12}&c_{13}&c_{14}&c_{15}&c_{16}\\c_{12}&c_{22}&c_{23}&c_{24}&c_{25}&c_{26}\\c_{13}&c_{23}&c_{33}&c_{34}&c_{35}&c_{36}\\c_{14}&c_{24}&c_{34}&c_{44}&c_{45}&c_{46}\\c_{15}&c_{25}&c_{35}&c_{45}&c_{55}&c_{56}\\c_{16}&c_{26}&c_{36}&c_{46}&c_{56}&c_{66}\end{bmatrix}\begin{bmatrix}\epsilon_{11}\\\epsilon_{22}\\\epsilon_{33}\\\gamma_{23}\\\gamma_{31}\\\gamma_{12}\end{bmatrix}$$

With $\gamma_{ij} = 2\,\epsilon_{ij}\,(i \neq j)$. Furthermore, if the studied crystal is cubic, because of the symmetry of the crystal, if the axes are mingles with the crystal axes, only three c_{mn} constants are enough to characterize the matrix (Hirth and Lothe, 1992):

$$c_{mn} = \begin{bmatrix}c_{11}&c_{12}&c_{12}&0&0&0\\c_{12}&c_{11}&c_{12}&0&0&0\\c_{12}&c_{12}&c_{11}&0&0&0\\0&0&0&c_{44}&0&0\\0&0&0&0&c_{44}&0\\0&0&0&0&0&c_{44}\end{bmatrix}$$

The three variables c_{11}, c_{12} and c_{44} are named elastic constants of the material and expresses the deformation induced by a stress in a special crystal. These variables can be computed using DFT calculations, and once computed, allow to retrieve the strain field of a dislocation ϵ_{ij}^{disloc}.

ii. Computing the C binding energies with the dislocation

The C atom is seen as a source of stress that can be defined by its elastic dipole P_{ij} (Veiga et al., 2011). The stress induced by a C atom spreads within the simulation box with respect to the inverse of the volume:

$$\sigma_{ij} = -\frac{1}{V}P_{ij} \tag{34}$$

For the simulation box's axes mingled with the crystal cubic lattice (i.e. [100],[010] and [001] axes for the simulation box), the C atom elastic dipoles P_{ij} can be easily found with a constant volume relaxation of a perfect crystal with a C atom in a O site or a T site. The elastic dipoles are found to be of the form:

$$P_{ij} = \begin{bmatrix}P_{xx}&0&0\\0&P_{yy}&0\\0&0&P_{zz}\end{bmatrix} \tag{35}$$

In the bcc Fe-C system, the C can be found in 3 different O sites types, whether the 2 Fe 1 NN of the C atom are along the [100], the [010] or the [001] axis. For a C atom in the [100] variant, the terms P_{yy} and P_{zz} are equals. The same logic applies to C atoms in the [010] variant and the [001] variant. Note however that these facts are true only if the axes of the simulation supercell match the cubic lattice. If

not, the elastic dipole as well as the stress field must be changed accordingly. The predicted values by our potential (Veiga et al., 2014) of the variables are found to be (Veiga et al., 2011):

	P_{xx}	$P_{yy} = P_{zz}$
O site [100] variant	8.03 eV	3.40 eV
T site [100] variant	4.87 eV	6.66 eV

Table 2: values of the elastic dipole terms for a C atom in a [100] O site variant and a C atom in a [100] T site variant.

The binding energy between a point defect and a dislocation is obtained by (Bacon et al., 1980):

$$E_{elasticity}^{binding} = P_{ij}\epsilon_{ij}^{disloc} \tag{36}$$

With ϵ_{ij}^{disloc} the dislocation induced strain field. The P_{ij} value can be taken for the C atom in a O site or a T site, leading respectively to the binding energy of a C atom in a O site with the dislocation and the binding energy of a C atom in a T site with the dislocation ($E_{C_O-dislocation}^{binding}$ and $E_{C_T-dislocation}^{binding}$).

Roberto Veiga (Veiga, 2011) showed that the agreement between elasticity and MS calculations is better for octahedral sites than for tetrahedral sites or more precisely the agreement between MS calculations and anisotropic elasticity holds closer to the dislocation line for octahedral sites than for tetrahedral sites as shown in Figure 25. We will take advantage of this in the study of the screw dislocation, in section "Chapter V. Results: the screw dislocation E. The 25 C – screw dislocation system".
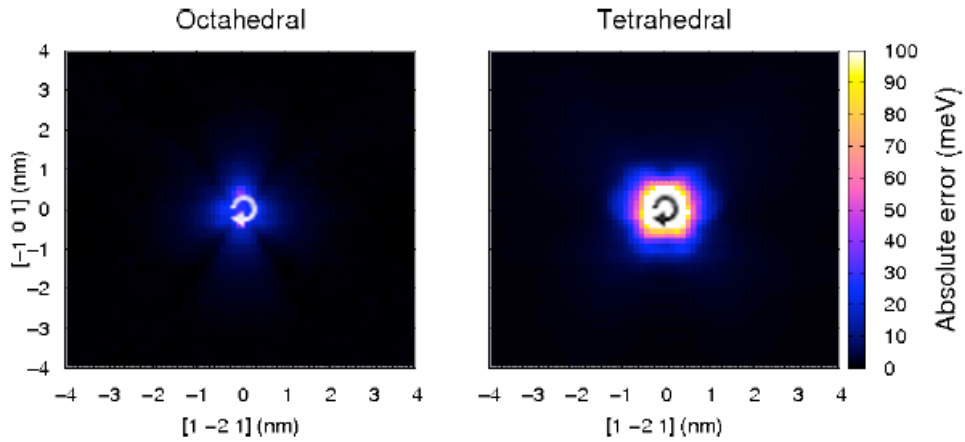
Figure 25: Mapping of absolute differences (errors) between the binding energies obtained by atomic simulations (MS) and anisotropic elasticity calculations as a function of carbon position around a screw dislocation (Veiga, 2011).

iii.   Taking into account the orientation of the system

The elastic dipole P_{ij} as well as the elastic constants c_{ijkl} (also called the Voigt matrix) have to be changed if the orientation of the system differs from ([100];[010];[001]). For example, the screw dislocation in bcc Fe has its line in a {111} plane. Therefore, it is much more convenient to orient the simulation box with a set of axes comprising the (111) directions, for example ([121];[-101];[1-11]). To perform such modifications, firstly the transition matrix T_{ij} between the basis R_{ini} ([100];[010];[001])

and the desired basis R_{fin}. Written in matrix notation, the basis R_{ini} becomes $e_i^{R_{ini}} = \begin{pmatrix} 1 & 0 & 0 \\ 0 & 1 & 0 \\ 0 & 0 & 1 \end{pmatrix}$.
The following relation allows to find the transition matrix T_{ij} associated to the change of basis:

$$e_i^{R_{ini}} = T_{ij}e_j^{R_{fin}} \tag{37}$$

Where $e_j^{R_{fin}}$ represents the basis R_{fin} in matrix notation. More practically, if one wants to change the orientation from R_{ini} ([100];[010];[001]) to R_{fin} ([121];[-101];[1-11]), the transition matrix associated with this rotation can be found:

$$e_1^{R_{fin}} = \frac{e_1^{R_{ini}} + 2e_2^{R_{ini}} + e_3^{R_{ini}}}{\sqrt{6}}$$

$$e_2^{R_{fin}} = \frac{-e_1^{R_{ini}} + e_3^{R_{ini}}}{\sqrt{2}}$$

$$e_3^{R_{fin}} = \frac{e_1^{R_{ini}} - e_2^{R_{ini}} + e_3^{R_{ini}}}{\sqrt{3}}$$

$$T_{ij} = \begin{pmatrix} \dfrac{1}{\sqrt{6}} & \dfrac{2}{\sqrt{6}} & \dfrac{1}{\sqrt{6}} \\ -\dfrac{1}{\sqrt{2}} & 0 & \dfrac{1}{\sqrt{2}} \\ \dfrac{1}{\sqrt{3}} & -\dfrac{1}{\sqrt{3}} & \dfrac{1}{\sqrt{3}} \end{pmatrix}$$

Note that the newly found vectors have to be normalized to match the length of the vectors in the R_{ini} basis, hence the denominators. The transition matrix T_{ij} is known, and allows to find the values of $e_j^{R_{fin}}$, $P_{ij}^{R_{fin}}$ and $c_{ijkl}^{R_{fin}}$ in the final basis R_{fin} with the following relations:

$$e_j^{R_{fin}} = {}^tT_{ij}e_i^{R_{ini}} \tag{38}$$

$$P_{ij}^{R_{fin}} = T_{ik}T_{jl}P_{kl}^{R_{ini}} = \sum_k \sum_l T_{ik}T_{jl}P_{kl}^{R_{ini}} \tag{39}$$

6. Selection of a transition and incrementing of time step

The selection of a transition and the incrementing of the time step is slightly different in the MLKMC than in standard KMCs. For standard KMCs, as previously said in section "Chapter II. Methods 5. C. b. Selection and execution of a transition among all the possible ones", a transition is selected among all the possible transitions than the system can perform. However, for the MLKMC, the transitions are found using two different methods depending on the atom performing the transition. Therefore, before selecting a transition, the program must take into account the transitions in the k-ART zone as well as the transitions in the rigid-lattice zone. For that purpose, a random number r_{zone} between the sum of the transitions states in the k-ART ($\sum T_r^{kart}$) plus the sum of transition states in the rigid-lattice ($\sum T_r^{rigid-lattice}$) zone is chosen. If r_{zone} is lower than $\sum T_r^{rigid-lattice}$, a transition among the ones in the rigid-lattice zone will be performed. On the contrary, if r_{zone} is greater than $\sum T_r^{rigid-lattice}$, a

transition among the k-ART ones will be performed. An example is provided on Figure 26 for comprehension sake where a rigid-lattice transition is chosen.

$$r_{zone}$$

$$\sum T_r^{rigid-lattice} \qquad \sum T_r^{k-ART}$$

$$\sum T_r^{total}$$
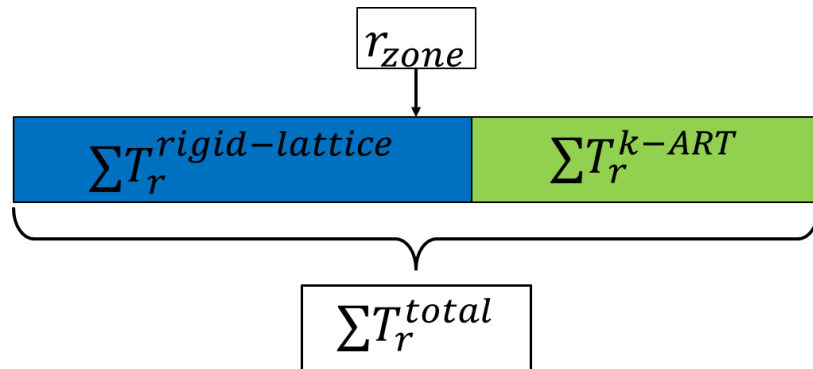
Figure 26: Selection of a program to perform the transition. The blue zone represents the sum of the transition rates obtained in the rigid-lattice zone, and the yellow zone represents the sum of the transition rates obtained in the k-ART zone. r_{zone} is lower than $\sum T_r^{rigid-lattice}$, therefore a transition among the rigid lattice ones will be performed.

Once the zone where the transition will occur is chosen, another random number will determine the transition that will be performed thanks to the method explained in "Chapter II. Methods 5. C. b. Selection and execution of a transition among all the possible ones".

The simulation time can be actualized by the addition of the time step, computed with the equation 27. Therefore, before performing a step, all the transitions in the k-ART zone and in the rigid-lattice zone must be known.

7. Interface between the soft lattice and the rigid lattice

A particular attention must be given at the interface between the k-ART zone and the on-lattice zone, especially for atoms going from a zone to the other. **Moreover, the atoms present on one side of the interface must have an effect on the atoms on the other side of the interface**, e.g. 2 C atoms at a distance of a_0, one C in the rigid lattice zone and one in the soft lattice zone, must have an impact on their respective migration energies.

Theoretically, this is a simple step to be done, as the positions of C atoms is updated after each step. **However, in the MLKMC, it was chosen to consider that the movement of C atoms in the bulk will not impact the migration energies of C atoms in the k-ART zone. Indeed, not doing this approximation would mean a recalculation of the C migration energies for the C atoms in the k-ART zone at each step, thus making the rigid-lattice approximation far less effective.**

However, if the C bulk movement do not have an impact on the k-ART zone C migration energies, C atoms in the rigid-lattice zone coming close to C atoms in the k-ART zone will have an impact on these energies. Therefore, it is necessary to take into account these C atoms coming close to the interface. An example is provided for a better comprehension: on *Figure* 27, the small blue atoms are Fe in the rigid-lattice zone, small green atoms are Fe in the k-ART zone, the dislocation is represented by the 3 columns of dark atoms (in the k-ART zone), the C atoms are the large red atoms and the circle represents the topology cut-off of the C atom in the k-ART zone (i.e. the zone on which the transitions are searched with k-ART). *Figure* 27 shows 4 steps (from a to b, from b to c, from c to d and from d to e) of a MLKMC simulation containing 2 C atoms in a bcc Fe bulk with a screw dislocation; these 4 steps being 4 consecutive rigid-lattice zone steps (only the C atom in the rigid-lattice zone moved). On the 5th configuration (*Figure* 27 e), after the 4th step, the C atom in the rigid-lattice zone entered the cut-

off of the C atom in the k-ART zone, thus having a direct impact on the transitions of the C in the k-ART zone. **The approximation made is that the 3 first steps on the example will not have any effect on the k-ART transitions. However, as the C in bulk enters to topology cut-off, the topology of the k-ART zone is reset. A topology reset is also made when a C atom in the rigid-lattice zone leaves the topology cut-off of a C atom in the k-ART zone: the C are now considered not to have an effect on each other migration. More practically, this means that it was chosen to tell k-ART that C atoms moved in the rigid-lattice zone only after a k-ART step or if a C in the rigid-lattice zone enters/leaves the topology of a C atom in the k-ART zone.** Note that the topology cut-off is chosen to be higher than the potential cut-off, usually around 6 Å.
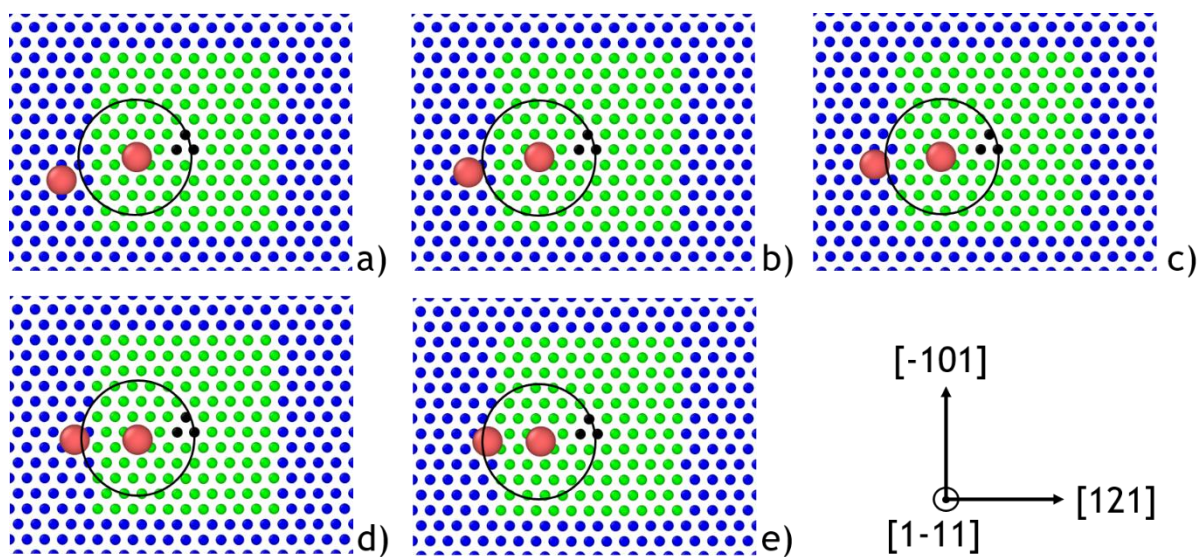
Figure 27: 5 steps (a, b, c, d and e) of a MLKMC simulation. On this simulation, the small blue atoms represent the Fe in the rigid-lattice zone, the small green atoms represent the Fe in the k-ART zone, the dark atoms represents the screw dislocation (in the centre of the k-ART zone), the large red atoms are the C atoms. The circle around the C atom situated in the k-ART zone represents the topology cut-off of the C atom, larger than the cut-off of the potential (usually around 6 Å). The C atom in the bulk does 5 successive steps until it arrives within the topology cut-off of the C atom of the k-ART zone.

A lot of issues arise from the interface between the k-ART zone and the rigid-lattice zone. One of them, linked to the use of the BMRM, is presented. Let's recall that the BMRM is the basin treatment to get rid of flickers done by k-ART and therefore a powerful tool to use. In a standard k-ART simulation, steps are followed one by one and thus the configuration is updated at each step. However, in a MLKMC simulation, k-ART is updated only after a k-ART step or if a C atom in the rigid-lattice zone enters/leaves the topology of a C atom in the k-ART zone. So, problems can arise if a C atom in the rigid-lattice zone enters a basin in the k-ART zone. Contrary to the topology cut-off allowing to know if a C atom in the rigid-lattice zone has an impact on C atoms in the k-ART zone, there is no such thing as a basin cut-off. Furthermore, the basins can change a lot during a simulation, as they can appear and disappear depending only on the configuration (and the minimum energy to be within a basin, parameter decided at the beginning of the simulation). Therefore, a C atom in the rigid-lattice zone can enter a basin previously set by k-ART. This results to an error and the end of the simulation, as k-ART has in memory a different basin than the one set by the MLKMC. **To get rid of this issue, it was chosen to deactivate the BMRM at the first step of the simulation and reactivate it only after a k-ART step. This means that the BMRM will be active only for successive k-ART jumps, thus an unnecessary step of a k-ART is made when the basin treatment is necessary.**

8. Example of a step in the MLKMC

An example of a step done by the MLKMC is provided for a better comprehension of all the aspects of the program. The system simulated is 2 C atoms in a bcc Fe bulk with a screw dislocation in the centre of the box; the step n of this system is presented on Figure 28. On this configuration, the C atoms are the large red atoms, 1 C atom is in the k-ART zone (where the Fe atoms are green), the other C atom is in the rigid-lattice zone (where the Fe are blue), and the dislocation is represented by the 3 columns of dark atoms in the k-ART zone.
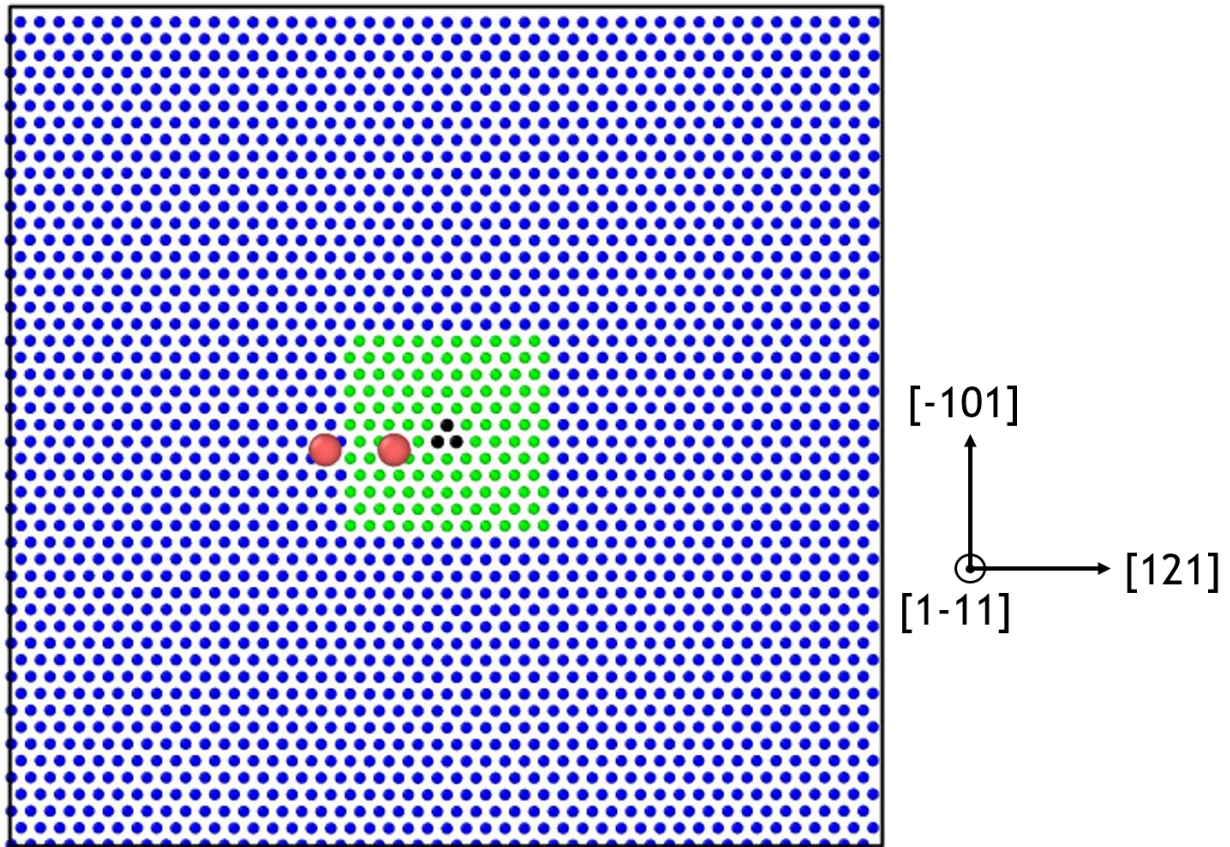
Figure 28: Simulation box containing 2 C atoms (large red atoms) in a bcc Fe matrix with a dislocation in the centre (represented by the 3 columns of dark atoms). The k-ART is delimited by the atoms in green (thus contains 1 C atom), the C atom between the blue atoms (Fe in the rigid-lattice zone) is treated with the rigid-lattice approximation.

The three steps of a KMC simulation – search of the possible transitions / Computation of the migration energies associated to each transition / Selection of a transition and incrementing of the time step – will be presented in this example.

Firstly, the transitions are searched for the 2 C atoms. Note that on Figure 28, the 2 C atoms are at a distance of 6.5 Å, meaning that they are two far to impact each other migration. On configuration seen Figure 28, 1 C is in the k-ART zone, and the other one is in the rigid-lattice zone, meaning that their transitions will be found by different programs. For the C atom in the k-ART zone, the transitions are searched by k-ART. The four possible transitions found have migration energies of respectively 0.73 eV, 0.76 eV, 0.83 eV and 0.83 eV as seen on Figure 29. For the C atom in the rigid-lattice zone, the four possible transitions have migration energies of 0.79 eV, 0.77 eV, 0.82 eV and 0.82 eV. The migration energies of the C atoms are different than the migration energy of a C atom in the perfect Fe lattice

because the influence of the dislocation was accounted. Therefore, the C migration energies of the rigid-lattice zone C was computed as such:

$$E_{mig} = E_{mig}^0 + E_{C_O-dislocation}^{binding} - E_{C_T-dislocation}^{binding}$$
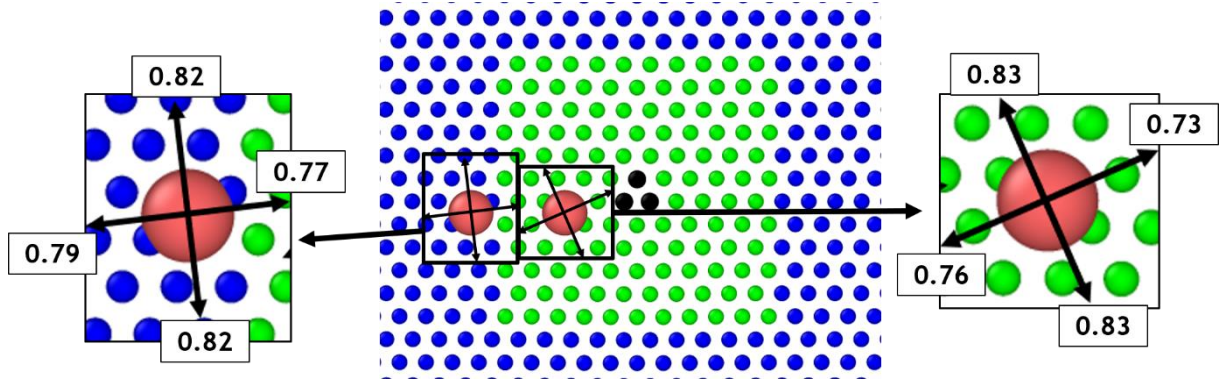
Figure 29: Zoom on the configuration presenting the migration energies of the C atoms (large red atoms) in eV within a bcc Fe matrix (blue and green atoms) containing a screw dislocation (represented by the 3 columns of dark atoms).

Now that all the transitions as well as their associated migration energies are known, one must be selected to perform a KMC step. For that, to each transition is associated a transition rate linked with the migration energy:

$$T_{r_i} = \omega_0 e^{-\left(\frac{E_{mig}^i}{k_B T}\right)}$$

With the prefactor $\omega_0 = 10^{13}$ Hz, the Boltzmann constant $k_B = 8.617.10^{-5}$ eV/K, the temperature $T = 300$ K and the migration energy associated to the transition E_{mig}. Therefore, the transitions rates associated to each energy are:

$$C(kart): T_r(0.73) = 5.446 \, ; T_r(0.76) = 1.706 \, ; \, 2 \times T_r(0.83) = 2 \times 0.114 = 0.228$$

$$C(rigid): T_r(0.77) = 1.159 \, ; T_r(0.79) = 0.535 \, ; \, 2 \times T_r(0.82) = 2 \times 0.168 = 0.336$$

Therefore, we have the sum of transitions rates:

$$\sum T_r^{kART} = 5.446 + 1.706 + 0.228 = 7.38$$

$$\sum T_r^{RL} = 1.159 + 0.535 + 0.336 = 2.03$$

$$\sum T_r^{total} = 7.38 + 2.03 = 9.41$$

A random number r_{zone} between 0 and 9.41 is generated. r_{zone} is equal to 1.07 and so is lower than $\sum T_r^{RL} = 2.03$, as seen on Figure 30. Therefore, the C atom performing the jump is within the rigid-lattice zone.
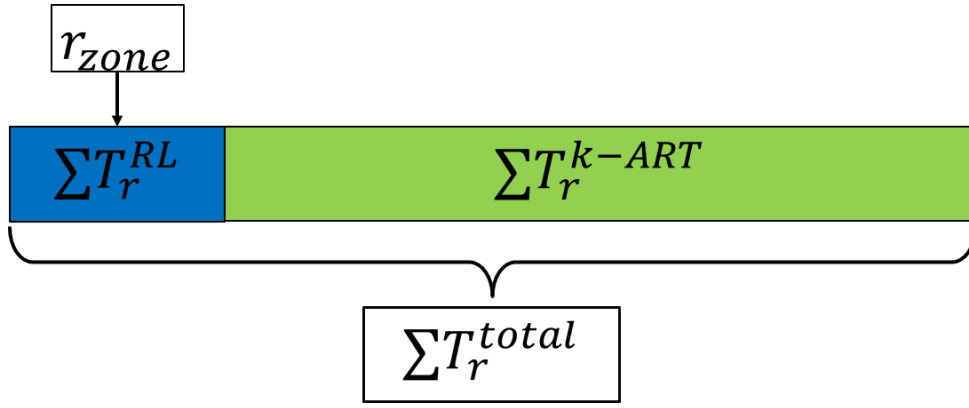
Figure 30: Selection of a program to perform the MLKMC step. r_{zone} is lower than $\sum T_r^{RL}$, therefore the C atom in the rigid-lattice zone will be chosen to perform a step.
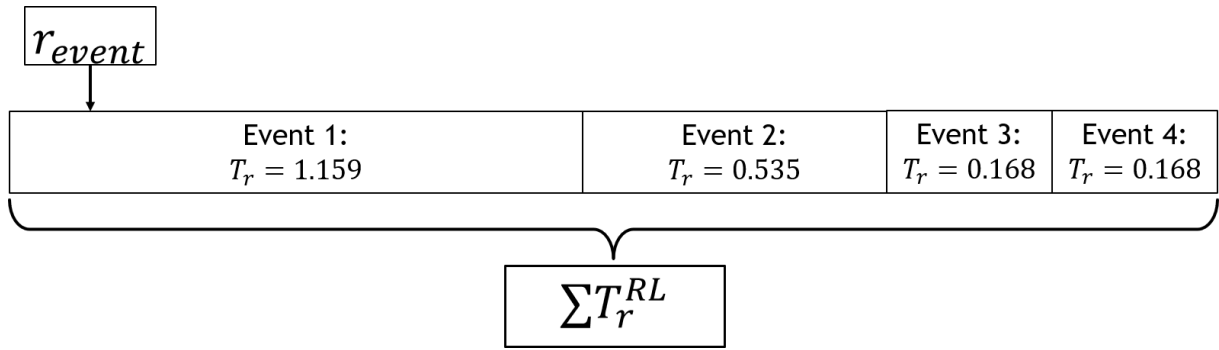
Figure 31: Selection of a transition among the rigid-lattice ones. r_{event} is lower than Tr of the event 1, therefore the event 1 is chosen and will be performed.

Another random number, $0 \leq r_{event} < \sum T_r^{RL}$, is generated to select a transition among all the transitions on the rigid-lattice zone, so on the C in the rigid-lattice zone in this example. $r_{event} = 0.31$ is generated, as seen in Figure 31. r_{event} is lower than the transition rate of the event 1, therefore the event 1 is chosen to be the transition. This transition is performed as showed on Figure 32.
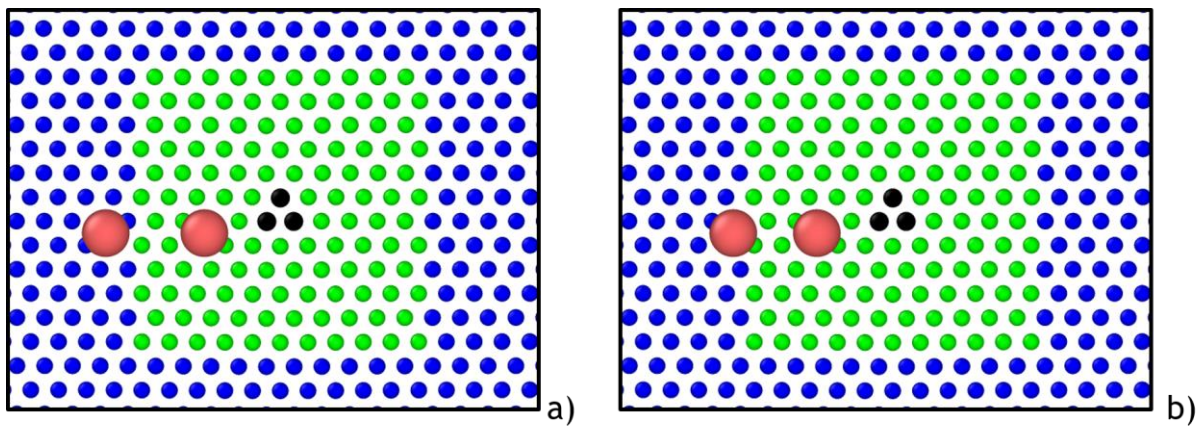
Figure 32: Configurations of the simulation before the execution of the event (a) and after the execution of the selected transition (b).

The time step $\tau = \frac{1}{\sum T_r} = \frac{1}{9.41} = 0.106$ s is added to the simulated time. Before doing another step, some verifications due to the interface between the rigid-lattice zone and the k-ART zone must be

made. As such, the distance between the C atom who moved and all the others C atom is computed, especially to determine if the movement of the C atom has an impact on this C atom and other C atoms or if the C atom changed zone during its jump. Indeed, the distance between the C atoms before the transition was 6.5 Å, and is now 5.7 Å. Therefore, the C in the rigid-lattice zone has entered the topology cut-off of the C in the k-ART zone. The topology of the C within the k-ART zone is reset to take into account the newly arrived C atom. The MLKMC is now ready to perform another step.

9. Validation of the model

The most common way to validate an interatomic potential fitted for diffusion is to plot $\log(D) = f(\frac{1}{T})$. This task is usually achieved through mean-square displacement (MSD) computations with MD simulations, allowing one to retrieve the diffusion coefficient as well as the activation energy of the diffusive atom. The potential used in this work has already passed this test with success (Becquart et al., 2007) (Veiga et al., 2014). However, the potential is not to be tested, but the method is. Therefore, if the MLKMC simulation predicts the C correct diffusion coefficient in α-Fe (and thus the correct migration energies of the C atom), the MLKMC method will be validated.

For that purpose, a total of nine 100 000 steps simulations with different parameters were launched to study their influence at $T = 300, 600, 900\ K$:

- $25 \times 25 \times 25$ Fe supercell (31250 atoms) with a single C, k-ART zone size of $4.5 \times 4.5 \times 4.5$ in the centre of the supercell, lattice parameter $a_0 = 2.85532$ for the three temperatures.
- $25 \times 25 \times 25$ Fe supercell (31250 atoms) with a C, k-ART zone size of $4.5 \times 4.5 \times 4.5$ in the centre of the supercell, lattice parameter a_0 changed according to the temperature induced lattice expansion for the three temperatures.
- $25 \times 25 \times 25$ Fe supercell (31250 atoms) with a C, k-ART zone size of $9.5 \times 9.5 \times 9.5$ in the centre of the supercell, lattice parameter $a_0 = 2.85532$ for the three temperatures.

Usually, MSD computations are done on MD simulations because the time step is constant, not on AKMC simulations. Nonetheless, as only 1 C atom will diffuse in a pure Fe matrix, the time step will be the same during the simulation. Free surfaces were applied during this work, as PBC could result in long jumps, harder to treat. When a C reaches the boundaries of the supercell, it is simply not allowed to perform the jump that crosses the boundary. This approximation is expected to have very poor effect on the kinetics as the C atom will spend most of its time within the supercell, not at its boundaries.

Figure 33 put on display the $\log(D) = f(\frac{1}{T})$ curve obtained for this dataset. The linear fit is close to perfect, thus ensuring the good reliability of the method. Furthermore, the slope of the linear fit ($a = -9472.6$) is directly related to the migration energy of the C atom:

$$E_a = k_B \times a \qquad (40)$$

Equation 40 returns a migration energy of 0.8163 eV, very close to the 0.8145 eV predicted by our potential. Therefore, the method does not affect the migration energy of the C atom and is thus validated.
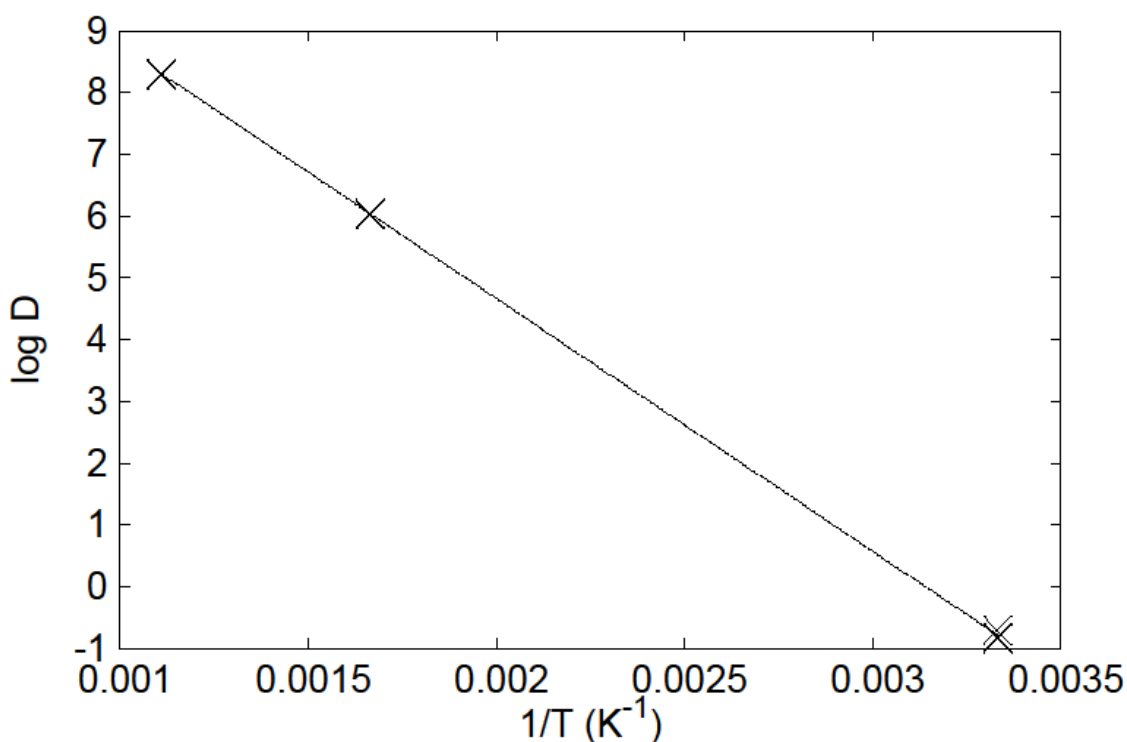
Figure 33: log(D) versus 1/T for the tested configurations (100 000 steps each). The blue crosses represent the tested configurations and the line is a linear fit operated on the data set. The straight line ensures the good reliability of the method.

10.   Efficiency

A test was launched to compare the efficiency of the mixed-lattice algorithm with k-ART. For that purpose, three simulations containing a 19 atoms SIA $\frac{1}{2}\langle 111 \rangle$ loop in a bcc Fe matrix with 11 C atoms were created: case 1, a k-ART simulation with 1479 atoms ($9 \times 9 \times 9$ bcc Fe box), case 2, a k-ART simulation with 16030 atoms ($20 \times 20 \times 20$ bcc Fe box) and case 3, a mixed-lattice simulation with 16030 atoms ($20 \times 20 \times 20$ bcc Fe box and a $9 \times 9 \times 9$ box, i.e. 1479 atoms matching the first simulation box treated by k-ART). As seen on Figure 34, the blue and the red lines, which show the evolution of the CPU time in the simulations with 1479 atoms treated with k-ART (i.e. case 1 and case 3) are almost combined, contrarily to the simulation with a 16030 k-ART box represented by the green line which takes more time to perform a step. The conclusion jumps out from Figure 34: the algorithm speed for a mixed-lattice simulation depends almost exclusively on the size of the k-ART zone, the size of the bulk is secondary. A step done by k-ART takes approximatively 100 s when all the possible transitions are known (refining of the transitions + update of the configuration) whereas a rigid-lattice KMC step takes approximatively 0.001, reducing the CPU time for a step in the rigid-lattice zone by at least a factor 100 000.
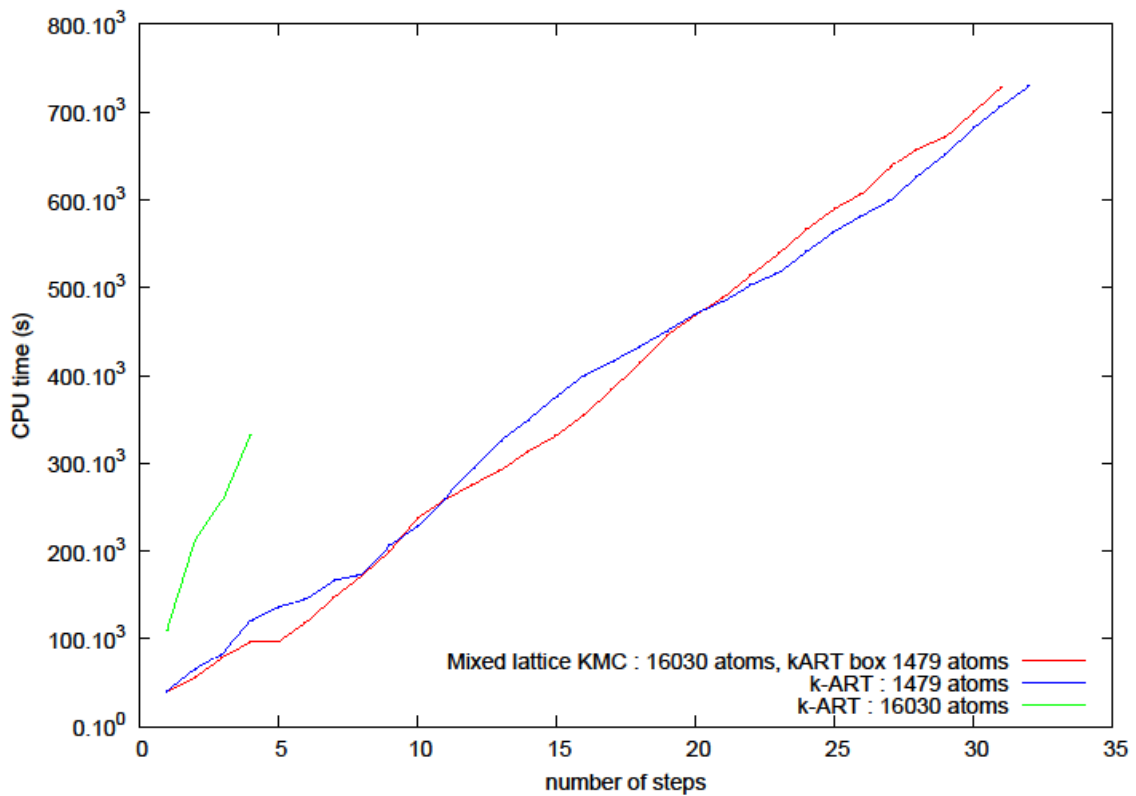
Figure 34: CPU time versus number of steps for three simulations containing a 19 atoms SIA $\frac{1}{2}\langle 111\rangle$ loop in a bcc Fe matrix with 11 C atoms: a k-ART simulation with 1479 atoms ($9 \times 9 \times 9$ bcc Fe box, blue line), a k-ART simulation with 16030 atoms ($20 \times 20 \times 20$ bcc Fe box, green line) and a mixed-lattice simulation with 16030 atoms ($20 \times 20 \times 20$ bcc Fe box with a $9 \times 9 \times 9$ matching the first simulation treated by k-ART, red line).

An AKMC able to find the possible transitions that the system can undergo using two different methods has been developed: the MLKMC. In the bulk zone (low distortion), a crude approximation where the Fe atoms are fixed after the introduction of the dislocation (called the rigid-lattice approximation) is used to find the possible jumps of the C atoms. The C migration energies are computed with the help of the anisotropic elasticity and a FISE model to take into account the C-C interactions. Near the distorted zone (e.g. the dislocation), a soft lattice AKMC, k-ART, is used to ensure that the MLKMC predicts the correct transitions. This combination allows to drastically reduce the time needed for the MLKMC to perform a step compared to k-ART alone as a rigid-lattice step is done at least 100 000 times faster than a k-ART step.

Chapter IV. Results: the SIA loop

In this chapter, we present the study of the interaction of 1 and 2 C atoms with a dislocation loop. As explained previously, the self-interstitial atom loops in Fe are considered as signature defects of irradiation due to the high formation energy of the SIA. In α-Fe, the reorganization of several SIA in the matrix leads to the formation of SIA loops. One kind of these loops is the $\frac{1}{2}a_0\langle 111 \rangle$ SIA loop, known to be the fastest loop in bcc Fe due to the very low migration energy of its crowdions along the (111) direction. As this defect is very mobile, it is expected to interact with many other defects, such as interstitials, dislocations, precipitates, loops or grain boundaries. Therefore, the study of this loop is of a primary importance to understand the mechanisms underlying the ageing of steels under irradiation. For that purpose, the interaction between a SIA loop constituted of 19 atoms (labelled as the i19 loop) and one or several C atoms was studied first using k-ART only, then using MD, then the MLKMC. The results obtained with k-ART only and MD have been published in a paper, appended at the end of the corresponding section, we thus summarize briefly here the main results. The simulations were pursued using the MLKMC, by encasing the k-ART or MD simulation boxes by Fe atoms, to obtain MLKMC simulation boxes containing 54000 Fe atoms, a dislocation loop and 10 C atoms. These simulation boxes were used to study the formation of a Cottrell atmosphere.

1. The k-ART study

Firstly, a $9 \times 9 \times 9$ system containing 1478 or 1479 atoms (1458 bulk Fe, 19 SIA forming a loop and 1 or 2 C atom(s)) was studied using k-ART only. The results are compiled in the article: "Interaction between interstitial carbon atoms and an $\frac{1}{2}\langle 111 \rangle$ SIA loop in an iron matrix: a combined DFT, off lattice KMC and MD study".

In this article, the preferential positions of the C atom with respect to the loop were studied using both DFT and MS calculations. We first calculated the binding energy (see equation 13 in section "Chapter II. Methods 3. Calculating the binding energy between several defects") between the loop and a C atom. Let's recall that with our definition, **a positive value of the binding energy corresponds to an attraction between the defects. On the contrary, a negative binding energy indicates repulsion between the defects.** It was observed that the results predicted by the DFT and the MS calculations were in good agreement despite slight differences in the values. **However, the trends remained the same, with the preference of the C atom to go at the external periphery of the loop (positive binding energies) and not within the loop (negative binding energies), as seen on** Figure 35**. Furthermore, the closer the C atom to the loop, the higher the binding energy between the loop and the C atom (for a C atom outside the loop).** This effect was linked to the local atomic volume[4] of the C atom: **the more space around a C atom, the higher the binding energy between the C and the i19 SIA loop.** It was thus deduced and proven that the C atom has more space at the external periphery of the loop.

---

[4] The local atomic volume of an atom is defined as the space closer to that atom than to any other atom. It was computed according to the method proposed by Domain and Becquart (Domain and Becquart, 2018).
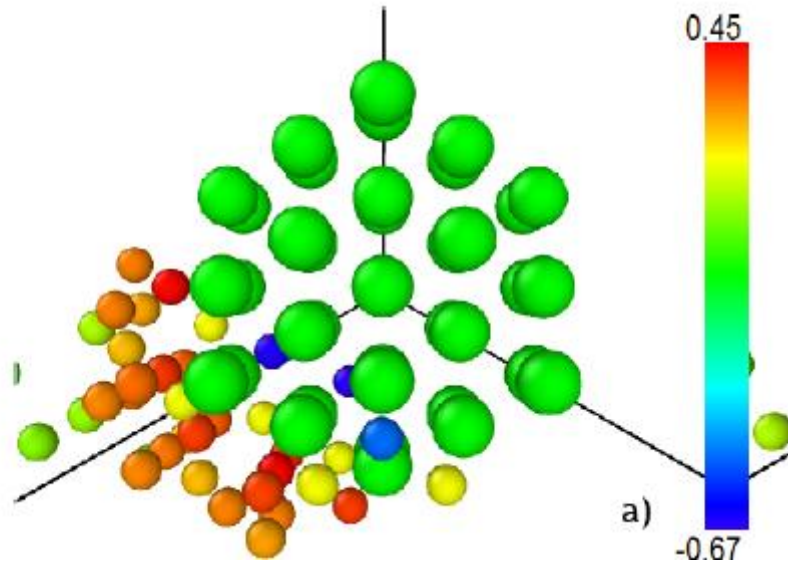
Figure 35: Binding energies of C atoms (small atoms) with the SIA loop (large green atoms) in bcc Fe. The C atoms are coloured depending on their binding energies with the loop (predicted by DFT), with a negative value indicating a repulsion between the C atom and the loop. Figure taken from (Candela et al., 2018).

Concerning the kinetics of the system, the loop was studied alone to estimate its high diffusivity. It was indeed observed that the migration energy of a crowdion is very low, around 50 meV. At 300 K, the time steps of the crowdion movements were observed to be between 10^{-13} and 10^{-16} s, thus confirming the very high mobility of the loop.

The 1C-loop configurations previously found by MS were used as starting configurations for k-ART simulations with the temperature set at 300 K. These configurations were divided in three categories: the high binding energies category ($E^{binding} > 0.3$ eV), the low binding energy category ($0 < E^{binding} < 0.3$ eV) and the repulsive category ($E^{binding} < 0$ eV). These categories are linked to the position of the C atom on the configuration: a C atom within the loop will be in the repulsive category, a C atom at the external periphery of the loop will be in the high binding energies category, and a C atom far from the loop belongs in the low binding energies category. The classification of the configurations is summarized on Figure 36:
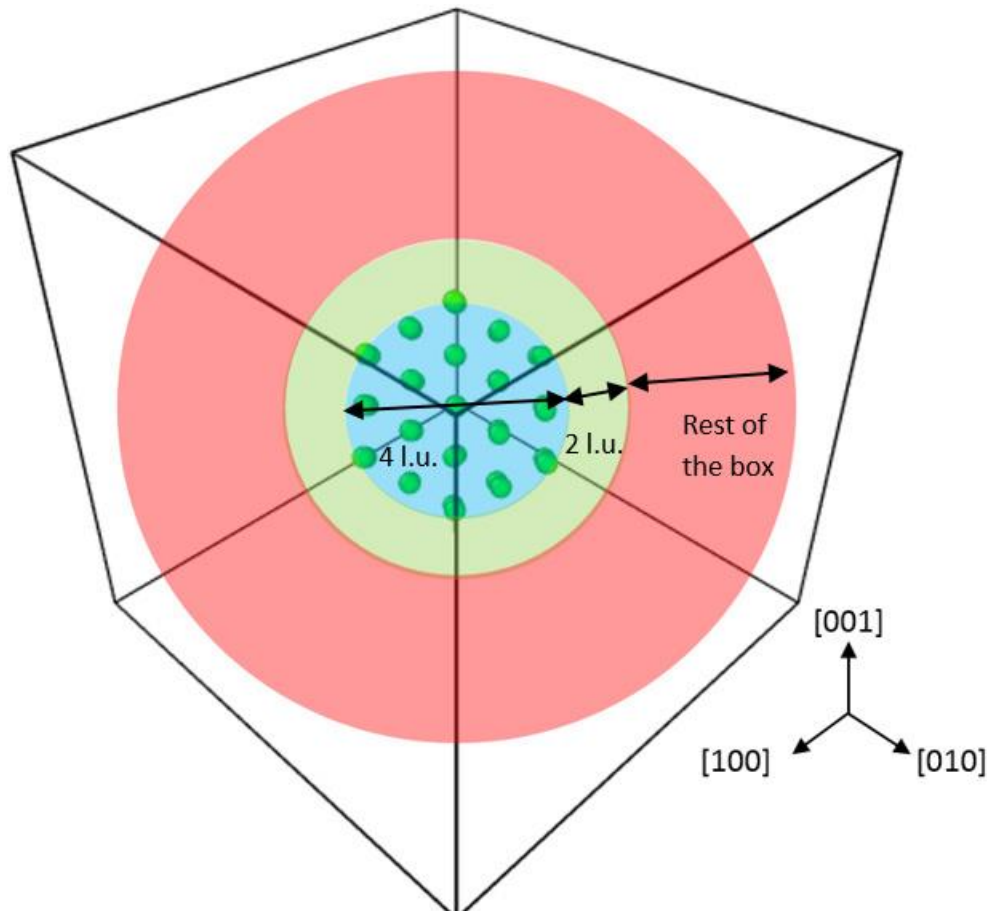
Figure 36: Classification of initial configurations depending on the C position. The green atoms represent the perfect i19 loop. C atoms in the blue zone are in the repulsive category, C atoms in the green zone are in the high binding energies category, and C atoms in the red zone are in the low binding energies category. Figure taken from (Candela et al., 2018).

Looking at the initial migration energies of the C atoms in the high binding energies category led us to think that a stability zone around the loop allows the C atom to freely move around the loop. Indeed, when looking at the k-ART simulation of the system, it was observed that C atoms at the external periphery of the loop did not leave the loop, they turned around thus pinning the loop for times up to 0.2 s at 300 K. This result is consistent with the observations made by Tapasa & al. where the loop can trap C atoms (Tapasa et al., 2007a). Concerning the other categories, it was either found that the C atoms move to the external periphery of the loop (in binding positions) or far from the loop where the C and the loop have no interaction. Another interesting result is the pinning mechanism of the loop by the C atom: the C atom will be strongly bound to some of the loop atoms, "forbidding" these loop atoms to move.

To complete the study, the kinetics of the 2C-loop system was studied with three kinds of initial configurations: 2 C atoms at the external periphery of the loop (binding configurations), 1 C atom within the loop and 1 C atom at the external periphery of the loop (low binding configurations), and 2 C atoms within the loop (repulsive configurations). For the initial binding configurations, the C atoms were observed to turn around the loop in the stability zone. For the initial repulsive configurations, the loop was observed to move promptly from the C atoms. However, for the initial low binding configurations, two different outcomes were found: either the loop moved away from the C atoms, or the C atom within the loop has the time to go from within the loop to the external periphery of the loop, i.e. in a binding configuration.

The temperature was then set at 600 K to study the influence of the temperature. In the KMC approach, increasing the temperature allows high energy transitions to be performed more often than at low temperatures. However, it was observed in the k-ART simulations that the very-low migration energy events (crowdions movement) were favoured at 600 K. We decided to launch MD simulations to estimate the effect of the temperature, as the simulated time of the k-ART simulations at 600 K was reachable by MD. Therefore, MD simulations matching the k-ART simulations were launched to validate the k-ART results (a loop with 1 or 2 C atoms, at 300 and 600 K). The same trends observed by k-ART were also observed by MD simulations, i.e. the C atoms moving around the loop and the loop moving promptly when the C atoms are within the loop. However, some differences are to note between k-ART and KMC simulations, especially the fact that in MD simulations, for configurations with 1 C within the loop and 1 C at the external periphery of the loop (low binding configurations of the 2C-loop system), the loop always moved away from the C atoms, leaving no time for the C atom within the loop to go outside the loop.

To have more information on the system, the configurations with 2 C atoms were launched with MD on larger simulation boxes, i.e. from 1458 Fe atoms to 16000 Fe atoms. This shift allowed to see another effect of the C atom on the loop: when the loop moves from the C atoms (because 2 C atoms are within the loop at the beginning), the loop was not observed to cross back the C atoms. This means that C atoms on the path of the loop have a repulsive effect on this loop.

Table 3 summarizes the k-ART simulation conditions, whereas Table 4 and Table 5 summarize the MD simulation conditions.

Type of simulations	K-ART
Defect investigated	I19 SIA loop
Simulation box size	X = 25.69788 Å, Y = 25.69788 Å, Z = 25.69788 Å
Number of Fe atoms	1458 +19 SIA
Number of C atoms	1 or 2
Box orientation	X = [100], Y = [010], Z = [001]
Boundary conditions	PBC in each direction
Temperature	300 K and 600 K
Number of cores	16
Average number of KMC steps	414
Average CPU time per core	13.2 days
Average simulated time at 300 K	0.12 s, from 10^{-11} s to 2.88 s

Table 3: Simulation conditions for k-ART simulations containing an i19 loop and 1 or 2 C atoms.

Type of simulations	MD
Defect investigated	I19 SIA loop
Simulation box size	X = 25.69788 Å, Y = 25.69788 Å, Z = 25.69788 Å
Number of Fe atoms	1458 +19 SIA
Number of C atoms	1 or 2
Box orientation	X = [100], Y = [010], Z = [001]
Boundary conditions	PBC in each direction
Temperature	300 K and 600 K
Number of cores	16
Number of MD steps	6.10^7 s
CPU time per core	9.5 days
Simulated time	6.10^{-8} s

Table 4: Simulation conditions for MD simulations containing an i19 loop and 1 or 2 C atoms.

Type of simulations	MD
Defect investigated	I19 SIA loop
Simulation box size	X = 57.1064 Å, Y = 57.1064 Å, Z = 57.1064 Å
Number of Fe atoms	16000 +19 SIA
Number of C atoms	2
Box orientation	X = [100], Y = [010], Z = [001]
Boundary conditions	PBC in each direction
Temperature	300 K and 600 K
Number of cores	16
Number of MD steps	$1. 10^6$ s
CPU time per core	17.6 days
Simulated time	$1. 10^{-8}$ s

Table 5: Simulation conditions for MD simulations containing an i19 loop and 1 or 2 C atoms in a 16000 Fe simulation box.

Finally, another interesting effect was observed both with MD and k-ART simulations: the loop was observed to drag the C atoms along with its movement for small distances (two lattice units at most). More precisely, the C atoms were sometimes observed to move around a distorted loop (due to the crowdions movement) thus resulting in the C atom moving in the crowdion axis direction.

To conclude, the ability of k-ART to produce reliable results on the C-i19 loop system was proven. At 300 K, k-ART is a method at least as efficient as MD for the study of the C-loop and the 2C-loop system (and can be up to 10^8 times more efficient) as seen on Figure 42.
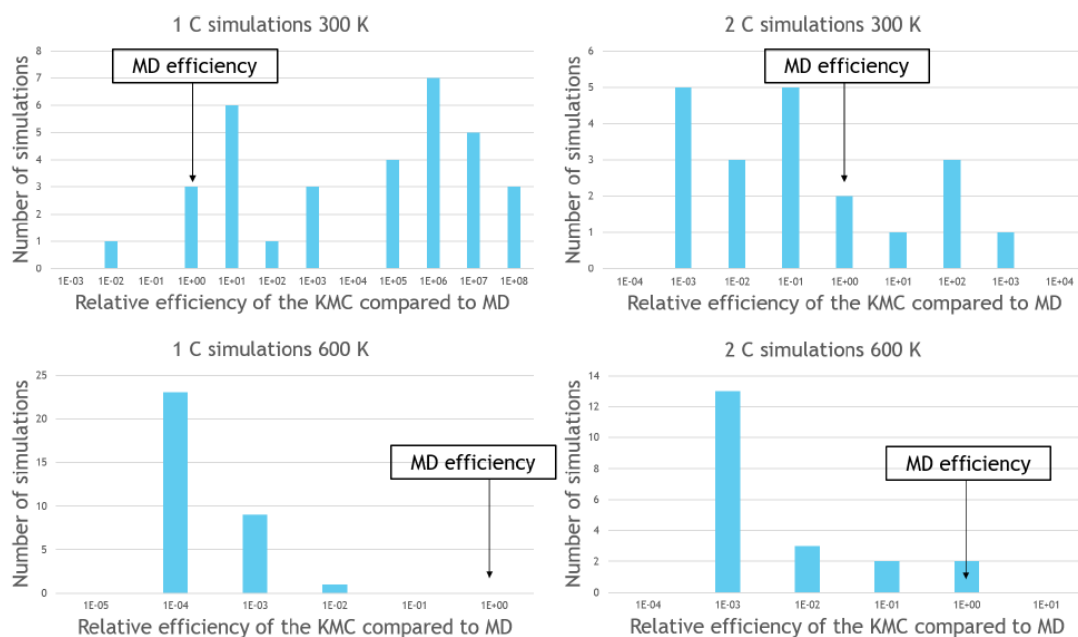
Figure 37: Relative efficiency of k-ART compared to MD for the simulations launched at 300 K and 600 K with 1 and 2 C atoms.

Interaction between interstitial carbon atoms and a ½ ⟨1 1 1⟩ self-interstitial atoms loop in an iron matrix: a combined DFT, off lattice KMC and MD study

R Candela[1,2] , N Mousseau[3], R G A Veiga[4] , C Domain[2,5] and C S Becquart[1,2]

[1] Univ. Lille, CNRS, INRA, ENSCL, UMR 8207, UMET, Unité Matériaux et Transformations, F 59 000 Lille, France
[2] Laboratoire commun EDF-CNRS Etude et Modélisation des Microstructures pour le Vieillissement des Matériaux (EM2VM), France
[3] Département de physique and Regroupement québécois sur les matériaux de pointe, Université de Montréal, Case postale 6128, succursale centre-ville, Montreal, QC H3C 3J7, Canada
[4] Universidade Federal do ABC, Center for Engineering, Modeling, and Social Applied Sciences (CECS), Av. dos Estados, 5001, Santa Terezinha, CEP 09210-580, Santo André/SP, Brazil
[5] EDF-R&D, Département Matériaux et Mécanique des Composants (MMC), Les Renardières, F-77818 Moret sur Loing Cedex, France

E-mail: charlotte.becquart@univ-lille1.fr

Abstract

A static and kinetic study of the interaction between a 19 ½ ⟨1 1 1⟩ self-interstitial atoms loop and C atoms in body-centred cubic iron is presented in this work. An empirical potential matching the density functional theory calculations is used to study the static properties of the system. The usual kinetic Monte-Carlo (KMC) on-lattice restriction is not valid when the material is highly distorted, especially in the presence of a dislocation loop. Therefore, the dynamics of the system are investigated using both molecular dynamics simulations and k-ART, a self-learning/off-lattice atomic kinetic Monte-Carlo. The presented work is thus a full study of the C-loop and the C2-loop systems. A good agreement is observed between the statics and the kinetics (e.g. the discovery of a zone of stability of the C atom around the Fe cluster where the C can almost freely move), even though the kinetics show some unexpected behaviours of the studied systems. The pinning time of the loop induced by the C atoms is also estimated.

Keywords: dislocation loop, molecular dynamics, irradiation, BCC steels, off-lattice kinetic Monte-Carlo, DFT

Supplementary material for this article is available online

(Some figures may appear in colour only in the online journal)

1. Introduction

Body-centred cubic (bcc) iron alloys are typically used in the nuclear industry, especially for reactor pressure vessels. Due to the high formation energy of self-interstitial atoms (SIA) in iron, defects such as SIA dislocation loops are found in materials that have been exposed to irradiation such as neutron irradiation: the concerned Fe–C alloys are the nuclear reactor vessel and the nuclear reactor internal parts. ½ ⟨1 1 1⟩ dislocations loops are known to have a very low migration

energy along the $\langle 1\,1\,1 \rangle$ direction [1] in pure Fe thus making it a mobile defect which can easily interact with other defects, as presented in the mechanism proposed by Xu *et al* leading to the formation of $\langle 1\,0\,0 \rangle$ loops by the interaction between two $\frac{1}{2}\langle 1\,1\,1 \rangle$ loops [2]. While the very mobile $\langle 1\,1\,1 \rangle$ loops may migrate to grain boundaries, the almost immobile $\langle 1\,0\,0 \rangle$ loops are expected to accumulate in the microstructure and act as sinks for mobile defects [2] and may as well hinder the dislocations movement. Therefore, quantifying the change of mobility of $\langle 1\,1\,1 \rangle$ loops due to the C atoms is of primary importance to have a better understanding of the evolution of the microstructure of irradiated steels. The addition of alloying elements in pure bcc Fe matrix has an influence on the loop mobility. Arakawa *et al* observed a lowering in the loop motion due to Cr segregation at the loop periphery for temperatures above 450 K [3]. As for interstitial impurities, the presence of even very small amount of carbon affects properties of Fe and Fe-based ferritic alloys. This comes from the fact that carbon exhibits strong interaction with lattice defects—see for instance [4]—and therefore influences their mobility [5], thus affecting the evolution of the microstructure. As an example, the strong affinity of carbon with vacancies in α-Fe leads to the formation of carbon–vacancy (*C*–*V*) complexes that can trap SIA loops [6]. Indeed, molecular dynamics (MD) simulations showed that *v*–*C* and *v*–*C*2 complexes can be responsible for the slowing down or even the complete stopping of $\frac{1}{2}\langle 1\,1\,1 \rangle$ SIA clusters [7]. The same authors showed that C decorated loops acted as strong obstacles for dislocations [8]. A single carbon atom was shown to hinder the movement of dislocations [9, 10] or $\langle 1\,0\,0 \rangle$ dislocation loops [8] in Fe, whereas Khater *et al* [11] showed that the stress level at 0 K due to a solid solution of C around an edge dislocation is lower than the Peierls stress leading to a softening of the material. On the contrary, these C atoms will tend to migrate towards the dislocation thus creating a well-known Cottrell atmosphere [12]. In these atmospheres, due to C atoms that occupy pinning positions, the unpinning stress is higher as shown very recently in a study combining Monte Carlo and MD [13].

The aim of this work is to study the interaction between C atom(s) and an $\frac{1}{2}\langle 1\,1\,1 \rangle$ dislocation loop composed of 19 iron SIA (i19 loop) within bcc Fe matrix. The i19 loop is expected to be representative of larger $\langle 1\,1\,1 \rangle$ loops because only the last shell of the loop and the first shell outside the loop are found not to be in a bcc environment [14]. Firstly, the static properties of the system are studied by density functional theory (DFT) and compared with the results of a well-assessed empirical potential [15] in order to determine the stability of the different configurations. This is done by calculating the binding energy between the C atom(s) and the loop. Secondly, the dynamic properties of the system are investigated at different temperatures for the different initial configurations given by the static study of the system. The aim of this dynamic study is to investigate the evolution in time of the loop and the C atom(s). A discussion will summarize the principal results of this work and show the consequences induced by the presence of C atoms near the loop.

2. Method

2.1. DFT calculations

DFT has been used within the projector augmented wave method as implemented in the Vienna *ab initio* simulation package (VASP) [16–19]. The Perdew and Wang [20] parameterization of the generalized gradient approximation has been used. For the spin interpolation of the correlation potential, the improved Vosko–Wilk–Nusair interpolation has been applied. Supercells of 1458 bcc positions ($9 \times 9 \times 9$ bcc two atoms unit cell with a_0 2.831 Å) were used with Gamma point representation of the Brillouin zone as the supercells are large. The plane wave energies were cut off at 300 eV. All the atoms were relaxed under constant volume condition.

The perfect interstitial $\langle 1\,1\,1 \rangle$ loop is introduced in the middle of the supercell and the influence of the pressure due to the use of constant volume has been evaluated using the method proposed by Varvenne *et al* [21] to take into account long range interactions. Once point defect energies have been calculated using VASP, they are corrected by subtracting artifactitious interaction energy arising from periodic boundary conditions. Because the introduction of an i19 $\langle 1\,1\,1 \rangle$ loop can induce a large pressure on the simulation box, the calculations were also done using a box size enlarged by 19 atomic volumes. The new lattice parameter a_{19} was then adjusted to match the new volume of the box. More precisely, this is done as such:

$$a_{19} = \frac{a_0}{N_{\text{box}}} \sqrt[3]{N_{\text{box}}^3 + \frac{19}{2}}$$

where N_{box} is the duplication of the unit cell in each direction ($N_{\text{box}} = 9$ for the DFT calculations).

It was found that these two methods to take into account the pressure applied return results that differ by less than 4% in the binding energies in average thus allowing one to confirm that the addition of 19 atomic volumes in the box is a valid correction. The local magnetic moments are calculated by taking the spin from the charge density difference integrated over spheres on each atom.

2.2. Cohesive model for the empirical potential calculations

Energy minimizations were done using the MD code DYMOKA [22] with simulation boxes of the same size as the ones used in the DFT calculations, i.e. $9 \times 9 \times 9$ boxes (1458 Fe atoms on a bcc lattice) with an i19 loop and a C atom. The empirical potential chosen is the one derived by Becquart *et al* [15] which was slightly modified by Veiga [23]. This Fe–C potential has been previously used to model Fe–C systems, with a particular focus on carbon-dislocation interactions [13, 24, 25] and the dynamics of carbon in bulk Fe[15] [26]. It was also used to model internal friction experiments [27], martensite properties [28], and C ordering in Fe–C crystallites at high C concentrations [29]. Periodic boundary conditions were applied along all the directions and the total energy of the system was minimized on both boxes with and without the correction on the lattice parameter due to the pressure

induced by the introduction of the i19 loop. Just like for DFT relaxation, a difference in the binding energies between the C atom and the loop was observed whether we adjust the lattice parameter or not to take into account pressure added by the addition of the loop.

2.3. Static properties

2.3.1. Binding energy. In a bcc Fe lattice containing N atomic sites, the total binding energy between n objects, i.e. vacancies, self-interstitial atoms, Fe or solute atoms, is the energy difference between the configuration where all the objects interact and the system where all the objects are far enough from one another to not interact anymore. Due to the limited supercell size, the total binding energy is calculated as follows:

$$E_{\mathrm{b}}\left(A_1, A_2, ..., A_n\right) = \sum_{i=1,...,n} E\left(A_i\right)$$
$$- \left[E\left(A_1 + A_2 + ... + A_n\right) + (n-1)\,E_{\mathrm{ref}}\right]$$

where E_{ref} is the energy of the supercell without any defects, $E\left(A_i\right)$ is the energy of the supercell with A_i, and $E\left(A_1 + A_2 + ... + A_n\right)$ is the energy of the cell containing all A_i interacting defects. All the supercells contain the same number of lattice sites, i.e. have the same size. More precisely, here are the binding energies for a system containing a loop with a C atom and a loop with two C atoms in a pure Fe matrix respectively, so for the systems studied in this paper:

$$E_{\mathrm{b}}\left(\mathrm{C} - \mathrm{loop}\right) = E\left(\mathrm{C}\right) + E\left(\mathrm{loop}\right)$$
$$- \left[\left(E\left(\mathrm{C\_and\_loop}\right) + E(\mathrm{perfect\_lattice})\right]\right.$$

$$E_{\mathrm{b}}\left(2\mathrm{C} - \mathrm{loop}\right) = 2 \times E\left(\mathrm{C}\right) + E\left(\mathrm{loop}\right)$$
$$- \left[\left(E\left(2\ \mathrm{C\_and\_loop}\right) + 2 \times E(\mathrm{perfect\_lattice})\right].\right.$$

With this definition, positive values correspond to binding (or attractive) configurations. The binding energy depicts the attraction/repulsion between the defects and so the overall stability of the system. Indeed, the higher the binding energy between a C atom and the loop, the more stable the configuration.

2.3.2. Distances between the loop centre of mass and the C atom. The loop centre of mass (CM) is defined as the centroid of all the Fe atoms composing the loop, i.e. all Fe atoms that are not close to the perfect bcc lattice. The C-CM distance is not enough to fully describe the carbon environment especially because the same distance may correspond to different configurations. Two variables are thus defined: D(C-CM), the distance between the CM and the C atom projection on the (1 1 1) plane comprising the CM and H(C-CM), the distance between the C atom and the (1 1 1) plane comprising the CM. In the square triangle defined by the C atom, the CM and H the orthogonal projection of the C atom to the (1 1 1) plane comprising the CM, the two variables are D(C-CM) and H(C-CM) are respectively the opposite side and the adjacent side of the right angle. Figure 1 represents these variables for a better understanding.
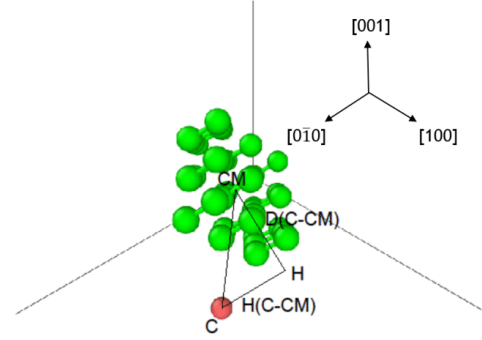
Figure 1. Representation of the variables D(C-CM) and H(C-CM) in the presence of an i19 loop (green atoms) and a C atom (in red) in a pure Fe matrix with CM the loop centre of mass and H the orthogonal projection of C on the (1 1 1) plane containing CM. For the sake of simplicity, the Fe matrix is not represented.

2.3.3. Local atomic volume. The local atomic volume of an atom corresponds to the space closer to this atom than to any other atom. It thus characterizes the real space an atom has. This local atomic volume was computed according to the methodology described by Domain and Becquart [14].

2.3.4. Coordination. In this work, the coordination is defined as the number of Fe atoms within a 2.3 Å radius sphere around the C atom. In an iron bcc lattice (lattice parameter at 0 K predicted by the EAM potential used throughout this work $a_0 = 2.855\,32$ Å), interstitial C atoms position themselves in octahedral sites rather than tetrahedral sites [30]. In pure iron, in an O site, the coordination is 6; there are two iron atoms at $\frac{a_0}{2} = 1.43$ Å and four iron atoms at $\frac{\sqrt{(2)}a_0}{2} = 2.02$ Å. The third closest neighbours of the C atom are eight iron atoms at $\frac{\sqrt{(5)}a_0}{2} = 3.19$ Å. According to the interatomic potential we use in this work, when a C atom is introduced in the O site and the structure is relaxed, the two Fe 1st nearest neighbours move away from the C atom from 1.43 Å to 1.79 Å whereas the four Fe 2nd nearest neighbours move closer to the C atom from 2.01 Å to 1.98 Å. Therefore, a coordination non-equal to 6 would mean a distorted lattice around the C atom because it would mean that an Fe atom moved by at least 0.3 Å.

2.4. Dynamic calculations: kinetic-ART

Contrary to standard AKMC methods, kinetic-ART (k-ART) is an off-lattice/self-learning AKMC, i.e. that it does not constraint atomic positions to a rigid lattice, and an event catalogue is constructed on-the-fly by the program as the simulation proceeds. It makes this technique especially suitable for the study of activated diffusion processes [31, 32] such as carbon diffusion in Fe [26] and reproduce the lattice even in distorted systems. K-ART identifies all the possible transitions for each local topology, defined by the graph composed of the links between the different atoms. For a given system, with a

specific potential, there is a bijection between the topology and the real lattice. Another important assumption made is that for a given topology, the possible transitions will remain the same. This means that for a topology, the transitions have to be computed only once. The relevant energy barriers, i.e. those with an occurrence probability of 0.01% or more, are recalculated at each step to ensure that the transitions, even if they are the same, have the right energy. This implies that k-ART, unlike more standard KMCs include exactly the effect of elastic deformations on minima and barriers, allowing one to study the diffusion of carbon near a dislocation core. The topologies of the system are managed by NAUTY [33]. K-ART uses a local transition searching method which finds all the jumps associated with a given system and their associated energies [34]. The method works by directly computing the lowest curvature using the iterative Lanczos algorithm, an efficient method allowing to follow a local eigendirection [35]. From a configuration in a local minimum, the program will find all the associated transitions barrier as well as the local minimum after the jump. Contrary to other saddle point searching methods such as the nudged elastic band method, only one local minimum is needed to find a transition barrier.

The simulations were launched in order to study the impact of the addition of C atom(s) near the i19 dislocation loop. Therefore, we introduced an i19 loop in a perfect Fe matrix with one or two C atoms. For all k-ART simulations, the temperature was set to 300 K or 600 K in a $9 \times 9 \times 9$ bcc supercell.

3. Results

3.1. Static properties

Figure 2 represents the $C - \frac{1}{2} \langle 1 1 1 \rangle$ loop binding energy for the DFT calculations as well as the empirical potential, and for the two investigated box sizes (the 1458 atomic volume box and the $1458 + 19$ atomic volume box). The binding energy is defined so that the most stable configurations are the ones with the highest binding energy (section 2.3.1).

Regarding the influence of the box volume on its energy, one could expect that it would only cause a shift in the simulation box energy (hence in the binding energy) equal to the constraint added by the 19 SIAs. However, figure 2 indicates that the addition of 19 atomic volumes to the simulation box volume does not induce a strict shift in the binding energy. This can be due to the fact that the lattice does not relax in the exact same configuration when the relaxation is done in the two different boxes or that deformations are sufficiently important to sample non-linear parts of the interaction. As seen on figure 2, the difference in binding energies between configurations relaxed by DFT with and without the addition of 19 atomic volumes is higher than the difference in binding energies between configurations relaxed by EP with and without the addition of 19 atomic volumes. Therefore, it is possible to deduce that DFT is more sensitive to the change of pressure than the empirical potential.

We can observe on figure 2 that the most stable configurations for the C atom are the ones at the external periphery
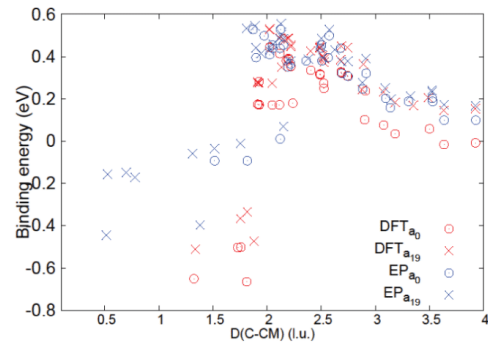
Figure 2. Binding energy between the C atom and the $\langle 1 1 1 \rangle$ loop (DFT and empirical potential calculations labelled as DFT and EP) versus D(C-CM) for lattice parameter taking and not taking into account the loop pressure induced dilatation (labelled as a_{19} and a_0 respectively). The results are presented for simulations containing a loop and a C atom as only defects in a $9 \times 9 \times 9$ bcc Fe matrix.

of the loop (D(C-CM) > 2 lattice unit (l.u.)), with a binding energy of 0.44 eV (resp. 0.50 eV) for the DFT (resp. for the empirical potential) calculations in the 1458 atomic volume box. The covalent Fe–C interaction potential derived by Hepburn [36] predicts binding energies of the same order. Note, however, that the Hepburn potential has been found to disagree with DFT calculations regarding the carbon-dislocation interaction. Indeed, as highlighted by Terentyev *et al* [7], the saddle point predicted by this potential as the C atom migrate is not the tetrahedral site, whereas the potential used in this work [15, 23] agrees qualitatively with the DFT calculations regarding the attractive carbon dislocation interaction of about 0.1 and 0.4 eV for carbon–carbon separations of 1*b* and 2*b* respectively [37]. Using a combination of an Fe potential developed by Ackland [38] and an FeC potential developed by Johnson [39], Tapasa *et al* [9] observe that the binding energy of C with small $\langle 1 1 1 \rangle$ loops decreases with the loop size from 0.86 eV for a four SIA loop to 0.42 eV for a 19 SIA loop, close to the value of 0.55 eV predicted by the potential used in this work for the binding energy between C and a 19 SIA loop. The strength of the C-loop interaction predicted by the empirical potential used through this work is in between that of the highest binding energy of C atom in a screw dislocation core (0.41 eV) and the highest binding energy of a C atom in an edge dislocation core (0.65 eV) [24] obtained with the same potential before the slight adjustment done by Veiga [23].

Even if the binding energies predicted by the DFT and the empirical potential are not strictly the same especially for repulsive configurations, there is an excellent agreement in the trend of the curves figure 1 thus confirming that the empirical potential is in good agreement with the DFT calculations. One can furthermore observe on figure 2 that for the same D(C-CM) different binding energies can be obtained. The main reason for this behaviour is due to the fact that the dumbbells constituting the loops have low migration barriers along the $\langle 1 1 1 \rangle$ direction; these can then move easily, therefore the energy of
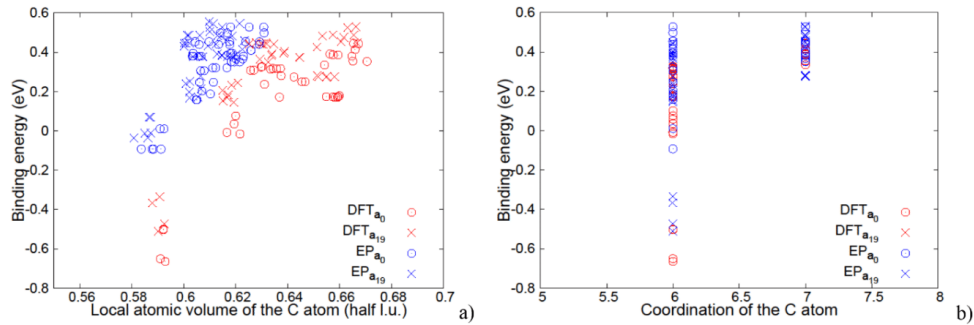
Figure 3. C-⟨1 1 1⟩ loop binding energies (DFT and empirical potential calculations) versus (a) the local atomic volume (b) the coordination number for lattice parameter taking and not taking into account the loop pressure induced dilatation. The results are presented for simulations containing a loop and a C atom as only defects in a $9 \times 9 \times 9$ bcc Fe matrix.

the box changes and so does the binding energy between the C and the loop. Despite this issue, figure 2 provides a good overview of the system: for a C-loop centre of mass distance under 1.9 l.u., all the binding energies are repulsive meaning that the loop and the C atom are likely to go far away from each other. Conversely, the most attractive configurations are the ones with the C atom at the external periphery of the loop (2–2.2 l.u.). Finally, one can observe that the empirical potential tends to underestimate the repulsion between the defects compared to DFT.

A correlation between the local atomic volume and the binding energy is emerging from figure 3(a): the more space a C atom has, the more attractive the interaction energy between the two defects. All configurations where the local atomic volume of the C atom is below 0.6 are repulsive. One can deduce from figures 2 and 3(a) that the most spacious configurations for the C atom are the ones where C is at the external periphery of the loop. Conversely, that the most stable configurations are the ones where the C atom is at the external boundary of the loop because this is where the carbon has the most space thus disturbing the less the iron matrix. Figure 3(a) also points out that the potential predicts smaller atomic volumes than DFT.

Figure 3(b) provides interesting information: the highest binding energies are obtained when the C atoms have seven Fe atoms closer than 2.3 Å to them. These configurations share a particular characteristic: the C atom is 2.3 Å close to only one or two atoms of the loop which corresponds to the carbon atom being at the external boundary of this loop. Inside the loop, the coordination is 6, which confirms that inside the loop the organization of Fe atoms is the same as for the bcc iron matrix. The surprising result is that the C atom is strongly bound to the loop when there are 7 Fe atoms close to it, so more than the C atom in pure iron. Strong binding energies also correspond to the largest local atomic volumes leading to the counter-intuitive fact that the more iron atoms in a 2.3 Å sphere around the C atom the larger the space around the C atom. A plot of the local atomic volume versus the coordination confirms that the C atoms having a coordination of 7 do have a high local atomic volume thus a strong binding energy between the defects.

Figure 4 summarizes the binding energy datasets obtained in this work. The main difference on these datasets is the change in the repulsive binding energies: on figure 4(a), (b) and (d), the most repulsive configurations have a binding energy below $-0.4\,\mathrm{eV}$ when on figure 4(c) the most repulsive configurations have a binding energy close to $-0.1\,\mathrm{eV}$. This is due to the differences in configurations, because for the empirical potential relaxation without the 19 atomic volumes, no C atom was found far within the loop after the relaxation and the closer the C atom to the loop centre of mass the greater the repulsion.

To summarize, one can observe in figure 5 that the most attractive configurations are the ones where the carbon is at the external boundary of the loop and close to the plane (1 1 1) containing the loop centre of mass. The sudden drop of the surface occurs at the loop boundary, confirming that the binding energy becomes repulsive when the C atom enters the loop.

A closer look at the binding energies of all the configurations leads us to sort the configurations in three sets of binding energies. Because no configuration relaxed by EP with the addition of 19 atomic volumes was found to have a binding energy between $0\,\mathrm{eV}$ and $0.069\,\mathrm{eV}$ and between $0.28\,\mathrm{eV}$ and $0.37\,\mathrm{eV}$, we decided to classify the configurations depending on their binding energy into three distinct categories, namely high binding energies category ($Eb > 0.3\,\mathrm{eV}$), low binding energy category ($0\,\mathrm{eV} < Eb < 0.3\,\mathrm{eV}$) and repulsive category ($Eb < 0\,\mathrm{eV}$). We thus expect to find the same kinetic behaviour for configurations in the same category.

Figure 6 summaries these three categories of initial configurations depending on the C position with respect to the loop: high binding energy configurations when the C is at the external periphery of the loop in green, low binding energy configurations when the C is far from the loop in red and repulsive configurations when the C is within the loop in blue (this colour code will be used throughout the whole paper). A precision must be added to the repulsive category, because the configurations with a repulsive binding energies close to $0\,\mathrm{eV}$ ($-0.01\,\mathrm{eV}$ and $-0.03\,\mathrm{eV}$) are the ones where the C atom is not directly within the loop and not even in the plane comprising
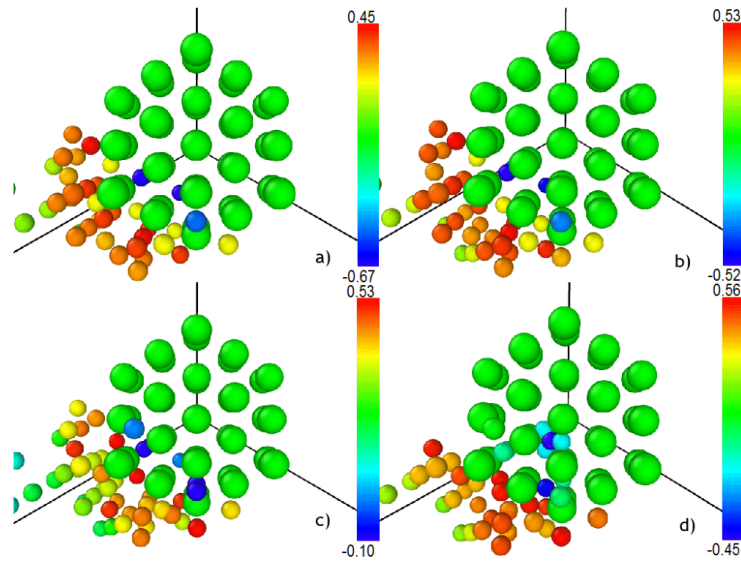
Figure 4. Binding energies in eV between the C atom (small colourized atoms) and the loop (large green atoms) for different configurations using the different relaxation techniques presented: (a) DFT without 19 atomic volumes added, (b) DFT with 19 atomic volumes added, (c) empirical potential without 19 atomic volumes added, (d) empirical potential with 19 atomic volumes added. The C atoms are colourized according to their binding energy with the loop. The perfect loop is showed for comprehension sake because the loop shape is different for each initial configuration.
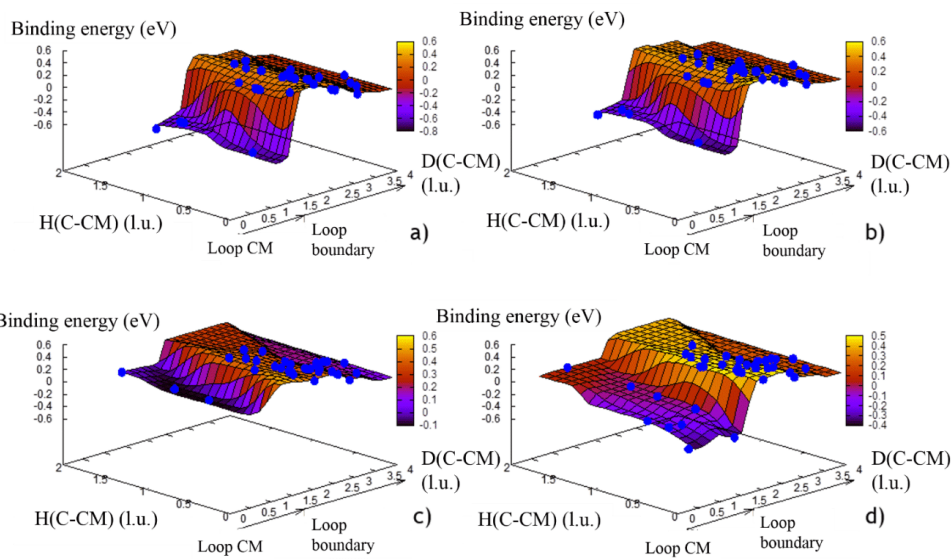
Figure 5. Binding energy surfaces constructed with the binding energy of initial configurations of simulations containing a loop and a C atom as only defects in a $9 \times 9 \times 9$ bcc Fe matrix (blue dots). The results for the different relaxation techniques are presented: (a) DFT without 19 atomic volumes added, (b) DFT with 19 atomic volumes added, (c) empirical potential without 19 atomic volumes added, d) empirical potential with 19 atomic volumes added. The *x* axis is D(C-CM) and the *y* axis is H(C-CM). The surface's colour refers to the Eb colour code.

6

85
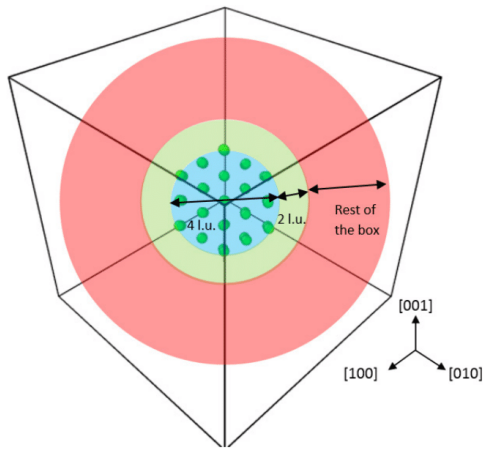
Figure 6. Classification of initial configurations depending on the C position. The green atoms represent the perfect loop for simplification sake. For C atoms in the blue zone, the configuration is repulsive (Eb < 0 eV); for C atoms in the red zone, the configuration is in the low binding energy category (0 eV < Eb < 0.3 eV); for C atoms in the green zone, the configuration is in the high binding energy category (Eb > 0.3 eV).
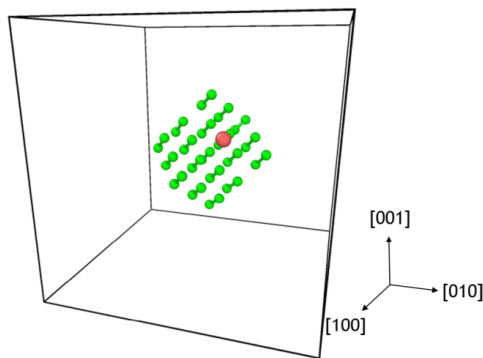
Figure 7. Configuration relaxed by the empirical potential with a binding energy, Eb = −0.13 eV indicating a repulsion between the C (red atom) and the loop (green atoms) even if the C atom is not on the same ⟨1 1 1⟩ plane as the loop. This system contains a loop and a C atom as only defects in a $9 \times 9 \times 9$ bcc Fe matrix (not represented for simplification sake).

the loop (e.g. figure 7). These configurations are thus the ones where H(C-CM) is high and D(C-CM) is lower than 2 l.u. Still, a repulsive energy between these defects suggests that the loop will likely go away from the C atom. This result may be easily explained by the fact that if the loop goes towards the C atom until the C is within the loop, the resulting configuration will be less stable than the original configuration, i.e. the configuration has a lower energy when the C atom is above the loop than the one where the C atom is within the loop.
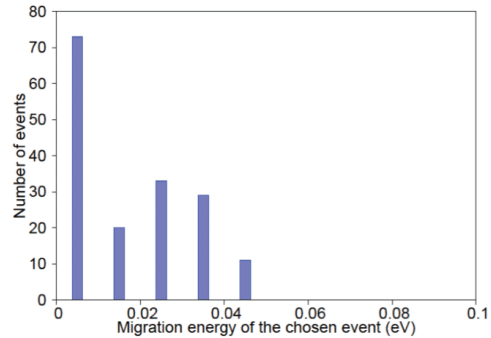
Figure 8. Migration energy of the events chosen by the KMC for a 176 step simulation containing the i19 loop as only defect in a $9 \times 9 \times 9$ bcc Fe matrix.

3.1.1. K-ART simulations. In order to have a good overview of all the simulations, a summary of each MD and KMC simulation is given in the table 'Summary of all simulations' in supplementary material (stacks.iop.org/JPhysCM/30/335901/mmedia).

3.1.1.1.Loop mobility in a pure Fe matrix. In pure iron, the i19 loop is known to be a very mobile defect. A simulation was launched with an i19 dislocation loop as only defect in a pure Fe matrix in a $9 \times 9 \times 9$ box at 300 K to confirm that result. The highest energy barrier found in a 176 step simulation is approximatively 0.05 eV for a crowdion to move as seen on figure 8.

Even if not a single crowdion was found far from the others, meaning that the loop will move as fast as its slowest crowdion, the energy barriers are so low that the overall mobility of the loop is enormous. For this simulation, the timestep of the different events were found to be between 10^{-13} s and 10^{-16} s.

3.1.1.2.Loop interaction with one C atom. We have run 40 k-ART simulations for an average computing time of 2.5×10^5 s at 300 K starting on the configurations relaxed by empirical potential with the addition of 19 atomic volumes, so for $9 \times 9 \times 9$ bcc Fe boxes with a C atom and an i19 loop. One first important result is that the average time step for a C jump is approximatively 10^7 times higher than the average time step for a crowdion displacement. The loop moves thus a lot faster than the C atom and the difference in the defect velocities suggests that the dislocation loop will move until it encounters a C atom.

The energy needed for the C atom to jump in the first step of all the simulations with 1 C atom at 300 K is presented figure 9. The simulations are divided in the three categories defined in 3.1. Knowing that the C migration energy predicted by our potential in a perfect Fe lattice is 0.815 eV, one can deduce from figure 9 that the loop has a high influence on the mobility of the C atom. When the C atom is initially inside the loop (repulsive category), the C migration energies are lower than the C migration energy in a perfect Fe bcc lattice
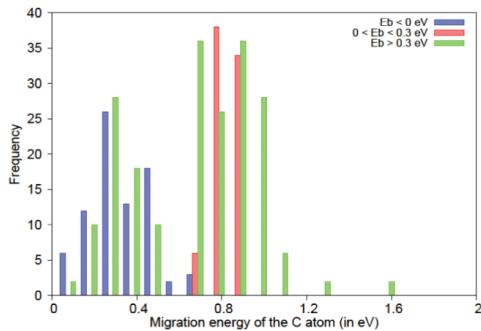
Figure 9. C migration energy for different initial configuration binding energy categories at the first step of the simulation: high binding energies category (Eb > 0.3 eV), low binding energies category (0 eV $<$ Eb < 0.3 eV) and repulsive category (Eb < 0 eV). The simulation boxes contain a loop and a C atom as only defects in a $9 \times 9 \times 9$ bcc Fe matrix.

($E_{\mathrm{mig}} < 0.8$ eV). This reflects that the loop will be likely to unpin from this C atom. For initial low binding energy configurations, the C jump energy is close to the migration energy of C in a perfect bcc lattice. From these configurations where the C atom is far from the loop, one can deduce that the interaction between the two defects is weak. More interestingly, for initial high binding energy configurations, two main areas divide the carbon migration energy. On the one hand, it was logically found that the C atom strongly linked to the loop has a close to or a higher jump energy than 0.8 eV. On the other hand, a lot of C migration energies are below that threshold of 0.8 eV, leading to the counter-intuitive idea that the C atom may move easily. A possible explanation linked to this observation is that a zone of stability around the loop exists thus allowing the C atom to move almost freely around the loop and staying in a strong binding position with it.

Representative simulations of the three categories are represented in figure 10(a) (for the high binding energy configurations), figure 10(b) (for the low binding energy configurations) and figure 10(c) (for the repulsive configurations). These representative simulations represent all the behaviours observed for the three categories of initial configurations with a loop and 1 C atom at 300 K.

As seen on figure 10(a), when the initial binding energy is high, the C-CM distance does not change much meaning that the loop does not move away from the C atom. For all these simulations, we never observed the loop leave the C atom. Even if in a few of these simulations the loop tends to go away from the C atom, it never really leaves it, e.g. when only one crowdion of the loop is close to the C atom while the others are far. This shows the pinning power the C atom has on the loop: strongly bound to a crowdion and because the cohesive force of the loop prevents its break-up, it is hard for the loop to move in these particular conditions.

Figure 10(b) represents the two different behaviours observed for initial low binding energy configurations (0 eV $<$ Eb < 0.3 eV). The first one (solid line) shows the ability of the loop to go away from the C atom when the two
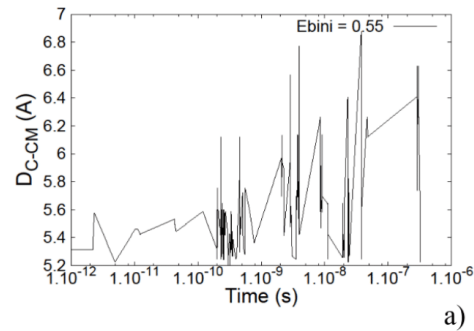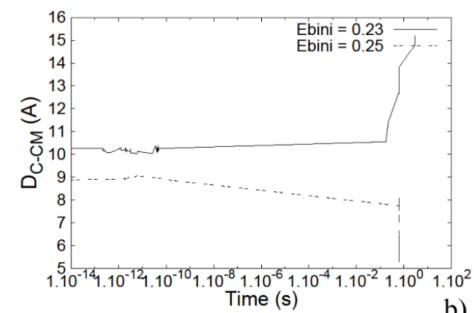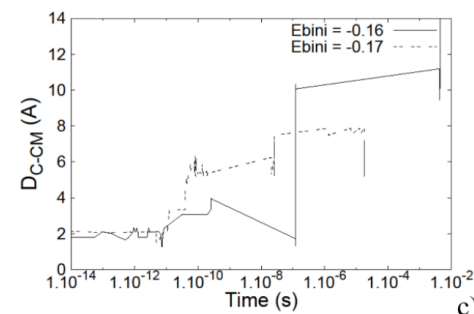
Figure 10. Evolution of the distance between the C atom and the loop centre of mass for representative simulations of the different categories of initial configurations: initial high binding energy configurations (a), initial low binding energy configurations (b) and initial repulsive configurations (c). The simulations contain a loop and a C atom as only defects in a $9 \times 9 \times 9$ bcc Fe matrix.

defects are not so close i.e. the interaction is low. On the contrary, the second one (dashed line) shows the ability of the C atom to move towards a more stable position, so towards the loop external periphery. Therefore, there is a competition between the C atom weakly pinning the loop and the loop movement. One can think that among the low binding energy configurations, the ones with the highest binding energy will lead to the migration of the C atom to the external periphery of the loop and the ones with the lowest binding energy will lead to the migration of the loop, but in fact it was found that even
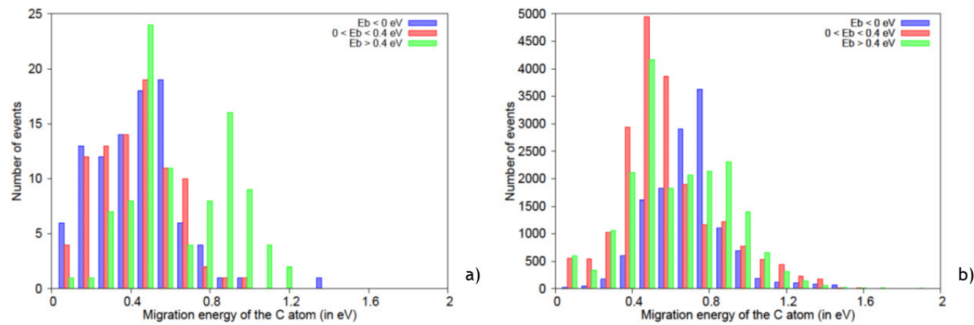
Figure 11. C migration energy for different initial configurations with two C atoms and a loop for the first step (a) and for the whole simulation (b). The initial configurations are divided into three categories: high binding energy (Eb > 0.4 eV), low binding energy (0 < Eb < 0.4 eV) and repulsive (Eb < 0 eV). The simulation boxes contain a loop and two C atoms as only defects in a $9 \times 9 \times 9$ bcc Fe matrix.

with binding energies of 0.17 eV the C atom can be found at the external periphery of loop and that the highest binding energy configuration (0.28 eV) lead to the loop moving with no movement of the C atom. This proves the stochastic character of this effect. This competition is found in two simulations, namely the ones with a binding energy 0.17 eV and 0.20 eV, in which the two effects are occurring at the same time: the loop moves a little away from the C atom but the C will still come to a strong binding position; at the end of these simulations, both defects have moved from their original places thus showing a weak enough anchoring of the loop for it to move but also a strong enough interaction between C and the loop for the C to migrate.

Figure 10(c) represents the two typical evolutions of the C-loop system found for initial repulsive configurations, namely the drive-away process of the loop from the C atom and the repositioning of the C atom to the most stable configurations. The first one (solid line) is simple to explain: the loop will move away from the C atom hindering the stability of the system. The simulation of the second behaviour (dashed line) shows a jump by jump migration of the C atom from within the loop through its external periphery. As shown in figure 9, the C migration energy within the loop is lower than the C migration energy in a perfect Fe lattice, suggesting a low energy migration pathway of the C atom to the external periphery of the loop. Once again, a competition occurs between the loop wanting to move and the C atom wanting to migrate to the most stable configurations. But for the C to migrate, the loop must be anchored a minimum. Therefore, even a C atom within the loop has a pinning effect on the loop although the two defects have a repulsive interaction.

To conclude on this first set of results at 300 K, only two different endings were found to all these simulations. Either the C atom is found at the external periphery of the loop, to the strongest pinning positions, or the pinning was not sufficient enough and the loop was found far from the C atom.

3.1.1.3. Loop interaction with two C atoms. We now investigate the impact of two C atoms on the mobility of the dislocation loop by launching 20 k-ART simulations at 300 K in

$9 \times 9 \times 9$ bcc Fe supercells with two C atoms and the i19 loop. Considering that there are three different categories for one C atom (see figure 6), six different combinations of initial configurations are possible for two C atoms simulations. However, as seen on figure 9, for initial low binding energy configurations where the C atom is far from the loop, the influence of the loop on the C migration energies is weak. We thus decided to focus our attention on simulations with C atoms in repulsive positions or in high binding energy positions. Therefore, only three different categories of initial configurations are possible: two C atoms within the loop, two C atoms at the external periphery of the loop and one C atom within the loop with one C atom at the external periphery of the loop. Looking at all the different initial configuration binding energies with two C atoms, we classify the configurations in three categories: repulsive category (Eb < 0 eV, two C atoms within the loop), low binding energy category (0 < Eb < 0.4 eV, one C atom within the loop and one C atom at the external periphery of the loop) and high binding energy category (Eb > 0.4 eV, two C atoms at the external periphery of the loop). The choice for these categories is, again, justified by the gap in the binding energies of the configurations: no configurations are found with an Eb between −0.36 eV and 0 eV and neither between 0.35 eV and 0.56 eV.

Figure 11 puts on display the migration energy of the C atom for all the simulations with two C atoms for the first step (a) and for all the steps (b). Doing the comparison between the initial C migration energy for configurations with one C atom (figure 9) and two C atoms (figure 11(a)) leads to the following observations.

– For initial high binding energy configurations, there are still the two distinct sets of migration energies, i.e. the low migration energy set ($E_{mig} < 0.8$ eV) and the high migration energy set ($E_{mig} \geqslant 0.8$ eV) meaning that the zone of stability of the C atom around the loop still exists.
– For initial repulsive configurations, whether one or two C atoms are within the loop, almost all the migration energies are low ($E_{mig} < 0.8$ eV) suggesting that the C atom and the loop are still likely to move away from each other.

9

– For initial low binding energy configurations, a difference in the C migration energies is observed whether the box contains one C atom or two C atoms. Indeed, when there is only one C atom (figure 9), C migration energies are close to C migration energy in a perfect bcc lattice ($E_{mig0} = 0.815$ eV) whereas when there are two C atoms, C migration energies are mostly low ($E_{mig} < 0.8$ eV). Remember that this is due to the differences in configurations: for the configurations in the initial low binding energy category with two C atoms, one C atom is in a strong attractive position and one C atom is in a repulsive position. Therefore, one should expect to observe low C migration energies due to the C atom in a repulsive position as well as both high and low C migration energies due to the C atom in a high binding energy position (as seen on figure 9). However, very few high energy barriers were found for the initial low binding energy configurations in figure 11. This means that the interaction between the two C atoms helps the C atom in a strong binding position to overcome the high energy barriers. The consequence of the interaction between the C atoms is then a lowering of the high energy barriers.

The evolution of the C-CM distance for the three categories of initial configurations with two C atoms is represented on figure 12. For the simulation initially in the high binding energies category so with two C at the external periphery of the loop (figure 12(a)), one can observe that the C-CM distance between the interstitials and the loop centre of mass did not evolve much. In fact, as seen on figure 13, the C atoms simply moved in the stability zone around the loop. An interesting phenomenon occurred in one of the simulations in the high binding energies category: the loop moved during the simulation while dragging the C atoms with it as seen in figure 14 through very-low migration energy transitions (around the meV). All the simulations in the high binding energies category were found to have the same ending, i.e. the two C atoms were situated in strong attractive positions at the end of the simulations.

For initial low binding energies configurations (with one C atom in a strong binding position and another one within the loop), two different endings of the simulations were reached. On the first scenario, the loop moves away rapidly from the C atoms because one C atom is within the loop. On the second scenario presented on figure 12(b) and illustrated on figure 15, the C atom within the loop moves as far as the loop periphery thus becoming strongly bound with the loop. Instead of having one C within the loop and only one anchoring point as the C atom at the external periphery like at the beginning of the simulation, there are now two strong anchoring points for the loop: the initial low binding energy configuration figure 15(a) became an initial high binding energy configuration figure 15(b) and just like other simulations of this category, the two C atoms moved freely around the loop (figure 15(c)). However, if the outcomes of the simulations in the low binding energies category are different, they share a particular detail: the C atom within the loop never moved towards the loop centre. This behaviour can be easily explained because
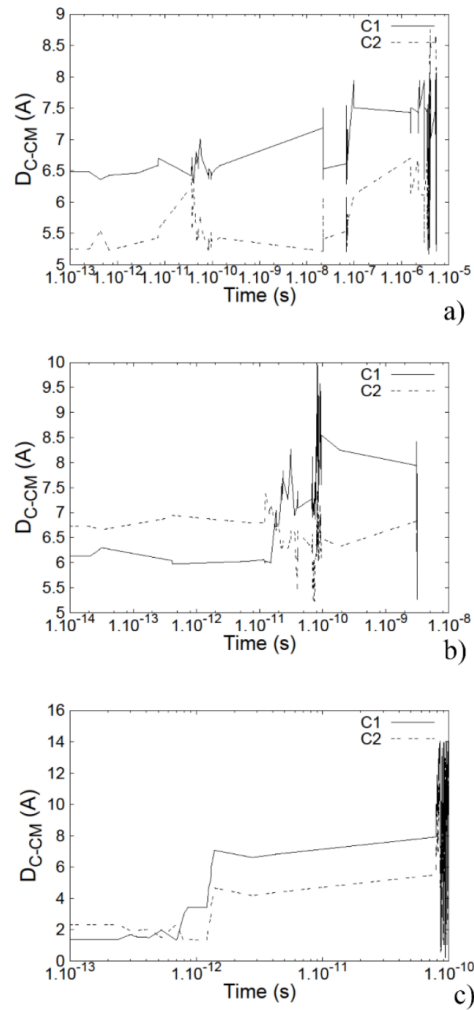
Figure 12. Evolution of the distance between the loop CM and the C atoms for k-ART simulations at 300 K with two C atoms representative of the three binding energy categories: high binding energies category (Eb = 0.91 eV (a)), low binding energies category (Eb = 0.23 eV (b)) and repulsive category (Eb = −1.29 eV (c)). The simulation boxes contain a loop and two C atoms as only defects in a $9 \times 9 \times 9$ bcc Fe matrix.

the closer the C atom to the loop centre of mass, the higher the total energy and so the lower the stability of the system.

The addition of another C atom tends to enhance all the phenomena occurring with one C atom, whether it is the loop unpinning from a C atom within it or the free movement of C interstitials around the loop. It can be easily explained for the first case because two repulsive forces will make the loop move faster. As for the second case, adding a C atom
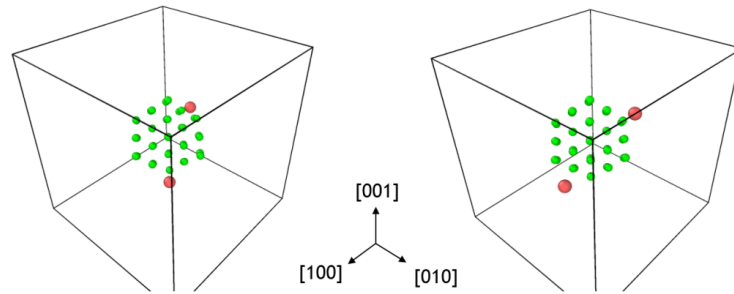
Figure 13. Initial (left) and final (right) configurations exhibiting the movement of the C atoms (red atoms) around the loop (green atoms) for a simulation with 2 C atoms bound to the loop at the beginning (Eb = 0.91 eV). The simulation contains a loop and two C atoms as only defects in a $9 \times 9 \times 9$ bcc Fe matrix (not represented for simplification sake).
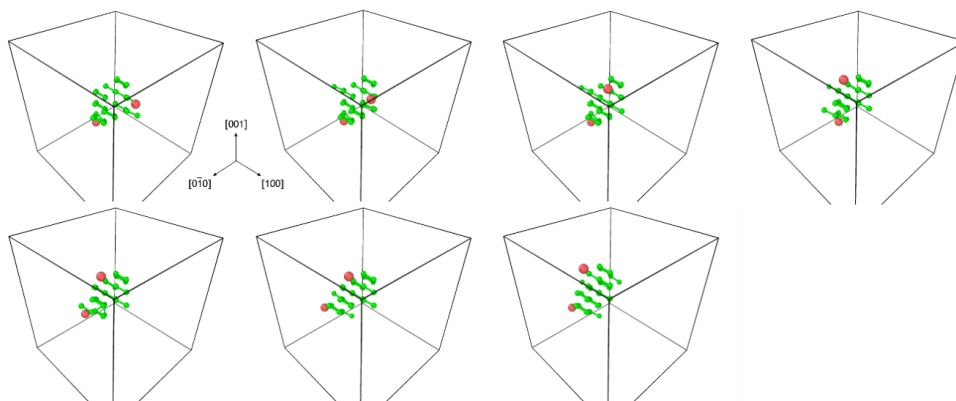
Figure 14. Snapshots of a k-ART simulation exhibiting the dragging effect of the loop (green atoms) which stays close to the C atoms (red atoms) when moving for a simulation with two C atoms bound to the loop at the beginning (Eb = 0.91 eV). The different snapshots were taken in a range of 20 steps with activation energies around 1 meV (steps with very low movements were skipped). Each step represents a simulated time between 10^{-15} s and 10^{-11} s. The box contains a loop and two C atoms as only defects in a $9 \times 9 \times 9$ bcc Fe matrix (not represented for simplification sake).
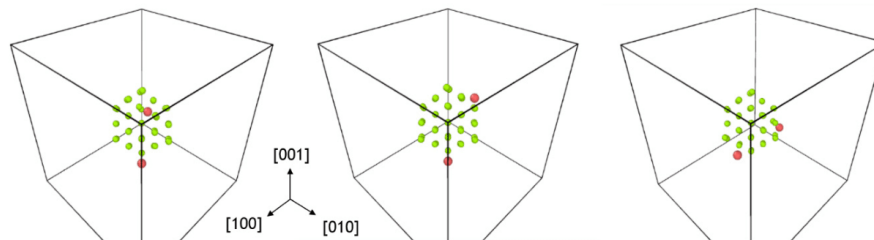
Figure 15. Representation of the evolution of a system with two C atoms (red atoms) and loop (green atoms) for an initial low binding energy configuration where 1 C is at the external periphery of the loop and the other one is within the loop (a). The snapshot (b) represents the moment the C atom within the loop went at the external periphery and (c) represents the end of the simulation. The simulation contains a loop and 2 C atoms as only defects in a $9 \times 9 \times 9$ bcc Fe matrix (not represented for simplification sake).

provides another anchoring point allowing the other C atom to move freely.

It seems obvious that two C atoms can pin the dislocation loop more efficiently than a single C atom because the second C atom provides an additional anchoring point; higher energy is therefore needed for the loop to unpin. Furthermore, just as in the case of the double kink mechanism [40], the whole loop can be dragged by the displacement of a single crowdion, therefore locking down two crowdions instead of one will result in lower chances for the loop to provide mobile crowdions which
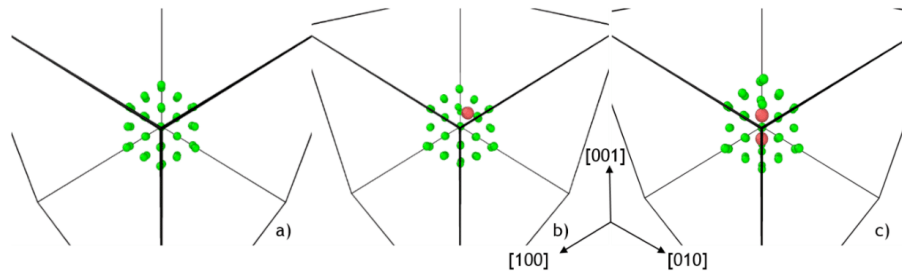
Figure 16. Loop distortion effect induced by the presence of two C atoms (red atoms) within the loop (green atoms), Eb = −0.60 eV (b) and Eb = −1.29 eV (c) comparing with the loop alone (a). The simulation contains a loop and two C atoms (only for (b)) and (c)) as only defects in a 9 × 9 × 9 bcc Fe matrix (not represented for simplification sake).

can drag the whole loop. However, no simulation with two C atoms has a simulated time higher than 10^{-4} s at 300 K so it is impossible to compare it with the simulations with one C atom. The main reason for that difference in the simulated time is linked to the presence of the second C atom. As this atom adds more possible transition at each step, with more low energy barriers (mainly between 0.2 and 0.5 eV, figure 11(b), the effective transition rate increases thus lowering drastically the time step. As seen previously, the great increase of the time step is due to a strong pinning of the loop removing the loop crowdions very-low barrier transitions thus leaving the C atom the only mobile defect. So adding another mobile C atom in this configuration results in a lower time step.

3.2. Influence of temperature

The temperature was then set at 600 K to investigate the effect of temperature. The main effect we observed is the enhanced mobility of the loop. Even in the simulations done with two C atoms, at this temperature, very few movements of the C atoms were found. The main drawback of this observation is the difficulty to interpret the results given by the simulations. Indeed, very-low migration energy events (flickers) lead to a significant decrease in the time step of KMCs and so on the simulated time. Fortunately, the simulated time of these simulations is reachable by molecular dynamics. Therefore, the effect of the temperature will be discussed only on MD simulations.

3.3. MD simulations

Simulations matching the KMC conditions were launched by MD, so with one and two C atoms, at 300 K and 600 K in a 9 × 9 × 9 box. For these simulations, the timestep is set to 1 fs in the NVE ensemble for a total simulated time of 100 ns. The same trends were found with both methods, even if some differences are observable: the C atoms still want to move towards the external periphery of the loop, the loop can be pinned by C atoms and when it is done, the C atoms can freely move around the loop. The main difference between KMC and MD simulation is the fact that for every simulation in the low binding energies category launched by MD with one C atom, the competition between the loop wanting to move and the C

atom wanting to go towards the loop periphery does not appear anymore. Indeed, at 300 K and even at 600 K, the C atom was never found to move to the external periphery of the loop, and while it can move a little, the loop rapidly goes away from it.

For all the simulations in the repulsive category launched (two C within the loop), at 300 K and 600 K, done by MD and KMC, the loop promptly goes away from the C atoms. Comparing this result with the simulations in the repulsive category with one C atom leads to the conclusion that even if the C atoms are pushed towards the loop external periphery, as proved by figures 11(a) and (b) where the migration energies of the C atoms are mostly lower than the migration energy of the C atom in a perfect Fe lattice, the repulsion between the loop and the two C atoms is too high for the loop to wait for the migration of the C atoms and so it rapidly moves away from the interstitials. The reason why the loop moves promptly can be explained by the high distortion of the loop induced by the presence of the two C atoms inside, even going as far as changing the crowdions alignment as seen on figure 16. The only possibility for the system to be stable again is the displacement of the loop. To prove the strength of this effect, even for an initial configuration with two C atoms very close (Eb = −0.6 eV), thus repelling each other, we observe that the loop moves first away from the C atoms, and then the two C atoms move away from each other. In only a very few number of simulations did we observe one of the C to jump before the loop went away, but the C atom never reached the loop external periphery. To conclude, the addition of a second C atom within the loop distorts the loop so much that it cannot stay close to the C atoms. They may rearrange but only after the loop has moved away.

Finally, the MD simulations with two C atoms were launched again but in a larger box, i.e. a 20 × 20 × 20 box (16 000 lattice Fe atoms, 19 SIA loop atoms and two C atoms) in order to check the impact of using small boxes and in particular interaction with the periodic images. An interesting phenomenon was observed for initial repulsive configurations. For all these simulations, at 300 K and 600 K, the loop rapidly moves away from the C atoms. However, when the loop comes back towards the C atoms because of the periodic boundary conditions, it moves back almost all of the time without crossing over the C atoms: the C atoms do not return back within the loop and so the loop is trapped in a back and forth movement
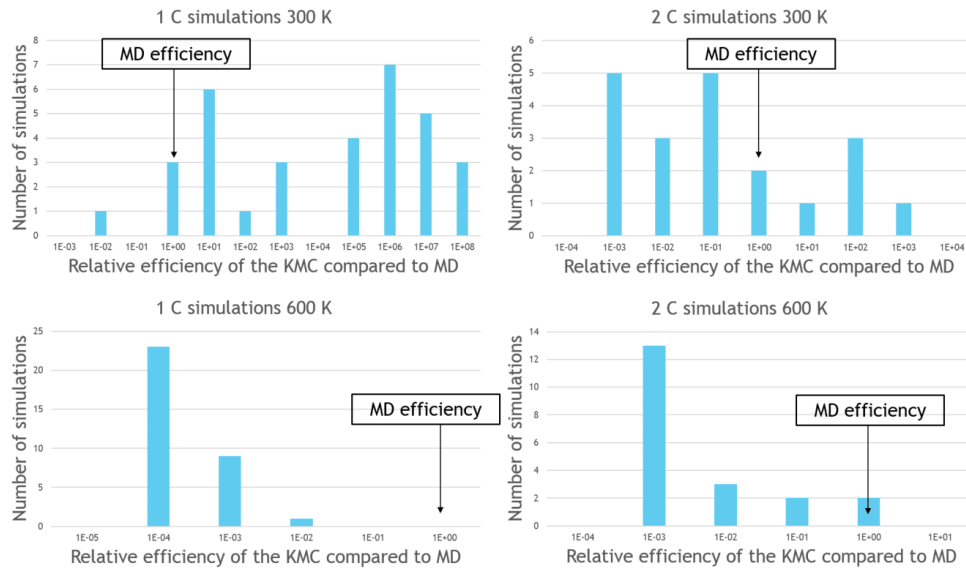
Figure 17. Relative efficiency of k-ART compared with MD for simulations with: one C atom at 300 K (a), two C atoms at 300 K (b), one C atom at 600 K (c) and two C atoms at 600 K (d).

between two C atoms. This indicates that a repulsion is occurring between the two C atoms and the loop even if the two C atoms are not directly within the loop: the loop needs a high energy in order to cross over these atoms. This can be seen on figure 7 where the C atom and the loop have a repulsing interaction even if the C atom is not within the loop.

This effect was not observed in $9 \times 9 \times 9$ simulations for two main reasons:

– the $9 \times 9 \times 9$ box is small, therefore the probability of the loop going back to the C atoms after it left is higher than in a $20 \times 20 \times 20$ and so is the probability of overcoming the energy barrier needed for the two C atoms to be in the loop again;

– as seen on figure 7, a repulsion is occurring between the loop and the C atom even if the C atom is not within the loop. In a $9 \times 9 \times 9$ box, the periodic images of C atoms help the loop to go through the C atoms in the initial box. In a $20 \times 20 \times 20$ box, the periodic images of C atoms are too far away from the loop to have an interaction with it.

4. Discussion

The interaction of solutes with interstitial loops stabilizes the i19 loop and reduce its mobility, which should slow down its growth. This is indeed observed with the effect of Mn and Ni (which have the largest concentration among other solutes in reactor pressure vessel materials) [41] in agreement with DFT calculations [14].

As seen in throughout this paper, the main effect of C atoms on loops is their pinning. The pinning time of the loop by the C atom can be estimated using an Arrhenius law with

an attempt frequency equal to 10^{13} Hz, the same as the one used by k-ART:

$$\frac{1}{t} = \omega_0 e^{-\left(\frac{E_d}{k_B T}\right)},$$

where t is the estimated average pinning time, ω_0 is the attempt frequency and $E_d = E_b + E_{migC}$ is the dissociation energy of the C-loop system. It was estimated that the loop will unpin from one C atom in 6.92×10^8 s at 300 K and in 0.008 32 s at 600 K. For the C2-loop system, if we suppose that the C atoms dissociates successively from the loop and do not recombine with it, the loop will unpin from the two C atoms in 1.38×10^9 s at 300 K and in 0.0166 s at 600 K. Therefore, at 300 K, the loop will never unpin from C atoms suggesting that the C-loop and the C2-loop systems needs to interact with other defects for the loop to unpin. However, at 600 K, the unpinning of the loop can occur with no external defects influence. The C2-loop system may even be hard to form because of the low pinning time of the loop by one C atom. Note that these calculations were done using the lowest value of a dissociation energy (i.e. $E_d = E_b + E_{migC} = 0.5 + 0.8 = 1.3$ eV) and that the pinning may be stronger between the loop and C atoms. This phenomenon is similar to what Veiga observed to C atoms in the vicinity of a screw dislocation [42] which have to overcome a high energy barrier to leave the dislocation. The pinning effect of C atoms can be extended to the study of the diffusion of carbon in a dislocation which is less mobile than a loop and then easier to pin (for same length defects). The main factor on the loop mobility is then related to the C concentration and more precisely the C atom placements. C atoms at the periphery of the loop will act as strong anchoring points, allowing other C atoms to come near.

13

Figure 17 summarizes the efficiency of the KMC and the MD methods for simulations at 300 K with one and two C atoms. The relative efficiency of the KMC compared to MD is calculated as such:

$$\eta = \frac{\text{Efficiency}_{\text{KMC}}}{\text{Efficiency}_{\text{MD}}} = \frac{\frac{\text{Simulatedtime}_{\text{KMC}}}{\text{CPUtime}_{\text{KMC}}}}{\frac{\text{Simulatedtime}_{\text{MD}}}{\text{CPUtime}_{\text{MD}}}}.$$

By looking at figure 17, one can observe the direct effect of the temperature on the relative efficiency of k-ART compared to MD: the rising of the temperature influenced only the KMC efficiency. The main reason of the lowering of the KMC efficiency can be seen in such that higher temperatures lead to higher transition rates and thus lower residence time. In order to enhance the KMC efficiency especially for high temperatures, a combination between a soft lattice where the system is distorted and a rigid lattice in the matrix can be made. Indeed, it seems wiser to develop a new method around the k-ART method than to a combination of meta-dynamics (for the thermodynamics of the system) and temperature accelerated dynamics to reach simulated times [43] of the second time scale at high temperatures.

5. Conclusions

We have determined the binding energy of a single C atom with a perfect $\langle 111 \rangle$ loop containing 19 SIA using DFT and a Fe–C empirical potential. Our results indicate that the most attractive configurations are the ones with the C atom at the external boundary of the loop (0.55 eV) because this is where they disturb the less the iron matrix and the most repulsive configurations are the ones with the C atom within the loop. Turning to kinetics, the main observation is the C atoms turning around the loop along a low-migration energy pathway at 300 K and 600 K.

At 300 K, when the C atom(s) are strongly bound to the loop, the pinning effect is so strong that the loop is never observed to go far from the C atoms in the simulation length spans (~0.2 s with one C atom and 10^{-5} s with two C atoms). When, in these configurations, the loop manages to move slightly, it drags the C atom(s) with it. At 600 K, one C atom does not provide a strong enough anchoring point to ensure that the loop will not unpin from it, however two C atoms in strong binding positions do most of the time. The dragging of the C atoms by the loop appear more often than at 300 K.

Within the short physical time simulated by accurate off lattice k-ART KMC, three possible mechanisms have been identified: unpinning of the loop from the almost immobile C atom, migration of the C atom around the loop, small motion of the loop dragging the C atom. Due to the time simulated, we have not been able to quantify these mechanisms in terms of diffusion coefficient or trapping time, indeed, the loop–C atom object is not immobile and some diffusion can be expected, as observed experimentally [44].

The k-ART method offers thus the possibility to explore complex mechanisms such as correlated migration of the SIA within the loop and the C atom migration in the distorted region around the loop. For the simulation of larger systems,

k-ART needs however to be coupled to metadynamics and/or lattice KMC.

ORCID iDs

R Candela ⬤ https://orcid.org/0000-0001-8263-9462
R G A Veiga ⬤ https://orcid.org/0000-0001-7035-1429

References

[1] Arakawa K *et al* 2014 One-dimensional glide motion of 'Naked' nanoscale 1/2$\langle 111 \rangle$; prismatic dislocation loops in iron *ISIJ Int.* **54** 2421–4
[2] Xu H, Stoller R E, Osetsky Y N and Terentyev D 2013 Solving the puzzle of $\langle 100 \rangle$ interstitial loop formation in bcc iron *Phys. Rev. Lett.* **110** 265503
[3] Arakawa K, Hatanaka M, Mori H and Ono K 2004 Effects of chromium on the one-dimensional motion of interstitial-type dislocation loops in iron *J. Nucl. Mater.* **329–33** 1194–8
[4] Becquart C S, Domain C and Foct J 2005 *Ab initio* calculations of some atomic and point defect interactions involving C and N in Fe *Phil. Mag.* **85** 533
[5] Becquart C S *et al* 2010 Modeling the long-term evolution of the primary damage in ferritic alloys using coarse-grained methods *J. Nucl. Mater.* **406** 39–54
[6] Anento N and Serra A 2013 Carbon–vacancy complexes as traps for self-interstitial clusters in Fe–C alloys *J. Nucl. Mater.* **440** 236–42
[7] Terentyev D *et al* 2011 Interaction of carbon with vacancy and self-interstitial atom clusters in α-iron studied using metallic–covalent interatomic potential *J. Nucl. Mater.* **408** 272–84
[8] Terentyev D, Anento N and Serra A 2012 Interaction of dislocations with carbon-decorated dislocation loops in bcc Fe: an atomistic study *J. Phys.: Condens. Matter* **24** 455402
[9] Tapasa K, Barashev A V, Bacon D J and Osetsky Y N 2007 Computer simulation of the interaction of carbon atoms

with self-interstitial clusters in α-iron *J. Nucl. Mater.*
361 52–61

[10] Chockalingam K, Janisch R and Hartmaier A 2014 Coupled
atomistic-continuum study of the effects of C atoms at α-Fe
dislocation cores *Model. Simul. Mater. Sci. Eng.* **22** 075007

[11] Khater H A, Monnet G, Terentyev D and Serra A 2014
Dislocation glide in Fe–carbon solid solution: from
atomistic to continuum level description *Int. J. Plast.*
62 34–49

[12] Cottrell A H and Bilby B A 1949 Dislocation theory of
yielding and strain ageing of iron *Proc. Phys. Soc.* A **62** 49

[13] Veiga R G A, Goldenstein H, Perez M and Becquart C S 2015
Monte Carlo and molecular dynamics simulations of screw
dislocation locking by Cottrell atmospheres in low carbon
Fe–C alloys *Scr. Mater.* **108** 19–22

[14] Domain C and Becquart C S 2018 Solute–$\langle 1 1 1 \rangle$ interstitial
loop interaction in α-Fe: a DFT study *J. Nucl. Mater.*
499 582–94

[15] Becquart C S *et al* 2007 Atomistic modeling of an Fe system
with a small concentration of C *Comput. Mater. Sci.*
40 119–29

[16] Kresse G and Hafner J 1993 *Ab initio* molecular dynamics for
liquid metals *Phys. Rev.* B **47** 558–61

[17] Kresse G and Hafner J 1994 Norm-conserving and ultrasoft
pseudopotentials for first-row and transition elements
Condens. Matter **6** 8245–57

[18] Kresse G and Hafner J 1994 *Ab initio* molecular-dynamics
simulation of the liquid-metal–amorphous-semiconductor
transition in germanium *Phys. Rev.* B **49** 14251

[19] Kresse G and Joubert D 1999 From ultrasoft pseudopotentials
to the projector augmented-wave method *Phys. Rev.* B
59 1758

[20] Perdew J P *et al* 1992 Atoms, molecules, solids, and surfaces:
applications of the generalized gradient approximation for
exchange and correlation *Phys. Rev.* B **46** 6671

[21] Varvenne C, Bruneval F, Marinica M-C and Clouet E 2013
Point defect modeling in materials: coupling *ab initio* and
elasticity approaches *Phys. Rev.* B **88** 134102

[22] Becquart C S *et al* 1997 Massively parallel molecular
dynamics simulations with EAM potentials *Radiat. Eff.
Defects Solids* **142** 9–21

[23] Veiga R G A, Becquart C S and Perez M 2014 Comments
on 'Atomistic modeling of an Fe system with a small
concentration of C' *Comput. Mater. Sci.* **82** 118–21

[24] Clouet E, Garruchet S, Nguyen H, Perez M and Becquart C S
2008 Dislocation interaction with C in α-Fe: a comparison
between atomic simulations and elasticity theory *Acta
Mater.* **56** 3450–60

[25] Veiga R G A, Perez M, Becquart C S, Clouet E and Domain C
2011 Comparison of atomistic and elasticity approaches
for carbon diffusion near line defects in α-iron *Acta Mater.*
59 6963–74

[26] Restrepo O A *et al* 2016 Diffusion properties of Fe–C systems
studied by using kinetic activation–relaxation technique
Comput. Mater. Sci. **112** 96–106

[27] Garruchet S and Perez M 2008 Modelling the carbon snoek
peak in ferrite: coupling molecular dynamics and kinetic
Monte-Carlo simulations *Comput. Mater. Sci.* **43** 286–92

[28] Gunkelmann N, Ledbetter H and Urbassek H M 2012
Experimental and atomistic study of the elastic properties
of α' Fe–C martensite *Acta Mater.* **60** 4901–7

[29] Sinclair C W, Perez M, Veiga R G A and Weck A 2010
Molecular dynamics study of the ordering of carbon in
highly supersaturated α-Fe *Phys. Rev.* B **81** 224204

[30] Domain C, Becquart C S and Foct J 2004 *Ab initio* study of
foreign interstitial atom (C, N) interactions with intrinsic
point defects in α-Fe *Phys. Rev.* B **69** 144112

[31] El-Mellouhi F, Mousseau N and Lewis L J 2008 Kinetic
activation-relaxation technique: an off-lattice self-learning
kinetic Monte Carlo algorithm *Phys. Rev.* B **78** 153202

[32] Béland L K, Brommer P, El-Mellouhi F, Joly J-F and
Mousseau N 2011 Kinetic activation-relaxation technique
Phys. Rev. E **84** 046704

[33] McKay B D 1981 Practical graph isomorphism *Congr. Numer.*
30 45

[34] Barkema G T and Mousseau N 1996 Event-based relaxation of
continuous disordered systems *Phys. Rev. Lett.* **77** 4358

[35] Malek R and Mousseau N 2000 Dynamics of Lennard-Jones
clusters: a characterization of the activation-relaxation
technique *Phys. Rev.* E **62** 7723

[36] Hepburn D J and Ackland G J 2008 Metallic-covalent
interatomic potential for carbon in iron *Phys. Rev.* B
78 165115

[37] Ventelon L *et al* 2015 Dislocation core reconstruction
induced by carbon segregation in bcc iron *Phys. Rev.* B
91 220102

[38] Ackland G J, Mendelev M I, Srolovitz D J, Han S and
Barashev A V 2004 Development of an interatomic
potential for phosphorus impurities in α-iron *J. Phys.:
Condens. Matter* **16** S2629

[39] Johnson R A, Dienes G J and Damask A C 1964
Calculations of the energy and migration characteristics
of carbon and nitrogen in α-iron and vanadium *Acta
Metall.* **12** 1215–24

[40] Domain C and Monnet G 2005 Simulation of screw
dislocation motion in iron by molecular dynamics
simulations *Phys. Rev. Lett.* **95** 215506

[41] Hernández-Mayoral M and Gómez-Briceño D 2010
Transmission electron microscopy study on neutron
irradiated pure iron and RPV model alloys *J. Nucl. Mater.*
399 146–53

[42] Veiga R G A 2011 Computational insights into the strain aging
phenomenon in bcc iron at the atomic scale *PhD Thesis*
INSA de Lyon

[43] Sorensen M R and Voter A F 2000 Temperature-accelerated
dynamics for simulation of infrequent events *J. Chem.
Phys.* **112** 9599–606

[44] Arakawa K *et al* 2007 Observation of the one-dimensional
diffusion of nanometer-sized dislocation loops *Science*
318 956–9

94

2. The MLKMC study

Having shown that C atoms can provide anchoring points for the loop, our next step is the study of a Cottrell atmosphere decorating the pinned loop. However, while being more efficient than MD on configurations with 1 or 2 C atoms at 300 K, adding more C atoms in the system will irremediably result in a drop in the time step of k-ART and thus a loss of efficiency. Therefore, the formation of the around the pinned loop has been studied using the MLKMC, considering that the loop will not unpin from the C atom. However, it was also observed that the migration energy of a C atom moving around the loop is lower than the C migration energy in the Fe bulk, thus making pointless the on-lattice zone as the only events that will be performed are the ones with the lowest energy. **To overcome this problem, it was chosen to divide the sum of transition rates for the k-ART zone by a factor 100 only if a unique C atom is present in the k-ART zone**. This approximation will not have much effect on C atoms outside of the k-ART zone, as the C-loop system will not move from the centre of the k-ART zone, but it will allow the MLKMC to get rid of undesired jumps that result only in the C atom in the k-ART zone turning around the loop. However, as a second C atom enters the k-ART zone, the sum of the transition rates returns to normal, as C atoms may now interact in the k-ART zone. Furthermore, the loop was observed to oscillate around its equilibrium position with very low energy barriers. These very low barriers (often called flickers in KMC simulations) make the KMC simulation impossible as very low energy events result in a very small time step. These oscillations of the loop are irrelevant when studying the formation of a Cottrell atmosphere of C atoms around the loop, as the loop is expected to be pinned to the C atom. **Therefore, another approximation made for these simulations is that Fe atoms are not allowed to move during the whole simulation in the k-ART zone, thus getting rid of the undesired and unrequired SIA loop movement. However, the Fe atoms will still be relaxed, meaning that the loop will always be in a local potential energy minimum.** Usually, this approximation can be applied simply by noticing it in the k-ART input file. However, for the particular case of the SIA loop, because the Fe atoms constituting the loop are very mobile, k-ART is likely to find transitions associated to Fe atoms. Therefore, to ensure that k-ART will not find Fe events, we specified in the additional conditions that no event related to Fe atoms shall be added in the catalogue. More precisely, even if k-ART is not researching events centred on Fe atoms (because we "told" k-ART not to do so), if during the generation of an event centred on a C atom a Fe atom has moved more than the C atom, this event will be categorized as a Fe event. Therefore, if during the generation of an event one of the Fe atoms has moved more than the C atom, the event is rejected (this condition was coded and added in the file "additional_conditions.f90").

A. Creation of the simulation box and systems studied

The studied system has approximatively 35 times more Fe atoms than the one studied by k-ART alone (in subsection 1. The k-ART study), i.e. a simulation box containing 54000 Fe atoms, a i19 loop and 10 C atoms. Ten simulations were launched with their only difference in the C atoms positions. Among the 10 C atoms in the system, 1 is placed directly next to the SIA loop in all the simulations to ensure the loop pinning. The other nine C atoms are placed randomly in one of all the O sites present in the system.

On these simulations, the k-ART zone is defined to match the k-ART simulations previously presented, i.e. a $9 \times 9 \times 9$ simulation box containing 1458 Fe atoms, a i19 DL and a C atom. One of the simulation supercells is presented on Figure 38 a), and the k-ART zone alone is shown on Figure 38 b).
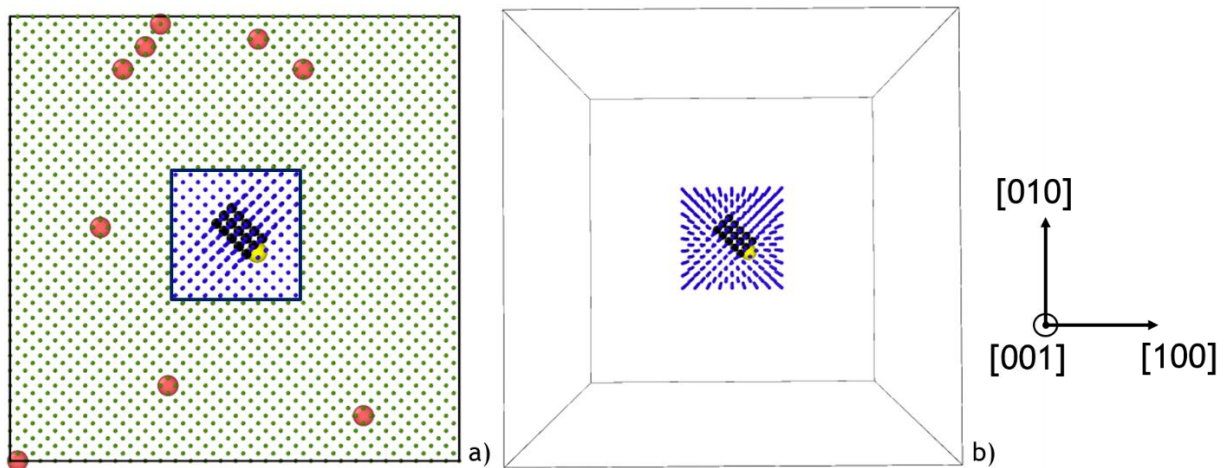
Figure 38: Example of a simulation box of a MLKMC simulation (a). The small green atoms are the Fe atoms in the rigid-lattice zone, the large red atoms are the C atoms in the rigid-lattice zone. All the atoms within the blue square are handled by k-ART, namely the Fe atoms (small blue atoms), the SIA loop (dark atoms) and the C atom (large yellow atom). The k-ART zone alone is displayed on b).

These ten simulations were launched at 300 K and 600 K, for a total of twenty simulations. The orientation of the system was ([100]; [010]; [001]), and PBC were applied in all directions. The BMRM was set with a barrier of 0.4 eV for an event to be considered in a basin. The migration energy for an event to be considered in a basin (and thus be treated with the BMRM) can not be higher than 0.4 eV or the whole zone around the loop might be considered as a single basin, meaning that a C atom coming at the vicinity of the DL should be expulsed right after coming due to the BMRM.

The migration energies of the C atom in the rigid-lattice zone were computed without the anisotropic elasticity, as the strain field induced by the dislocation loop is entirely covered by the k-ART zone. Indeed, it was observed in the k-ART study of the C-loop system that a C atom far from the DL had a migration energy very close to the migration energy of a C atom in a perfect Fe lattice. This means that only the C-C interactions are taken into account on the rigid-lattice zone.

Table 6 summarizes the simulation conditions.

Type of simulations	MLKMC
Defect investigated	I19 SIA loop
Simulation box size	X = 85.6596 Å, Y = 85.6596 Å, Z = 85.6596 Å
Number of Fe atoms	54 000 + 19 SIA
Number of C atoms	10
Box orientation	X = [100], Y = [010], Z = [001]
Boundary conditions	PBC in each direction
Temperature	300 K and 600 K
Size of k-ART zone	X = 25.69788 Å, Y = 25.69788 Å, Z = 25.69788 Å
Approximation in the k-ART zone	No Fe event, $\sum T_r$ in the k-ART zone divided by 100 if 1 C atom is in the k-ART zone
Approximation in the rigid lattice zone	$E_{mig_C} = E^0_{mig_C} + \Delta E_{C-C}$
Number of cores	16
Average number of KMC steps	5010
Average CPU time per core	4.5 days
Average simulated time at 300 K	0.4 hours
Average simulated time at 600 K	1.82 10^{-5} s

Table 6: Simulation conditions for MLKMC simulations containing an i19 loop and 10 C atoms in a 54000 Fe simulation box.

B. Results

The evolution of the distance between the centre of the loop and all the C atoms, C-DL, is a simple way of inspecting the formation of the Cottrell atmosphere. This distance is expected to lower as the Cottrell atmosphere grows, and to stabilize when the Cottrell atmosphere is fully formed. Indeed, the most stable configurations for the C atoms are at the external periphery of the loop, and therefore the C atoms will irremediably be found at the most stable configurations for long enough simulations due to the nature of Monte-Carlo methods. Therefore, the C-DL distances are presented on Figure 39 (simulations at 300 K) and Figure 40 (simulations at 600 K).
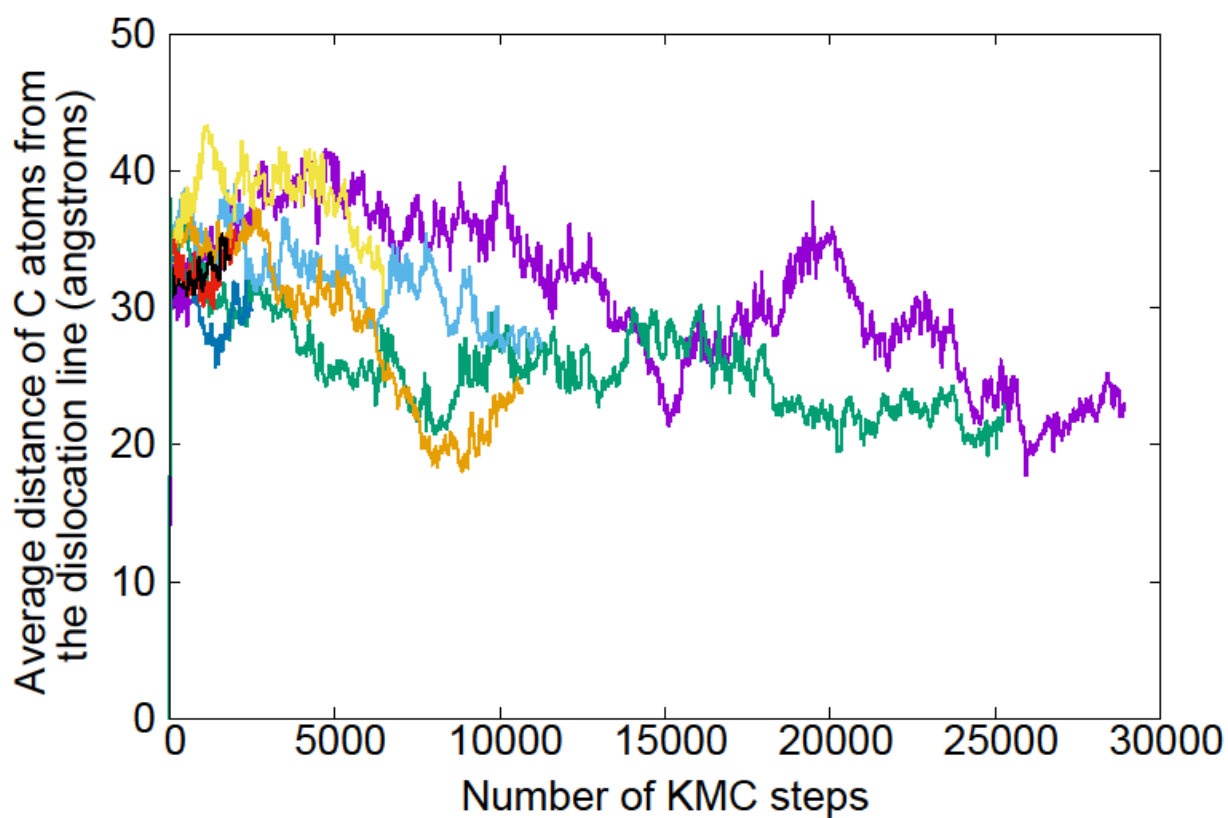
Figure 39: C-DL distances versus the number of steps for all the MLKMC simulations launched at 300 K containing a i19 DL and 10 C atoms. One line represents one simulation.
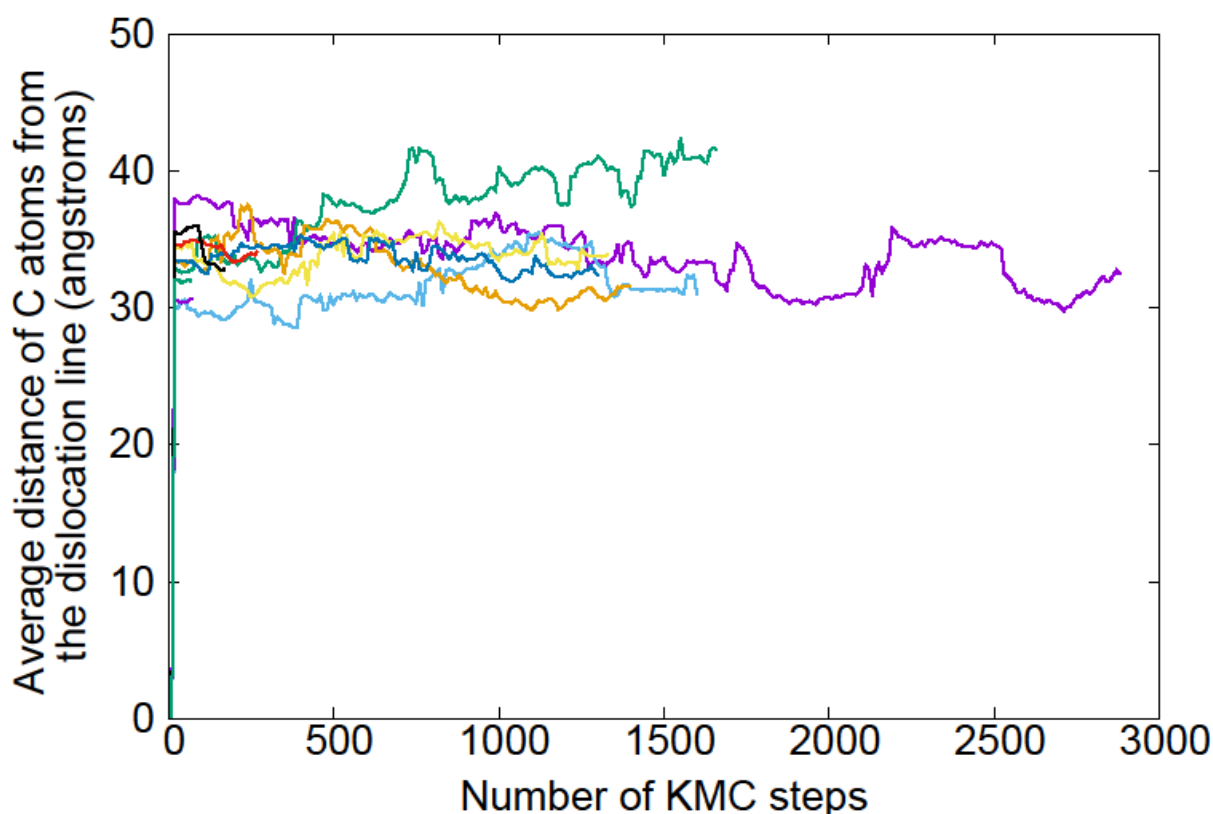
Figure 40: C-DL distances versus the number of steps for all the MLKMC simulations launched at 600 K containing a i19 DL and 10 C atoms. One line represents one simulation.

It was observed that at 300 K (Figure 39), only 4 simulations have done more than 10 000 steps (purple, light blue, green and orange lines). For these three simulations, the overall C-DL distance has decreased by approximatively 10 Å (from 33 to 23 Å). However, on all the other simulations whether the temperature is set at 300 or 600 K, the average C atoms-dislocation loop distances were not observed to evolve much. This effect is particularly striking for the simulations at 600 K (Figure 40), where only few steps were made and where all the lines are overall flat despite an average CPU time of 5 days for simulations running on 16 cores.

The same behaviour was observed for all the simulations launched at 600 K, therefore only one representative example will be detailed to explain the small number of steps of these simulations. For this simulation, we represent in Figure 41 a) the initial configuration and in Figure 41 b) a configuration observed in the simulation where the C atom went a little away from the loop (while still being strongly bound to the loop). For the initial configuration of this simulation (Figure 41 a)), the migration energies of the C atom in the k-ART zone are too low for any other C atom to move. This effect lasts for approximatively 50 steps until the C atom at the external DL periphery (so in the k-ART zone) goes a little further away from the loop in a configuration where its migration energies are higher (an example of this configuration is shown on Figure 41 b)). For the configuration shown in Figure 41 b), the lowest migration energy of the C atom close to the DL (in blue) is 0.72 eV. Considering that the other C atoms have migration energies of 0.815 eV, the atom close to the DL should move again. However, because of the approximation made to divide by 100 the sum of the transitions rates of k-ART if 1 C atom is in the k-ART zone, the C atoms in the rigid-lattice zone are able to perform some steps. After few tens or

hundreds of steps in the rigid-lattice zone, the C atom in the k-ART zone moves again close to the dislocation loop where it has very low migration energies until it reaches a configuration where it has higher migration energies, thus repeating the same loop of events.
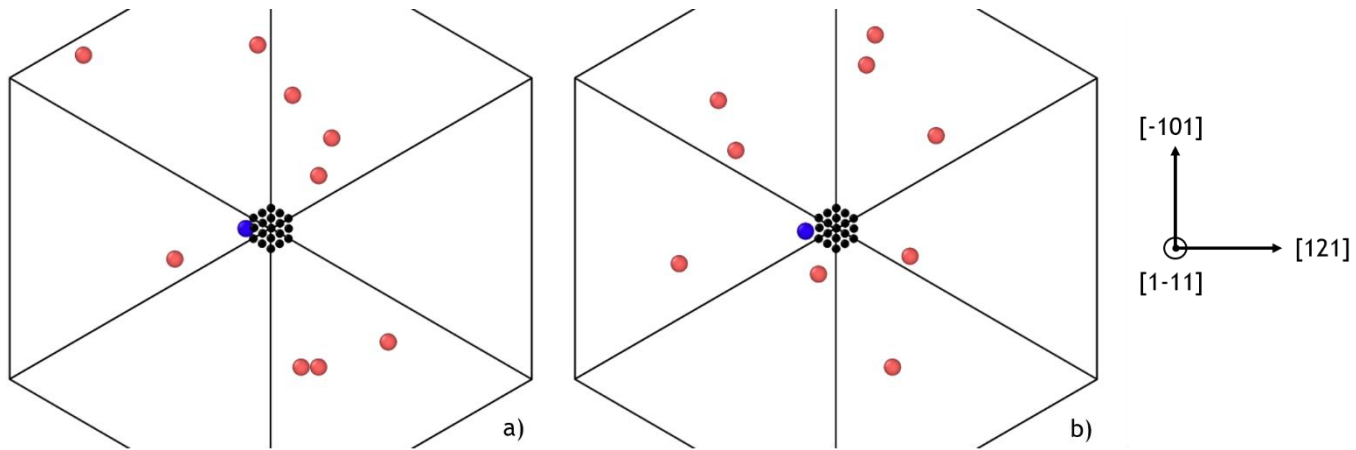
Figure 41: Example of an initial configuration a) and a configuration where the C atom in the k-ART zone has high migration energies b) of the 10C-loop system. Only when the C atom is further away from the DL, can the other C atoms move in the simulation box. The dark atoms represent the loop, the red atoms are the C atoms in the rigid-lattice zone, and the blue atom is the C atom in the k-ART one (close to the DL). The Fe matrix is not represented for comprehension sake.

However, when another C atom finally enters the k-ART zone, the sum of transitions rates of the C atoms in the k-ART zone is not divided by 100 anymore. This means that the C atom close to the dislocation loop will have more chance to move even when in a configuration with high migration energies. For instance, on the presented simulation, the configuration Figure 41 b) represents the step 1098. On the same simulation, another C atom enters the k-ART zone at the step 1164. The migration energies for the C atoms in the k-ART zone are shown in Figure 42 for the steps 1097, 1098 and 1165, so respectively for the step where the C close to the DL goes to in a configuration where it has high energy barriers, the step where the C atom close to the DL has high energy barriers, and the step after another C atom entered the k-ART zone.

As seen on Figure 42 (the blue column), the C atom close to the DL has 2 possible events with a 30 meV migration energies at step 1097. This very-low barriers means that the chosen event will be an event treated with the BMRM, and the C atom was put a little further away from the loop (as seen on Figure 41 b)). On this particular configuration (thus at step 1098), the C atom close to the DL has higher energy barriers, from 0.72 to 0.92 eV (Figure 42, red bars). When another C atom enters the k-ART zone at step 1164 (configuration shown in Figure 43), the migration energies of the C atom close to the DL are not impacted: on Figure 42, the green bars match the red bars. On the meantime, the other C atom in the k-ART zone has migration energies very close to the C migration energies in the Fe bulk (4 jumps at 0.81 eV, yellow bar on Figure 42). The important result is that now that another C atom has entered the k-ART zone, the C atom close to the dislocation line will move much more until the other C atom leaves the k-ART zone because the sum of transition rates of C atoms in the k-ART zone is not divided by 100 anymore. In other terms, it will be hard to construct a Cottrell atmosphere using the MLKMC because of this effect. However, it could be possible to avoid this problem by different means:

- It can be possible to fix C atoms when they are at the external periphery of the loop by coding it in the additional conditions file (the same method applied to fix the loop). It would require to know the position of the centre of mass of the DL and each of the crowdion constituting the

loop for all steps performed in the k-ART zone. If a C atom arrives close enough to the loop centre of mass and is very close to one or two crowdions only, this C atom is fixed. Indeed, if the C atom is very close to more than 2 crowdions, it means that the C is under or above the loop when looking at the ⟨111⟩ direction (in a repulsive configuration), and not at the external periphery of the loop. However, fixing C atoms as they arrive close to the DL could bias a lot the kinetics. Indeed, the C-C interactions being repulsive, a single C atom moving rapidly around the loop could prevent any other C atom to come close to the DL.

- Another possible mean to deal with this problem would be to implement in k-ART a way to treat analytically the C atom(s)-loop system, or to treat the C-loop system as an object in a hybrid AKMC/OKMC simulation. In this method, the C-loop system would be given emission and absorption properties, allowing the loop to absorb or expel C atoms.

- Finally, the method used to study the formation of a Cottrell atmosphere around a loop could be completely changed, and one could use temperature accelerated MD (Sorensen and Voter, 2000) to see if other C atoms can come close to the dislocation loop when a C atom is moving around this loop.
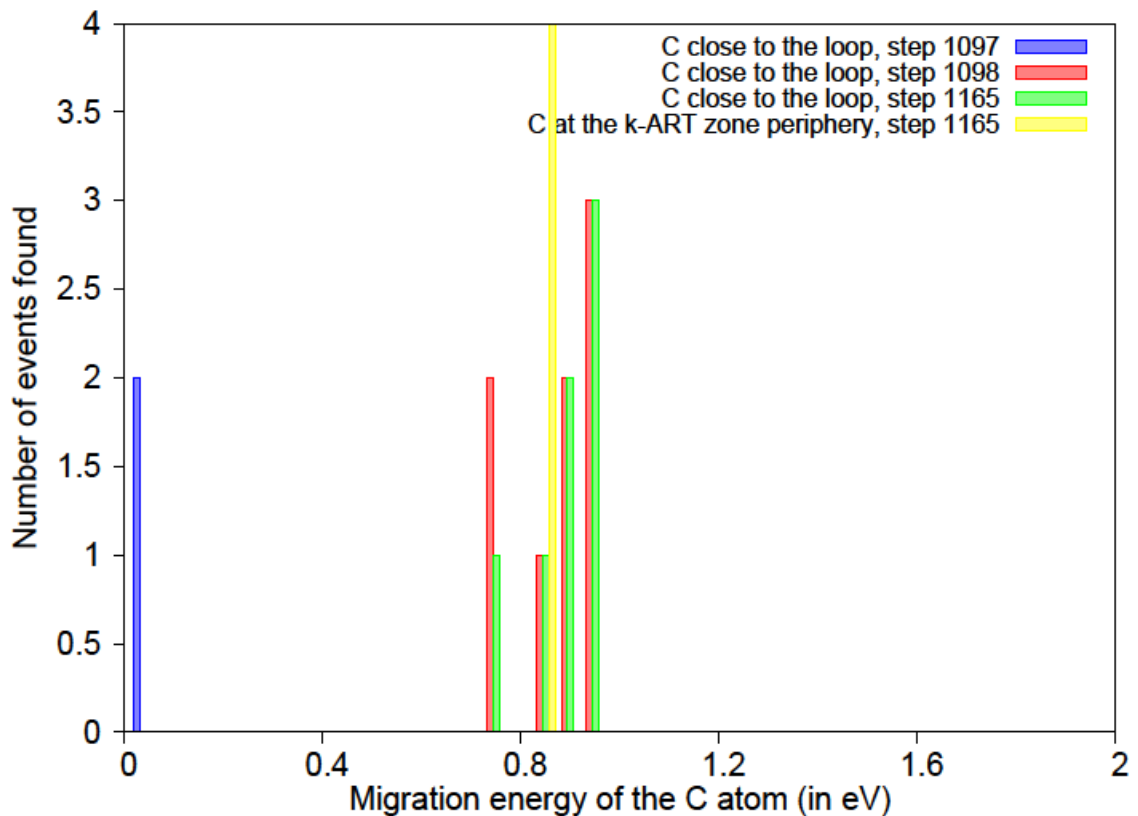
Figure 42: Migration energies for the C atoms in the k-ART zone for a typical MLKMC simulation containing 10 C atoms and a DL. At step 1164, another C atom enters the k-ART zone (for a total of 2 C atoms in the k-ART zone), therefore its migration energies are also shown in this histogram for the step following its arrival to the k-ART zone.
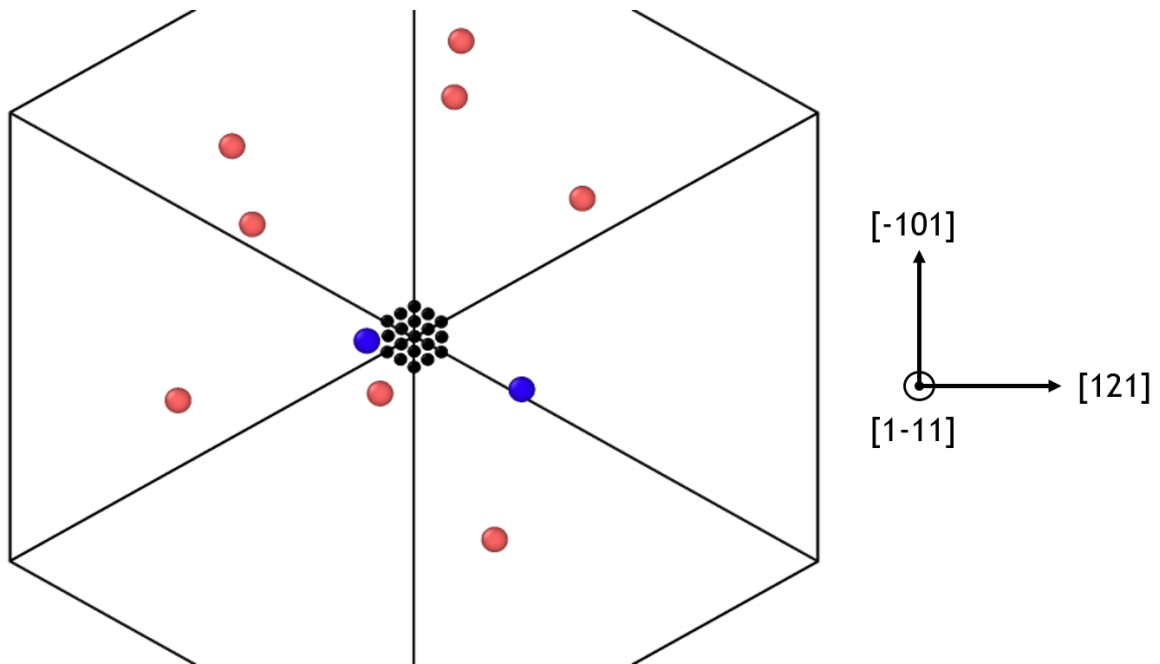
Figure 43: Configuration at the beginning of step 1165 on the chosen simulation where another C atom has entered the k-ART zone. The dark atoms represent the loop, the red atoms are the C atoms in the rigid-lattice zone, and the blue atoms are the C atoms in the k-ART one. The Fe matrix is not represented for comprehension sake.

DFT and EP calculations showed that the most stable configurations for the C atoms are at the external periphery of the loop. It was also shown that a stability zone around the loop allows the C atoms to freely move around the loop with low energy barriers. Pursuing the study using our MLKMC approach, we show that the method is not really suitable to study the formation of a Cottrell atmosphere around the loop, even if one fixes the Fe atoms so as to remove all the Fe low energy migrating events corresponding to the crowdions motions in the loop. The issue in this particular simulation is the low migration energies of the C atoms around the loop which prevent the other C from moving. A possible solution to deal with this issue would be to fix the C atoms as they arrive at the loop external periphery, but this would bias the physics too much as the C atom moving around the loop could prevent other C atoms arrival.

Chapter V. Results: the screw dislocation

In this chapter, we present MLKMC simulations containing a screw dislocation in a 36 000 Fe atoms simulation box with 10 or 25 C atoms. The aim of these simulations is to study the kinetics of the Cottrell atmosphere formation.

A. Creation of the simulation box

The creation of a system containing a dislocation is not a trivial operation. In our case, we followed the procedure described below:

- First comes the creation of a unit cell of Fe atoms for the desired orientation. If the orientation is different from ([100][010][001]), this task can be performed with atomsk (Hirel, 2015). Then, this unit cell is duplicated to match the user's will.

- Secondly, all the different O sites and T sites of the system are found. For that purpose, it is important to remember that O sites are found between two Fe separated by a_0 Å. The Fe-Fe distances are thus computed, and if equal to a_0, an O site is detected and stored. The variant of the O site is computed as well (it is needed for the binding energies between the C atom in this O site and the dislocation computed with anisotropic elasticity (equation 36)). Once all the O sites are found, the T sites are researched between two adjacent O sites separated by a distance of $\frac{a_0}{2}$ Å. The T site variant can be easily deduced from its adjacent O sites variants. At the end of this step, all the O and T sites of the system as well as their variants are computed.

- The dislocation is then introduced within the simulation box using the anisotropic elasticity theory. This step is done using the code Babel (Clouet, 2007). During this operation, the binding energies of a C atom within each O site and T site with the dislocation is computed according to their variant. Therefore, at the end of this step, all O and T site positions along with the Fe atoms are known with respect to the dislocation.

- Then, the O sites and the T sites are linked. More precisely, the four adjacent O sites and T sites are found for each O site, and the two adjacent O sites are searched for each T sites. These values are then stored to be used whenever a C atom is in the on-lattice zone.

- Finally, the appropriate number of C atoms is added (as defined by the user) randomly on different O sites. Note that one C atom has to be added close to the dislocation in order to provide an anchoring point for the dislocation. Furthermore, the MLKMC can not be launched when no event is present in the k-ART zone (k-ART does not allow it for now). The simulation box is then be relaxed; however, this is not a necessary step as k-ART relaxes the whole configuration before the first step. The relaxation before k-ART does it may even induce some undesired effects on particular systems, for example in high C concentrations systems, the bulk can be distorted enough on some particular points for the MLKMC algorithm not to be able to determine if two C atoms 4 NN have or have not a Fe atoms between them.

With this newly created system along with the O sites and T sites list, the MLKMC simulation can be launched.

B. Calculating the migration energies

Unlike the case of a SIA loop, introducing a screw dislocation within the simulation box induces a long-range distortion in the Fe matrix. This effect is notably expressed in the change of the C migration energy when a C atom goes from the on-lattice zone to the k-ART zone. Indeed, in addition to finding the possible transitions as well as their associated migration energies, k-ART is also able to find the inverse transitions of each of the transitions find. More practically, this means that when a C atom enters the k-ART zone at step n, k-ART will also compute, at step $n + 1$, the migration energy of the event that allowed the C atom to enter the k-ART zone at step n. Therefore, by comparing the migration energies predicted by k-ART and the migration energies predicted by the on-lattice KMC for the same event, one can check whether a continuity in the migration energy exists between the k-ART zone and the on-lattice zone. If this continuity was indeed observed for a C atom approaching a SIA dislocation loop, discrepancies were observed for almost all events for a C atom approaching the screw dislocation. This means that the elastic effect of the dislocation must be considered to ensure kinetically correct simulations.

For that purpose, as seen in section "Chapter III. Results: the Mixed-Lattice Kinetic Monte-Carlo 5. B. c. Taking into account the distortion of the system", the impact of the dislocation on the migration energy of the C atom in the bulk can be computed. Knowing that a C jump consists in the C movement between two adjacent O sites with the saddle point in a T site, the possible transitions can be easily found knowing the distances between O and T sites. The migration energies are then easily computed with equation 28. Therefore, the migration energies of the C atom can be mapped (Figure 44).
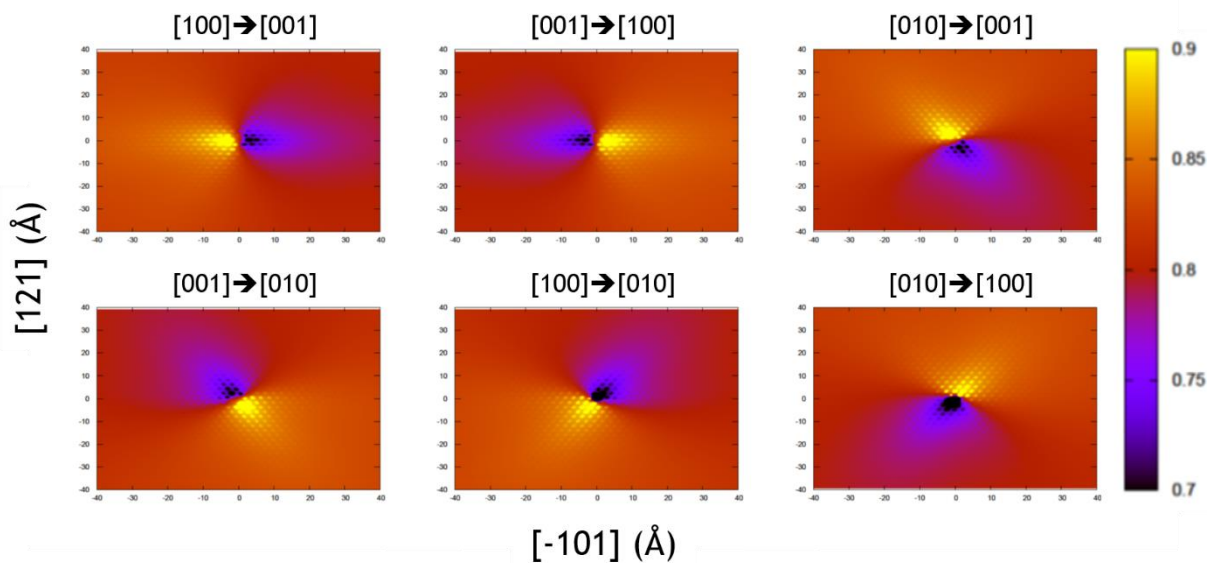
Figure 44: Mapping of the C migration energies (in eV) for C positions around a screw dislocation. The migration energies are predicted by anisotropic elasticity and displayed for the 6 possible different variant jumps.

These results can be compared with the ones obtained by Veiga & al. (Veiga et al., 2011). While a direct comparison is nearly impossible because the list of all migration energies was not displayed, one can notice that the trends are the same between the results obtained in this work and the ones obtained by Veiga. In order to implement these results in the rigid-lattice KMC, the list of all O sites and T sites along with the binding energies of a C atom in these sites must be provided (the results obtained with Babel).

Two main results are obtained from this set of data:

Firstly, the way for a C atom to reach the dislocation is not so straightforward, as can be seen on Figure 44, as the C possible jumps are strongly impacted by the O site variant the C atom is in. A schematic representation of the impact of the 6 variants shown on Figure 44 is presented on Figure 45 a). It is possible to deduce from this representation that there are zones where a C atom will not be seen in a particular O site variant because of the high energy needed for a C atom to go in that variant. These zones are represented on Figure 45 b): the red zone represents the area where a C atom will not jump to an O site in the variant [001], the green zone represents the area where a C atom will not jump to an O site in the variant [010] and the blue zone represents the area where a C atom will not jump to an O site in the variant [100]. **Furthermore, the overlapping of two zones indicates that only one variant will be favoured, meaning that a C atom in the overlap of two zones will be trapped in a high migration energies configuration.**

Secondly, the sink effect of the dislocation, while being visible in the migration energies, is not significant enough to drag the C atom towards the dislocation. For example, a C atom in the [100] variant has almost the same migration energies when jumping to an adjacent [001] O site whether the C moves towards the dislocation or away from it (the differences between the migration energies is lower than 10 meV). To prove that point, the migration energies of the C atom predicted by k-ART are shown on Figure 46 for several C-dislocation distances. On this figure, it is shown that the asymmetry in the migration energies, i.e. the sink effect of the dislocation, is visible only for C-screw dislocation distances lower than 8 Å. **In other terms, the screw dislocation in α-Fe is a narrow sink, attracting the C atoms only if the C atom is 8 Å from the dislocation. However, the dislocation impacts the C migration even at long range (the C migration energies are changed according to the variant the C atom is in).**

a)   b)
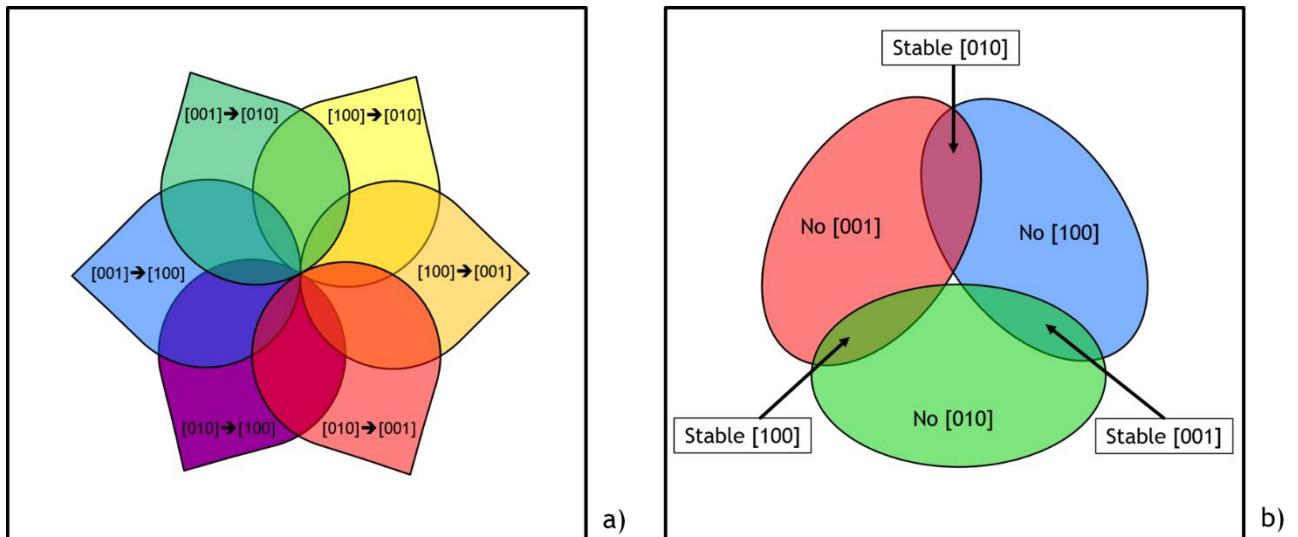
Figure 45: Schematic representation of the preferred variant diffusion (addition of all the 6 images presented on Figure 44) a) and representation of the zones where one variant type are excluded b). Figure b) is simply obtained by summation of Figure a). On Figure b), the red zone represents the area where a C atom will not jump to an O site in the variant [001], the green zone represents the area where a C atom will not jump to an O site in the variant [010] and the blue zone represents the area where a C atom will not jump to an O site in the variant [100]. The overlapping of two zones means that a single variant will be favoured, i.e. that a C atom can be trapped.
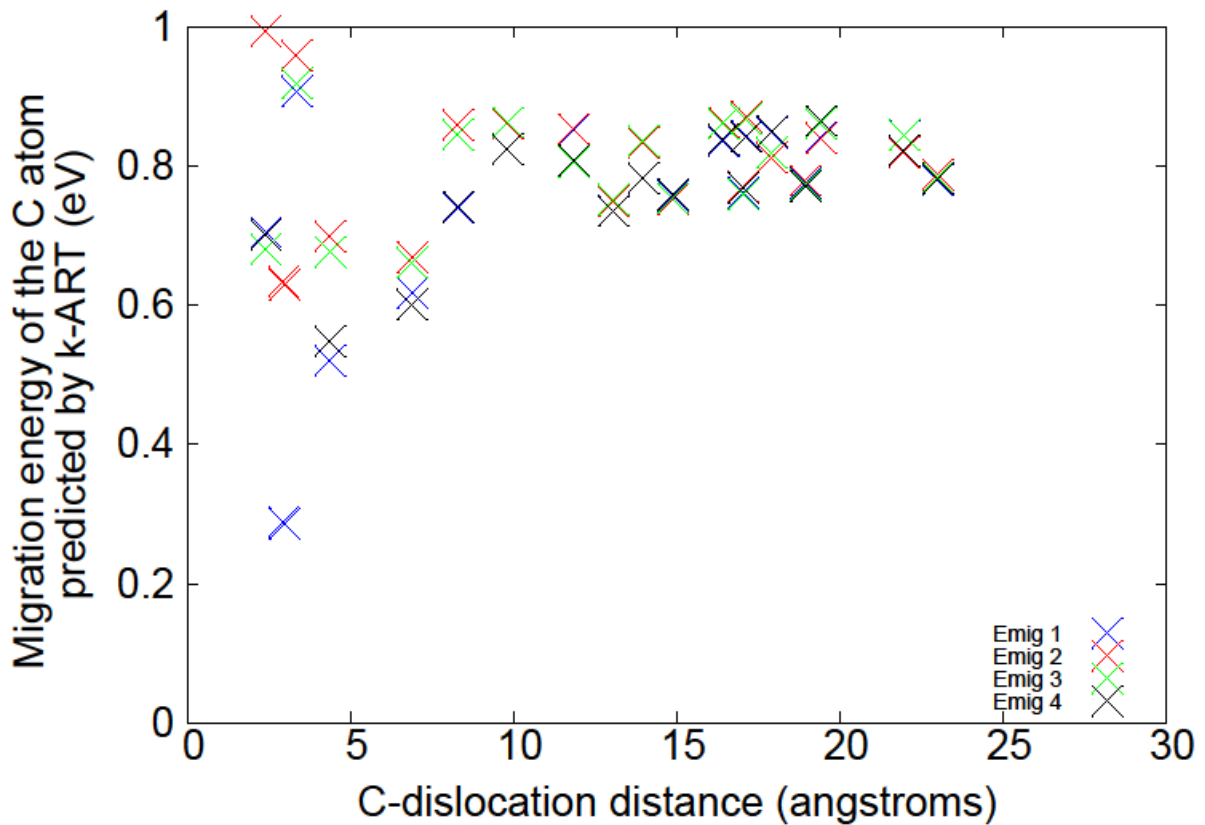
Figure 46: C migration energies predicted by k-ART for several C-dislocation distances in a simulation box containing 1 C atom and a screw dislocation in the centre of the box. The asymmetry in the migration energies, i.e. the fact that depending on the motion direction (towards or outwards the dislocation line), the migration energies are different, starts to show for C-dislocation distances lower than 8 Å. The migration energies higher than 1 eV are not shown in this plot because they will never be chosen in the KMC.

We can conclude from this set of data by saying that all the C possible positions with respect to the dislocation are not equivalent (some configurations are highly improbable). **More practically, this means that is it very likely to see the C atoms diffuse through the same paths, and knowing that the screw dislocation is $\frac{1}{2}\langle 111 \rangle$ periodic, it is very probable to see several C atoms lined up in the $\langle 111 \rangle$ direction.** Furthermore, as seen on Figure 47 which represents the binding energies of the C atoms in different O sites with the screw dislocation, not all C positions are stable according to the dislocation. Indeed, the higher the C-dislocation binding energy, the more stable the configuration. Therefore, it is expected to see the C atoms go at the most stable positions, namely O sites numbered 6, 15, 16, 20, 23, 32, 34, 35 and 37 in Figure 47.
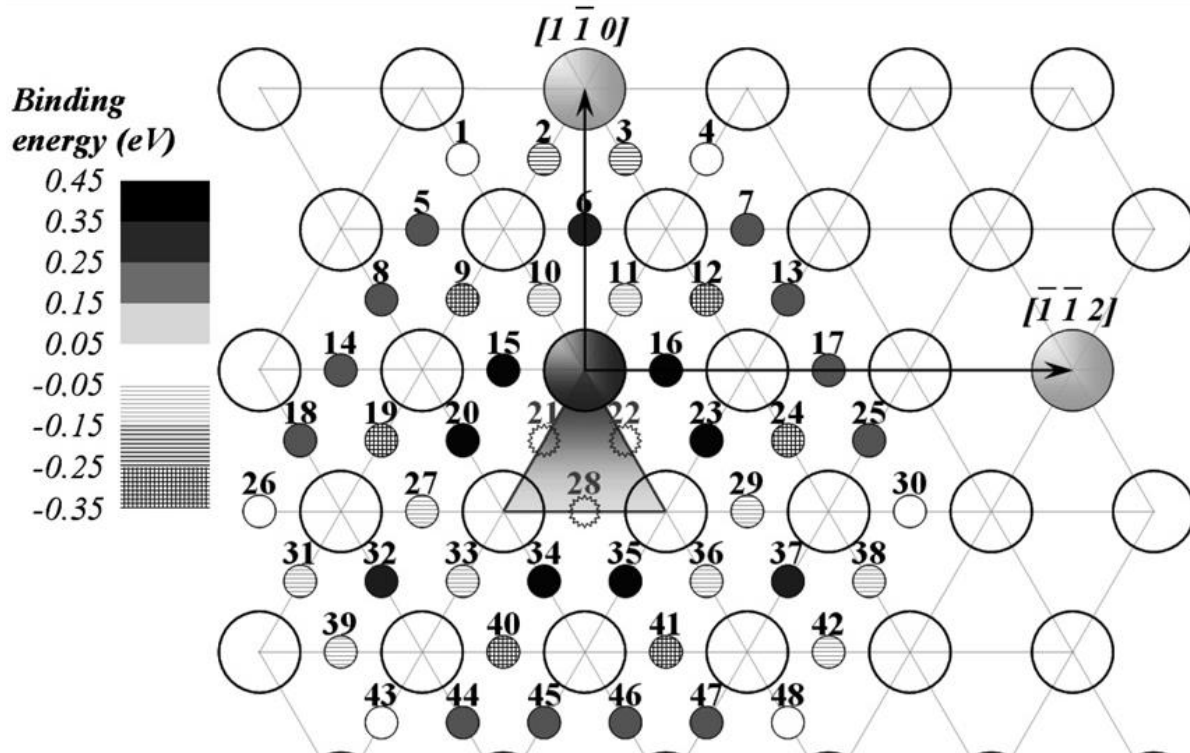
Figure 47: Binding energies of the C atoms in O sites with the screw dislocation. The O sites are represented by the small numbered circles which are coloured according to the binding energies between the C atom and the dislocation. The large circles represent the Fe atoms, and the screw dislocation is represented by the triangle. Figure taken from reference (Becquart et al., 2007).

C. Optimizing the k-ART parameters

The time needed for k-ART to perform a step is approximatively 10^5 to 10^7 times higher than the time needed for an on-lattice step to be performed. This means that, even during a simulation where a thousand times more steps are performed in the rigid-lattice zone than in the k-ART zone, k-ART is still the time limiting factor. Furthermore, without a proper parametrization, false events can be generated (e.g. and C jumping to a 2nd NN O site instead of the 1st) or some events can be missed. Therefore, a series of k-ART only calculations testing the different parameters has been launched with a simulation box containing 1 C atom and a screw dislocation. The different parameters that need to be optimized are among others the energy for an atom to be considered within a basin (for the BMRM treatment) and the number of searches per topology to ensure that k-ART will find all the possible transitions at each step. For that purpose, the same simulation box containing a single C atom within a screw dislocation line as shown in Figure 48 was launched 13 times with different parameters (see "Annexes 2. Parameters optimized for the MLKMC simulations containing a screw dislocation").

Even if these 13 simulations were not all fully optimized (as their purpose was to search for the optimal parameters), the results they provide can still be exploited (except in some rare cases), because the consequences of not being fully optimized are that simulations can take more time to perform steps, or that some events can be missed.
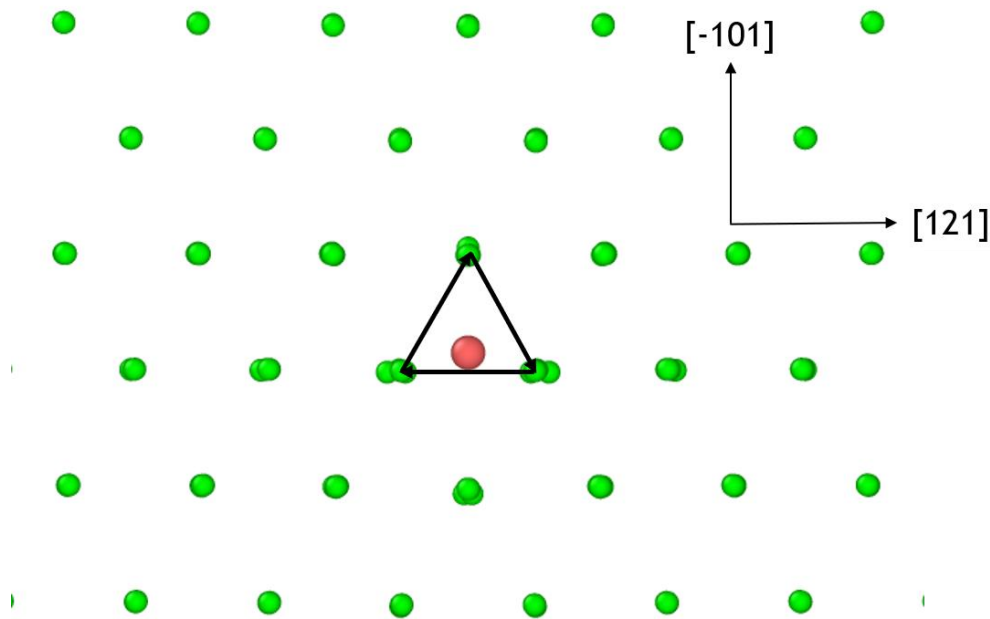
Figure 48: Initial configuration of a C atom (red atom) within the dislocation line in Fe (green atoms). The arrows represents the dislocation.

In most of the cases, the C atom went out of the dislocation line through a small energy barrier path (7 meV). This event was found to be highly asymmetrical, meaning that the energy barrier of the inverse event is different from this event energy. Indeed, for the C atom to get back into the dislocation line, the energy was predicted by k-ART to be 0.45 eV. One can deduce from these statements that a C atom alone is unlikely to be found within the dislocation line. Note however, that even if the energy to get back to the dislocation is close to 100 times more than the energy to go out of the dislocation line, it is still low compared to the C migration energy in bulk (0.815 eV). As a result, in all these test cases, the C atom was never once observed to leave the dislocation (i.e. go further than 5 Å from the dislocation line) for times up to $3.6 \ 10^3$s, reinforcing the idea of the dislocation acting as a sink for C atoms.

On three different simulations, it was observed that a C atom had diffused within the dislocation line. This pipe diffusion occurs with the C atom jumping from three equivalent positions according to the threefold symmetry of the screw dislocation, as seen on Figure 49 (four different positions a, b, c and d corresponding to three events, from a to b, from b to c and from c to d). Because all of these positions are equivalent due to the dislocation symmetry, the C migration energy of the three events seen on Figure 49 are the same, i.e. 0.413 eV. This mechanism is presented in this section to prove that the number of searches per topology is an essential k-ART parameter to optimize, as a low number could result in false kinetics. Indeed, the pipe diffusion was observed especially because the event for the C atom to move outside the dislocation line was not found by k-ART, indicating that a high number of researches per topology is a necessity for a complete description of the C migration close to the dislocation. This number was thus set at 60 to ensure that all events are found at each step by k-ART.
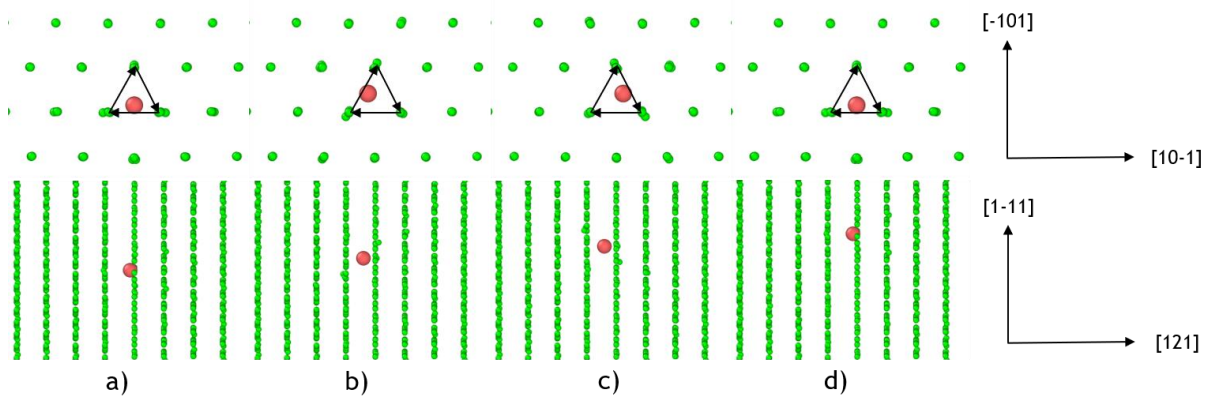
Figure 49: Pipe diffusion occurring for the C atom (red atom) within the screw dislocation line represented by the arrows in a α-Fe matrix (green atoms). The four configurations of the C atoms represented (a, b, c, d) represents the four first steps of the KMC. The positions a, b, c and d are equivalent according to the threefold symmetry of the screw dislocation. Moreover, the positions a and d are also equivalent according to the screw dislocation line, i.e. distanced by exactly $\frac{1}{2}a_0\|\overrightarrow{111}\|$.

It is important to notice that Veiga also observed pipe diffusion for a single C atom close to the screw dislocation line, but with a migration energy of 0.738 eV (Veiga, 2011) when we find a migration energy for the pipe diffusion at 0.413 eV. Two differences can explain this discrepancy. The first one is that Veiga observed pipe diffusion for temperatures above 750 K while our simulations are launched at 300 K. The second one is that Veiga observe pipe diffusion for C atom – screw dislocation distances up to 1 nm, while the only pipe diffusion we observe is when the C atom is within the dislocation line (i.e. C atom – screw dislocation distances up to 1 Å).

D. The 10 C – screw dislocation system

Ten different configurations containing 10 C atoms, 36 000 Fe atoms and a screw dislocation placed in the centre of the simulation box were the starting point of MLKMC simulations. These simulations were launched at 300 K and 600 K, for a total of twenty simulations. Contrary to the dislocation loops simulations, PBC were applied only in the dislocation line direction and free surfaces were applied on the other directions. The BMRM was activated with an energy barrier of 0.4 eV for an event to be considered within a basin. The orientation of the system was ([121];[-101];[1-11]).

To accelerate the formation of the Cottrell atmosphere, we added the following approximation: the sum of the transition rates of C atoms in the k-ART zone was divided by 100 to force the MLKMC to perform rigid-lattice steps. As rigid-lattice events are performed instantly compared to k-ART events, this approximation should let the C atoms move to the k-ART zone. When at least 8 C atoms have arrived at the k-ART zone, the simulation is continued with k-ART only to avoid interface issues. Indeed, if all the C atoms are in the k-ART zone, MLKMC simulations can be longer than pure k-ART simulations due to the checks that are made to ensure a good compatibility between the two different lattices (i.e. between the k-ART zone and the rigid-lattice zone).

Because of this approximation, the simulated times will not be perfectly accurate and only an estimate of the order of magnitude of the time needed to reach the dislocation, i.e. to form the Cottrell atmosphere, will be obtained.

The conditions of these simulations are summarized in Table 7.

Type of simulations	MLKMC
Defect investigated	screw dislocation
Simulation box size	X = 104.9 Å, Y = 100.9 Å, Z = 39.6 Å
Number of Fe atoms	36 000
Number of C atoms	10
Box orientation	X = [121], Y = [-101], Z = [1-11]
Boundary conditions	PBC along the dislocation line direction [1-11], free surfaces in other directions
Temperature	300 K and 600 K
Size of k-ART zone	X = 25 Å, Y = 25 Å, Z = 39.6 Å
Approximation in the k-ART zone	$\sum T_r$ in the k-ART zone divided by 100
Approximation in the rigid lattice zone	$E_{mig_C} = E^0_{mig_C} + \Delta E_{C-C} + \Delta E_{elasticity}$
Number of cores	16
Average number of KMC steps	27 000
Average CPU time per core	8.3 days
Average simulated time at 300 K	1.9 hours
Average simulated time at 600 K	$1.3\ 10^{-3}$ s

Table 7: Simulation conditions for MLKMC simulations containing a screw dislocation and 10 C atoms in a 36000 Fe simulation box.

Firstly, the evolution of the C-dislocation distances are shown for all simulations at 300 K (Figure 50) and 600 K (Figure 51). As expected, for all the simulations the average C-dislocation distances are decreasing as the simulation performs more steps, expressing the formation of a Cottrell atmosphere. Note however that this is partially due to the choice of dividing the sum of transitions rates of C atoms in the k-ART zone by 100, meaning that C atoms entering the k-ART zone will be almost immobile (the probability for these C atoms to jump is divided by 100).
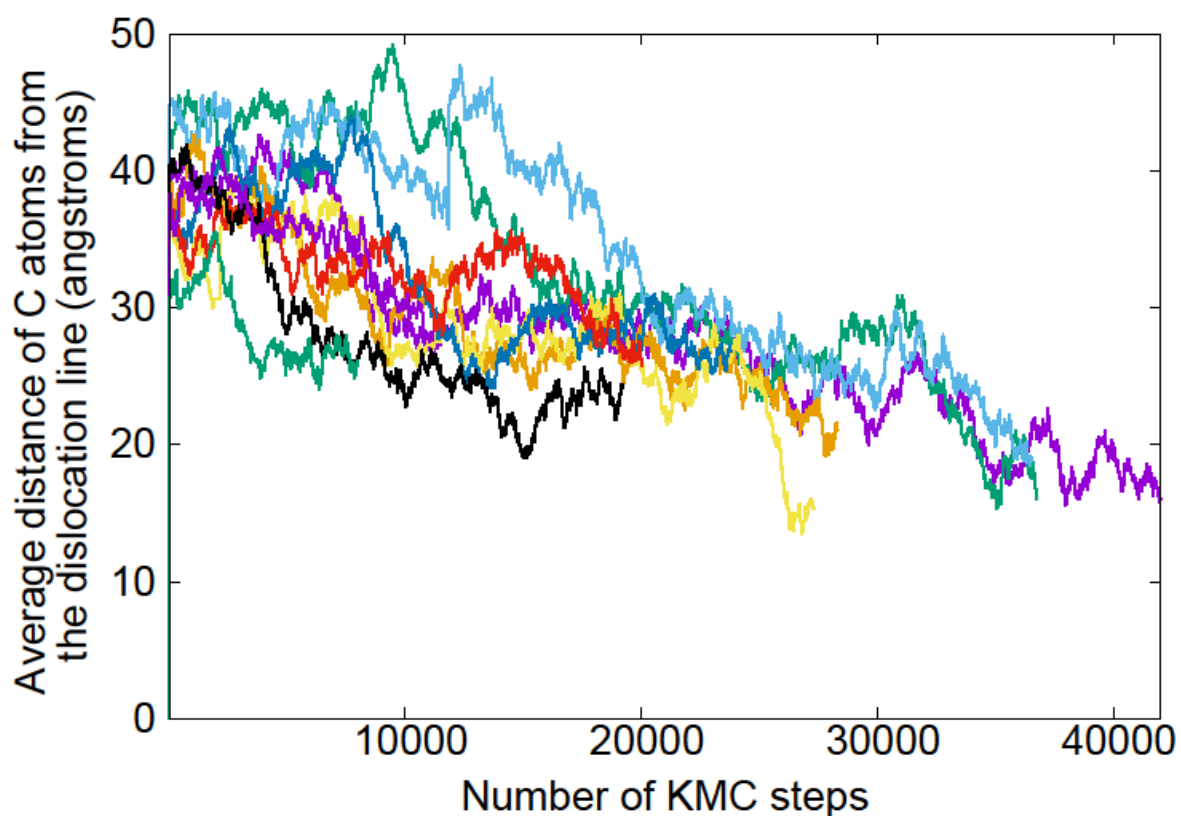
Figure 50: C-dislocation distances versus the number of steps for all the MLKMC simulations launched at 300 K containing a screw dislocation and 10 C atoms. One line represents one simulation. The average simulated time of the simulations is 1.9 hours for a CPU time of 8.3 days per core (16 cores).
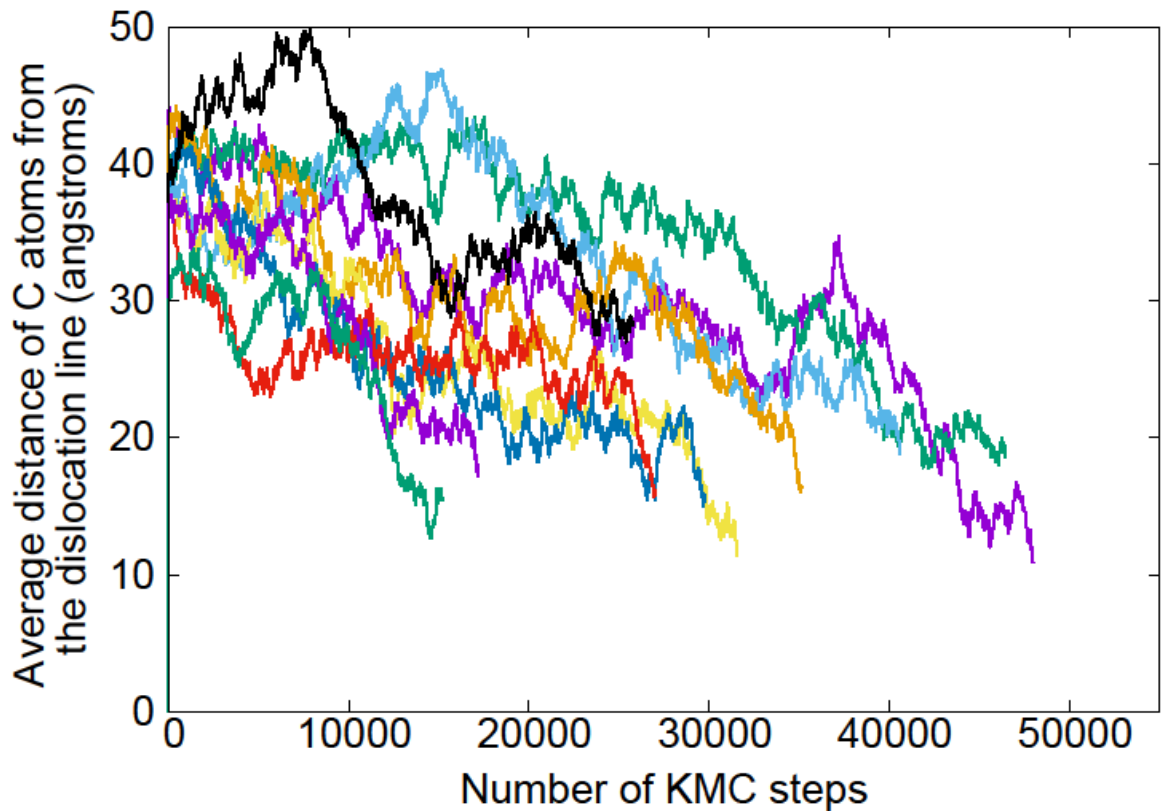
Figure 51: C-dislocation distances versus the number of steps for all the MLKMC simulations launched at 600 K containing a screw dislocation and 10 C atoms. One line represents one simulation. The average simulated time of the simulations is 1.3 millisecond for a CPU time of 8.3 days per core (16 cores).

As expected, on several simulations two or more C atoms share the same position with respect to the dislocation, meaning that they are lined up along the ⟨111⟩ direction. More precisely, on five among the twenty simulations, 2 C atoms were lined up along the ⟨111⟩ direction, expressing the few means that the C atom has to come towards the dislocation.
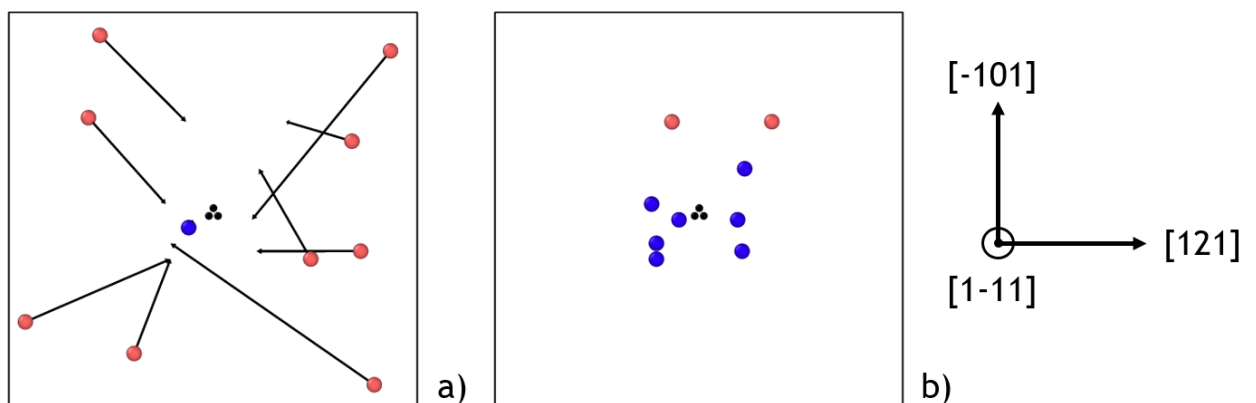
Figure 52: Initial a) and final b) configurations of a MLKMC simulation where 2 C atoms are lined up along the ⟨111⟩ direction. The blue atoms are the C atoms in the k-ART zone, the red atoms are the atoms in the rigid-lattice zone, and the dark atoms represent the dislocation. The arrows on the initial configuration a) represent the total displacement of C atoms. CPU time of 4.4 days on 16 cores for a simulated time of 2.3 hours.

After all the C atoms are either on the k-ART zone or far from the dislocation, the simulations are continued with k-ART only to get rid of interfaces issues, especially the checks performed at each step that can result in an extension of the time needed to perform a step. The last configuration of a MLKMC simulation will therefore be used as initial configuration for the k-ART simulation. The aim of these k-ART simulations is therefore to study the mechanisms of C atoms going towards the dislocation.

Table 8 summarizes the simulation conditions.

Type of simulations	k-ART
Defect investigated	screw dislocation
Simulation box size	X = 104.9 Å, Y = 100.9 Å, Z = 39.6 Å
Number of Fe atoms	36 000
Number of C atoms	10
Box orientation	X = [121], Y = [-101], Z = [1-11]
Boundary conditions	PBC along the dislocation line direction [1-11], free surfaces in other directions
Temperature	300 K and 600 K
Number of cores	16
Average number of KMC steps	208
Average CPU time per core	12.4 days
Average simulated time at 300 K	3 seconds
Average simulated time at 600 K	$3.0 \ 10^{-6}$ s

Table 8: Simulation conditions for k-ART simulations containing a screw dislocation and 10 C atoms in a 36000 Fe simulation box. These simulations continue the MLKMC simulations.

The most surprising effect observed is the tendency of C atoms to diffuse through the same paths even if two or more C atoms are close. This indicates that the influence of the dislocation on the C migration energies is stronger than the C-C repulsion. To prove that point, the smallest C-C distance is plotted for all simulations at 300 K and 600 K in Figure 53. The important thing to notice in Figure 53 is that the smallest C-C distance is often under 5 Å, so where the C atoms start to repel each other. **Therefore, we observe that the C-C repulsion is not strong enough to compete with the influence of the dislocation on the C migration energies. In other terms, the dislocation appears to have more impact on the C migration than the C-C interactions. It is this effect that allows the Cottrell atmosphere to be formed.**
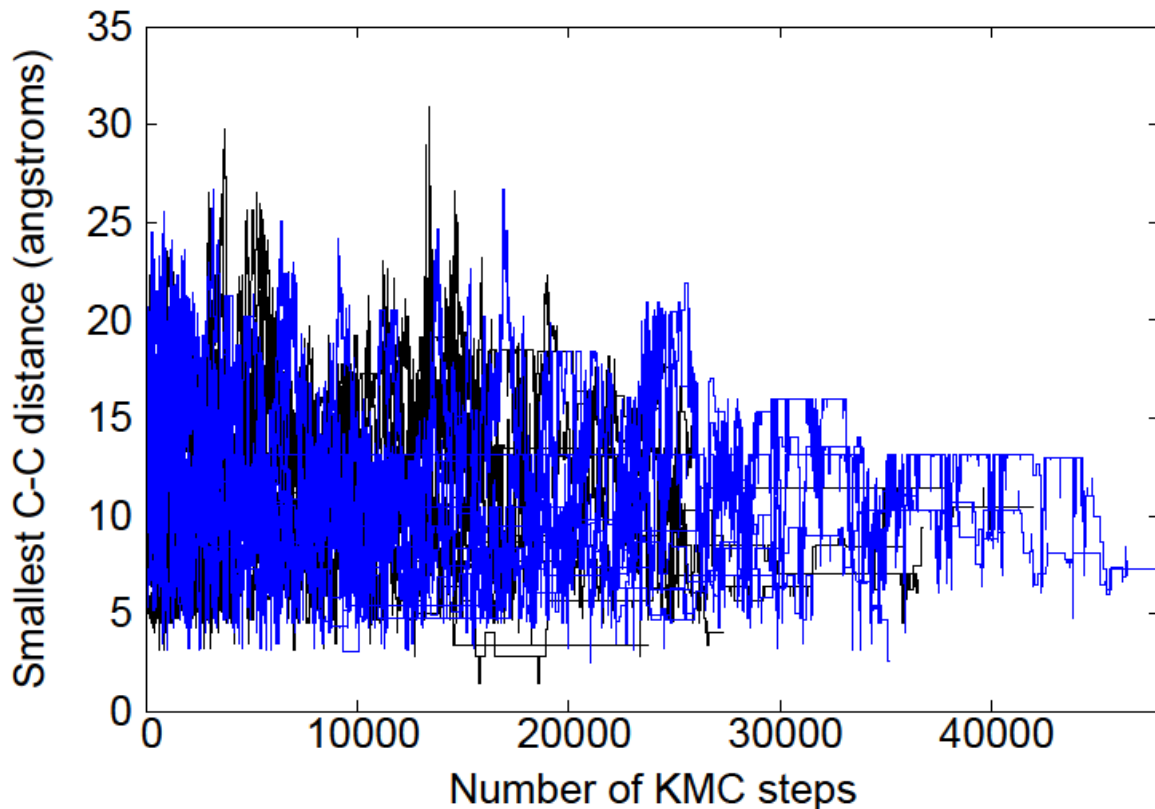
Figure 53: Smallest C-C distance observed for all simulations at 300 K (dark lines) and 600 K (blue lines) versus the number of steps of the simulation.

E. The 25 C – screw dislocation system

To measure the influence of the C concentration on the formation of a Cottrell atmosphere, the same Fe matrix presented in the previous subsection (D. The 10 C – screw dislocation system, 36 000 Fe atoms with a screw dislocation in it) with the only difference of adding 25 C to the system instead of 10, corresponding to 150 ppm of C (ultra-low carbon steels). Ten different simulations were launched with their only difference on the C positions at 300 K. Five of these simulations were also launched at 600 K, the other five are launched at 300 K and the temperature will be changed to 600 K when several C atoms arrive In the k-ART zone. Indeed, increasing the temperature in a KMC simulation results in a lower influence of the dislocation, meaning that the C atoms are less attracted by the dislocation. Therefore, putting the temperature at 300 K and changing the temperature at 600 K will allow us to study the reorganization of C atoms when they are close to the dislocation line even at 600 K. PBC were applied only in the dislocation line direction, free surfaces are applied on the other directions. The BMRM was activated with an energy barrier of 0.4 eV for an event to be considered within a basin. The orientation of the system was ([121];[-101];[1-11]).

As explained in the previous subsection (D. The 10 C – screw dislocation system), some assumptions must be made to speed up the simulations at the cost of the "kinetic validity" of the simulations. In this case, the precedent assumption to divide by 100 the sum of the transitions rates of atoms in the k-ART zone can not stand for this system; as the C concentration grows up, some effects may appear at the interface between the k-ART zone and the on-lattice zone. Indeed, dividing the sum of the k-

ART transitions rates by 100 means that a C atom entering the k-ART zone will be less likely to move. Therefore, C atoms who just entered the k-ART zone will not be likely to move, thus lowering the possibility of other C atoms coming through the same path towards the dislocation. If for this system with 10 C atoms this effect is not likely to be seen, with 25 C atoms it is very likely to find C atoms "stuck" at the interface between the k-ART and the on-lattice zone repulsing other C atoms going towards the dislocation. Therefore, another assumption must be made to allow the possibility of studying the formation of a 25 C Cottrell atmosphere around a screw dislocation in a 36 000 Fe matrix.

The most straightforward approximation to be made is to reduce the size of the k-ART zone, at the cost of less precise C migration energies. However, as stated by Clouet & al. (Clouet et al., 2008), the agreement between the anisotropic elasticity theory predictions and the atomistic predictions is close to perfect for the binding energies of C atoms within O sites for C − screw dislocation distances higher than 2 Å. Let's remind that when taking into account the elastic field of the dislocation, the migration energy of C single atom in the on-lattice zone is computed as:

$$E_{mig}C = E^0_{mig}C + \Delta E_{elastic}$$

Where $E^0_{mig}C$ is the migration energy of a C atom in the Fe bulk (predicted to be 0.815 eV by the empirical potential used) and $\Delta E_{elastic}$, the elastic contribution of the dislocation, which is computed as:

$$\Delta E_{elastic} = E^{binding}_{C_O-dislocation} - E^{binding}_{C_T-dislocation}$$

Where $E^{binding}_{C_O-dislocation}$ is the binding energy between a C atom in a O site and $E^{binding}_{C_T-dislocation}$ is the binding energy of a C atom in a T site, with the O and T site above-mentioned corresponding respectively to the O site the C atom is in and the T site the same C atom goes through to perform a jump.

Clouet & al. (Clouet et al., 2008) and Veiga & al. (Veiga et al., 2011) showed that the elastic computations for $E^{binding}_{C_O-dislocation}$ match the atomic computations for C-dislocation distances greater than 2 Å. However, for the tetrahedral site, the elastic approximation does not hold as close to the dislocation core as shown in Figure 25. Therefore, computing these values using atomic calculations could extend the size of the rigid lattice with only the small cost of performing some MS computations before launching the simulation.

For a better overview of how the MLKMC will compute the C migration energies, a simplified schema is shown on Figure 54. On this picture, the large blue zone represents the area where the C migration energies are computed with the approximation $E_{mig}C = E^0_{mig}C + \Delta E_{elastic}$, with both $E^{binding}_{C_O-dislocation}$ and $E^{binding}_{C_T-dislocation}$ computed within the anisotropic elasticity theory (binding energies given by Babel in less than a second). When a C atom is in the intermediate yellow zone, the migration energies associated with the 4 jumps are still predicted with the equation 28, but contrary to the blue zone, the different values of $E^{binding}_{C_T-dislocation}$ are given by molecular statics simulations (one binding energy computation takes approximatively 30 s). Finally, the red zone containing the dislocation line is where the C migration energies are fully computed by k-ART.

Figure 54: Representation of the different zones where the C migration energy is computed. The small red zone represents the k-ART zone where the screw dislocation is and where the C events are found by k-ART. The large blue zone represents the area where the C migration energy is computed with $E_{mig}C = E_{mig}^0 C + \Delta E_{elastic}$, with both $E_{CO-dislocation}^{binding}$ and $E_{CT-dislocation}^{binding}$ computed within the anisotropic elasticity theory. The yellow intermediate zone represents the area where the C migration energy is computed with $E_{mig}C = E_{mig}^0 C + \Delta E_{elastic}$, but $E_{CT-dislocation}^{binding}$ is computed with molecular statics whereas $E_{CO-dislocation}^{binding}$ is computed with elasticity. Note however that the sizes of the different zones are not at the correct scale, as the sizes depends on the system launched.

Considering the C atom and the dislocation as two different defects in the Fe matrix, the binding energies for a C atom in a T site with the dislocation can be computed as expressed previously in equation 12:

$$E_{CT-dislocation}^{binding} = E_{CT-dislocation}^{box} + E_{perfect\ lattice}^{box} - (E_{CT}^{box} + E_{dislocation}^{box}) \qquad (41)$$

Where $E_{CT-dislocation}^{box}$ is the energy of the whole simulation box containing a C in a T site and a screw dislocation, $E_{perfect\ lattice}^{box}$ is the energy of the simulation box of a perfect Fe lattice, E_{CT}^{box} is the energy of the box with a C in a T site and $E_{dislocation}^{box}$ is the energy of the simulation box containing only a screw dislocation. More practically, the binding energy between a C atom in a T site and the screw dislocation can be computed as the difference in energies between the simulation box where the two defects are interacting and the simulation box where the two defects are not interacting.

The conditions of these simulations are summarized in Table 9.

Type of simulations	MLKMC
Defect investigated	screw dislocation
Simulation box size	X = 104.9 Å, Y = 100.9 Å, Z = 39.6 Å
Number of Fe atoms	36 000
Number of C atoms	25
Box orientation	X = [121], Y = [-101], Z = [1-11]
Boundary conditions	PBC along the dislocation line direction [1-11], free surfaces in other directions
Temperature	300 K, 600 K and 300 K continued at 600 K when at least 3 C atoms are in the k-ART zone
Size of k-ART zone	X = 12.5 Å, Y = 12.5 Å, Z = 39.6 Å
Approximation in the k-ART zone	$\sum T_r$ in the k-ART zone divided by 100 if 1 C atom is in the k-ART zone
Approximation in the rigid lattice zone	$E_{mig_C} = E^0_{mig_C} + \Delta E_{C-C} + \Delta E_{elasticity}$
Number of cores	16
Average number of KMC steps	6177
Average CPU time per core	7.2 days
Average simulated time at 300 K	0.11 hours
Average simulated time at 600 K	$2.4\ 10^{-5}$ s
Average simulated time for simulations started at 300 K and continued at 600 K	0.13 hours

Table 9: Simulation conditions for MLKMC simulations containing a screw dislocation and 25 C atoms in a 36000 Fe simulation box.

The average C-dislocation distances are presented for the simulations at 300 K (Figure 55), at 600 K (Figure 56) and for the simulations who changed from 300 K to 600 K after several C atoms have come to the k-ART zone (Figure 57). As seen on these figures, the average C-dislocation distances are slightly decreasing through the simulation. However, the decrease is not as fast as the decrease observed for the average C-dislocation distances in a MLKMC simulation containing only 10 C atoms (Figure 50 and Figure 51) due to the higher number of C atoms. However, when looking at an initial and a final configuration of a MLKMC simulation (Figure 58), the start of the formation of a Cottrell atmosphere is undeniable. Furthermore, as the C-C interactions are repulsive, it will take more time for the C atoms to find an equilibrium position in simulations containing more C atoms, as the first C atoms coming close to the dislocation line will hinder the arrival of other C atoms.
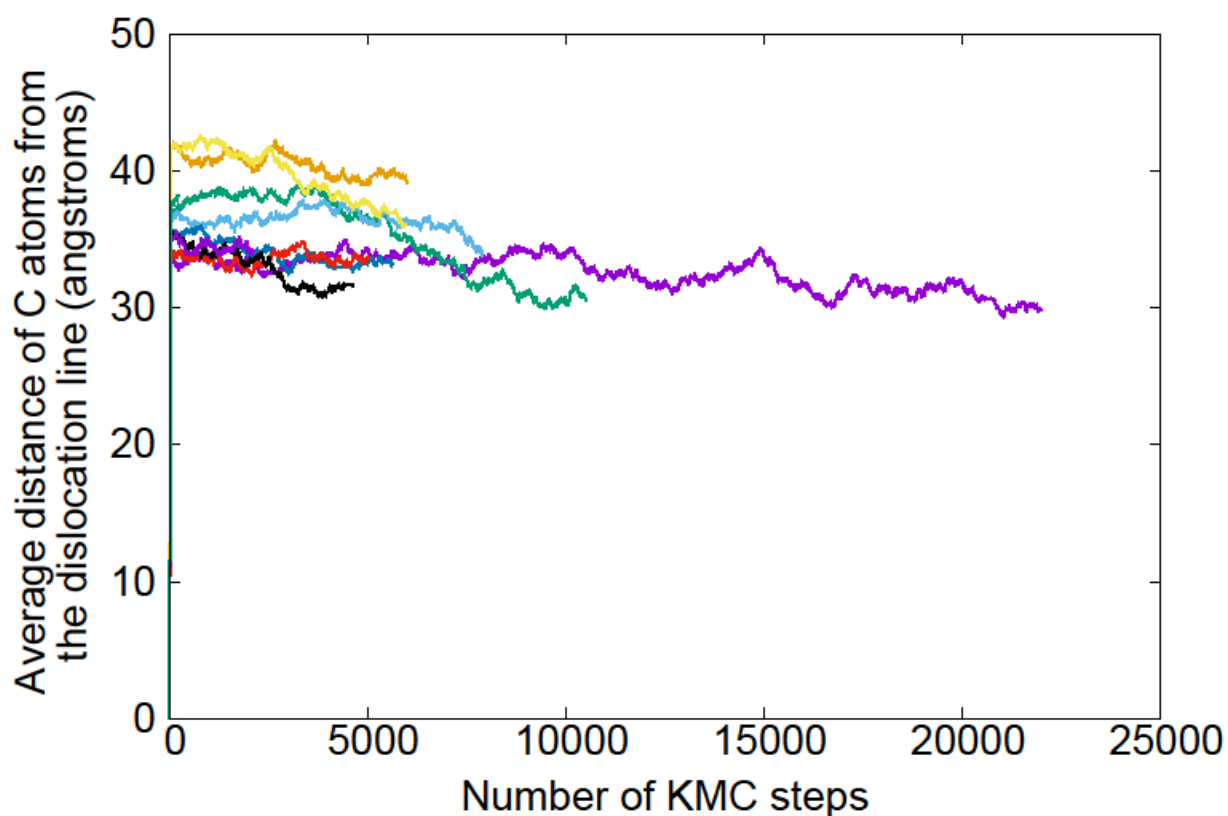
Figure 55: Average C-dislocation distances versus the number of steps for all the MLKMC simulations launched at 300 K containing a screw dislocation and 25 C atoms. One line represents one simulation. The average simulated time of the simulations is 0.11 hours for a CPU time of 7.2 days per core (16 cores).
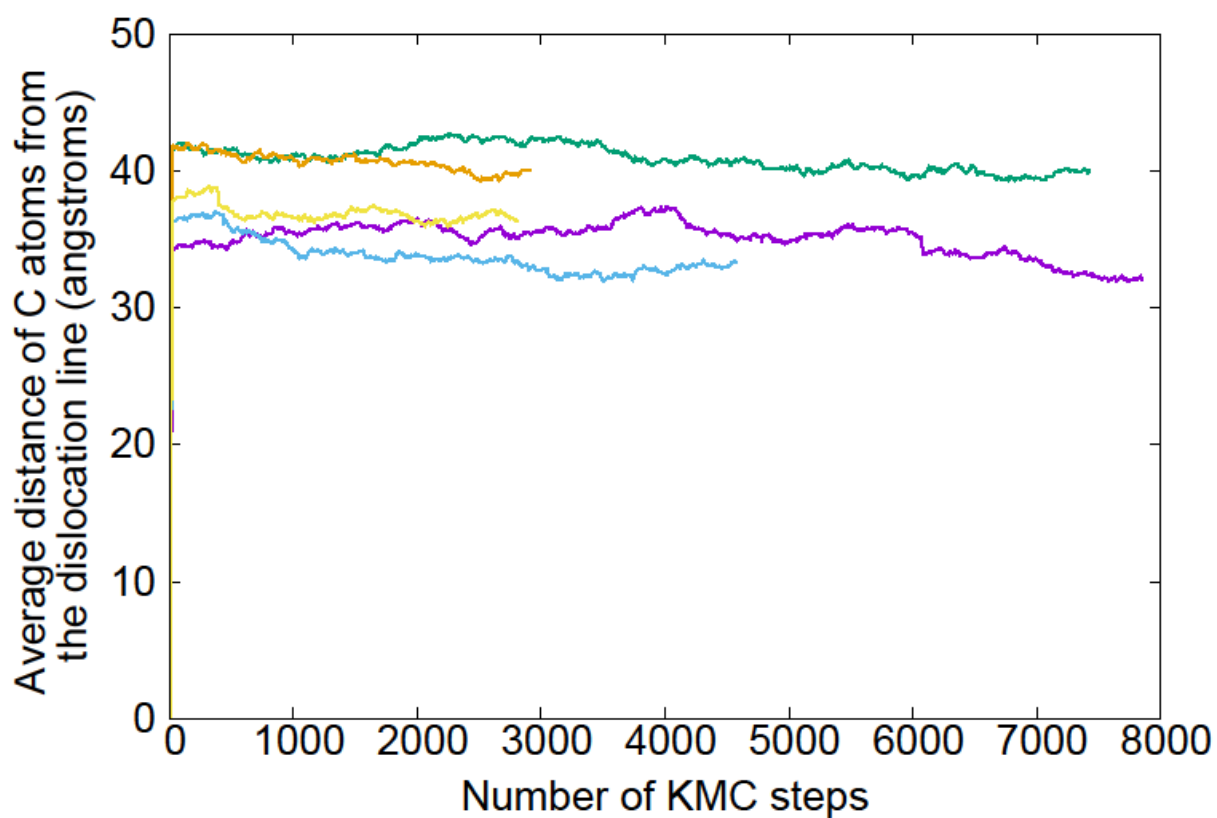
Figure 56: C-dislocation distances versus the number of steps for all the MLKMC simulations launched at 600 K containing a screw dislocation and 25 C atoms. One line represents one simulation. The average simulated time of the simulations is 2.4 10^{-5} s for a CPU time of 7.2 days per core (16 cores).
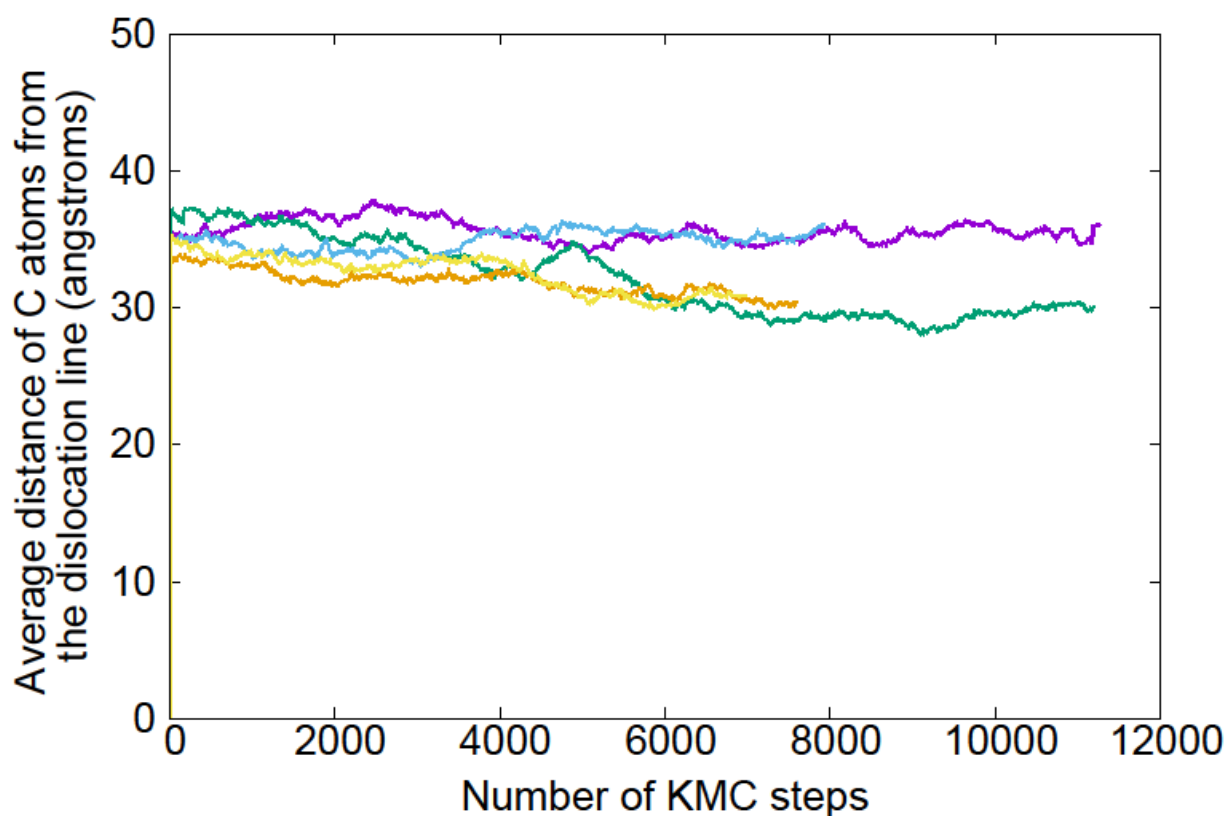
Figure 57: C-dislocation distances versus the number of steps for all the MLKMC simulations launched at 300K and continued at 600 K containing a screw dislocation and 25 C atoms. One line represents one simulation. The average simulated time of the simulations is 0.13 hours for a CPU time of 7.2 days per core (16 cores).
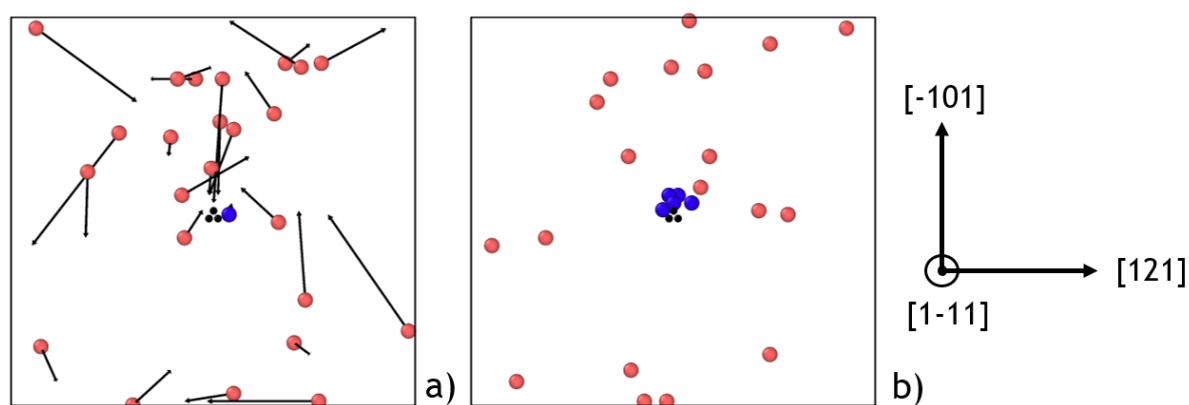
Figure 58: Initial (a) and final (b) configurations of a MLKMC simulation containing a screw dislocation and 25 C atoms. The blue atoms represent the C atoms in the k-ART zone, the red atoms are the C in the rigid-lattice zone and the dark atoms represent the screw dislocation. CPU time of 9.4 days for a simulated time of 0.10 hours.

An interesting mechanism was discovered in the simulations launched at 300 K and continued at 600 K when at least 3 C atoms arrived in the k-ART zone. During the simulation at 300 K, two C atoms arrived close to the dislocation line and were separated by only 4.9 Å, meaning that a small repulsion occurs between these C atoms. This configuration was the starting point of the simulation at 600 K. This mechanism is showed on Figure 59. On the initial configuration (Figure 59 a), the C atom circled and the C atom where the arrow starts from are separated by 4.9 Å. However, one C atom will leave will go away from the other one, firstly going at 7.25 Å (Figure 59 b) and then leaving the dislocation vicinity (Figure 59 c C-C distance equal to 10 Å, Figure 59 d C-C distance equal to 11 Å). Then, the C atom will come back very close to the dislocation line but at 7.5 Å from the C atom originally at 4.9 Å.
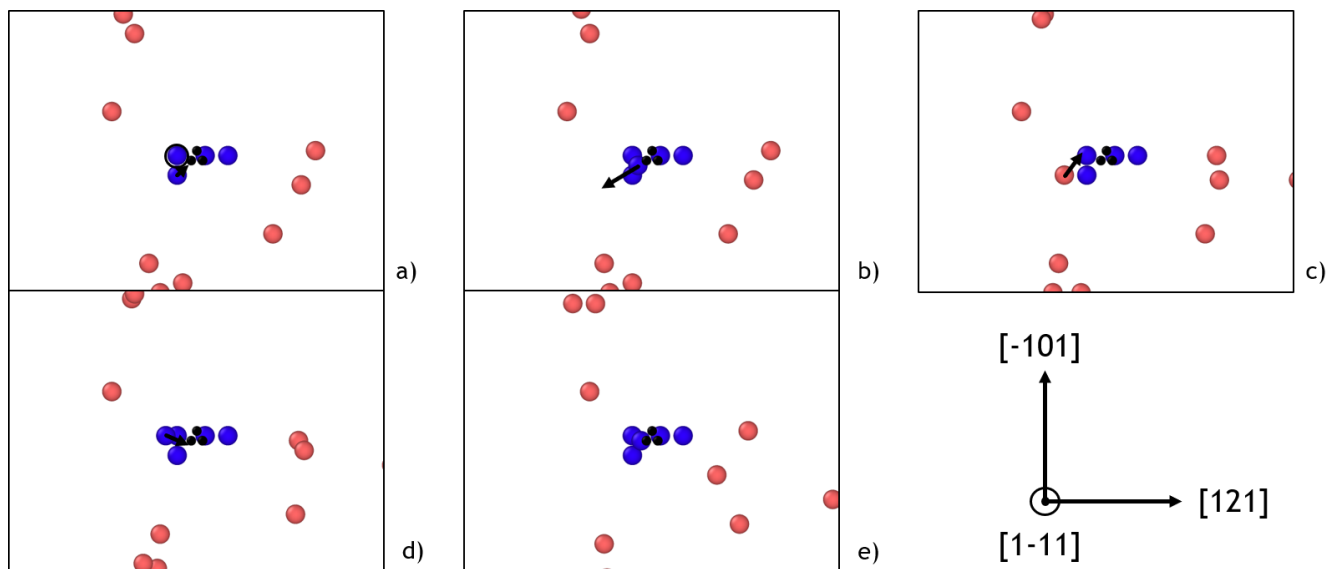
Figure 59: Mechanism showing the reorganization of 2 C atoms when continuing a 300 K MLKMC at 600 K. At first, when putting the simulation at 600 K, the 2 C atoms (the circled one and the one where the arrow starts from) are a at distance of 4.9 Å (a). One of these atoms leaves the dislocation vicinity (b, c, d, C-C distances respectively of 7.25 Å, 10 Å and 11 Å) to finally come back close to the dislocation loop but more far from the other atom than the initial configuration (7.5 Å) (e). The blue atoms are the C atoms in the k-ART zone, the red atoms are the C atoms in the rigid-lattice zone, the dark atoms represent the screw dislocation and the arrows represents the C displacement. CPU time of 1.8 days for a mechanism happening in less than a 10^{-3} s.

Another interesting mechanism observed is that C atoms in stable configurations close to the dislocation line will repel others C atoms that want to come towards the dislocation. This mechanism is presented on Figure 60 where a C atom close to the dislocation line (circled in configuration a, in blue) repels another C atom (circled in configuration a, in red). The C atom repelled finds a way to the dislocation vicinity (bumping a few times into the C atom in a stable position), and then forces the other C atom to leave its stable position at the final configuration (Figure 60 j). **Therefore, we can deduce from the two mechanisms presented that even if the C-C repulsion is not as strong as the dislocation influence on the migration energies (e.g.** Figure 60 **i, the 2 C atoms presented are at 3.9 Å thus repelling each other), it plays a major role in the C reorganization for C atoms close to the dislocation line.**
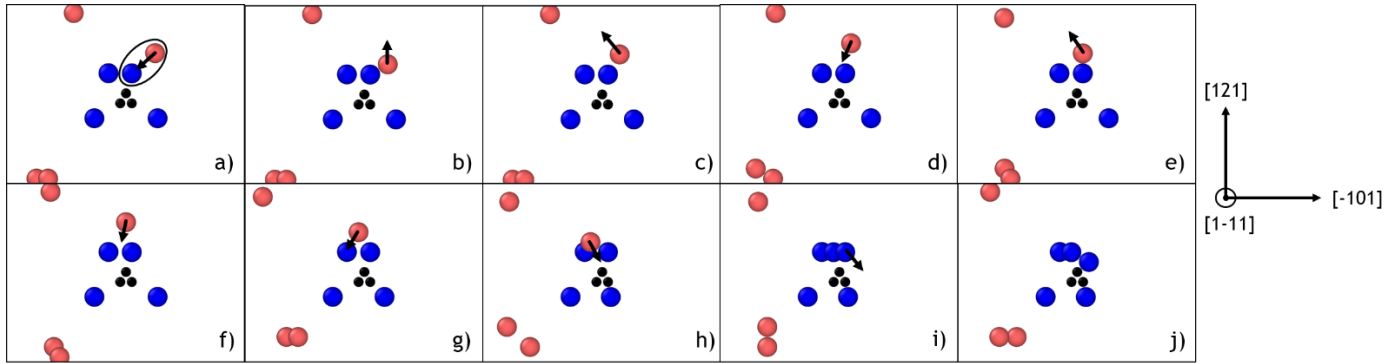
Figure 60: Mechanism showing the arrival of a C atom close to the dislocation line while being hindered by the presence of a C atom. On configuration a, the circled atoms are the atoms interacting together. The red circled atom wants to move towards the dislocation line but is hindered by the presence of the blue circled atom. All the other configurations show the path found by the red circled atom to finally reach the vicinity of the dislocation. The C-C distances for all the configurations are respectively 7.4 Å (a), 4.7 Å (b), 4.7 Å (c), 6.2 Å (d), 4.7 Å (e), 7.3 Å (f), 5.6 Å (g), 6.3 Å (h), 3.9 Å (i) and 6.2 Å (j). The blue atoms are the C atoms in the k-ART zone, the red atoms are the C atoms in the rigid-lattice zone, the dark atoms represent the screw dislocation and the arrows represents the C displacement. The CPU time required for the whole mechanism presented is 1.8 days for a simulated time of 153 s.

F. Discussion

The Cottrell atmosphere decorating a screw dislocation is known to be a stable configuration, i.e. a low energy configuration (Veiga et al., 2015). Therefore, as the MLKMC simulations run and thus as the Cottrell atmosphere is formed, the energy of the simulation box is expected to lower. The energies of the initial and final configurations is shown for all MLKMC simulations, respectively for simulations launched with 10 C atoms at 300 K (Figure 61) and 600 K (Figure 62), with 25 C atoms at 300 K (Figure 63) , 600 K and 300 K and continued at 600 K (both simulations at 600 K and 300 K and continued at 600 K in Figure 64). However, on these figures, even if the majority of the simulations led to a decrease on the total energy of the simulation boxes, an increase in energy was also observed for several simulations, especially for the simulations 6 and 7 with 25 C at 600 K (Figure 64). The increase of the total energy happens even if for the particular case of the simulation 6 on Figure 64, 5 C atoms have arrived to the k-ART zone as seen on Figure 65. **This means that the beginning of the formation of a Cottrell atmosphere is not always linked with a decrease in the total energy of the simulation box.** All the simulated times and the CPU times are presented in Table 10.
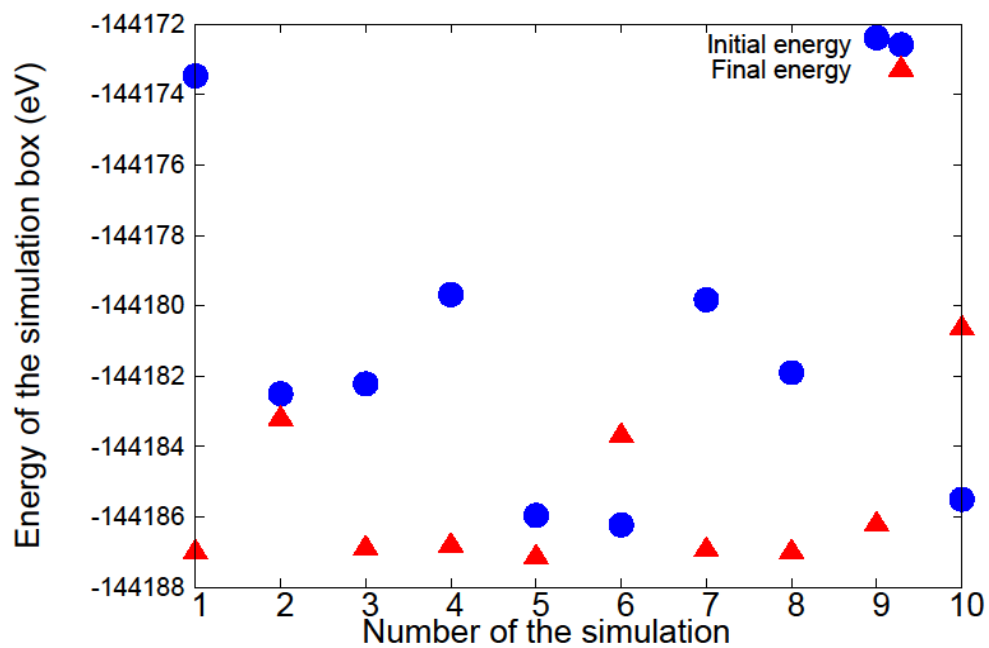
Figure 61: Energy of the initial and the final states of all the MLKMC simulations containing 10 C atoms and a screw dislocation at 300 K.
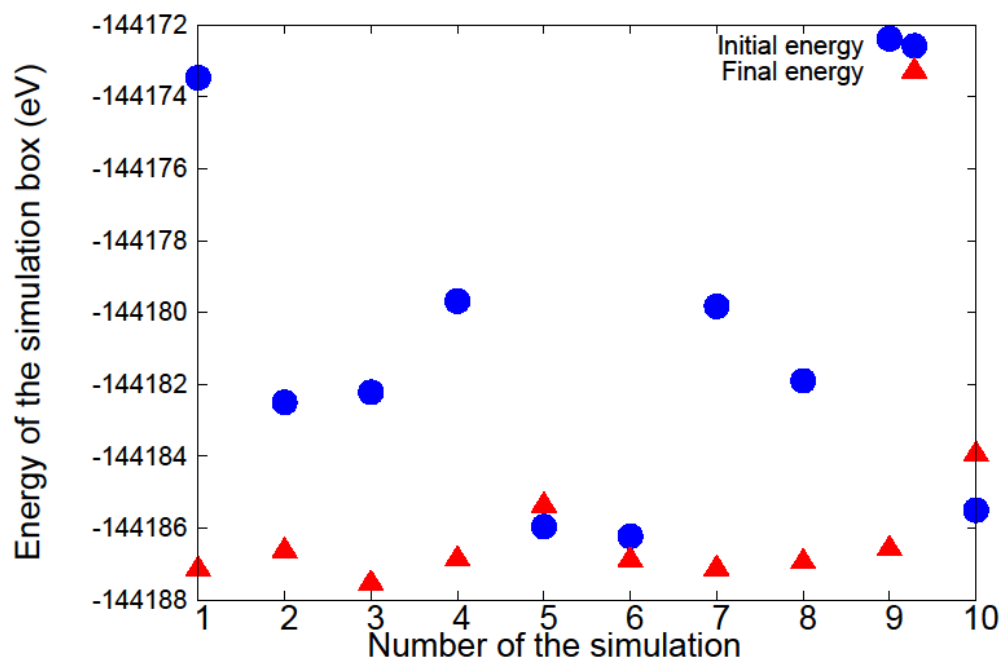
Figure 62: Energy of the initial and the final states of all the MLKMC simulations containing 10 C atoms and a screw dislocation at 600 K.
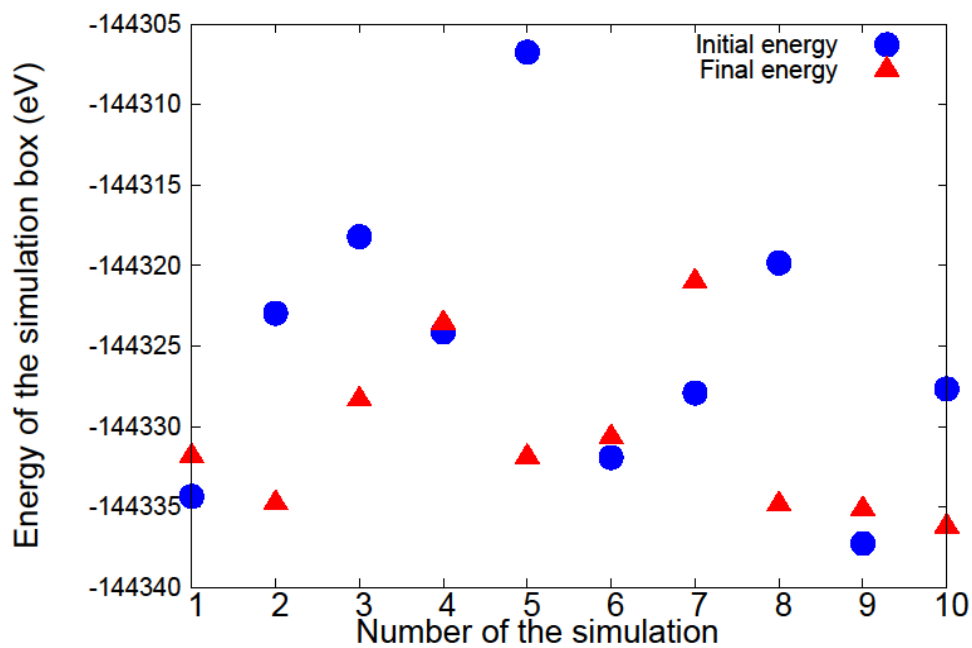
Figure 63: Energy of the initial and the final states of all the MLKMC simulations containing 25 C atoms and a screw dislocation at 300 K.
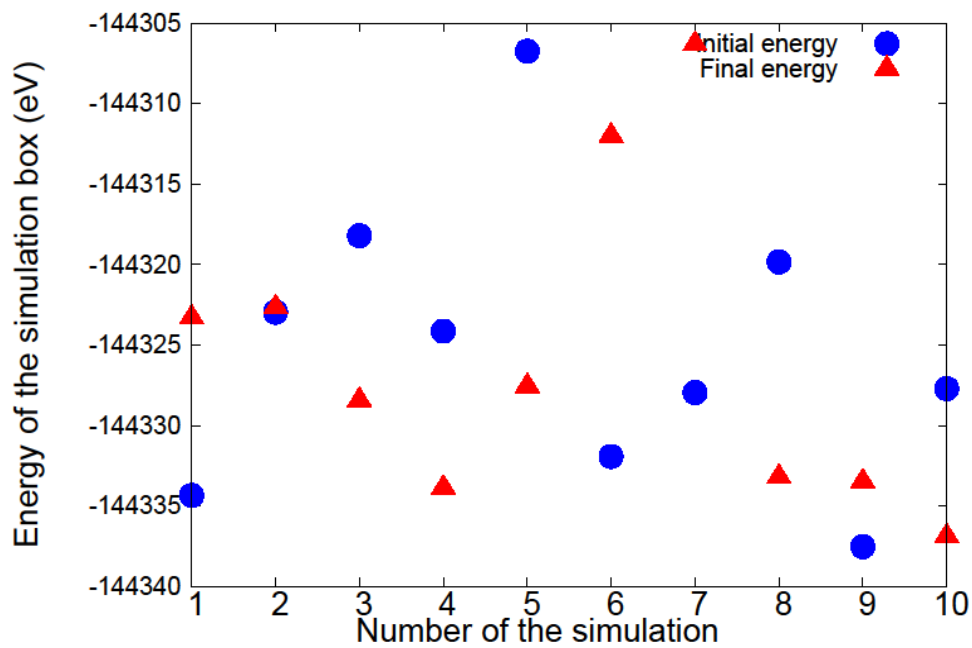
Figure 64: Energy of the initial and the final states of all the MLKMC simulations containing 25 C atoms and a screw dislocation at 600 K and at 300 K then continued at 600 K.
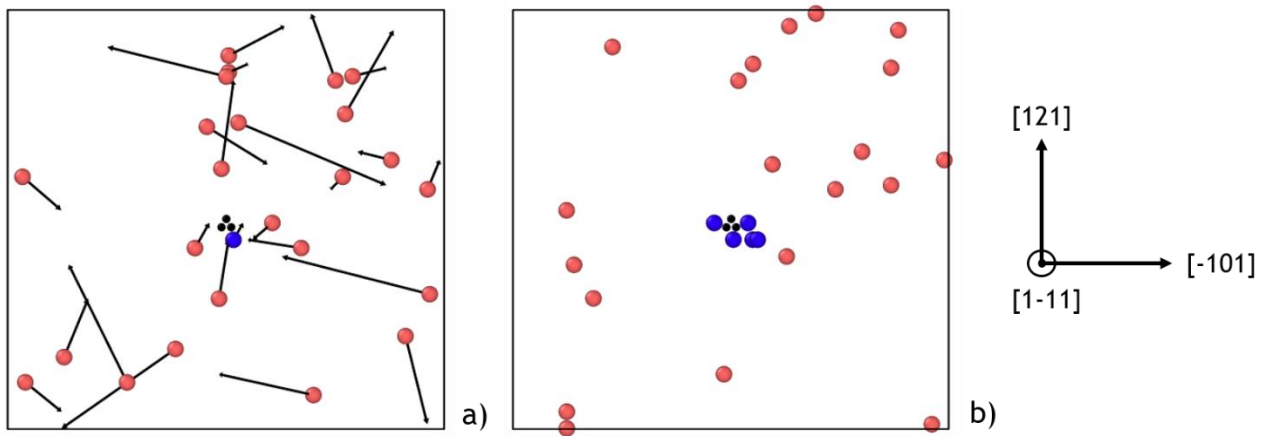
Figure 65: Initial (a) and final (b) configurations of the MLKMC simulation 6 presented on Figure 64 containing a screw dislocation and 25 C atoms started at 300 K and continued at 600 K. The blue atoms represent the C atoms in the k-ART zone, the red atoms are the C in the rigid-lattice zone and the dark atoms represent the screw dislocation. CPU time of 7.7 days, simulated time of 296 s.

Number of the simulation	Number of C atoms	Temperature	Simulated time (s)	Simulated time (hours)
1	10	300	1,47E+04	4,08
2	10	300	6,20E+03	1,72
3	10	300	7,91E+03	2,20
4	10	300	6,14E+03	1,70
5	10	300	8,33E+03	2,31
6	10	300	2,12E+03	0,59
7	10	300	6,83E+03	1,90
8	10	300	8,61E+03	2,39
9	10	300	4,03E+03	1,12
10	10	300	2,22E+03	0,62
1	10	600	6,68E-04	0,00
2	10	600	1,12E-03	0,00
3	10	600	1,65E-03	0,00
4	10	600	1,58E-03	0,00
5	10	600	1,37E-03	0,00
6	10	600	6,90E-04	0,00
7	10	600	2,22E-03	0,00
8	10	600	1,53E-03	0,00
9	10	600	7,83E-04	0,00
10	10	600	1,39E-03	0,00
1	25	300	1,56E+03	0,43
2	25	300	2,87E+02	0,08
3	25	300	3,25E+02	0,09
4	25	300	3,63E+02	0,10
5	25	300	7,68E+02	0,21
6	25	300	1,46E+02	0,04
7	25	300	3,71E+02	0,10
8	25	300	1,51E+02	0,04
9	25	300	1,26E+01	0,00
10	25	600	3,34E+02	0,09
1	25	300 then 600	5,18E+02	0,14
2	25	300 then 600	3,54E+02	0,10
5	25	300 then 600	6,25E+02	0,17
6	25	300 then 600	2,96E+02	0,08
8	25	300 then 600	5,13E+02	0,14
3	25	600	1,23E-05	0,00
4	25	600	2,87E-05	0,00
7	25	600	5,05E-05	0,00
9	25	600	1,66E-05	0,00
10	25	600	1,21E-05	0,00

Table 10: Simulated time and CPU time for all the MLKMC simulations launched with a screw dislocation and 10 or 25 C atoms.

At least two different effects can explain the increase in the total energy of a system during the formation of a Cottrell atmosphere. The first one is the temperature, as a higher temperature in an AKMC simulation results in more steps to stabilize the system because more energetically unfavourable jumps are performed. Indeed, the increase in the total energy was especially seen at 600 K rather than at 300 K. The other explanation is linked to the C-C interactions. Initially, the atoms are placed randomly, which means that no or few C atoms will be close to each other. However, as the simulation performs more steps, the influence of the dislocation will put C atoms close to each other.

Indeed, as seen on Figure 66, the smallest C-C distance evaluates during the simulation and is often found below 5 Å, meaning that these 2 C will have a repulsing interaction and thus will increase the total energy of the system.
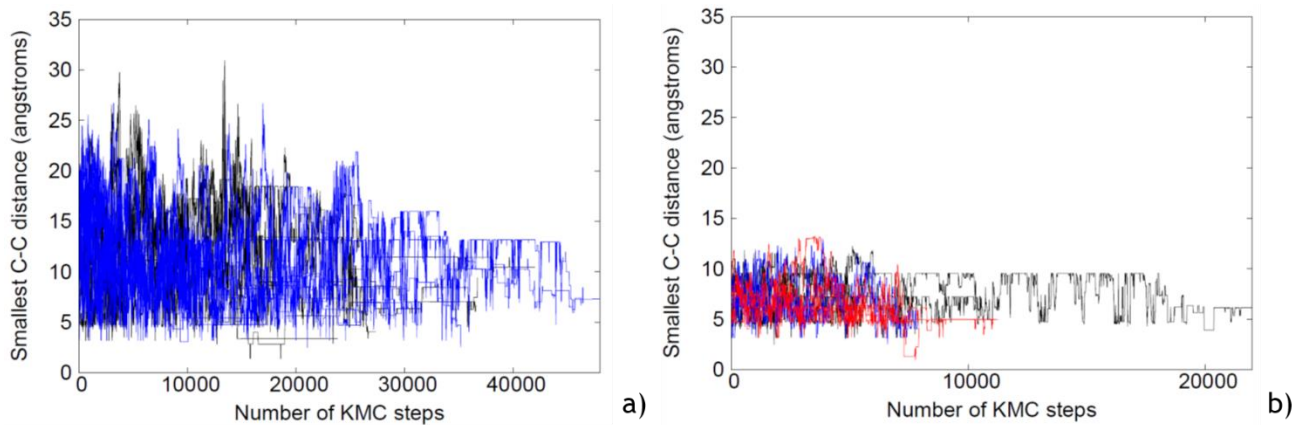
Figure 66: Smallest C-C distance observed for all MLKMC simulations containing a screw dislocation and 10 C atoms (a) or 25 C atoms (b) at 300 K (dark lines), 600 K (blue lines) and launched at 300 K and continued at 600 K (red) versus the number of steps of the simulation.

However, if the total energy of the system can sometimes increase during a MLKMC simulation, it is important to note that the C atoms in the k-ART zone (i.e. close to the dislocation) are in stable positions. To prove that, the C migration energies (blue bars) as well as the energies of the inverse transitions for the C atoms in the k-ART zone (therefore for C atoms close to the dislocation) are represented on Figure 67 and Figure 68. One can clearly observe that the C migration energies are higher than the energy of the inverse events, thus indicating that the C atoms in the k-ART zone are in stable configurations. It is interesting to note that this effect is more pronounced for the simulations containing 25 C atoms (Figure 68) than for simulations containing 10 C atoms (Figure 67) because the k-ART zone is smaller for simulations with 25 C atoms, and therefore the dislocation has more impact on the C atoms in the k-ART zone. This issue needs to be further explored and for this purpose we launched a series of simulations containing 10 C atoms and a screw dislocations with a reduced k-ART zone. Unfortunately, no results are available yet as the simulations are still running.
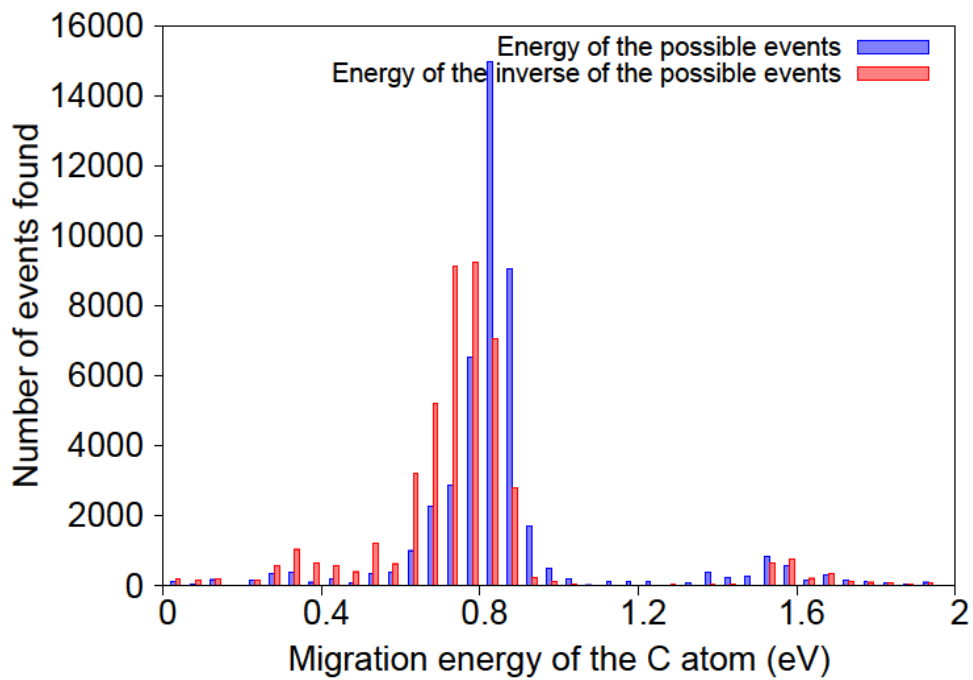
Figure 67: Migration energies of the C atoms in the k-ART zone for all the steps in the MLKMC simulations containing a screw dislocation and 10 C atoms. The blue bars represent the migration energies of the C atoms, the red bars represent the migration energies of the inverse events of C atoms.
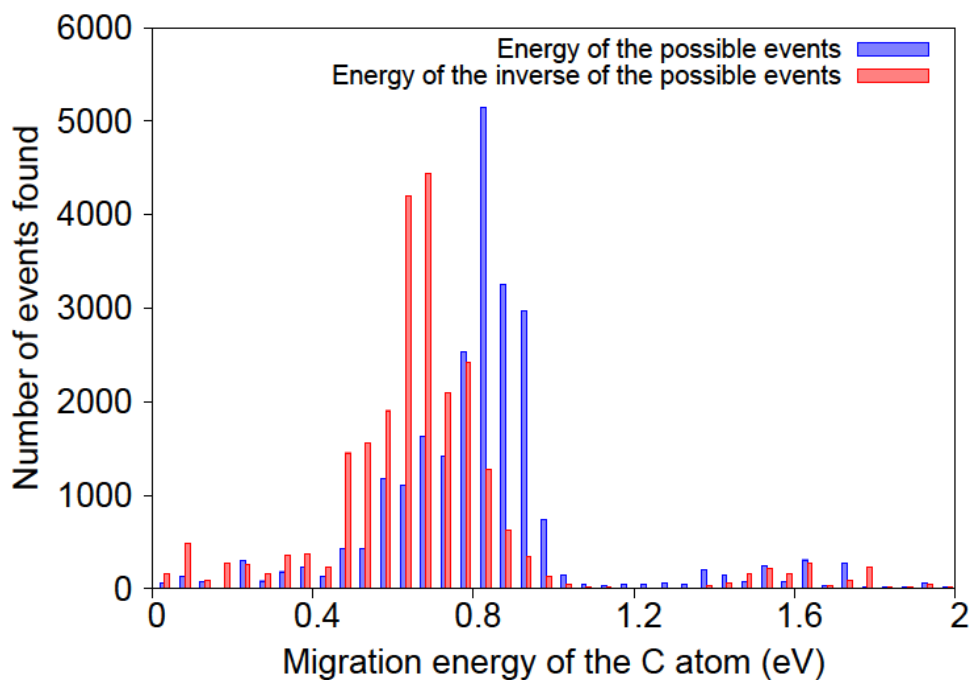
Figure 68: Migration energies of the C atoms in the k-ART zone for all the steps in the MLKMC simulations containing a screw dislocation and 10 C atoms. The blue bars represent the migration energies of the C atoms, the red bars represent the migration energies of the inverse events of C atoms.

The MLKMC simulations showed the beginning of the Cottrell atmosphere formation. It was observed that the first C atoms rapidly come close to the dislocation line in stable positions, and that the C atoms close to the dislocation line can repel other C atoms that arrive close to the dislocation line. Furthermore, small C-C distances were observed during the simulations, which indicates that the impact of the dislocation on C migration energies is higher than the C-C repulsion. This is indeed a necessary condition for a Cottrell atmosphere to be formed. We proposed a methodology to reduce the size of the k-ART zone for the system containing 25 C atoms, which is advised for future work with the MLKMC. The simulations containing a screw dislocation and 10 C atoms with the k-ART zone reduced to its limits are running and will be compared to the results with the 25 C – screw dislocation system.

Chapter VI. Results: the Cottrell atmosphere

In this final chapter, we present an investigation of the behaviour of a Cottrell atmosphere constructed with a static model. This configuration containing a screw dislocation in bcc Fe decorated by a 34 C atoms Cottrell atmosphere was studied using k-ART only. Indeed, as the Cottrell atmosphere is already formed (and thus all the C atoms are close to the dislocation line), there is no need for the rigid-lattice. This configuration was provided by R.G.A. Veiga and constructed with a MC/MD model (method explained in reference (Veiga et al., 2015)). The initial configuration of the simulations is shown on Figure 69. Table 11 summarizes the simulation conditions.
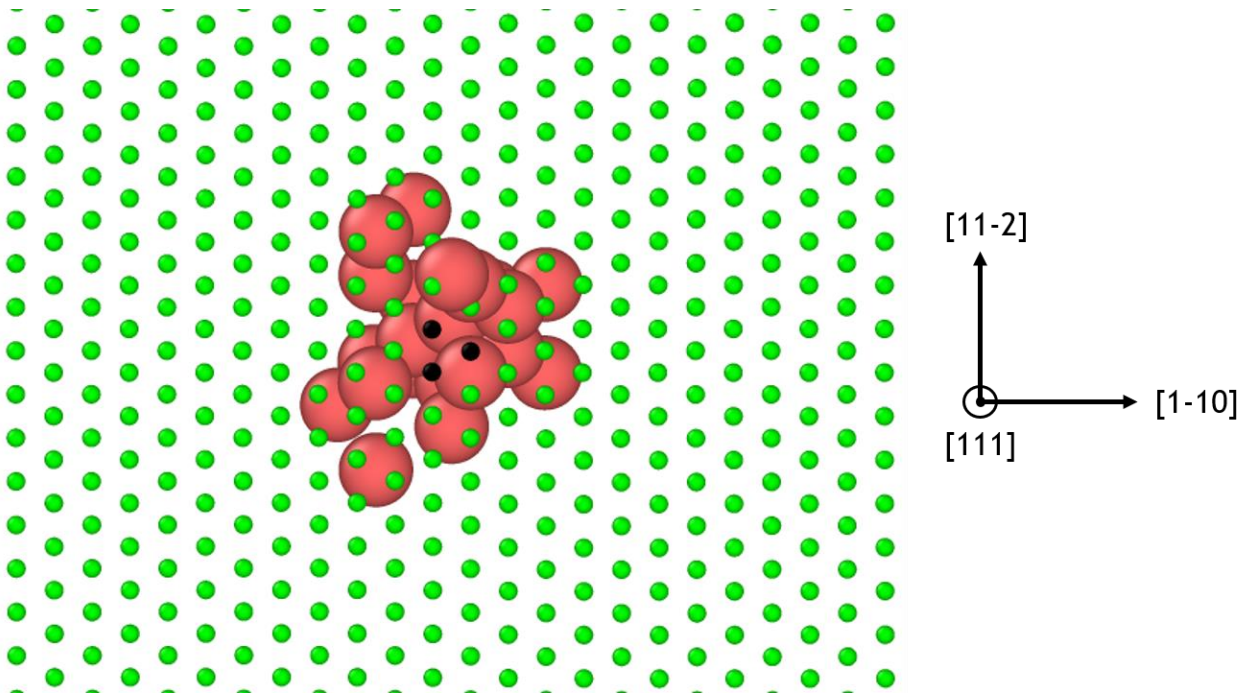
Figure 69: Initial configuration of the k-ART simulations. The box contains a screw dislocation (dark atoms) in a 85 000 bcc Fe atoms (green atoms) and 34 C atoms forming a Cottrell atmosphere. This atmosphere was created using the MC/MD method detailed in reference (Veiga et al., 2015).

Type of simulations	k-ART
Defect investigated	screw dislocation
Simulation box size	X = 104.9 Å, Y = 100.9 Å, Z = 39.6 Å
Number of Fe atoms	84 000
Number of C atoms	34
Box orientation	X = [11-2], Y = [1-10], Z = [111]
Boundary conditions	PBC along the dislocation line direction [111], free surfaces in other directions
Temperature	300 K
Number of cores	16
Average number of KMC steps	42
Average CPU time per core	9.4 days
Average simulated time	3.6×10^{-3} s

Table 11: Simulation conditions for MLKMC simulations containing a screw dislocation and decorated by a 34 C atoms Cottrell atmosphere in an 84 000 Fe simulation box.

The k-ART simulations were unfortunately too costly for any kinetic behaviour to be observed (approximatively 4 days of CPU time to perform the first 10 steps).

Nonetheless, it is possible to show the migration energies of all the C atoms for all the steps made. Furthermore, as said previously in section "Chapter II. Methods 5. C. e. i. Finding the transitions", k-ART also finds the migration energy of the inverse events. The migration energies of C atoms as well as the migration energies of the inverse events found are presented on Figure 70. On this figure, the blue bars represent the migration energies of the C atoms and the red bars represent the migration energies of the inverse events of C atoms. One can see that the energies of the possible events are higher than the energies of the inverse possible events. **This proves, in agreement with the results of Veiga (Veiga et al., 2015), that the screw dislocation acts as a sink to C atoms, as the migration energies of C atoms are higher to leave the Cottrell atmosphere configuration than to form it.**
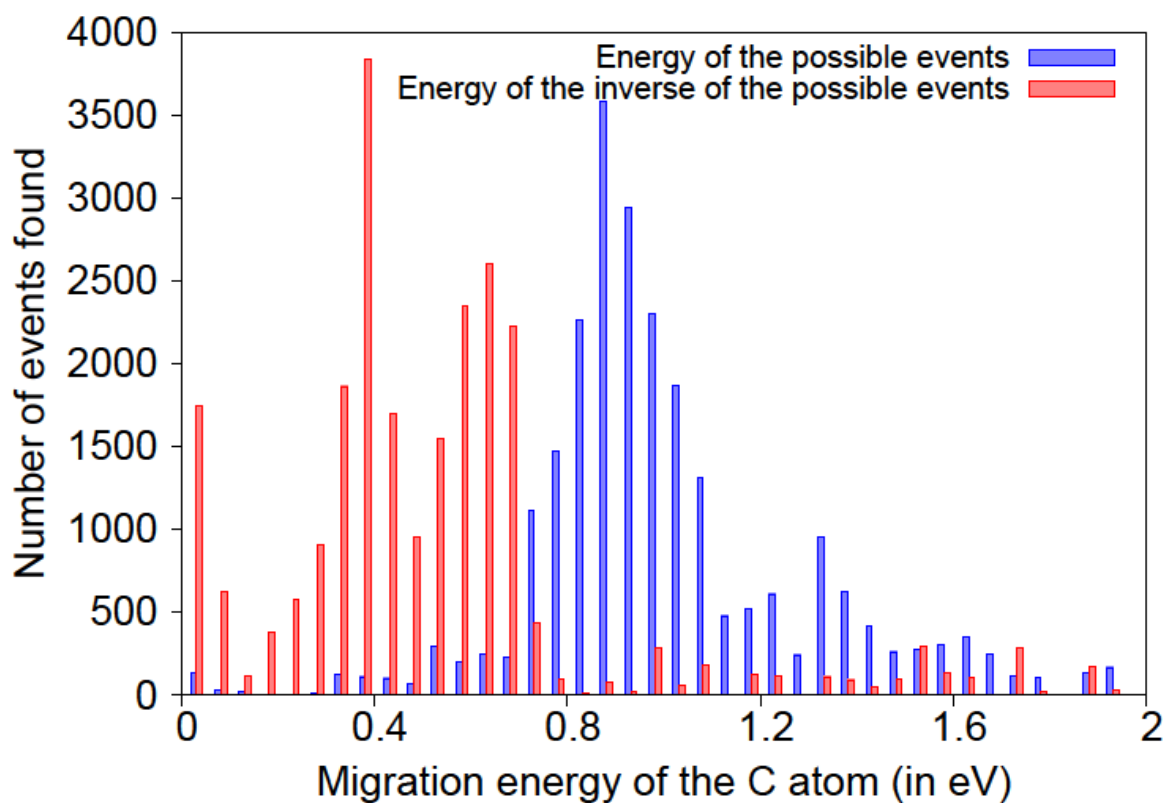
Figure 70: Migration energies of all the C atoms for all the steps in the k-ART simulations containing a screw dislocation decorated by a 34 C atoms Cottrell atmosphere. The blue bars represent the migration energies of the C atoms, the red bars represent the migration energies of the inverse events of C atoms.

The k-ART study of a Cottrell atmosphere revealed the stability of the Cottrell atmosphere. Indeed, the migration energies of C atoms forming a Cottrell atmosphere are higher than the inverse events. More practically, this means that it is easier for C atoms to stay in a Cottrell atmosphere arrangement than to leave this arrangement.

Conclusion and perspectives

We studied the interaction of C atoms with SIA dislocation loops and with the screw dislocation in bcc Fe. For that purpose, we developed a mixed lattice Kinetic Monte Carlo code which combine k-ART, a soft lattice on the fly self-learning KMC approach with a much simpler atomic approach on a rigid lattice. The combination of the state of the art approach with a much cruder one, allows one to increase the physical time that can be reached with this approach. By using the rigid-lattice approximation when focusing on events far from a distorted zone, the average CPU time needed for MLKMC to perform a jump is reduced drastically compared to k-ART alone. This is a necessary condition to allow to study the formation of Cottrell atmosphere as the interstitial requires many steps to form this atmosphere (10^6 to 10^8 expected depending on the box size). The developed code is easy to compile and can be freely distributed as a k-ART addition. Indeed, just by adding an option in the k-ART Makefile (i.e. -DON_LATTICE), the MLKMC can be compiled as well.

A study using k-ART only was done on the 1 or 2 C atom – SIA loop in α-Fe system. it was found that the most stable positions for the C atoms are at the external periphery of the loop, because it is where the C atoms have the most space. The C atoms thus provide strong anchoring points for the loop, hindering their motion. Furthermore, the C atoms were observed to move rapidly around the loop with a low migration energy path, possibly preventing other C atoms to come close to the loop. The interaction of 10 C atoms with the loop was then studied with the MLKMC. However, due to the low migration energy path of C atoms around the loop, the MLKMC simulations had too few steps for a kinetic behaviour of C atoms to be determined.

The formation of a C Cottrell atmosphere was also studied using the MLKMC. The migration energies in the rigid-lattice zone were computed within the anisotropic elasticity theory, thus taking into account the impact of the dislocation on the C migration. It was observed that C atoms had preferred migration path and more favourable positions with respect to the dislocation. We found also that the influence of the dislocation on the C migration energies is greater than the C-C repulsion as many C atoms were close during the formation of a Cottrell atmosphere: this is a necessary condition for a Cottrell atmosphere to be formed. It was also shown that the first C atoms come very fast towards the screw dislocation: within an hour of simulated time (at 300 K) in a 150 ppm C simulation, several C atoms were found very close to the dislocation line. It is expected for other C atoms to come as well, but it may take longer time as C in the dislocation line may repel C arriving at the dislocation.

Finally, a Cottrell atmosphere decorating a screw dislocation that had been obtained using a static approach by R. Veiga (Veiga et al., 2015) was studied using k-ART only. It was shown that the Cottrell atmosphere is a stable configuration, as the C migration energies are high to leave the dislocation. Furthermore, the inverse events of C atoms leaving the atmosphere were very low, thus emphasizing the stability of Cottrell atmosphere and validating the MC method proposed by Veiga (Veiga et al., 2015).

However, several issues arise from the combination of a rigid-lattice with k-ART. The first one is the difficulty to find the right input parameter settings. Indeed, in addition to the needed knowledge of k-ART which can either be very simple or more complicated depending on the system studied, one must as well be careful about the on-lattice part in order to find the appropriate compromise between speed and physics. Indeed, just the creation of the simulation box itself can turn out to be quite a difficult task to achieve, especially when adding the elastic effects to the O and T sites (absolutely needed when studying a dislocation).

Nonetheless, the MLKMC method has proven its worth. For the first time, the beginning of the formation of a Cottrell atmosphere surrounding a screw dislocation was simulated at the atomic scale using a KMC simulation with times up to the hour at 300 K. It was shown that the first C atoms come very fast close to the dislocation line. The other C atoms are expected to come as well, but this can take a lot more KMC steps as the C atoms close to the dislocation line repel the other C atoms.

Concerning the possible improvements of the methods, several actions can be made: firstly, when studying a moving defect such as a dislocation loop, the k-ART box may need a readjustment. Therefore, redefining these values within the code to be centred on the centre of mass of this loop can allow the program to study the movement of these loops. Secondly, the possibility of adding other k-ART boxes to the system could allow the program to study the interaction between large defects, such as two loops or a loop and a dislocation. Concerning the kinetics of the system, the prefactor is fixed at the moment. Even if at low temperatures this approximation may not impact the kinetics much as the governing factor is the activation energy, going to higher temperatures can lead to kinetically wrong results. For that purpose, k-ART, as it is an evolving code, will be soon provided with the possibility to compute on-the-fly prefactors within the harmonic transition state theory (Mousseau, 2019).

Another issue is the possibility of using the MLKMC for substitutional atoms such as Mn atoms for instance. This would require that a valid interatomic potential exist, which to our knowledge is not the case. Furthermore, the influence of Mn would also need to be taken into account in the rigid-lattice zone, which is not the case for now. This would require to compute the difference in energies of between the Fe-C pair and Mn-C pair for several C-Mn and Fe-C distances. Moreover, using the link-cell method, each C atom would know the neighbouring Fe and Mn atoms, and the energy of the configurations of the C atom before and after its possible jumps could be computed. More practically, another corrective term in the migration energy calculation can be added and computed with the help of a FISE model just by knowing the energies of Fe-C pairs and Mn-C pairs for different C-Fe and C-Mn distances.

Along with bringing comprehensive elements to the mechanisms occurring at the micro scale, atomic simulations may also serve as the first step of larger scale simulations. Indeed, mesoscopic laws can be determined from the atomic behaviour of a material. For instance, Gilbert & al. and Queyreau & al. dedicated their study of the dynamical behaviour of a dislocation computed by MD to serve as a law for DD simulations (Queyreau et al., 2011) (Gilbert et al., 2011). Phase-Field (PF) methods can also be parametrized using smaller scale data, such as Rouchette & al. who performed PF simulations to study the sink strength of dislocation on point defects, with the Vegard tensor of these point defects being computed by DFT (Rouchette et al., 2014b). Going to the macro-scale, the finite element method[5] can reproduce the behaviour of large systems, with a parametrization that can be determined by mesoscopic simulations. Therefore, data such as the time needed for C atoms to form a Cottrell atmosphere or the C migration energies for C atoms close to the dislocation line could be used to model the behaviour of steels at higher scales.

---

[5] Method consisting in a separation of the system in several parts (the finite elements) on which different properties can be applied, such as pressure, displacement, etc.

References

Ackland, G.J. (2012). Interatomic Potential Development. In Comprehensive Nuclear Materials, (Elsevier), pp. 267–291.

Ackland, G.J., Mendelev, M.I., Srolovitz, D.J., Han, S., and Barashev, A.V. (2004). Development of an interatomic potential for phosphorus impurities in α-iron. Journal of Physics: Condensed Matter 16, S2629.

Allen, M.P., and Tildesley, D.J. (1987). Computer Simulations of Liquids, Oxford Science Publications.

Amino, T., Arakawa, K., and Mori, H. (2016). Detection of one-dimensional migration of single self-interstitial atoms in tungsten using high-voltage electron microscopy. Sci Rep 6, 26099.

Anento, N., and Serra, A. (2013). Carbon–vacancy complexes as traps for self-interstitial clusters in Fe–C alloys. Journal of Nuclear Materials 440, 236–242.

Arakawa, K., Hatanaka, M., Mori, H., and Ono, K. (2004). Effects of chromium on the one-dimensional motion of interstitial-type dislocation loops in iron. Journal of Nuclear Materials 329–333, 1194–1198.

Arakawa, K., Hatanaka, M., Kuramoto, E., Ono, K., and Mori, H. (2006). Changes in the Burgers Vector of Perfect Dislocation Loops without Contact with the External Dislocations. Physical Review Letters 96.

Arakawa, K., Ono, K., Isshiki, M., Mimura, K., Uchikoshi, M., and Mori, H. (2007). Observation of the One-Dimensional Diffusion of Nanometer-Sized Dislocation Loops. Science 318, 956–959.

Arakawa, K., Amino, T., Isshiki, M., Mimura, K., Uchikoshi, M., and Mori, H. (2014). One-Dimensional Glide Motion of "Naked" Nanoscale 1/2<111> Prismatic Dislocation Loops in Iron. ISIJ International 54, 2421–2424.

Bacon, D.J., and Osetsky, Y.N. (2009). Dislocation—Obstacle Interactions at Atomic Level in Irradiated Metals. Mathematics and Mechanics of Solids 14, 270–283.

Bacon, D.J., Barnett, D.M., and Scattergood, R.O. (1980). Anisotropic continuum theory of lattice defects. Progress in Materials Science 212.

Barkema, G.T., and Mousseau, N. (1996). Event-based relaxation of continuous disordered systems. Physical Review Letters 77, 4358.

Barralis, J., and Maeder, G. (2005). Précis de métallurgie, Nathan.

Beachem, C.D. (1972). A new model for hydrogen-assisted cracking (hydrogen "embrittlement"). Metallurgical and Materials Transactions B 3, 441–455.

Becquart, C.S., Decker, K.M., Domain, C., Ruste, J., Souffez, Y., Turbatte, J.C., and Van Duysen, J.C. (1997). Massively parallel molecular dynamics simulations with EAM potentials. Radiation Effects and Defects in Solids 142, 9–21.

Becquart, C.S., Raulot, J.M., Bencteux, G., Domain, C., Perez, M., Garruchet, S., and Nguyen, H. (2007). Atomistic modeling of an Fe system with a small concentration of C. Computational Materials Science 40, 119–129.

Béland, L.K., Brommer, P., El-Mellouhi, F., Joly, J.-F., and Mousseau, N. (2011). Kinetic activation-relaxation technique. Physical Review E *84*.

Bhatia, M.A., Groh, S., and Solanki, K.N. (2014). Atomic-scale investigation of point defects and hydrogen-solute atmospheres on the edge dislocation mobility in alpha iron. Journal of Applied Physics *116*, 064302.

Bitzek, E., Koskinen, P., Gähler, F., Moseler, M., and Gumbsch, P. (2006). Structural Relaxation Made Simple. Phys. Rev. Lett. *97*, 170201.

Blavette, D. (1999). Three-Dimensional Atomic-Scale Imaging of Impurity Segregation to Line Defects. Science *286*, 2317–2319.

Bonny, G., Terentyev, D., Zhurkin, E.E., and Malerba, L. (2014). Monte Carlo study of decorated dislocation loops in FeNiMnCu model alloys. Journal of Nuclear Materials *452*, 486–492.

Bortz, A.B., Kalos, M.H., and Lebowitz, J.L. (1975). A new algorithm for Monte Carlo simulation of Ising spin systems. Journal of Computational Physics *7*, 10–18.

Caillard, D. (2010a). Kinetics of dislocations in pure Fe. Part I. In situ straining experiments at room temperature. Acta Materialia *58*, 3493–3503.

Caillard, D. (2010b). Kinetics of dislocations in pure Fe. Part II. In situ straining experiments at low temperature. Acta Materialia *58*, 3504–3515.

Caillard, D. (2011). An in situ study of hardening and softening of iron by carbon interstitials. Acta Materialia *59*, 4974–4989.

Caillard, D., and Bonneville, J. (2015). Dynamic strain aging caused by a new Peierls mechanism at high-temperature in iron. Scripta Materialia *95*, 15–18.

Candela, R., Becquart, C.S., Mousseau, N., Veiga, R.G., and Domain, C. (2018). Interaction between interstitial carbon atoms and an ½ ⟨1 1 1⟩ SIA loop in an iron matrix: a combined DFT, off lattice KMC and MD study. J. Phys. 17.

Chockalingam, K., Janisch, R., and Hartmaier, A. (2014). Coupled atomistic-continuum study of the effects of C atoms at α -Fe dislocation cores. Modelling and Simulation in Materials Science and Engineering *22*, 075007.

Clouet, E. (2007). Babel, http://emmanuel.clouet.free.fr/Programs/Babel/index.html (CEA).

Clouet, E. (2011). Dislocation core field. I. Modeling in anisotropic linear elasticity theory. Physical Review B *84*.

Clouet, E., Garruchet, S., Nguyen, H., Perez, M., and Becquart, C.S. (2008). Dislocation interaction with C in α-Fe: A comparison between atomic simulations and elasticity theory. Acta Materialia *56*, 3450–3460.

Cong, Z., and Murata, Y. (2011). Dislocation Density of Lath Martensite in 10Cr-5W Heat-Resistant Steels. Mater. Trans. *52*, 2151–2154.

Cottrell, A.H., and Bilby, B.A. (1949). Dislocation theory of yielding and strain ageing of iron. Proceedings of the Physical Society. Section A *62*, 49.

Dalla Torre, J., Bocquet, J.L., Doan, N.V., Adam, E., and Barbu, A. (2006). JERK, an event-based Kinetic Monte Carlo model to predict microstructure evolution of materials under irradiation. Philosophical Magazine *85*, 549.

Daw, M.S., and Baskes, M.I. (1983). Semiempirical, quantum mechanical calculation of hydrogen embrittlement in metals. Physical Review Letters *50*, 1285.

Daw, M.S., and Baskes, M.I. (1984). Embedded-atom method: Derivation and application to impurities, surfaces, and other defects in metals. Physical Review B *29*, 6443–6453.

Domain, C., and Becquart, C.S. (2018). Solute – ⟨111⟩ interstitial loop interaction in α-Fe: A DFT study. Journal of Nuclear Materials *499*, 582–594.

Domain, C., and Monnet, G. (2005). Simulation of Screw Dislocation Motion in Iron by Molecular Dynamics Simulations. Physical Review Letters *95*.

Domain, C., Becquart, C.S., and Foct, J. (2004). *Ab initio* study of foreign interstitial atom (C, N) interactions with intrinsic point defects in α -Fe. Physical Review B *69*.

El-Mellouhi, F., Mousseau, N., and Lewis, L.J. (2008). Kinetic activation-relaxation technique: An off-lattice self-learning kinetic Monte Carlo algorithm. Physical Review B *78*.

Eyring, henry (1935). The Activated Complex in Chemical Reactions. The Journal of Chemical Physics *3*, 107–115.

Fichtorn, K.A., and Weinberg, W.H. (1991). Theoretical foundations of dynamical Monte Carlo simulations. J. Chem. Phys. *95*.

Fomin, E.S. (2010). Comparison of the Verlet Table and cell-linked list algorithms on parallel architectures. Numerical Methods and Programming 8.

France, and Commissariat à l'Energie Atomique (2016). Les matériaux du nucléaire: Modélisation et simulation des matériaux de structure (Paris: Le Moniteur).

Ganesan, H., Begau, C., and Sutmann, G. (2018a). MC/MD Coupling for Scale Bridging Simulations of Solute Segregation in Solids: An Application Study. In Simulation Science, M. Baum, G. Brenner, J. Grabowski, T. Hanschke, S. Hartmann, and A. Schöbel, eds. (Cham: Springer International Publishing), pp. 112–127.

Ganesan, H., Teijeiro, C., and Sutmann, G. (2018b). Parallelization comparison and optimization of a scale-bridging framework to model Cottrell atmospheres. Computational Materials Science *155*, 439–449.

Gao, N., Perez, D., Lu, G.H., and Wang, Z.G. (2018). Molecular dynamics study of the interaction between nanoscale interstitial dislocation loops and grain boundaries in BCC iron. Journal of Nuclear Materials *498*, 378–386.

Gilbert, M.R., Dudarev, S.L., Derlet, P.M., and Pettifor, D.G. (2008). Structure and metastability of mesoscopic vacancy and interstitial loop defects in iron and tungsten. J. Phys.: Condens. Matter *20*, 345214.

Gilbert, M.R., Queyreau, S., and Marian, J. (2011). Stress and temperature dependence of screw dislocation mobility in α -Fe by molecular dynamics. Phys. Rev. B *84*, 174103.

Hatakeyama, M., Tamura, S., and Yamagata, I. (2014). Direct observation of solute–dislocation interaction on screw dislocation in a neutron irradiated modified 316 stainless steel. Materials Letters *122*, 301–305.

Henkelman, G., Jóhannesson, G., and Jónsson, H. (2002). Methods for Finding Saddle Points and Minimum Energy Paths. In Theoretical Methods in Condensed Phase Chemistry, S.D. Schwartz, ed. (Dordrecht: Kluwer Academic Publishers), pp. 269–302.

Hestenes, M.R., and Stiefel, E. (1952). Methods of conjugate gradients for solving linear systems. Journal of Research of the National Bureau of Standards *49*, 28.

Hirel, P. (2015). Atomsk: A tool for manipulating and converting atomic data files, http://pierrehirel.info/codes_atomsk.php?lang=eng. Comput. Phys. Comm. *197*, 212.

Hirth, J.P., and Lothe, J. (1992). Theory of dislocations (Malabar, FL: Krieger Pub. Co).

Hohenberg, P., and Kohn, W. (1964). Inhomogeneous Electron Gas. Physical Review *136*, B864–B871.

Hull, D., and Bacon, D.J. (2001). Introduction to dislocations (Butterworth-Heinemann).

Jiang, D.E., and Carter, E.A. (2003). Carbon dissolution and diffusion in ferrite and austenite from first principles. Physical Review B *67*.

Johnston, W.G., and Gilman, J.J. (1959). Dislocation Velocities, Dislocation Densities, and Plastic Flow in Lithium Fluoride Crystals. Journal of Applied Physics *30*, 129–144.

Jonsson, H., Mills, G., and Jacobsen, K.W. (1998). Nudged elastic band method for finding minimum energy paths of transitions. In Classical and Quantum Dynamics in Condensed Phase Simulations, (B. J. Berne, G. Ciccotti, and D. F. Coker), p. 385.

Kang, H.C., and Weinberg, W.H. (1989). Dynamic Monte Carlo with a proper energy barrier: Surface diffusion and two-dimensional domain ordering. The Journal of Chemical Physics *90*, 2824–2830.

Khater, H.A., Monnet, G., Terentyev, D., and Serra, A. (2014). Dislocation glide in Fe–carbon solid solution: From atomistic to continuum level description. International Journal of Plasticity *62*, 34–49.

Kresse, G., and Hafner, J. (1993). Ab initio molecular dynamics for liquid metals. Physical Review B *47*, 558–561.

Kresse, G., and Hafner, J. (1994a). Norm-conserving and ultrasoft pseudopotentials for first-row and transition elements. Condens. Matter *6*, 8245–8257.

Kresse, G., and Hafner, J. (1994b). Ab initio molecular-dynamics simulation of the liquid-metal–amorphous-semiconductor transition in germanium. Physical Review B *49*, 14251.

Kresse, G., and Joubert, D. (1999). From ultrasoft pseudopotentials to the projector augmented-wave method. Physical Review B *59*, 1758.

Kuramoto, E., Ohsawa, K., and Tsutsumi, T. (2005). Interrelation between dislocation loops and an edge dislocation. Materials Transactions *46*, 450–456.

Lavaire, N., Merlin, J., and Sardoy, V. (2001). Study of ageing in strained ultra and extra low carbon steels by thermoelectric power measurement. Scripta Materialia *44*, 553–559.

Lavaire, N., Massardier, V., and Merlin, J. (2004). Quantitative evaluation of the interstitial content (C and/or N) in solid solution in extra-mild steels by thermoelectric power measurements. Scripta Materialia *50*, 131–135.

Le Chatelier, A. (1909). Influence du temps et de la température sur les essais au choc. Rev. Met. Paris *6*, 914–917.

Li, W.-Y., Zhang, Y., Zhou, H.-B., Jin, S., and Lu, G.-H. (2011). Stress effects on stability and diffusion of H in W: A first-principles study. Nuclear Inst. and Methods in Physics Research *269*, 1731.

Liu, Y.-L., Zhou, H.-B., and Zhang, Y. (2011). Investigating behaviors of H in a W single crystal by first-principles: from solubility to interaction with vacancy. Journal of Alloys and Compounds *509*, 8277.

Love, G.R. (1964). Dislocation pipe diffusion. Acta Metallurgica *12*, 731.

Lüthi, B., Ventelon, L., Rodney, D., and Willaime, F. (2018). Attractive interaction between interstitial solutes and screw dislocations in bcc iron from first principles. Computational Materials Science *148*, 21–26.

Malek, R., and Mousseau, N. (2000). Dynamics of Lennard-Jones clusters: A characterization of the activation-relaxation technique. Physical Review E *62*, 7723.

Malerba, L., Marinica, M.C., Anento, N., Björkas, C., Nguyen, H., Domain, C., Djurabekova, F., Olsson, P., Nordlund, K., Serra, A., et al. (2010). Comparison of empirical interatomic potentials for iron applied to radiation damage studies. Journal of Nuclear Materials *406*, 19–38.

Marais, A. (2012). Influence du vieillissement statique sur la transition ductile-fragile des aciers au C-Mn.

McKay, B.D. (1981). Practical Graph Isomorphism. Congressus Numerantium *30*, 45–87.

Mendelev, M.I., Han, S., Srolovitz, D.J., Ackland, G.J., Sun, D.Y., and Asta, M. (2003). Development of new interatomic potentials appropriate for crystalline and liquid iron. Philosophical Magazine *83*, 3977–3994.

Metropolis, N., and Ulam, S. (1949). The Monte Carlo Method. Journal of the American Statistical Association *44*, 335–341.

Metropolis, N., Rosenbluth, A.W., Rosenbluth, M.N., Teller, A.H., and Teller, E. (1953). Equation of State Calculations by Fast Computing Machines. 7.

Meyer, W., and Neldel, H. (1937). Z. Tech. Phys. *12*.

Miller, M.K. (2006). Atom probe tomography characterization of solute segregation to dislocations. Microscopy Research and Technique *69*, 359–365.

Monnet, G. (2006). Investigation of precipitation hardening by dislocation dynamics simulations. Philosophical Magazine *86*, 5927–5941.

Monnet, G., and Terentyev, D. (2009). Structure and mobility of the 1/2<111>{112} edge dislocation in BCC iron studied by molecular dynamics. Acta Materialia *57*, 1416–1426.

Mousseau, N. (2019). Private communication.

Mousseau, N., and Barkema, G.T. (1998). Traveling through potential energy landscapes of disordered materials: The activation-relaxation technique. Physical Review E *57*, 2419–2424.

Myers, S.M., Baskes, M.I., Birnbaum, H.K., Corbett, J.W., DeLeo, G.G., Estreicher, S.K., Haller, E.E., Jena, P., Johnson, N.M., Kirchheim, R., et al. (1992). Hydrogen interactions with defects in crystalline solids. Reviews of Modern Physics *64*, 559–617.

Nabarro, F.R.N. (1947). Dislocations in a simple cubic lattice. Proceedings of the Physical Society *59*, 256–272.

Nedelcu, S., Kizler, P., Schmauder, S., and Moldovan, N. (2000). Atomic scale modelling of edge dislocation movement in the alphaFe-Cu system. Modelling Simul. Mater. Sci. Eng. *8*, 12.

Ngayam-Happy, R., Becquart, C.S., and Domain, C. (2013). First principle-based AKMC modelling of the formation and medium-term evolution of point defect and solute-rich clusters in a neutron irradiated complex Fe–CuMnNiSiP alloy representative of reactor pressure vessel steels. Journal of Nuclear Materials *440*, 143–152.

Nguyen, H. (2009). Etude à l'échelle atomique des interactions des hétéro-interstitiels (C et N) avec les défauts étendus : effets sur la plasticité du Fe. Lille.

Olsson, P., Klaver, T.P.C., and Domain, C. (2010). *Ab initio* study of solute transition-metal interactions with point defects in bcc Fe. Physical Review B *81*.

Pascuet, M.I., Martínez, E., Monnet, G., and Malerba, L. (2017). Solute effects on edge dislocation pinning in complex alpha-Fe alloys. Journal of Nuclear Materials *494*, 311–321.

Pascuet, M.I., Monnet, G., Bonny, G., Martínez, E., Lim, J.J.H., Burke, M.G., and Malerba, L. (2019). Solute precipitation on a screw dislocation and its effects on dislocation mobility in bcc Fe. Journal of Nuclear Materials *519*, 265–273.

Peierls, R. (1940). The size of a dislocation. Proceedings of the Physical Society *52*, 34.

Perdew, J.P., Chevary, J.A., Vosko, S.H., Jackson, K.A., Pederson, M.R., Singh, D.J., and Fiolhais, C. (1992). Atoms, molecules, solids, and surfaces: Applications of the generalized gradient approximation for exchange and correlation. Physical Review B *46*, 6671.

Plimpton, S. Fast Parallel Algorithms for Short–Range Molecular Dynamics. 42.

Queyreau, S., Marian, J., Gilbert, M.R., and Wirth, B.D. (2011). Edge dislocation mobilities in bcc Fe obtained by molecular dynamics. Phys. Rev. B *84*, 064106.

Restrepo, O.A., Mousseau, N., El-Mellouhi, F., Bouhali, O., Trochet, M., and Becquart, C.S. (2016). Diffusion properties of Fe–C systems studied by using kinetic activation–relaxation technique. Computational Materials Science *112*, 96–106.

Rodney, D., Ventelon, L., Clouet, E., Pizzagalli, L., and Willaime, F. (2017). Ab initio modeling of dislocation core properties in metals and semiconductors. Acta Materialia *124*, 633–659.

Rouchette, H., Thuinet, L., Legris, A., Ambard, A., and Domain, C. (2014). Influence of shape anisotropy of self-interstitials on dislocation sink efficiencies in Zr: Multiscale modeling. Phys. Rev. B *90*, 014104.

Sheppard, D., Terrell, R., and Henkelman, G. (2008). Optimization methods for finding minimum energy paths. The Journal of Chemical Physics *128*, 134106.

Shewchuk, J. (1974). An Introduction to the Conjugate Gradient Method that Even an Idiot Can Understand. 62.

Simonetti, S., Pronsato, M.E., Brizuela, G., and Juan, A. (2003). The electronic effect of carbon and hydrogen in an () edge dislocation core system in bcc iron. Applied Surface Science *217*, 56–67.

Smith, G.D.W., Hudson, D., Styman, P.D., and Williams, C.A. (2013). Studies of dislocations by field ion microscopy and atom probe tomography. Philosophical Magazine *93*, 3726–3740.

Soisson, F., Barbu, A., and Martin, G. (1996). Monte Carlo simulations of copper precipitation in dilute iron-copper alloys during thermal ageing and under electron irradiation. Acta Materialia *44*, 3789–3800.

Soisson, F., Becquart, C.S., Castin, N., Domain, C., Malerba, L., and Vincent, E. (2010). Atomistic Kinetic Monte Carlo studies of microchemical evolutions driven by diffusion processes under irradiation. Journal of Nuclear Materials *406*, 55–67.

Soneda, N., and de la Rubia, T.D. (1998). Defect production, annealing kinetics and damage evolution in α-Fe: An atomic-scale computer simulation. Philosophical Magazine A *78*, 995–1019.

Soneda, N., Ishino, S., and de la Rubia, T.D. (2001). Vacancy loop formation by "cascade collapse" in a-Fe: A molecular dynamics study of 50keV cascades. Philosophical Magazine Letters *81*, 649–659.

Sorensen, M.R., and Voter, A.F. (2000). Temperature-accelerated dynamics for simulation of infrequent events. The Journal of Chemical Physics *112*, 9599–9606.

Swope, W.C., Andersen, H.C., Berens, P.H., and Wilson, K.R. (1982). A computer simulation method for the calculation of equilibrium constants for the formation of physical clusters of molecules: Application to small water clusters. The Journal of Chemical Physics *76*, 637–649.

Tapasa, K., Barashev, A.V., Bacon, D.J., and Osetsky, Yu.N. (2007a). Computer simulation of the interaction of carbon atoms with self-interstitial clusters in α-iron. Journal of Nuclear Materials *361*, 52–61.

Tapasa, K., Osetsky, Y., and Bacon, D. (2007b). Computer simulation of interaction of an edge dislocation with a carbon interstitial in α-iron and effects on glide. Acta Materialia *55*, 93–104.

Taylor, G.I. (1934). The Mechanism of Plastic Deformation of Crystals. Part I. Theoretical. Proceedings of the Royal Society A: Mathematical, Physical and Engineering Sciences *145*, 362–387.

Tchitchekova, D.S., Morthomas, J., Ribeiro, F., Ducher, R., and Perez, M. (2014). A novel method for calculating the energy barriers for carbon diffusion in ferrite under heterogeneous stress. The Journal of Chemical Physics *141*, 034118.

Terentyev, D., and Martin-Bragado, I. (2015a). Evolution of dislocation loops in iron under irradiation: The impact of carbon. Scripta Materialia *97*, 5–8.

Terentyev, D., and Martin-Bragado, I. (2015b). Evolution of dislocation loops in iron under irradiation: The impact of carbon. Scripta Materialia *97*, 5–8.

Terentyev, D., Grammatikopoulos, P., Bacon, D.J., and Osetsky, Yu.N. (2008). Simulation of the interaction between an edge dislocation and a ⟨100⟩ interstitial dislocation loop in α-iron. Acta Materialia *56*, 5034–5046.

Terentyev, D., Osetsky, Yu.N., and Bacon, D.J. (2010). Competing processes in reactions between an edge dislocation and dislocation loops in a body-centred cubic metal. Scripta Materialia *62*, 697–700.

Terentyev, D., Anento, N., Serra, A., Jansson, V., Khater, H., and Bonny, G. (2011). Interaction of carbon with vacancy and self-interstitial atom clusters in α-iron studied using metallic–covalent interatomic potential. Journal of Nuclear Materials *408*, 272–284.

Terentyev, D., Anento, N., and Serra, A. (2012). Interaction of dislocations with carbon-decorated dislocation loops in bcc Fe: an atomistic study. Journal of Physics: Condensed Matter *24*, 455402.

Terentyev, D., He, X., Bonny, G., Bakaev, A., Zhurkin, E., and Malerba, L. (2015). Hardening due to dislocation loop damage in RPV model alloys: Role of Mn segregation. Journal of Nuclear Materials *457*, 173–181.

U.S.NRC PWR, https://www.nrc.gov/reading-rm/basic-ref/students/animated-pwr.html.

Van der Ven, A., Ceder, G., Asta, M., and Tepesch, P.D. (2001). First-principles theory of ionic diffusion with nondilute carriers. Physical Review B *64*.

Varvenne, C., Bruneval, F., Marinica, M.-C., and Clouet, E. (2013). Point defect modeling in materials: Coupling *ab initio* and elasticity approaches. Physical Review B *88*.

Veiga, R. (2011). Computational insights into the strain aging phenomenon in bcc iron at the atomic scale. Industrial & Engineering Chemistry Research *26*, 726–731.

Veiga, R.G.A., Perez, M., Becquart, C.S., Domain, C., and Garruchet, S. (2010). Effect of the stress field of an edge dislocation on carbon diffusion in α -iron: Coupling molecular statics and atomistic kinetic Monte Carlo. Physical Review B *82*.

Veiga, R.G.A., Perez, M., Becquart, C.S., Clouet, E., and Domain, C. (2011). Comparison of atomistic and elasticity approaches for carbon diffusion near line defects in α-iron. Acta Materialia *59*, 6963–6974.

Veiga, R.G.A., Becquart, C.S., and Perez, M. (2014). Comments on "Atomistic modeling of an Fe system with a small concentration of C." Computational Materials Science *82*, 118–121.

Veiga, R.G.A., Goldenstein, H., Perez, M., and Becquart, C.S. (2015). Monte Carlo and molecular dynamics simulations of screw dislocation locking by Cottrell atmospheres in low carbon Fe–C alloys. Scripta Materialia *108*, 19–22.

Ventelon, L., Willaime, F., Clouet, E., and Rodney, D. (2013). Ab initio investigation of the Peierls potential of screw dislocations in bcc Fe and W. Acta Materialia *61*, 3973–3985.

Ventelon, L., Lüthi, B., Clouet, E., Proville, L., Legrand, B., Rodney, D., and Willaime, F. (2015). Dislocation core reconstruction induced by carbon segregation in bcc iron. Physical Review B *91*.

Verlet, L. (1967). Computer "Experiments" on Classical Fluids. I. Thermodynamical Properties of Lennard-Jones Molecules. Physical Review *159*, 98–103.

Vincent, E., Becquart, C.S., Pareige, C., Pareige, P., and Domain, C. (2008). Precipitation of the FeCu system: A critical review of atomic kinetic Monte Carlo simulations. Journal of Nuclear Materials *373*, 387–401.

Vítek, V., Perrin, R.C., and Bowen, D.K. (1970). The core structure of ½⟨111⟩ screw dislocations in b.c.c. crystals. Philosophical Magazine *21*, 1049–1073.

Volterra, V. (1907). Sur l'équilibre des corps élastiques multiplement connexes. Annales scientifiques de l'École normale supérieure *24*, 401–517.

Wang, S., Hashimoto, N., and Ohnuki, S. (2013). Hydrogen-induced change in core structures of {110}[111] edge and {110}[111] screw dislocations in iron. Scientific Reports *3*.

Waseda, O., Veiga, R.G., Morthomas, J., Chantrenne, P., Becquart, C.S., Ribeiro, F., Jelea, A., Goldenstein, H., and Perez, M. (2017). Formation of carbon Cottrell atmospheres and their effect on the stress field around an edge dislocation. Scripta Materialia *129*, 16–19.

Xu, H., Osetsky, Y.N., and Stoller, R.E. (2011). Simulating complex atomistic processes: On-the-fly kinetic Monte Carlo scheme with selective active volumes. Physical Review B *84*.

Xu, H., Stoller, R.E., Osetsky, Y.N., and Terentyev, D. (2013). Solving the Puzzle of ⟨ 100 ⟩ Interstitial Loop Formation in bcc Iron. Physical Review Letters *110*.

Young, W.M., and Elcock, E.W. (1966). Monte Carlo studies of vacancy migration in binary ordered alloys: I. Proceedings of the Physical Society *89*, 735–746.

Zhao, Y., and Lu, G. (2011). QM/MM study of dislocation—hydrogen/helium interactions in α-Fe. Modelling and Simulation in Materials Science and Engineering *19*, 065004.

Annexes

1. On-the fly computation of the migration energies in the rigid-lattice zone

Another transition-searching method was developed for the rigid-lattice zone: instead of searching the transitions before the simulation starts, the transitions on the rigid-lattice zone can be computed on-the-fly.

Some of the MLKMC principles explained previously are to be remembered to understand the method to construct the rigid configuration: Firstly, the configuration is divided in two parts, i.e. the k-ART zone (distorted lattice) and the on-lattice zone (lattice close to perfect). Secondly, within the on-lattice zone, the only defects present are C atoms, disturbing the matrix locally (only the 6 atoms constituting the O site containing a C atom are considered to move compared to the perfect matrix). Therefore, the most straight-forward way to create a rigid-lattice is to reverse the local C induced lattice distortion. An example of how the program manages to perform this step is displayed for a single C atom. Firstly, the program identifies the Fe 1st and 2nd nearest neighbours (NN) to the C atom in the rigid lattice. Then, the vectors $\overrightarrow{d_{Fe_n-C}}$ between the Fe nearest neighbours and the C atoms are found:

$$\overrightarrow{d_{Fe_n-C}} = \begin{pmatrix} x_C - x_{Fe_n} \\ y_C - y_{Fe_n} \\ Z_c - Z_{Fe_n} \end{pmatrix} \tag{42}$$

Where Fe_n represents one of the six Fe nearest neighbours to the C atom (two Fe 1st NN, four Fe 2nd NN) and $x_C, y_C, z_C, x_{Fe_n}, y_{Fe_n}, z_{Fe_n}$ represents the coordinates of the C atom and the Fe atom respectively. In a perfect bcc Fe lattice, the Fe 1st NN to the C atom are at a distance of $\frac{a_0}{2}$ (1.43 Å with the potential used) and while Fe 2nd NN are at $\frac{\sqrt{2}}{2} \times a_0$ (2.01 Å with the potential used). However, in a relaxed configuration, the Fe atoms are displaced due to the presence of the C atom: the Fe 1st NN are at approximatively 1.79 Å and the Fe 2nd NN are at approximatively 1.97 Å with the potential used. The coordinates of the Fe atoms after the relaxation are noted $x_{Fe_n}^{relaxed}, y_{Fe_n}^{relaxed}, z_{Fe_n}^{relaxed}$. The coordinates of the C atom and the relaxed Fe atoms are known, yet the coordinates of the Fe atoms on the rigid lattice are to be determined. They can be found using a combination of the next equations:

$$\left\| \overrightarrow{d_{Fe_n-C}} \right\| = \sqrt{\left(x_C - x_{Fe_n}\right)^2 + \left(y_C - y_{Fe_n}\right)^2 + \left(Z_c - Z_{Fe_n}\right)^2} \tag{43}$$

$$\left\| \overrightarrow{d_{Fe_n^{relaxed}-C}} \right\| = \sqrt{\left(x_C - x_{Fe_n^{relaxed}}\right)^2 + \left(y_C - y_{Fe_n^{relaxed}}\right)^2 + \left(Z_c - Z_{Fe_n^{relaxed}}\right)^2} \tag{44}$$

$$\left\| \overrightarrow{d_{Fe_n-C}} \right\| = k \times \left\| \overrightarrow{d_{Fe_n^{relaxed}-C}} \right\| \tag{45}$$

In equation 45, k represents a real positive scalar. The variables $\overrightarrow{d_{Fe_n-C}}$ and $\overrightarrow{d_{Fe_n^{relaxed}-C}}$ are represented on Figure 71, with $n = 1$ for the Fe 1 NN and $n = 2$ for the Fe 2 NN for comprehension sake.
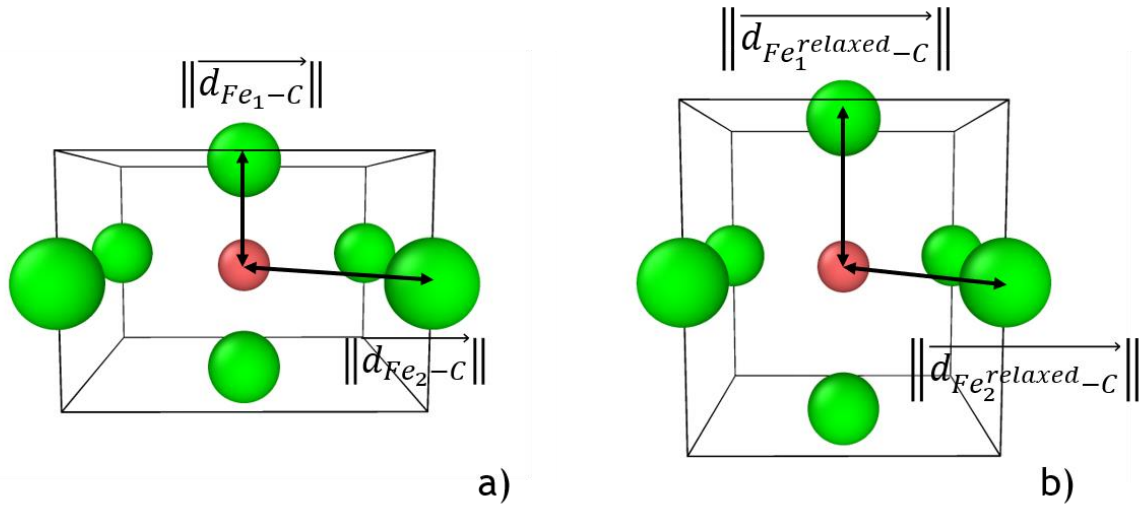
Figure 71: Representation of the variables $\overrightarrow{d_{Fe_n-C}}$ (a) and $\overrightarrow{d_{Fe_n^{relaxed}-C}}$ with $n=1$ for the Fe 1 NN and $n=2$ for the Fe 2 NN.

Because the vectors $\overrightarrow{d_{Fe_n-C}}$ and $\overrightarrow{d_{Fe_n^{relaxed}-C}}$ are collinear, equation 45 can be rewritten as follow:

$$\nabla\overrightarrow{d_{Fe_n-C}} = k \times \nabla\overrightarrow{d_{Fe_n^{relaxed}-C}} \tag{46}$$

Or in other terms:

$$\begin{pmatrix} x_C - x_{Fe_n} \\ y_C - y_{Fe_n} \\ Z_c - Z_{Fe_n} \end{pmatrix} = \begin{pmatrix} x_C - k \times x_{Fe_n^{relaxed}} \\ y_C - k \times y_{Fe_n^{relaxed}} \\ Z_c - k \times Z_{Fe_n^{relaxed}} \end{pmatrix} \tag{47}$$

Equation 47 allows the program to find the coordinates of the Fe atom in the perfect rigid lattice. More practically, the C-Fe NN directions are found and the Fe atoms are moved along this direction only by a factor corresponding to the ratio of the distances between the C atom and the Fe in the relaxed configuration to the C atom and the Fe in the rigid lattice position (i.e. $\frac{a_0}{2}$ Å). This can be done in two steps once the Fe NN to the C are known. Firstly, identification of the C-Fe directions (Figure 72 a) ; secondly, displacement of the Fe along the Fe-C direction previously found (Figure 72 b). The rigid-lattice is then constructed (Figure 72 c).
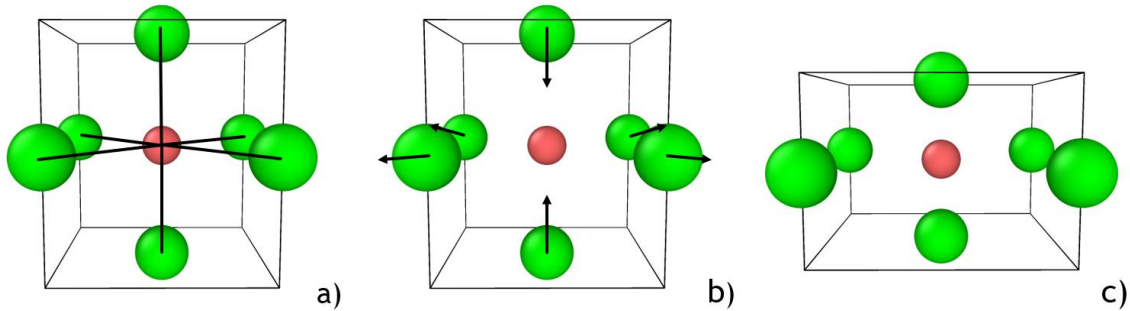

Figure 72: Construction of the rigid lattice in two steps, i.e. identification of the C-Fe distances (a) and displacement of the Fe atoms along the Fe-C direction previously computed (b). The rigid lattice is created from a relaxed configuration (c).

A C atom can perform jumps only from an O site to one of the fours adjacent O sites. Knowing that these adjacent O sites are situated between two Fe 2 NN to the C atoms distanced by a_0 Å, the transitions that the system can undergo are easily retrievable. Firstly, the Fe NN to each C atom must be known at each step. This step is managed using the cell-linked lists method for a fast finding of the Fe NN. Knowing the positions and indexes of the Fe 2 NN to a C atom, the program computes the distances between the different Fe 2 NN to find between which Fe the C atoms can jump. This is done for each C atom at each step to find all the positions of each C transitions. Unfortunately, this method fails especially when the simulated system contains a lot of C atoms. Indeed, surprisingly a single C atom induces a great distortion of the system, especially in the direction given by the 2 Fe 1st NN, up to 6 Å far from the C atom, while the C induced distortion was expected local. As one can see on Figure 73 where the displacement of Fe atoms due to the presence of a C atom is showcased, the distortion is not restricted only to Fe 1st and 2nd NN to the C atom. More precisely, the numerical values of the Fe displacement are displayed on Figure 74, with a positive value meaning that the Fe atoms moved away from the C atoms and a negative value meaning that the Fe moved towards the C atoms. Three main conclusions jump out from Figure 73 and Figure 74:

- The C-induced Fe displacement is not restricted on the direction C-Fe, which makes the equation 47 irrelevant for certain Fe ;
- The main Fe displacement is at 0.36 Å (for the Fe 1 NN to the C), but the C still induces a great distortion of the lattice even for Fe 9th NN to the C atom (or a C-Fe distance of 5.9 Å). This implies that the presence of a single C atom disturbs the bulk as far as distances of 5.9 Å, moving Fe atoms at this distance of 0.04 Å ;
- On Figure 74, the Fe atoms 5th and 9th NN to the C atom both have a positive and a negative displacement. More precisely, because all the Fe 5th and 9th NN are not equivalent (i.e. while the C-Fe distance is the same, some Fe are in the [100] direction passing by the C atom thus directly impacted by it), some atoms will be pushed by the C while the other will compensate this distortion by going towards the C atom.
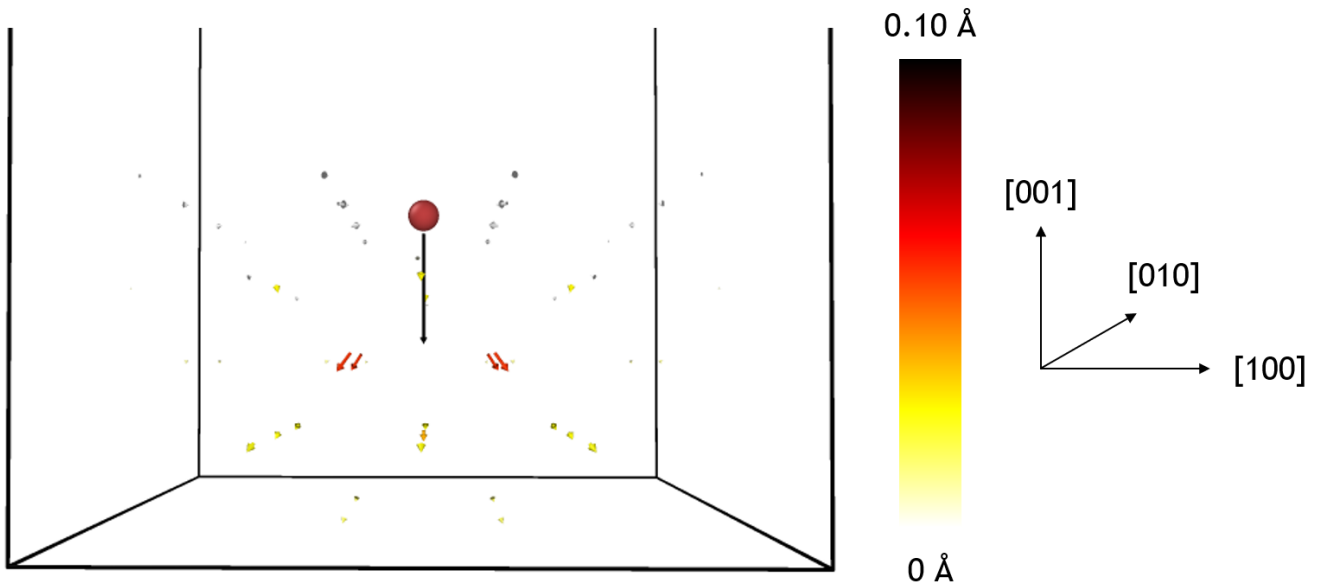
Figure 73: Displacement of the Fe atoms (displacement represented by the arrows, the Fe atoms are not presented for comprehension sake) induced by the introduction of 1 C atom in the bulk (red atom) for Fe atoms up to the 10th Fe nearest neighbour to the C atom. Only half of the Fe displacements are shown, as the $(00z_c)$ plane is a plane of symmetry. Arrows displaying the displacement of Fe are scaled and colorized according to the value of the above-mentioned displacement (color scale goes from 0 to 0.1 Å for a better visualization even if the greatest Fe displacement is at 0.36 Å).
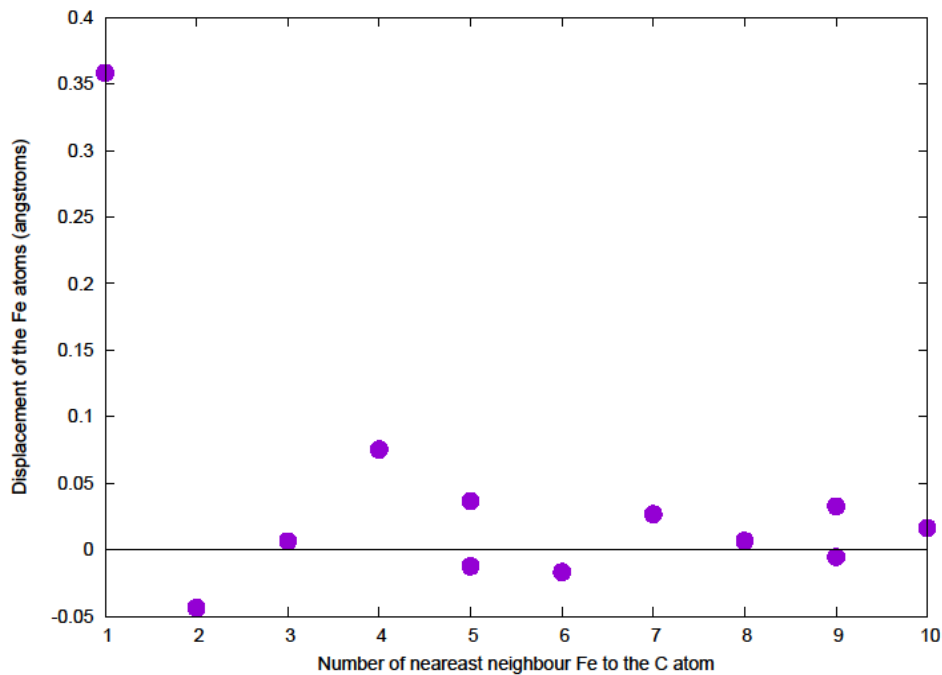

Figure 74: Displacement of Fe atoms versus their number of nearest neighbour to the C atom (e.g. x=3 means that the displacement is showed for the Fe 3 NN to the C). A positive value for the Fe displacement means that the Fe atoms have moved away from the C atom and a negative displacement means that the Fe atoms have moved towards the C atom.

As a result, because of the combination of the distortions of different C atoms on the matrix, the creation of a perfect lattice from a distorted one is a much more complicated task than what intuition suggests. Therefore, the correction presented on equation 47 is not valid for a great C concentration, or more precisely if at least 2 C atoms are close enough to both have an influence on the same area of the bulk. However, this method can be applied to not too much distorted lattices, such as the study of C migration towards a SIA dislocation loop in Fe.

It is also important to note that this method results in higher times needed for the MLKMC to perform a step. Indeed, this method is approximatively 100 times slower than computing the transitions before the simulation starts. Nonetheless, computing the transitions on-the-fly on the rigid-lattice zone is still 10^3 to 10^5 faster than using k-ART. The main advantage of using this method is that the possible transitions do not have to be computed before the simulation starts, thus making the construction of the simulation box much easier.

2. Parameters optimized for the MLKMC simulations containing a screw dislocation

Table 12 summarizes the different k-ART parameters tested for the MLKMC simulations containing a screw dislocation. More precisely, the use of the BMRM or not, the energy of an event to be considered within a basin, the number of searches per topology and the minimum distance for 2 atoms to be linked in a topology were optimized. Furthermore, several other parameters are also tested to determine their relevance (Table 12 4th column: Additional parameters).

BMRM	Energy of an event to be considered in a basin (eV)	Number of searches per topology	Additional parameters
No	/	30	/
Yes	0.35	50	Fe active
Yes	0.35	50	/
Yes	0.35	50	No reversibility
Yes	0.70	50	/
Yes	0.70	50	No local forces
Yes	0.70	100	/
Yes	0.70	50	No reversibility
No	/	50	Fe active
No	/	50	/
No	/	50	No reversibility
Yes	0.70	150	/

Table 12: K-ART parameters tested for the MLKMC simulations containing a screw dislocation.

It was found that BMRM treatment is a necessity in these simulations as low energy events can result in a C atom oscillating near an energy minimum position (spurious steps). The energy for an event to be considered within a basin (for the BMRM treatment) was thus investigated. It was found that only one 0.2 eV event could hinder the simulation, the second higher migration energy event being at 0.6 eV. It was therefore chosen to consider that events with a migration energy lower than 0.4 eV will be treated with the BMRM for all the MLKMC simulations. When k-ART performs only 30 event searches per topology, it was observed (rarely) that some events could be missed, resulting in false predictions of the kinetics of the system. However, 50 event searches per topology ensures that all the events are found for a particular configuration. As the simulations are launched on 16 cores, (1 master 15 slaves searching for transitions), a multiple of 15 is recommended for the transition searches (otherwise some

slaves will wait the other to finish). Therefore, it was chosen to perform 60 searches per topology for all simulations containing a screw dislocation and 10 C atoms, and 45 searches per topology for all simulations containing a screw dislocation and 25 C atoms (not to have a too long simulated time). Finally, several different parameters were investigated. Firstly, k-ART was allowed to search transitions on Fe atoms (labelled as "Fe active" on Table 12 4th column). This resulted in too many possible events for a step in addition to a CPU time of 2 days to perform a step. Furthermore, many of these Fe steps were minor reorganizations such as 0.05 eV steps. Therefore, for the MLKMC simulations, it was chosen not to search transitions centred on Fe atoms. K-ART has the possibility to check whether an event is reversible or not. It was determined that deactivating this option could result in false kinetics, and thus this option was set in all the MLKMC simulations. The last parameter tested was to compute the forces of all atoms for the search of transitions rather than on a zone of about 2 000 atoms around the atom the topology is centred on (labelled as "No local forces" on Table 12 4th column). As the results were the same, it was chosen to use the local forces, i.e. to compute the forces of approximatively 2 000 atoms around the atom the topology is centred on.

Résumé de la thèse

Dans les réacteurs à eau pressurisée, les tuyaux des circuits secondaires sont soumis à de fortes pressions et des températures élevées (70 bars, 600 K). Ils sont constitués d'aciers Fe-Mn-C qui sont donc soumis au vieillissement statique, i.e. la formation d'atmosphères de Cottrell qui décorent les dislocations. Les dislocations sont des défauts linéaires dans une matrice, et le mouvement de ces dislocations est responsable de la plasticité dans les matériaux. Les dislocations agissent de plus comme des puits pour les hétéro-interstitiels : il est donc possible d'observer la formation d'atmosphère de Cottrell, ce qui impacte les propriétés macroscopiques de ces aciers en ayant un effet d'ancrage sur les dislocations. Par ailleurs, sous irradiation dans l'acier de cuve, les boucles de dislocation d'auto interstitiels sont des défauts bien plus mobiles que les dislocations dans le fer bcc. A cause de la haute énergie de formation d'un atome auto interstitiel, ces boucles sont un des défauts de la microstructure irradiée. Leur très grande mobilité fait qu'elles impactent grandement la microstructure du matériau étudié en interagissant avec beaucoup d'autres défauts. Une méthode de simulation atomique est développée donc afin d'étudier la cinétique de formation des atmosphères de Cottrell : le Mixed-Lattice Kinetic Monte-Carlo (MLKMC). Le MLKMC consiste en une division spatiale de la boîte de simulation pour traiter les zones distordues avec k-ART, un KMC sur réseau souple, et traiter les zones non distordues avec l'approximation du réseau rigide. Le modèle est tout d'abord testé pour retrouver le coefficient de diffusion du carbone dans le fer bcc avec succès. Il est ensuite testé sur des dislocations vis et sur des boucles de dislocations d'auto interstitiels dans le fer bcc. Pour la première fois, la formation d'une atmosphère de Cottrell est observée à l'échelle atomique, avec des temps simulés de l'ordre de l'heure à 300 K. Des mécanismes intéressants sont également observés et expliqués, comme l'impact de la dislocation sur la migration des atomes de carbones.

Abstract

In pressurized water reactors, the pipes of secondary circuits go under high pressures and temperatures (70 bars, 600 K). They are constituted of Fe-Mn-C steels which are thus subject to static ageing, i.e. the formation of Cottrell atmospheres decorating dislocations. Dislocations are linear defects in a matrix, and their movement is responsible for the plasticity in materials. Dislocations act as sinks for hetero-interstitials: as such, Cottrell atmosphere can be made, impacting the macro properties of these steels by pinning the dislocations. On the other hand, in pressure vessel steels, under irradiation, dislocation loops made of auto-interstitials are defects much more mobile than dislocations in bcc iron. Because of the high formation energy of a SIA, dislocation loops are considered signature defects of irradiation. Due to their high mobility, these loops will impact a lot the microstructure studied by interacting with numerous other defects. An atomic simulation method is developed in order to study the kinetics of the Cottrell atmosphere formation: the Mixed-Lattice Kinetic Monte Carlo (MLKMC). It consists in dividing spatially the simulation box to treat the distorted zones with k-ART, a soft-lattice KMC, and treat the not distorted zones under the rigid-lattice approximation. The model is able to accurately find the C diffusion coefficient in bcc Fe. Then, it is used on screw dislocation and SIA dislocations loops in bcc Fe. For the first time, the formation of a Cottrell atmosphere is observed at the atomic scale, with simulated times close to the hour at 300 K. Furthermore, interesting mechanisms of are observed and explained, such as the dislocation impact on the carbon atoms migration.